The role of plasmodesmata regulation in root responses to macronutrient and water availability

Philip John Kirk

Submitted in accordance with the requirements for the degree of

Doctor of Philosophy (PhD)

The University of Leeds

Faculty of Biological Sciences

July 2022

The candidate confirms that the work submitted is his own, except where work which has formed part of jointly authored publications has been included. The contribution of the candidate and the other authors to this work has been explicitly indicated below. The candidate confirms that appropriate credit has been given within the thesis where reference has been made to the work of others.

In the Introduction chapter, Figure 1.7 was published in the following publication: Amsbury, S., Kirk, P. and Benitez-Alfonso, Y. 2018. Emerging models on the regulation of intercellular transport by plasmodesmata-associated callose. *Journal of Experimental Botany*. **69**(1), pp.105-115. The figure was constructed by the candidate with input from the other authors.

In Chapter 3 and Chapter 4, Figure 3.1,-3.5; 3.8, 3.9-3.12 and 4.11 were constructed from data presented in the following publication: Kirk, P., Amsbury, S., German, L., Gaudioso-Pedraza, R. and Benitez-Alfonso, Y. 2022. A comparative meta-proteomic pipeline for the identification of plasmodesmata proteins and regulatory conditions in diverse plant species. *BMC biology*. **20**(1), pp.1-21. Meta-transcriptomics of *Arabidopsis thaliana* was performed jointly by the candidate and Dr Sam Amsbury. Meta-transcriptomics of *Medicago truncatula* was performed by Liam German. All subsequent analysis and construction of figures were performed by the candidate. Figure 3.12 was also constructed from data presented in the following publication: Gaudioso-Pedraza, R., Beck, M., Frances, L., Kirk, P., Ripodas, C., Niebel, A., Oldroyd, G.E.D., Benitez-Alfonso, Y. and de Carvalho-Niebel, F. 2018. Callose-Regulated Symplasmic Communication Coordinates Symbiotic Root Nodule Development. *Curr Biol.* **28**(22), pp.3562-3577 e3566. The transformation plasmid *pUBI::MtBG2* was generated by Dr Rocio Gaudioso-Pedraza. The subsequent transient expression of this plasmid in *M. truncatula*, photography of roots and confocal analysis using symplasmic reporter was performed by the candidate.

In Chapter 4, Figure 4.12 was constructed from data presented in the following publication: Grison, M.S., Kirk, P., Brault, M.L., Wu, X.N., Schulze, W.X., Benitez-Alfonso, Y., Immel, F. and Bayer, E.M. 2019. Plasma Membrane-Associated Receptor-like Kinases Relocalize to Plasmodesmata in Response to Osmotic Stress. *Plant physiology*. **181**(1), pp.142-160. The data for this figure was generated solely by the candidate.

In Chapter 6, Figure 6.3 was constructed from data generated by Dr Lei Yang from the Kragler group, Max Planck Institute of Molecular Plant Physiology, Germany.

Acknowledgements

My first thank you must go to my super supervisor Yoselin. Yoselin is one of the kindest people I have ever met, and she always goes above and beyond to help support her staff and students. She has taught me almost everything I know about being a scientist and has helped me learn a great deal about myself too. I will always be greatly indebted to you. I pay a special thanks to my colleague, lab mentor and good friend Dr Sam Amsbury for everything he did to help me through my project. Thank you to everyone else at the Centre for Plant Sciences who also helped me along the way.

None of this would have been possible without the unwavering love and support of my partner Jade, parents John and Clare, my grandparents Les and Barbara, my brother Joe, and the rest of my family. Meeting Jade was the highlight of my PhD, and I cannot express enough how her encouragement and advice helped me through the most challenging periods of this project. I wouldn't have ventured into a PhD without the love of learning instilled in me by my mum and grandma who always encouraged me to achieve the best that I could. I can attribute my fascination of biology with times spent catching and observing tadpoles, newts and sticklebacks under the supervision of my wise and always encouraging grandpa. My dad is a continuing source of inspiration who shared with me the need to know how things work and the meaning of perseverance in the face of challenges. Fear of Joe beating me at anything has been a consistent motivation all my life. In many ways except the literal sense, Joe is my big brother and without him, I wouldn't have had the confidence to undertake this project.

Abstract

Modulation of root morphology allows plants to intercept resources whilst avoiding areas of soil with suboptimal conditions. Plasmodesmata (PD) are membranous pores embedded in the cell wall that connect the cytoplasm of neighbouring cells. Regulation of this symplasmic connectivity by proteins that localise to PD, such as PD-located beta-1,3 glucanases and callose synthases control root morphology. Technical constraints hamper efforts to dissect PD proteomes and understand the regulation of PD transport. Here, the tool PIP1 (Plasmodesmata *in silico* Proteome 1) was developed that uses comparative proteomics to predict PD proteins in different species. PIP1 was validated by comparing *in silico* - and experimentally derived PD proteomes obtained from *Arabidopsis thaliana* and poplar. In combination with meta-transcriptomics, PIP1 was used to identify conditions that may involve regulation of PD in *A. thaliana*. Predictions were experimentally tested by measuring symplasmic transport of GFP using confocal microscopy and promoter reporter lines. Low nitrate, osmotic challenge and elevated NaCl reduced phloem unloading of GFP in root tips. This correlated with a 35-51% reduction in primary root length. Meta-transcriptomics revealed that *PD CALLOSE BINDING PROTEIN 4* (*PDCB4*) was upregulated up to 2.3 $\log_2$ fold change under osmotic challenge. Primary root length of CRISPR-Cas9 generated *pdcb4* showed an insensitivity to osmotic challenge and salt stress suggesting that PDCB4 is a regulator of these root morphological responses. A role for SHAVEN3-LIKE1 (SVL1) in regulating root morphology was explored. *SVL1* mRNA was previously identified as shoot to root mobile in response to changes in nutrient conditions. Mutant *svl1* was found to be defective in root growth and symplasmic movement of GFP; a phenotype that was likely linked to changes in cell wall composition. Together, this work suggests that plants use mechanisms involving the regulation of symplasmic transport to mediate root responses to water availability, salinity and nutrient conditions.

Table of Contents

List of tables

List of figures

List of abbreviations

ABA	abscisic acid
AIR	alcohol insoluble residue
APL	ALTERED PHLOEM DEVELOPMENT
ARF2	AUXIN RESPONSE FACTOR
AKT1	*ARABIDOPSIS* K TRANSPORTER 1
ATP	adenosine triphosphate
ATS	*Arabidopsis* salts media
BAM	BARELY ANY MERISTEM
BG	(1,3)-β-glucanase
BIN2	BR INSENSITIVE 2
BR	brassinosteroids
BRL3OE	BR INSENSITIVE 1 LIKE 3
CALS	CALLSOE SYNTHASE
CC	companion cells
CDTA	2-diaminocyclohexane tetraacetic acid
CEP	C-TERMINALLY ENCODED PEPTIDE
CEPD	CEP DOWNSTREAM
CEPH	CEPD-induced phosphatase
CFDA	5-Carboxyfluorescein diacetate
CLE	CLAVATA3/ESR-RELATED
CLV	CLAVATA
CNX2	CALNEXIN2
CRK	CYSTEINE-RICH RLK
DE	Differential expression
dpg	days post germination

dpt	days post transfer
DT	desmotubule
ELISA	enzyme-linked immunosorbent assay
EPF	EPIDERMAL PATTERNING FACTORs
ER	endoplasmic reticulum
EXPA	EXPANSIN
FITC	fluorescein isothiocyanate
FRAP	fluorescence recovery after photobleaching
GAT	GFP ARRESTED TRAFFICKING
GDPD	GLYCEROPHOSPHODIESTER PHOSPHODIESTERASE
GFP	GREEN FLUORESCENT PROTEIN
GL2	GLABRA2
GO	gene ontology
GPD	glycerophosphoryl diesters
GPI	glycosylphosphatidylinositol anchor
GSL	glucan synthase-like
HAK5	HIGH AFFINITY K TRANSPORTER 5
HG	homogalacturonans
IMK2	INFLORESCENCE MERISTEM KINASE 2
InsP8	inositol Pyrophosphate
ISE	INCREASED SIZE EXCLUSION
JIM	John Innes Monoclonal antibody
KN1/STM	KNOTTED 1/SHOOTMERISTEMLESS
KO	knock out mutant
LM	Leeds Monoclonal antibody
LST8	LETHAL WITH SEC THIRTEEN 8

MCTP	MULTIPLE C2 DOMAIN AND TRANSMEMBRANE REGION PROTEIN
MS	Murashige and Skoog media
NCAP	non-cell autonomous proteins
NHEJ	non homologous end joining
OE	over expressor
ONPS	organelle-nucleus-plasmodesmata signalling
PBS	phosphate buffered saline
PD	plasmodesmata
PDBG	PD-localised BG
PDCB	PD-LOCALISED BINDING PROTEIN
PDLP	PD-LOCALISED PROTEIN
PEF	PD-enriched fraction
PEG	polyethylene glycol
PHR	PHOSPHATE STARVATION RESPONSE 1
Pi	inorganic phosphate
PI	propidium iodine
PIP1	Plasmodesmata *in silico* Proteome 1
PLS-DA	partial least squares discriminant analysis
PM	plasma membrane
PME	PECTIN METHYL ESTERASE
PMEIs	PME INHIBITOR
PPT	phosphinothricin
QC	quiescent centre
QSK1	QIAN SHOU KINASE 1
RAM	root apical meristem
RAP2.11	RELATED TO AP2 11

RBOHD	RESPIRATORY BURST OXIDASE HOMOLOG D
RG	rhamnogalacturonan
RLK	receptor-like kinases
ROS	reactive oxygen species
RSA	root system architecture
SCR	SCARECROW
SE	sieve element
SEL	size exclusion limit
SHR	SHORTROOT
SHV3	SHAVEN 3
SLV1	SHV3 LIKE 1
SNRK2.2	SNF1-RELATED PROTEIN KINASE
SP	signal peptide
SPCH	SPEECHLESS
SUC2	SUCROSE TRANSPORTER 2
SUNN	SUPER NUMERIC NODULE RECEPTOR
SYT	SYNAPTOTAGMINS
TET	TETRASPANNINS
TF	transcription factor
TM	transmembrane domain
TMO7	TARGET OF MONOPTEROS 7
TMV	tobacco mosaic virus
TOR	TARGET OF RAPAMYCIN
WOX5	WUSCHEL RELATED HOMEOBOX 5
WT	wildtype
XTH	XYLOGLUCAN ENDO-TRANSGLYCOSYLASE/HYDROLASE

Chapter 1 Introduction

1.1 Preamble

As the human population grows and economies develop, demands for food are increasing in the face of ever scarcer fresh water, mineral fertilisers and fuel resources (Mbow et al., 2019). In a tragic irony, the use of these resources for agriculture is generating environmental damage that is further harming our ability to produce food (Godfray et al., 2010). Every avenue to make better use of these resources whilst generating more food needs to be explored including modifications in the below ground physiology of plants to improve resource use efficiency.

Plants are sessile organisms, and it is essential that plants can modulate their growth to respond to their nutritional and water requirements. This requires plants to detect the availability of each resource, integrate this information and elicit responses to maintain nutrient requirements. Modern crop production relies heavily on fertiliser application, particularly of the macronutrients fixed nitrogen (N), inorganic phosphate (Pi) and potassium (K) (Heffer and Prud'homme, 2016; Mbow et al., 2019). P and N are crucial elements for all life as it is a constituent of many biomolecules, including nucleic acids, lipids, chlorophyll, proteins and adenosine triphosphate (ATP) (López-Arredondo et al., 2013). Plants also require K for protein synthesis, osmoregulation, turgor driven growth and many core metabolic processes (Alemán et al., 2011). In 2017, global fertiliser production of N was over 100 million tonnes, over 40 million tonnes for Pi and 35 million tonnes for K and demands for fertiliser are only set to increase over the coming decades (FAOSTAT, 2021). These agricultural inputs are dwarfed by the quantity of freshwater withdrawn from water sources for agriculture which stood at 3 trillion tonnes in 2014 (AQUASTAT, 2021). Up to 25% of global cropland at any one time can be subject to water scarcity (Rosa et al., 2020). Around 40% of crop production is supported by irrigation and in areas such as the Arabian Peninsula, North Africa and India, ground water is being 'mined' at a rate that exceeds the rate of natural replenishment (D'Odorico et al., 2018). Climate change is increasing the occurrence of droughts (Harvey et al., 2014) influencing soil salinity and osmolarity (Singh, 2021). Unlike mineral nutrients, water availability can fluctuate wildly thus crops may experience both flooding and drought in the same season (Iijima et al., 2016). The environmental costs and risks to food security that stem from our reliance on these resources are severe and even small improvements in nutrient- and water- use efficiency could cut down demands for fertiliser and water (Spiertz, 2009;

Parris, 2010). One path towards this goal is to improve our understanding how plants acquire and respond to nutrient availability and water stress (Sharma et al., 2015).

Improving plant roots' ability to take up water and nutrients has many facets. On the macroscopic scale, improving plant root system architecture (RSA), the spatial and temporal distribution of roots in the soil substrate, would allow roots to intercept resources more effectively in the heterogeneous soil environment (Lombardi et al., 2021). Specific RSA traits such as deeper primary roots are associated with better nutrient and water uptake and higher yields (Uga et al., 2013; El Hassouni et al., 2018; Ye et al., 2018; Stangoulis, 2019) and genetic manipulation of RSA can improve growth traits (Xu et al., 1995; Koevoets et al., 2016). Plants can adapt their RSA via alterations in root development in response to changes in internal and external conditions. In order to achieve this, plants must balance system requirements for specific or multiple resources with information about the local availability of those resources in different parts of the root system (Zhang and Forde, 1998). This level of coordination across the whole plant requires systemic signalling. Certain aspects of these signalling pathways have received more attention than others. For example, a great deal has been reported about the role that the plant hormone auxin plays in regulating root morphology (Lewis et al., 2013; Roychoudhry et al., 2017; Hu et al., 2021). A much smaller body of work exists that tie changes in cell-to-cell transport via the symplasm (intercellular cytoplasmic bridges formed by membranous pores named plasmodesmata) to changes in root morphology (Li et al., 2021). Plasmodesmata (PD) are embedded in the primary cell wall of plants (Amsbury et al., 2018) and regulate cell-to-cell communication and signalling responses to internal and external cues. Despite their critical role, our understanding of PD composition and function remains limited.

The focus of this thesis is to develop our understanding of the role of symplasmic transport in the regulation of root development in response to macronutrients (with a focus on N, Pi and K) and water availability in the model plant *Arabidopsis thaliana*. In the Introduction, *Arabidopsis* root architecture and the signalling pathways involved in root development are described. The root responses to changes in nitrate, phosphate, potassium as the major plant nutrients and to water availability are also introduced. Particular attention is paid to the potential role that symplasmic transport plays in these responses. Finally, the aims and objectives for this thesis are listed.

1.2 *Arabidopsis* as a model system for root development

A. thaliana (*Arabidopsis*) emerged as a model organism about 35 years ago (Koornneef and Meinke, 2010). Arguably, the most important factor that makes *Arabidopsis* one of the most valuable model species for root development is the vast number of techniques, tools and resources that have been developed for this species; far more than could be discussed here. A PubMed literature search of *Arabidopsis* identifies nearly 80,000 papers which is far more than any other plant species. This rich and diverse collection of published materials is the most valuable resource as it represents the collective understanding of *Arabidopsis* biology and is the framework to build and test new hypotheses against. It is in this manner that function, development and structure of *Arabidopsis* roots will be briefly introduced here as it is integral to understand the phenotypes observed in this work.

As for all plant species, the function of *Arabidopsis* roots is multifaceted. Roots provide anchorage to the substrate and are used to find, acquire and, in some cases, store resources (Kellermeier et al., 2014; Zierer et al., 2021). The function of roots is enabled by a body plan that is laid down during embryogenesis and continually adapted post-embryonically (Park and Harada, 2008). The body plan can be considered along two axes: the apical-basal axis and the radial axis. The apical-basal axis is apparent after the asymmetric first division of the zygote which generates a terminal and basal cell. The terminal cell develops into the hypocotyl and the shoot whilst the basal cell gives rise to the radicle (Mansfield and Briarty, 1991). First, the basal cell develops into the suspensor which is composed of approximately 7 cells (Figure 1.1, Palovaara et al., 2016; Verna et al., 2019). The uppermost suspensor cell forms the hypophysis and the other suspensor cells provide auxiliary roles in support, nutrient delivery and ensuring correct patterning of the meristem (Du and Scheres, 2018; Downs and Jones, 2020). The hypophysis divides asymmetrically to form a lens-shaped cell that is the progenitor of the quiescent centre (QC) and a larger basal cell that will form the distal meristem cells (Colette et al., 2015). All root cells are derived from stereotypic divisions of meristematic cells which are laid down in concentric layers of tissue forming the radial axis of the root. Starting from the centre, in the differentiation zone, these tissue layers are the phloem, procambium and xylem (forming the vascular cylinder), the pericycle, the endodermis, the cortex and the epidermis (Figure 1.1 B,C). All tissues converge at the QC which is mitotically inactive and forms the organising centre (Van den Berg et al., 1995). The QC is maintained in an undifferentiated state by initial cells which surround it. The initial cells are the progenitors of the tissues and there are 4

types: a type that forms the columella, a type that forms the vasculature, a type that forms the lateral root cap (a tissue that surround the epidermis in the meristem region) and the epidermis and a type that forms the ground tissues (i.e. endodermis and cortex) (Augstein and Carlsbecker, 2018).

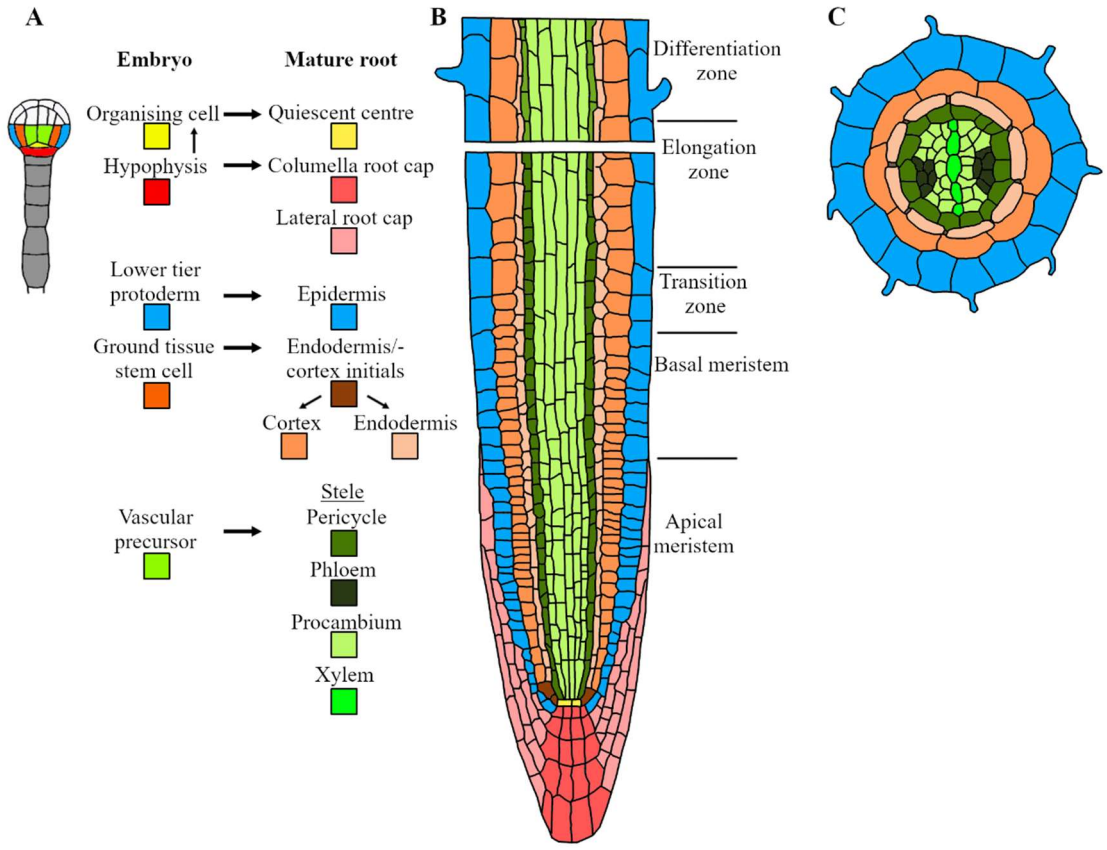

Figure 1.1 Root tissue development and organisation in *Arabidopsis*. (A) Longitudinal section of an early-globular stage embryo. Cells filled in grey form part of the suspensor. The identity of cells and root tissues is mentioned in the figure and are referenced by colour in the key. Arrows indicate cell identity progression from progenitor cells in the embryo to mature root tissues. (B) Longitudinal section of mature root displaying developmental zones and tissue organisation. (C) Cross section of mature root taken across the differentiation zones displaying tissue organisation. In addition to the key which identifies tissues, the spaces in-between endodermal cells represent the suberised cell wall of the Casparian strip. This figure was adapted from (De Smet, 2012).

Divisions of the initials, and to greater extent, their daughter cells lead to files of differentiated cells that form the tissues. The root tip region can be divided into two sections: the apical meristem where most of the cell division takes place and the basal

meristem where division slows down. After the basal meristem, cells start to elongate forming the elongation zone. The region when cell division stops, and elongation starts is called the transition zone. Once cells have acquired their final length and shape, they leave the elongation zone, and form the differentiation zone which is considered mature root (Figure 1.1 B).

Each mature tissue serves a different purpose. Almost all vascular plant roots are tipped with a root cap (Augstein and Carlsbecker, 2018). In *A. thaliana*, the root cap is divided into the columella root cap and the lateral root cap. The root cap provides protection of the delicate meristem cells and plays a role in detecting and propagating environmental signals. Columella cells are large cells that sit at the very tip of the root and contain starch filled plastids called statoliths that facilitate the sensing of gravity (Konstantinova et al., 2021). Lateral root cap cells are located to the side of columella cells that continue distally enveloping most of the apical root meristem. The root epidermis is a 1-cell thick outermost layer that serves as the interface between the root and the environment and consists of cells of two identities: root hair cells (trichoblasts) and non-hair cells (atrichoblasts) (Dolan et al., 1993). Root hair cells start to emerge in the differentiation zone and their function is to increase the surface area available for nutrient and water acquisition. *Arabidopsis* and other Brassicaceae have 'type 3' epidermal patterning where the cortex plays an important role in specifying trichoblasts and atrichoblasts cells. Under certain conditions, the number of cortex files increase and, concomitantly, root hair density also increases (Zhang et al., 2003; Janes et al., 2018).

The cortex adjoins the endodermis which in *Arabidopsis* is one cell thick (Grebe, 2011). The endodermal cell wall in mature roots is rich in suberins (an impermeable substance) forming what is known as the Casparian strip. The Casparian strip impedes the diffusion of ions which effectively separates the apoplastic regions of the cortex from the pericycle and the vasculature. The pericycle surrounds the vasculature and can be divided into the xylem pole and phloem pole cells with marked differences in size and gene expression (Parizot et al., 2008). Functions of the pericycle include xylem loading and is the site of lateral root formation in angiosperms. Different species display a stereotyped arrangement of vascular tissue and *Arabidopsis* has a diarch arrangement with two strands of phloem and two strands of xylem interspaced with parenchyma cells (Figure 1.1 C) (Parizot et al., 2008). The vasculature is involved in the long distance transport of substances connecting root and shoots and other organs in the plant body.

One fascinating aspect of plants is that, unlike animals, their body plan is not set exclusively at the embryonic stage. Roots display a remarkable degree of post-embryonic plasticity (Lombardi et al., 2021). The ability of the root system to fulfil the plants requirements for resource acquisition and anchorage is determined by the RSA. RSA is controlled in a multitude of ways including regulation of the rate of root growth, root branch patterning and orientation of root growth (Khan et al., 2016). *A. thaliana* forms two predominant root types: the primary and lateral roots. The primary root develops from the embryonic root whereas lateral root development initiates post-embryonically in response to environmental and developmental cues (Bhalerao et al., 2002; Dubrovsky et al., 2008). To form lateral roots, new root meristems develop in mature roots from xylem-pole pericycle cells (Du and Scheres, 2018). First, lateral root founder cells are specified from competent xylem-pole pericycle cells. These founder cells divide to form the lateral root primordium (Malamy and Benfey, 1997). As the lateral root primordium develops, coordination between the nascent lateral root and the overlying tissue is required to allow for lateral root emergence. Lateral roots emerge with a tissue organisation that resembles the embryonic root meristem. In most plants, adventitious roots also emerge from non-root tissues in a related, but distinct way, to lateral roots (Verstraeten et al., 2014). The orientation of roots is controlled post embryonically. Directed root growth enables the plant to respond to environmental conditions that can, for example, improve the effectiveness of resource scavenging (Roychoudhry et al., 2017; Izzo and Aronne, 2021; Konstantinova et al., 2021). A major influence on root orientation is the angle they are maintained relative to gravity; named the gravitropic setpoint angle. Much work on root gravitropic setpoint angle has focused on lateral roots as they naturally grow away from the parent root in a non-vertical direction. The gravitropic setpoint angle is regulated by internal and external cues including hormone signalling (Roychoudhry et al., 2017).

1.3 Signalling pathways controlling root development and responses to water and nutrients

Signalling molecules play a critical role in coordinating development and responses to the environment. Many of the smaller signalling molecules are classed as phytohormones. At least 10 classes of phytohormone have been discovered including auxins, cytokinins, salicylic acid, abscisic acid (ABA), brassinosteroids (BR) and gibberellins with many links to responses to environmental cues (Signora et al., 2001; Kieffer et al., 2010; Tylewicz et al., 2018; Gupta et al., 2020; Zhao et al., 2021). Mobile proteins and RNAs are also

important signalling factors in the local and the systemic response to biotic and abiotic stresses (Table 1-1). The focus of the following sections is a brief overview of the known signalling pathways involved in the sensing of nutrient availability (with a focus on N, Pi and K) and their effect on root system architecture.

Table 1-1 Mobile macromolecules with a role in signalling. Key for references: 1- Zhang et al., 2018; 2-Buhtz et al., 2010; 3-Jones-Rhoades and Bartel, 2004; 4-Vatén et al., 2011; 5-Tabata et al., 2014; 6-Ohkubo et al., 2017a; 7-Takahashi et al., 2018; 8-Chen et al., 2016; 9-Chen et al., 2008; 10-Ye et al., 2016; 11- Ye et al., 2017; 12-Koizumi and Gallagher, 2013; 13-Pi et al., 2015; 14- Lu et al., 2018.

Mobile factor	Stress	Plant species	Reference
<u>mRNA</u>			
PS	Pathogen	Tomato	1
miRNA			
mi399	Phosphate deprivation	*Arabidopsis*	2
miR395	Sulphur deprivation	*Arabidopsis*	3
mirR165/6	Negative regulator of SHR		4
<u>Peptides</u>			
C-TERMINALLY ENCODED PEPTIDE (CEP)	Nitrate deprivation (7 CEPs)	*Arabidopsis*	5
CEP DOWNSTREAM1, 2	Nitrate deprivation	*Arabidopsis*	6
CLAVATA3/EMBRYO-SURROUNDING REGION-RELATED 25	Water availability	*Arabidopsis*	7
<u>Proteins</u>			
ELONGATED HYPOCOTYL 5 (HY5)	Nitrate deprivation/ Light	*Arabidopsis*	8
ACYL-COA-BINDING PROTEIN 6	Cold exposure	*Arabidopsis*	9-11
SHORTROOT (SHR)	TF involved in cellular patterning, movement regulated by PD	*Arabidopsis*	4, 12
WUSCHEL RELATED HOMEOBOX 5 (WOX5)	TF involved in cellular patterning, movement regulated by PD	*Arabidopsis*	13
TM07	TF involved in cellular patterning, movement regulated by PD	*Arabidopsis*	14

1.3.1 Nitrate scarcity: Signalling pathways regulating root system architecture responses

The predominant forms of inorganic N that plants can utilise are nitrate and ammonium. Nitrate is normally present at higher concentrations in agricultural settings and is the predominant form of N used by plants (Ho and Tsay, 2010). Plants modulate RSA in response to nitrate availability in the soil. For example, severe N starvation inhibits primary and lateral root growth (Araya et al., 2014) but milder N deprivation induces root branching to facilitate N acquisition (Gruber et al., 2013). RSA has been modelled to have a profound influence on the ability of roots to intercept nitrate (Dunbabin et al., 2004). Nitrate uptake from the soil is performed by at least 4 different protein families including NITRATE TRANSPORTER (NRT) and nitrate TRANSPORTER 1/PEPTIDE TRANSPORTER FAMILY (NPF) which are high and low affinity nitrate– transporters families, respectively (O'Brien et al., 2016). One member of the latter, NRT 1.1 (also known as NPF6.3) functions not only as a high and low affinity transporter but also as a key part of the nitrate sensing apparatus that integrates nitrate signalling with auxin signalling as NRT 1.1 also transports auxin in low nitrate conditions (Ho et al., 2009).

NRT 1.1 regulates a suite of responses to low nitrate including modulation of RSA (Swarup et al., 2008; Krouk et al., 2010; Porco et al., 2016; Maghiaoui et al., 2020). Under low nitrate conditions, NRT1.1 facilitates the basipetal movement of auxin away from lateral root primordia and inhibits their emergence (Krouk et al., 2010). NRT1.1 controls auxin distribution further by inhibiting expression of the auxin influx carrier *LIKE AUXIN1 3* (*LAX3*), involved in auxin-dependent cell wall loosening required for lateral root emergence (Figure 1.2). NRT1.1 also regulates *TRYPTOPHAN AMINOTRANSFERASE RELATED 2* (*TAR2*) which in turns regulates auxin biosynthesis in the root stele (Swarup et al., 2008; Porco et al., 2016; Maghiaoui et al., 2020). At higher N concentrations, NRT1.1 no longer transports auxin and therefore no longer inhibits lateral root proliferation (Sun and Zheng, 2015). Another regulatory mechanism regulating lateral root patterning under low nitrate conditions is the CLE (CLAVATA3/ESR-related)-CLAVATA1 (CLV1) regulatory modules. CLE peptides bind the receptor like kinase (RLK) CLV1 and control cellular differentiation in shoot and root meristems (Strabala et al., 2006; Araya et al., 2014). Under low nitrate, CLE3,4,7 are upregulated in the pericycle (Araya et al., 2014). Over expression of CLE3 was shown to supress lateral root emergence but not in the *clv1* background suggesting that that CLE3-CLV1 form a regulatory module regulating lateral

root proliferation under low nitrate. CLV1 is known to localise at PD which raises the possibility that PD play a role in this response (Stahl et al., 2013). Root orientation also appears to be regulated by nitrate availability. Under nitrate starvation, lateral root gravitropic setpoint angle was maintained at a more horizontal angle (Roychoudhry et al., 2017). This behaviour may be a strategy to intercept nitrate from surface soil layers as it is carried to lower soil layers by water. Gravitropic setpoint angle modulation by low nitrate may be controlled by the *miR393*/*AUXIN SIGNALLING F-BOX 3* (*AFB3*) regulatory module, which also plays a role in regulating lateral and primary root growth in response to nitrate availability (Vidal et al., 2010). Other classes of RNA may also have a role in regulating responses to low nitrate. mRNAs have been found to be mobile under N stress and miRNAs induced by low N have been found in the phloem sap (Thieme et al., 2015). Sugar signalling also has links with the regulation of nitrate responses. For example, in high nitrate conditions, high sugar status stimulates leaf development and photosynthesis but under low nitrate, high sucrose has an inhibitory effect of genes involved in photosynthesis (Martin et al., 2002; Cho et al., 2010). Overexpressing the major sugar signalling kinase *TARGET OF RAPAMYCIN* (*TOR*) leads to an insensitivity to high nitrate and inhibition of root proliferation (Deprost et al., 2007).

Split root experiments, demonstrate that plants are coordinating responses to both local and systemic N status (Figure 1.3) (Zhang and Forde, 2000). Lateral roots under N stress produce a family of peptides derived from proteolysis, known as C-terminally Encoded Peptides (CEPs) which are transported to the shoot through the apoplast (Taleski et al., 2018). These 'hunger' signals are then perceived by CEP-receptors in the leaves. This induces the production of class III glutaredoxin family polypeptides CEPD1 and CEPD2 which are transported to the root via the phloem (Ohkubo et al., 2017). CEPD1/2 regulates CEPD-induced phosphatase (CEPH) which in turn dephosphorylates NRT2.1, a factor that facilitates nitrate uptake (Ohkubo et al., 2021). In nitrate rich areas of the substrate, NRT1.1 induces the expression of factors such as MADS-box transcription factor *ARABIDOPSIS NITRATE REGULATED 1* (*ANR1*) which stimulates lateral root growth (Remans et al., 2006). This lateral root growth is absent in *auxin resistant 4* (*axr4*) suggesting a role for AXR4 in this response (Zhang et al., 1999).

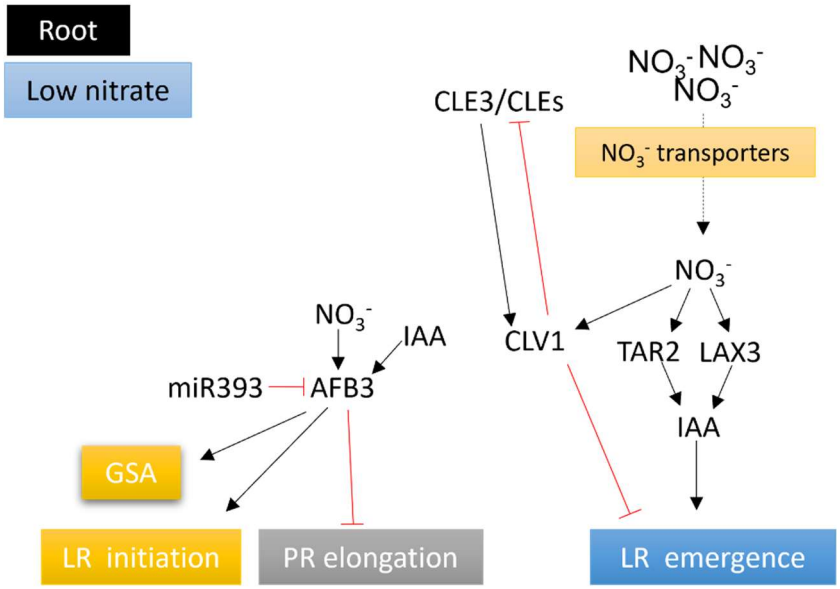

Figure 1.2 Signalling pathways regulating root system architecture in response to low nitrate. The tip of lines with arrows and blunt ends indicates induction or suppression of signalling steps, respectively. Under low nitrate, nitrate transporters such as NITRATE TRANSPORTER 1.1 regulate nitrate responsive genes such as *TRYPTOPHAN AMINOTRANSFERASE RELATED 2* (*TAR2*) and *LIKE AUXIN1 3* (*LAX3*) which in turn regulate lateral root emergence. Under nitrate limiting conditions, CLE3 (CLAVATA3/ESR-related) is detected by CLAVATA1 (CLV1) to induce lateral root development. Primary root length and gravitropic setpoint angle (GSA) may also regulated under low nitrate by the *miR393*/*AUXIN SIGNALLING F-BOX 3* (*AFB3*) complex.

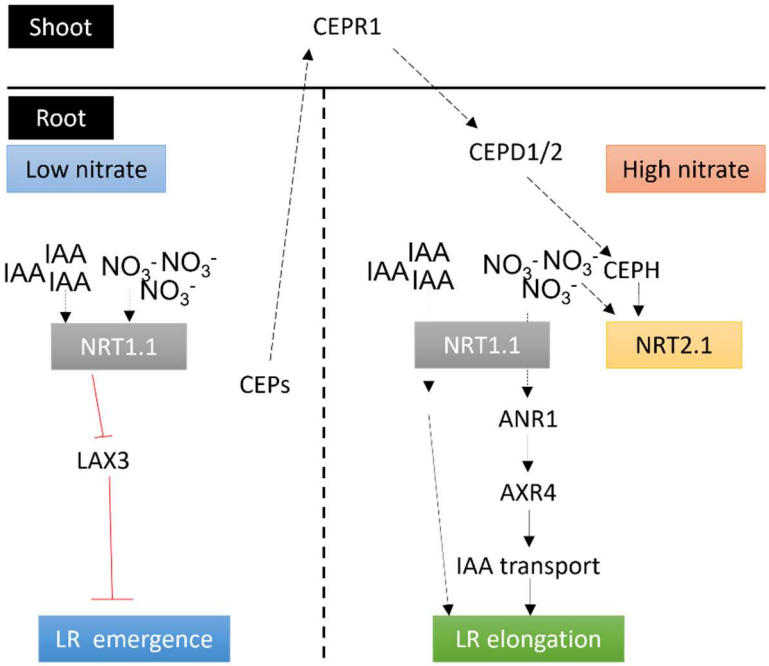

Figure 1.3 Signalling pathways controlling responses to heterogeneity in nitrate-availability. The left and right regions separated by the bold dotted line represent areas of the root with locally low and high nitrate concentrations, respectively. Other dotted lines show movement/transport or signals. The tip of lines with arrows and blunt ends indicates induction or suppression of signalling steps, respectively. Under low nitrate conditions, NITRATE TRANSPORTER 1.1 (NRT1.1) represses expression of *LIKE AUXIN1 3* (*LAX3*). LAX3 is involved in lateral root emergence responses. C-terminally Encoded Peptides (CEPs) move to the shoot where they are perceived by CEP RECEPTOR 1 (CEPR1). This induces the expression of CEP DOWNSTREAM (CEPD) peptides which are transported to the root and regulate NRT2.1 nitrate uptake via CEPD-induced phosphatase (CEPH). In areas of high nitrate availalbity NRT1.1 regulates lateral root development via induction of *ARABIDOPSIS NITRATE REGULATED 1* (*ANR1*) that may involve the activity of AUXIN RESISTANT 4 (AXR4).

1.3.2 Phosphate scarcity: Signalling pathways regulating root system architecture responses

Plants predominantly acquire P in an inorganic form (Pi) (Wang et al., 2004). In 60% of agriculture settings around the world, low Pi is a major limitation to crop yields (Cordell et al., 2009). Even when there is sufficient Pi in the soils, it is often recalcitrant and inaccessible to plants. Free Pi in soil is readily fixed, either precipitating with cations such as Fe or Al, or by becoming closely associated with soil colloids (Schachtman et al., 1998;

Pound et al., 2016). Additionally, free Pi can also form complexes with organic molecules and these forces conspire to make the availability of Pi in the soil one of the lowest of any nutrient (Kobayashi et al., 2007). Consequently, plants rely extensively on 'root interception' where roots must grow in close proximity in order to liberate and acquire Pi. Indeed, 20% of Pi uptake is at the point of interception, the root cap (Kanno et al., 2016). To accomplish efficient Pi interception, plants must first sense where Pi is and respond appropriately to exploit the Pi supply (Tilsner et al., 2016). To sense phosphate levels, plants monitor inositol pyrophosphate (InsP8) levels, which are affected by intracellular Pi (Qi et al., 2017). InsP8 directly binds to SYG1/Pho81/XPR1 DOMAIN-CONTAINING PROTEIN 1 (SPX1) (Figure 1.4) (Dong et al., 2019). Under Pi-replete conditions, SPX1 interacts with PHOSPHATE STARVATION RESPONSE 1 (PHR1), the central regulator of Pi starvation responses, to inhibit its function (Puga et al., 2014; Qi et al., 2017). Up to 2,000 genes may be regulated by PHR1 under Pi depleted conditions (Castrillo et al., 2017). PHR-independent signalling has also been described in low Pi responses (Azevedo and Saiardi, 2017; Puga et al., 2017; Ham et al., 2018) highlighting the complex nature of Pi signalling. Sugar-, phytohormone- and other macronutrients are all known to play a role in low Pi signalling pathways (Smith and Jackson, 1987; Farquharson, 2008; Rouached et al., 2011). Long distance signalling between the shoot and root regulates Pi responses. Grafting experiments showed that the miRNA miR399 is a phloem mobile signal that accumulates in roots under Pi deficiency in a PHR1-dependent fashion (Buhtz et al., 2010). miR399 promotes low phosphate responses by causing degradation of ubiquitin E2 conjugase PHOSPHATE 2 (PHO2) transcripts. PHO2 is a negative regulator of phosphate responses by causing degradation of PHR1.

One significant low phospate response is seen in RSA. Of the 73 *Arabidopsis* ecotypes assayed in one study, 50 % displayed reductions in primary and lateral root growth in response to low Pi (Chevalier et al., 2003). Several studies have shown that low phosphate has a negative impact on primary root growth in the widely studied ecotype Col-0 (Nacry et al., 2005; Svistoonoff et al., 2007; Ticconi et al., 2009). Reduction in primary root growth in response to low phosphate is due to meristem exhaustion and dependent on Fe (Sánchez-Calderón et al., 2005). Low Pi leads to callose deposition in the root tip in a Fe-dependent fashion leading to restriction in the movement of the cell fate determining factor SHORTROOT (SHR) (Müller et al., 2015). This mechanism restricts root meristem growth and is mediated by the ferroxidase LOW PHOSPHATE ROOT 1 (LPR1) and the P5-type ATPase PHOSPHATE DEFICIENCY RESPONSE 2 (PDR2), which induces callose

deposition possibly via redox signalling (Müller et al., 2015). In contrast to primary root growth, there is no consensus in the literature on the effect of low Pi availability on lateral root growth with some reporting increased proliferation or growth (Al-Ghazi et al., 2003#; Chen et al., 2016) and other reporting inhibition (Jain et al., 2007; Gruber et al., 2013). Exogenous sucrose, the use of agar with high levels of phosphate and also the amount of light can affect the extend of low-Pi root growth inhibition, which could account for these contradictory findings (Liu, 2021).

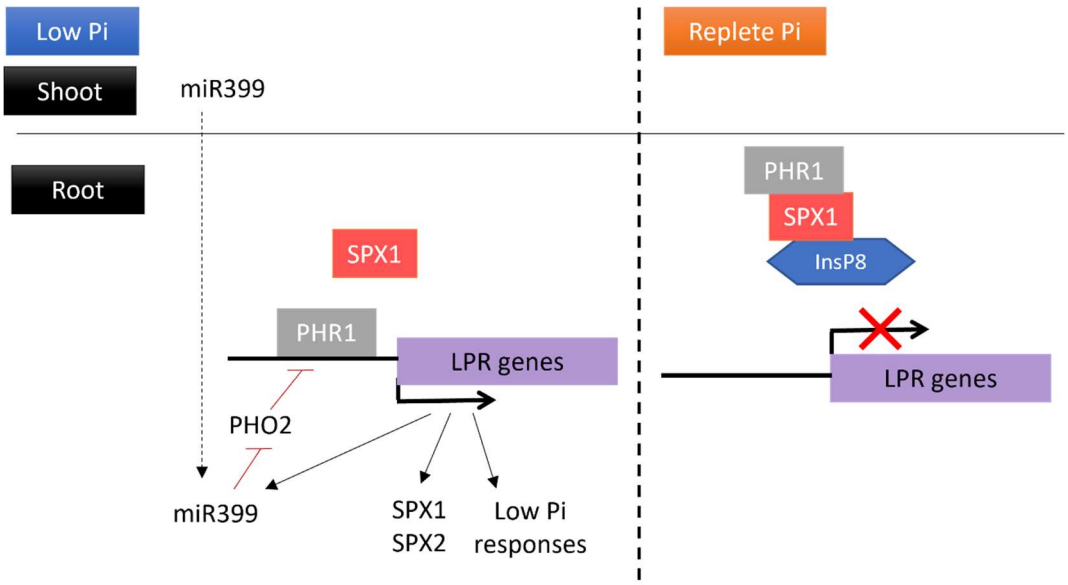

Figure 1.4 PHR1 is a master regulator of low phosphate response (LPR) genes. The transcription factor PHOSPHATE STARVATION RESPONSE 1 (PHR1) binds the promotor region of LPR genes which increases their expression. Low phosphate conditions promote the expression of miR399 which is transported from the shoot to the root which it represses PHOSPHATE 2 (PHO2); a negative regulator of PHR1. In the presence of high levels of inositol pyrophosphate (InsP8), YG1/Pho81/XPR1 DOMAIN-CONTAINING PROTEIN 1 (SPX1) binds PHR1 which represses expression of LPR genes.

RSA can have a major influence on phosphate acquisition. For example, a quantitative trait locus for root angle strongly co-segregated with yield under low Pi (Lynch and Brown, 2001; Liao et al., 2004). In beans, low phosphate was shown to lead to a more horizontal gravitropic setpoint angle leading to a shallower root system hypothesised to improve subsurface phosphate scavenging (Bonser et al., 1996; Liao et al., 2001). In *Arabidopsis*, lateral roots maintain a more vertical gravitropic setpoint angle in low Pi conditions, which is abolished in the double mutant between *transport inhibitor response 1* (*tir1*) (an auxin receptor mutant) and *afb3* (*tir1afb3*), supporting the role of auxin in the regulation of this

gravitropic setpoint angle response (Roychoudhry et al., 2017). Auxin also plays a role in the regulation of root hairs in response to Pi. Root hairs proliferate in areas of the soil rich in phosphate (Janes et al., 2018). Mutants in the auxin transporter *auxin1* display stunted root hairs in low Pi conditions, which negatively affects its ability to acquire Pi (Bhosale et al., 2018). Expression of AUXIN1 in the lateral root cap rescued the root hair phenotype, demonstrating that auxin signalling and transport, is important for root hair response to low Pi.

1.3.3 Potassium scarcity: Signalling pathways regulating root system architecture responses

Between 2-10% of the dry weight of plants is K^+, making it the most abundant cation (Leigh and Wyn Jones, 1984). A small deficiency in K can cause chlorosis and reductions in growth, whilst large deficiencies can lead to meristem death and eventually the death of the plant (Thomas et al., 2008). The regulation of K is closely related to that of Na and, in physiological conditions, plants tend to maintain a low Na^+ /K^+ ratio. High salinity not only inhibits growth due to osmotic stress, but also due to toxic concentrations of Na^+ that, at least in part, disturb K uptake (Horie et al., 2009; Ali et al., 2021).

Little is known about the processes regulating K supply relative to other macronutrients. It is currently unknown how plants detect low K levels, but detection in the root is mainly within a small group of post meristematic cells in the transition zone, leading to reactive oxygen species (ROS) -dependent transduction of downstream responses (Figure 1.5) (Wang et al., 2021a). Plants respond to low K in several ways including the induction of *HIGH AFFINITY K TRANSPORTER 5* (*HAK5*) to improve uptake from the soil (Gierth et al., 2005; Wang et al., 2021a) and changes in RSA. *HAK5* up regulation under low K is promoted by the transcription factor RELATED TO AP2 11 (RAP2.11) and ROS. The transcription factor AUXIN RESPONSE FACTOR 2 (ARF2) represses *HAK5* expression by binding the gene's promotor which explains why *arf2* displays an increased tolerance to low K conditions (Zhao et al., 2016). HAK5 and other K transporters including *ARABIDOPSIS* K TRANSPORTER 1 (AKT1) are post-translationally regulated by the CALCINEURIN B-LIKE PROTEINS (CBL) - CBL-INTERACTING PROTEIN KINASE 23 (CIPK23) complex (Wang et al., 2021b). CBL1 (and CBL9 in the case of AKT1 regulation) activates CIPK23 which in turn phosphorylates AKT1 and HAK5 which increases the rate of K+ uptake (Xu et al., 2006; Ragel et al., 2019). HAK activity is further promoted by

phosphorylation by INTEGRIN-LINKED KINASE 1 in conjunction with CALMODULIN-LIKE 9 (Brauer et al., 2016).

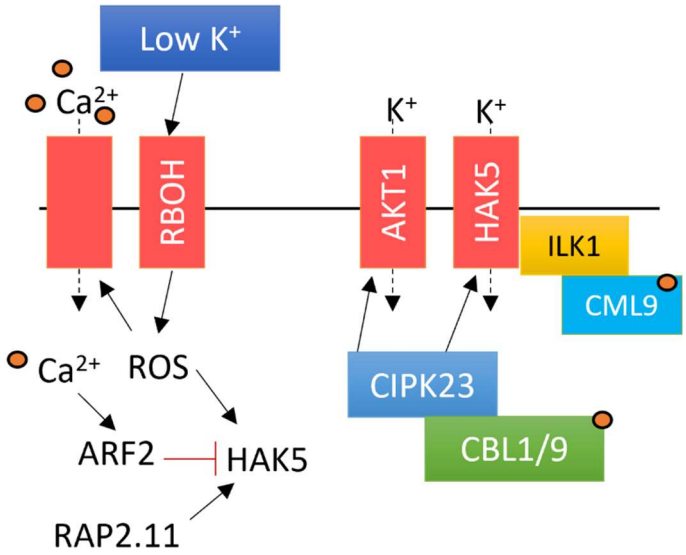

Figure 1.5 Signalling pathway regulating K+ uptake in root cells. Reactive oxygen species (ROS) are generated downstream of low K+ perception which leads to an influx of Ca^{2+} (represented by orange circles). Ca^{2+} regulates expression and post transcriptional regulation of potassium transporters. Transporters involved in K+ import include *ARABIDOPSIS* K TRANSPORTER 1 (AKT1) and HIGH AFFINITY K TRANSPORTER 5 (HAK5) which are positively regulated by the CALCINEURIN B-LIKE PROTEINS (CBL) - CBL-INTERACTING PROTEIN KINASE 23 (CIPK23) complex.

K^+ is highly mobile and heterogeneously distributed in soil, with higher concentrations of K^+ in the higher soil strata (Jobbagy and Jackson, 2001). RSA is modulated to improve K foraging when low, but these responses are not as strong as those described for nitrate or Pi (Drew, 1975; Kellermeier et al., 2013; Kellermeier et al., 2014; Song et al., 2018). RSA responses to low K are difficult to classify as they are diverse between ecotypes and species (Drew, 1975; Rengel and Damon, 2008; Kellermeier et al., 2013) with some strategies more effective than others. Some *Arabidopsis* ecotypes respond to K deficiency by favouring lateral root elongation over primary root elongation, whilst others cease to elongate lateral roots and invest instead in continuing elongation of primary roots (Kellermeier et al., 2013). Interestingly, the primary root of Col-0 is relatively insensitive to changes in K^+ availability which may have hampered efforts to identify the molecular components of such responses (Kellermeier et al., 2013).

Low K shifts lateral root development towards the production of 2nd order lateral roots (new organs developing from 1st order laterals) at the expenses of 1st order laterals concurrent with proliferation in root hairs (Jung et al., 2009; Kellermeier et al., 2014). Auxin signalling seems to be a negative regulator of low K^+ responses. Using the auxin biosensor *ProDR5::GFP*, Li et al. (2017) were able to demonstrate that auxin accumulation in root tips is supressed and protein expression of PIN-FORMED 1 is reduced under low K^+. The knockout *myb77* (targeting the transcription factor MYB DOMAIN PROTEIN 77 which Interacts with ARF7 and regulates the expression of some auxin responsive genes) displays reduction in lateral root numbers in low K conditions, linking changes in lateral root architecture and auxin signalling (Shin et al., 2007). Furthermore, gene expression analysis demonstrated that this transcription factor positively regulates *HAK5* expression (Feng et al., 2021). Expression of *HAK5* has also been found to be regulated by ethylene. *ethylene insensitive 1* (*ein1*) mutant had reduced, but not abolished, expression of *HAK5* pointing to an ethylene- dependent gene regulation pathway for K^+ uptake (Jung et al., 2009). When in K deficient conditions, *ein1* and *ein2* displayed increased chlorosis and reduced growth relative to wildtype and a mutant with constitutive ethylene response (*constitutive triple response 1*). *ein1* and *ein2* also showed reduced root hair length in low K^+ suggesting the proliferation of root hairs under low K^+ may be related with ethylene signalling (Jung et al., 2009).

1.3.4 Water scarcity: Signalling pathways regulating root system architecture responses

To overcome water scarcity, plants can employ responses that fall into 3 broad categories: drought escape, dehydration tolerance and dehydration avoidance (Kooyers, 2015; Blum and Tuberosa, 2018). Drought escape strategies are exemplified by *A. thaliana*'s 'live fast, die young' life strategy to produce seed and complete its life cycle before water resources are limited later in the season (Martignago et al., 2020). Dehydration tolerance strategies aim to facilitate continued physiological activity under osmotic stress. Such strategies include the production of osmoprotectants and antioxidants and are often under the control of gibberellic acid signalling. Dehydration avoidance responses enable a plant to maintain a high relative water content even under water scarcity (Martignago et al., 2020). Dehydration avoidance strategies include ABA-dependent regulation of stomatal conductance and leaf curling to improve water use efficiency (Bertolino et al., 2019).

The modulation of RSA is a key dehydration avoidance strategy that can have a significant impact on a plants ability to acquire water (Roycewicz and Malamy, 2012; Uga et al., 2013; Grison et al., 2019; Hunter et al., 2019). Optimal RSA is dependent on where water resources are in the soil. Deep rooting architectures can tap into longer term water reserves whilst shallow rooting architectures are able to intercept water from infrequent precipitation events before it is lost to lower soil strata (Lynch, 2013). Adopting one style of RSA over another can have a major effect on productivity in water limited conditions such as deeper rooting cultivars of durum wheat (*Triticum durum*) which displayed up to 35% increase in yield relative to shallow rooting cultivars when grown in rain fed environments in the Middle East and North Africa (El Hassouni et al., 2018).

RSA responses in *Arabidopsis* to water stress include a reduction in primary root growth and reduction in lateral root proliferation which are under the control of ABA signalling (van der Weele et al., 2000). For example, when grown in 60 mM mannitol, lateral roots appear many times longer in *aba deficient 2* (*aba2*) and *aba3* seedlings than in wildtype (González-Guzmán et al., 2002; Deak and Malamy, 2005). Plants can sense differential water potentials as demonstrated by hydrotropic responses (Eapen et al., 2005) and can target growth to intercept water in the soil. Laser ablation or manual removal of columella and root meristems does not prevent hydrotropism (Dietrich et al., 2017). This finding demonstrates that this response is distinct from auxin-controlled gravitropic responses for which the root tip is critical. Supporting a role for ABA, the mutant *snf1-related protein kinase* (*snrk2.2)*, a receptor kinase involved in ABA signal transduction displays a much weaker hydrotropic response than wildtype (Dietrich et al., 2017). There is significant crosstalk between ABA and BR signalling. ABA activates the negative regulator of BR signalling, BR INSENSITIVE 2 (BIN2) which in turn activates *SNRK2* genes (Gupta et al., 2020). Another link between BR signalling with hydrotropism is demonstrated by overexpression of the BR receptor BR INSENSITIVE 1 - LIKE 3 (BRL3OE) which leads to increased hydrotropic response, increased levels of osmoprotectants and improved growth under drought (Fàbregas et al., 2018). Intriguingly, improved drought tolerance of BRL3OE was not at the cost of growth as normally observed with increased drought tolerance phenotypes (Shao et al., 2008; Fàbregas et al., 2018).

As for Pi and N, responses to water scarcity are regulated systemically. Under drought conditions, roots produce CLE25 peptide which is transported to the shoot via the vasculature (Figure 1.6) (Takahashi et al., 2018)). CLE25 was discovered by applying CLE peptides to roots and measuring the expression of the *NINE-CIS-EPOXYCAROTENOID*

DIOXYGENASE 3 (*NCED3*); a key gene involved in the synthesis of ABA and the shoot response to dehydration stress. BARELY ANY MERISTEM (BAM) 1 and BAM3 function as the receptors of CLE25 in leaves, triggering the upregulation of *NCED3* which in turn regulates stomatal aperture via *NCED3* -expression-mediated ABA accumulation. CLE25, along with CLE26 and CLE 27, is expressed during root development where it works downstream of the BREVIS RADIX and OCTOPUS; key regulators of protophloem development (Gou, 2022).

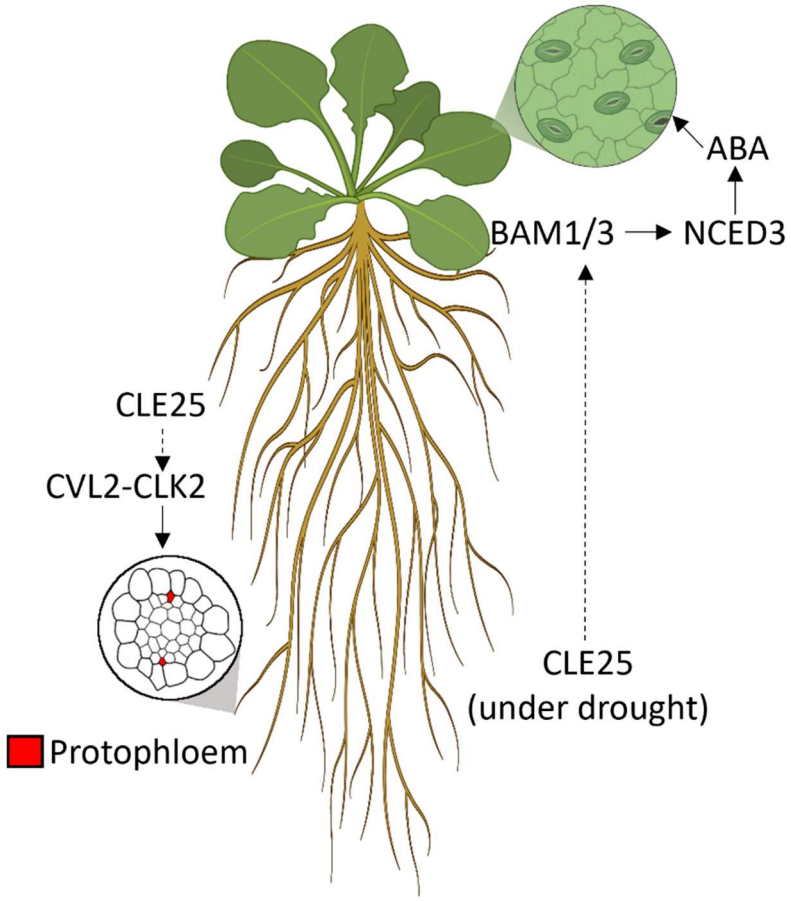

Figure 1.6 CLE25 regulates systemic responses to drought and is also involved in phloem development. Under water scarcity, CLE25 peptides are transported to the shoot where they are detected by BAM1 and BAM3 triggering upregulation of *NCED3*. NECD3 increases ABA production and triggers stomatal closure. In the developing root, CLE25 is detected by a CLV2/CLERK receptor complex that promotes protophloem cell differentiation.

1.4 Introduction to intercellular transport

Without the ability of cell-cell communication, multicellular plants would be amorphous clumps of cells unable to respond effectively to environmental change, predation or pathogen attack. Plants have evolved two major pathways for cell-cell exchange of signals and resources: the apoplastic pathway and the symplasmic pathway (Stahl and Simon, 2013). The apoplastic pathways require molecules to be secreted into the extracellular space (named the apoplast), where they can diffuse within cell walls and be either, actively imported into neighbouring cells or interact with membrane receptors in the cell surface. The apoplastic pathway is the predominant way used to acquire resources from the soil (Sattelmacher, 2001). Nutrients, water and soil borne signals pass into the epidermal apoplastic space and migrate towards deeper tissues or be imported into the cell via specialised transporters. Apoplastic transport employs a vast array of channels and transporter proteins to facilitate passive and active movement of substances including water, mineral ions, hormones and sugars (Ruan et al., 2001; Krouk et al., 2010; Park et al., 2017a; Durand et al., 2018). This includes, for example, aquaporins, which are channel proteins involved in the transfer of water and other small solutes across the membrane (Singh et al., 2020). In mature root tissue, apoplastic movement of substance from the epidermis is blocked at the endodermis by the Casparian strip: a diffusion barrier that effectively separates the apoplast exposed to the environment from the apoplast that connects to the vasculature (Grebe, 2011). To pass this barrier, substances selectively enter the endodermal cell, and move via the symplasm into deeper tissues.

Due to the nature of the extracellular space (and the porosity of cell walls), apoplastic transport is limited to small molecular weight compounds such as water, inorganic nutrients, sugars and hormones. Larger molecular weight compounds such as proteins and RNAs are generally too large to effectively pass through the cell wall matrix of the apoplastic space. Instead, transport of these compounds is predominantly via cytoplasm to cytoplasm connections (the symplasm) formed by PD (Amsbury et al., 2018). PD are pores in the cell wall formed by plasma membrane (PM) and a modified endoplasmic reticulum (ER) termed the desmotubule (DT) (Figure 1.7). The gap between the PM and DT is a cytoplasmic sleeve (CS) considered to be the main conduit of symplasmic transport. Regulation of PD is often mediated by callose: a cell wall polysaccharide which turnover (by PD-located enzymes) determines PD conductivity. High PD connectivity between groups of cells creates symplasmic domains where exchange of signals and

resources is relatively unrestricted (Bayer et al., 2008). Low PD connectivity can effectively prevent large signalling molecules from moving into neighbouring cells (Grison et al., 2019). PD also connect the vasculature with the surrounding tissues allowing for the systemic distribution of sugars and other signalling molecules. The vasculature offers a highway for signals to move around the plant. The next section will introduce phloem transport as an essential part of the signal transport apparatus.

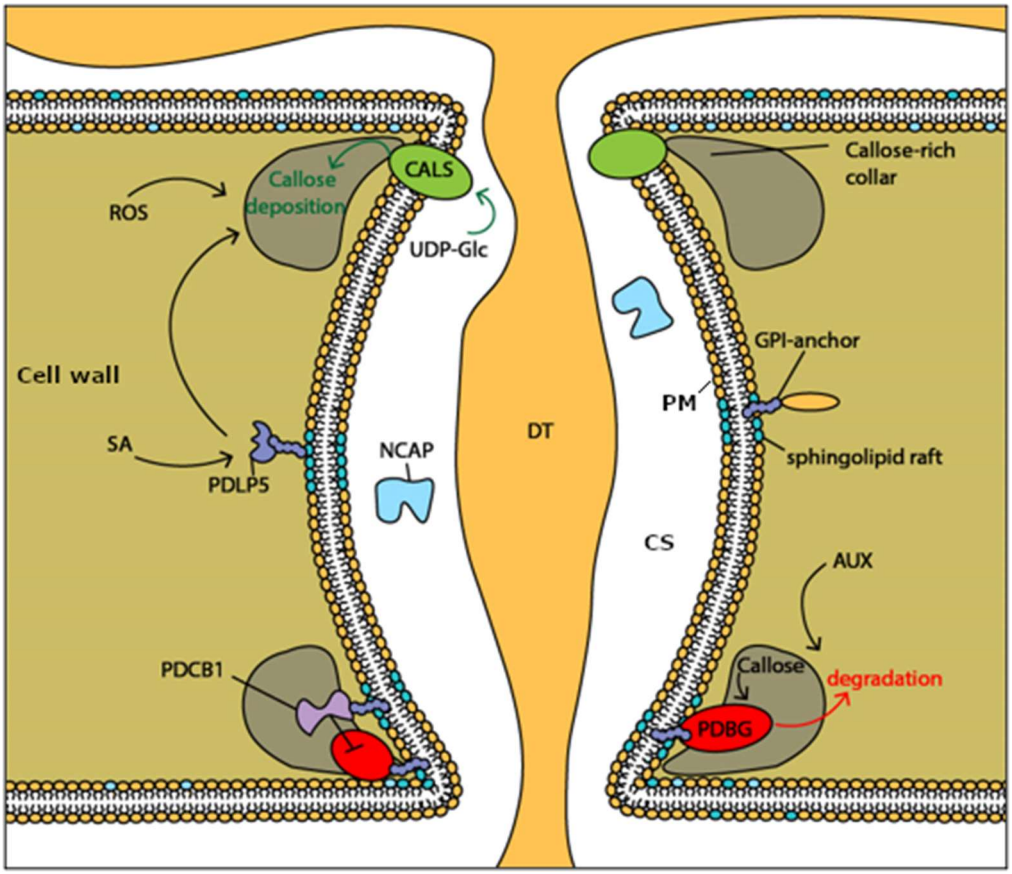

Figure 1.7 Structure and regulation of plasmodesmata (PD). PD have a cell wall, endoplasmic reticulum-derived desmotubule (DT) and plasma membrane (PM). Substances can travel symplasmically via the cytoplasmic sleeve (CS) between the DT and PM. Callose turnover at the neck region of PD is regulated by callose synthases (CalS) and PD-localised (1,3)-β-glucanases (PDBG). Callose is stabilised by PD–callose-binding proteins (PDCB), which might inhibit PDBG activity. PDBG and PDCB have specialised glycosylphosphatidylinositol (GPI) anchors, which tether them to micro-domains of the PM at PD, which are rich in sphingolipids. Callose deposition is enhanced by salicylic acid (SA) and by reactive oxygen species (ROS), in a mechanism mediated by PDLP proteins. Some PDBG are regulated by hormones including auxins (AUX). Callose restricts the aperture of PD and the size of macromolecules (such as non-cell autonomous proteins; NCAP) that can pass through the cytoplasmic sleeve formed between the desmotubule (DT) and the PM. Placement of proteins reflects putative localisation within the PD. This figure, as published in Amsbury et al. (2018), was developed by this author.

1.4.1 Phloem loading and unloading mechanisms: long distance translocation of signals and resources

Phloem is a primary conduit for the translocation of resources and signals across the plant. Phloem tissue is composed of chains of sieve elements (sieve tubes) that form the main conducting tissue in association with ancillary cell types (De Schepper et al., 2013). Sieve elements (SE), although living, lack a nucleus and other organelles and instead rely on companion cells for its metabolic needs. Companion cells (CC) contain a high number of mitochondria and ribosomes and are symplasmically connected to SE by a high number of PD (De Schepper et al., 2013). Key resources that are transported via phloem are photoassimilates. Photoassimilates synthesised in leaves are transported to mesophyll cells (MC) where excess sucrose can be stored in vacuoles and act as a buffer to balance cytosolic sucrose levels via the activities of TONOPLAST MONOSACCHARIDE TRANSPORTERS (Xu and Liesche, 2021). Sucrose and some types of sugar alcohols (polyols) move from MC towards the phloem passing through various cell types including bundle sheath cells, phloem parenchyma cells, intermediary cells and CC. Several phloem loading mechanisms have been proposed. One mechanism requires sucrose or polyols to be released by permeases from the phloem parenchyma cells into the apoplast and then actively pumped into SE by symporters such as SUCROSE TRANSPORTER 2 (SUC2) at the SE-CC PM boundary (Chen et al., 2012). In the polymer trap model, photoassimilates are converted to large compounds such as raffinose oligosaccharides in intermediary cells. These oligosaccharides are considered too large to move symplasmically back into neighbouring phloem parenchyma cells thus they are 'forced' to travel via PD into the adjoining SE to enter the phloem stream (Turgeon and Gowan, 1990; Bonnemain, 1991). Symplasmic movement of sucrose and other sugars can also occur when sugar concentrations are high, creating a gradient that drives the passive diffusion from MC to SE (Zhang et al., 2014b). The loading of sugars and other solutes in the phloem reduces the water potential which draws in water from surrounding tissues generating pressure-driven bulk flow of sap within sieve tubes. This pressure gradient is maintained by phloem unloading into sink (developing or metabolically demanding) tissues.

Phloem symplasmic unloading occurs via specialised funnel-shaped PD found between proto-SE and neighbouring cells in multiple dicots and monocots (Ostermeyer et al., 2021). Live cell imaging, electron microscopy and modelling provide compelling evidence that funnel PD can allow the passage of relatively large macromolecules (at least 112 KDa)

and facilitate unloading by a combination of bulk flow and diffusion (Ross-Elliott et al., 2017). Phloem unloading can also occur via apoplastic pathways mediated by sucrose transporters as described for some fruits (Paniagua et al., 2021). A structural study determined that SE-CC complexes in the developing sink tissues of apple fruits do not contain PD and the symplasmic dye carboxyfluorescein remained constricted to phloem tissue indicating apoplastic phloem unloading (Zhang et al., 2004). In grape, on the other hand, SE-CC complexes possess PD with neighbouring parenchyma cells, but these become occluded during ripening (Zhang et al., 2006). This occlusion coincides with an increase in cell wall acid invertases that hydrolyse sucrose which suggest that there is a switch from symplasmic to apoplastic phloem unloading during fruit development.

The vascular bulk flow of substance created by the source-loading of solutes, primarily sugars, carries many other classes of substances including proteins and RNA (Yang et al., 2019). The loading and unloading of RNAs and proteins have received much less attention than sugars. All classes of RNAs (including ribosomal, messenger, tRNAs, etc.) have been found in phloem sap and several of these RNAs play important roles in shoot/root signalling (Table 1-1). Transport of RNAs via the phloem has some degree of selectivity. RNAs harbouring phloem transport signals are aided in translocation by RNA-binding proteins (Yang et al., 2019). The exact mechanisms of how RNAs are selectively loaded in the phloem are poorly understood. Similarly, a large proportion of the plant proteome can also be found in the phloem sap (Malter and Wolf, 2011; Rodríguez-Celma et al., 2016), but the function of phloem mobile proteins is not fully characterised.

1.5 The symplasmic pathway: Plasmodesmata

The capacity of a substance to cross the CS is dependent on physical characteristics of both the PD and the substance. One parameter routinely used to describe PD transport capability is the maximum size of a molecule that can pass through it, termed the size exclusion limit (SEL) (Goodwin, 1983; Oparka et al., 1999). SEL is often estimated by comparing the relative permeability of fluorescent dyes of small molecular weight with that of larger protein-based fluorophores such as GREEN FLUORESCENT PROTEIN (GFP), either as a protein tag, in free form or in its multimeric configurations (Itaya et al., 2002; Benitez-Alfonso et al., 2009; Burch-Smith and Zambryski, 2010; Gerlitz et al., 2018). SEL is not the only factor that influences transport through PD, but it is a useful framework to conceptualise simple non-specific PD transport. PD are dynamic structures and SEL and

molecular flux through PD are regulated in response to internal and external cues (Li et al., 2021).

1.5.1 Development and diversity of plasmodesmata

PD are diverse and can be classified by how they are developed, their size, shape and properties. PD can form during cytokinesis (primary PD) or *de novo* in existing cell walls (secondary PD) (Burch-Smith et al., 2011b) (Figure 1.8). Primary PD develop in the cell plate that forms during cytokinesis trapping a portion of the ER that will form the DT (Hawes et al., 1981; Hepler, 1982). Secondary PD are formed in existing cell walls or in cells forming graft junctions and host/parasite interfaces (Kollmann and Glockmann, 1991; Fischer et al., 2021). Secondary PD are thought to be formed by local thinning of the cell wall, insertion of ER, PM fusion between cells and further modifications to the cell wall (Ehlers and Kollmann, 2001; Burch-Smith et al., 2011b). Primary PD are randomly distributed in the cell wall whereas secondary PD are often clustered together, with primary PD, forming pit fields (Faulkner et al., 2008). Structurally, primary and secondary PD closely resemble each other (Burch-Smith et al., 2011b). Both primary and secondary PD can develop simple or branched morphologies (Figure 1.8). PD can be further classified based on how tightly the DT is associated with the PM (Nicolas et al., 2017). Type I PD have barely any CS between the PM and DT whilst type II PD conform more to the standard model of PD transport with a significant CS. Each of the domains of PD (cell wall, PM, DT and CS) contribute to PD function. The following subsections will describe how each domain of PD along with their associated proteome influence PD form and function.

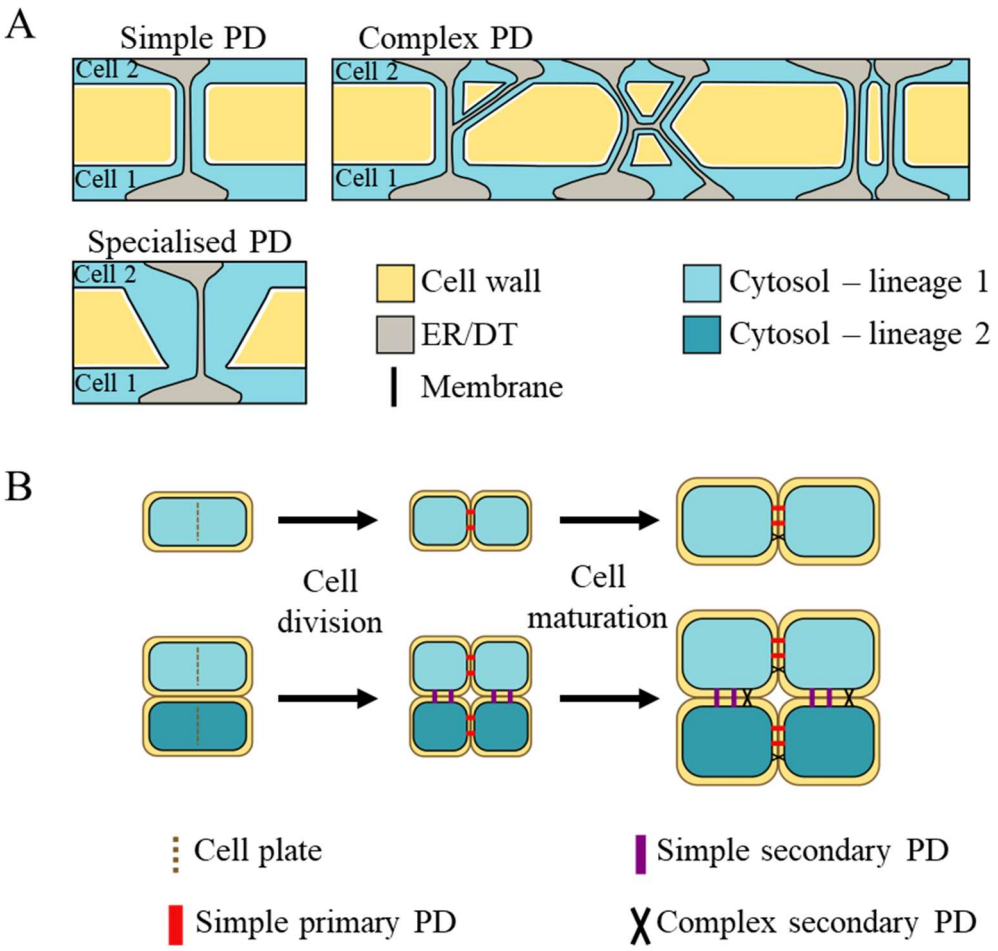

Figure 1.8 Plasmodesmata (PD) can be classified based on their structure and by whether they developed during or after cytokinesis. (A) PD have been found with different structures including simple and complex forms, which include 'Y'-shaped, 'H'-shaped, and twinned PD. PD can have specialised structures to serve specific functions such as funnel PD that are adapted for phloem unloading. (B) Primary PD are generated during cytokinesis where portions of the ER are trapped within the cell plate as it forms. Secondary PD develop *de novo* in existing cell walls. Complex PD morphologies are thought to develop from simple primary or secondary PD. PD can also be classified by whether there is a significant cytoplasmic sleeve or not. Adapted from Lee and Sieburth (2010).

1.5.2 Composition and function of PD membranous domains

Lipidomic analysis of PD fractions have been carried out and plant membrane lipids can be broadly subdivided into 3 types with distinct properties: glycerophospholipids, sterols, and sphingolipids (Harayama and Riezman, 2018). Differences in lipid composition are likely to reflect changes in PM membrane composition given that it is more abundant than

the DT at PD (Li et al., 2021). The composition of lipids at PD are distinct from other membranous domains. For example, glycerophospholipids at PD have a higher saturation level and the sphingolipid glycosyl inositol phospho ceramides and sterols are enriched at PD relative to the PM (Grison et al., 2015). Sterols and sphingolipids have a high affinity for one another (Harayama and Riezman, 2018) which results in the formation of microdomains within membranes referred to as lipid rafts. Specific PD proteins like REMORINs (REM) and TETRASPANNINS (TET) are involved in lipid nanodomain specification and organisation at PD (Wang et al., 2015; Huang et al., 2019). Not only do lipid rafts recruit specific proteins to PD (Grison et al., 2015), nanodomain specification may be crucial in the specification of PD. This is exemplified by the recent finding that heterologous expression of plant REM in mammalian cells resulted in cell-cell membrane channels that were reminiscent of PD and were able to transport macromolecules between cells (Wei et al., 2020).

In comparison to the PD PM region, much less is known about the composition and function of the DT. The exact lipid composition of the DT is not possible to disentangle from that of the PM or the rest of the ER due to the technical challenge of purifying PD membranous fractions (Li et al., 2021). Only a minority of currently identified PD proteins interact with the DT: CALNEXINS, RETICULONS and MULTIPLE C2 DOMAIN AND TRANSMEMBRANE REGION PROTEINS (MCTPs) (Knox et al., 2015; Liu et al., 2017a; Brault et al., 2019). DT are tethered to the PM by MCTPs and SYNAPTOTAGMINS (SYT) (Brault et al., 2019; Ishikawa et al., 2020). The PM and DT interact at characteristic spoke like features seen in electron micrographs of PD which may function as membrane contact sites where lipid-associated proteins can be exchanged (Li et al., 2021). Originally these spoke like patterns were thought to be related to the cytoskeleton and there is debate about what contribution the cytoskeleton plays (Overall and Blackman, 1996; Tilsner et al., 2016). PD-localising FORMINS are thought to anchor actin to PD and both actin and myosin have been detected in the PD pore (Tilsner et al., 2011; Diao et al., 2018). Microinjection experiments have demonstrated that molecules can move between cells directly through the DT lumen and this pathway has been postulated as a potential route for the transport of lipids and specific membrane bound proteins (Barton et al., 2011; Li et al., 2021). More work is required to determine the extent and significance of transport directly via the ER-DT continuum.

The CS is often attributed as the main conduit for symplasmic transport but much of the pore aperture is occupied by the DT. One may assume that cytosolic transport through PD

may be easier if the DT were simply not there. However, recent modelling suggests that the presence of a DT increases the transport capacity of the PD for a given SEL (Deinum et al., 2019). This may seem counterintuitive at first but if one assumes that the diameter of the CS is the effective SEL of the pore and transport is possible around the whole ring of CS around the DT, without a DT, the pore would have to be much narrower to achieve the same SEL and would therefore have less cross-sectional area available for transport. The DT has also been proposed to control flux through the CS under osmotic stress or wounding events (Park et al., 2019). Under these conditions, a pressure wave is created, and modelling suggests that the DT complex may flow under these conditions and plug the pore thus restricting fluid loss and mitigating damage.

1.5.3 Cell wall microdomains around plasmodesmata

Cell walls are a defining feature of plant cells providing strength and protection to the interior of the cell and the whole plant body. Cell walls are often conceptualised as a highly complex matrix of interacting polysaccharides and proteins (Knox and Benitez-Alfonso, 2014). PD are mainly found bridging primary cell walls thus secondary cell wall formation is not discussed here. The use of proteomics, high resolution microscopy and immunochemistry techniques have demonstrated that cell walls around PD have a distinct structure and composition relative to the rest of the cell wall (Faulkner et al., 2008; Fitzgibbon et al., 2010). The cell wall domain surrounding PD is known to play a critical role in their development and function (Amsbury et al., 2018). Despite its importance, many questions remain about the true extent the cell wall plays in the biology of PD. In this subsection, cell wall structure and composition will be explored.

1.5.3.1 Callose at plasmodesmata cell wall domains

Callose, a β-1,3-glucan with some minor β-1,6-branching, accounts for a small proportion of the composition of the cell wall but is found in relative abundance around PD (Knox and Benitez-Alfonso, 2014). Callose is synthesised *in situ* from glucose (in the form of uridine diphosphate glucose) by CALLOSE SYNTHASES (CalS) (Figure 1.9). The deposition of callose by PD specific CalSs pushes the PM against the DT narrowing the CS (Figure 1.7). This effectively limits the SEL for diffusible molecules (Hunter, 2007; Pound et al., 2013; Sinclair et al., 2017). The orientation of the glucose molecules impedes close association of callose chains which adopts an amorphous structure (Amsbury et al., 2018). This makes callose more amenable to enzymatic digestion and high turnover than the highly ordered β glucan cellulose. Degradation of callose into glucose is performed by β-

1,3-glucanases (BGs) (Figure 1.9). PD-localising BGs (PDBGs) work antagonistically with PD CalSs to regulate levels of PD callose and thereby the regulate PD permeability (Figure 1.2).

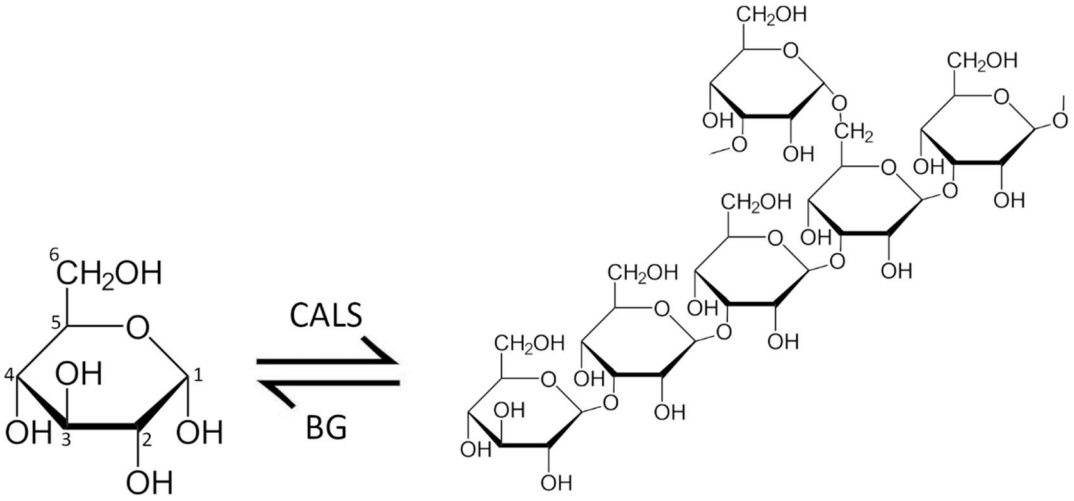

Figure 1.9 Callose is primarily composed of glucose molecules linked by 1,3 glycosidic bonds with some minor 1,6 branching. Callose is synthesised from glucose by callose synthases (CALS) and degraded by 1,3-β-glucanases (BG).

The capacity for rapid turnover is not the only functional property of callose in PD biology. Callose has been shown to interact with cellulose *in vitro*, making a more elastic mixture (Abou-Saleh et al., 2018). Functionally, the elasticity of callose/cellulose mixtures could help the cell wall to be more resilient in areas of high stress. The cell wall is effectively punctured to form PD which may subject the cell wall around these perforations to higher degrees of stress. This may be more apparent in pit fields where there is a higher density of PD and a larger area of thin cell wall (Faulkner et al., 2008). Callose, therefore, may be playing a dual role: regulating PD pore aperture and allowing the cell wall to cope with the stresses imposed by PD perforations.

1.5.3.2 Pectins at plasmodesmata cell wall domains

Pectins are a complex class of polysaccharides with an acid backbone of mainly homogalacturonans (HG) or rhamnogalacturonans (RG-I and RG-II) with a diverse set of side chains including arabinans, galactans and arabinogalactans (Chen et al., 2015). Methyl ester groups are added to pectins such as HG during synthesis (Vidal et al., 2013). These methyl ester groups can be removed later by pectin methylesterases (PMEs) which are regulated by PME inhibitors (PMEIs) (Clauw et al., 2015). Non-methyl esterified poly galacturonans can become crosslinked by mutual binding of calcium ions forming a gel

(Jarvis, 1984) thus the degree of pectin methyl esterification is a major regulator of cell walls properties. Levels and/or composition of pectins at PD are distinct relative to the bulk cell wall and this may contribute to the physical properties of PD or be involved directly in the regulation of symplasmic transport (Amsbury et al., 2018). Immuno-labelling of sectioned plant material with antibodies specific to cell wall epitopes is a powerful technique that can be used to assess the relative abundance of polysaccharides *in situ*. Immuno-labelling with the antibody JIM5 (John Innes Monoclonal 5, specific to low-esterified HG) have shown high levels of this epitope in the pit fields of tomato fruit pericarp (Casero and Knox, 1995; Orfila and Knox, 2000) and cell wall domains around PD in apple (Roy et al., 1997). Similarly, immuno-labelling with LM6 (Leeds Monoclonal 6), which specific to RG-I-(1-5)-α-L-arabinan (Lewis et al., 2013), showed that this epitope is enriched in cell wall surrounding PD and in pit fields in tomato and tobacco (Orfila and Knox, 2000; Faulkner et al., 2008). Pectins have been linked with controlling cell wall porosity and is often characterised as a glue that holds together other cell wall constituents (Knox and Benitez-Alfonso, 2014). Members of the PMEs and PMEIs families have been identified in PD proteomes (Brault et al., 2019) which suggests that pectin modification maybe linked with the regulation of PD. The movement protein of tobacco mosaic virus (TMV) interacts with a native PME and this interaction is required for protein movement and virus spreading (Zhang et al., 2016). PME activity regulates apoplastic Ca2+ levels which has been associated with responses to stress and also with PD modifications (Wu et al., 2018). Although it has been known for 20 years that PD have distinct populations of pectin, it is still not clear what the function significance of this is.

1.5.3.3 Cellulose at plasmodesmata cell wall domains

Cellulose is the most structurally significant component of the cell wall. Cellulose is a β 1,4 -glucan that forms strong linear crystalline structure called microfibrils (Li et al., 2014). Microfibrils arrangement is deliberately controlled to regulate the anisotropic properties of the cell wall to direct cell expansion (Li et al., 2014). Given that cell walls around PD are thinner and may be under stress due to perforations, it is intriguing that pit fields contain less cellulose than other cell wall domains (Faulkner et al., 2008). It has been postulated that having less cellulose may make the cell wall more flexible and that this is a requirement of regulated symplasmic transport (Gronnier et al., 2017). For example, interactions between cellulose microfibrils are loosened by expansins (Stahl et al., 2009; Benitez-Alfonso et al., 2013) and a PD-specific expansin (that increases the transport of a viral movement protein) was identified in Nicotiana benthamiana (NbEXPA1) (Park et al.,

2017b). Pectin and callose has been shown to interact with cellulose *in vitro* indirectly suggesting that regulation of cellulose arrangement might be important in determining the properties of PD (Deak and Malamy, 2005; Abou-Saleh et al., 2018).

1.5.3.4 Hemicelluloses at plasmodesmata cell wall domains

Hemicelluloses are a group of polysaccharides that are classified together largely because they do not readily fall into the other classifications of cell wall polysaccharides (Paul Knox, personal comms.). The predominant hemicellulose in *Arabidopsis* primary cell walls is xyloglucan. Xyloglucans have historically been considered an essential component for cellulose microfibrils arrangement (Keegstra et al., 1973). However, double mutants in *xylosyltransferase 1/2*, which have little to no detectable xyloglucan, do not show major growth defects suggesting that cellulose crystallinity is not affected (Cavalier et al., 2008; Park and Cosgrove, 2012; Kuki et al., 2020). Almost nothing is known about the role hemicelluloses play at PD. Several families of proteins that are related with xyloglucan synthesis/remodelling are present in PD proteomes (Fernandez-Calvino et al., 2011; Park et al., 2017b; Leijon et al., 2018; Brault et al., 2019). These families include glycosyl hydrolases family 31 proteins which hydrolyse the terminal xylose residue from xyloglucan (Larsbrink et al., 2011) and XYLOGLUCAN ENDO-TRANSGLYCOSYLASE/HYDROLASE (XTH) that remodel the xyloglucan matrix by cleavage and rearrangement of xyloglucan (Nishitani and Tominaga, 1992; Rose et al., 2002). The presence of these enzymes at PD indicates a potential, yet unknown, function for xyloglucans at PD.

1.5.4 The plasmodesmata proteome

PD proteomes of several plant model species have been published in the last decade which have greatly improved our understanding of what factors may associate with PD (Fernandez-Calvino et al., 2011; Park et al., 2017b; Leijon et al., 2018; Brault et al., 2019). However, identification of a protein in a PD proteome is not confirmation of PD localisation as isolation of these domains within cell walls often carries contamination with non-PD structures such as the bulk PM, the cell walls and the endoplasmic reticulum (ER) (Brault et al., 2019). PD proteomes are derived from cell-cultures that are purified to produce fractions enriched in PD membranes that are sequenced by mass spectrometry (Figure 1.10). A major handicap is the fact that PD isolation has been so far optimised for cell cultures thus the dynamics of PD proteomic composition associated with plant development and responses to the environment are often missed. An additional problem is that proteins identified to target PD are often

members of large families with multiple functions and no distinctive domains linked to PD localisation. These proteomic studies are relatively resource intensive and therefore have only been performed on a small number of species. Moreover, there is no evidence, hitherto, that the proteins identified are conserved between plant species.

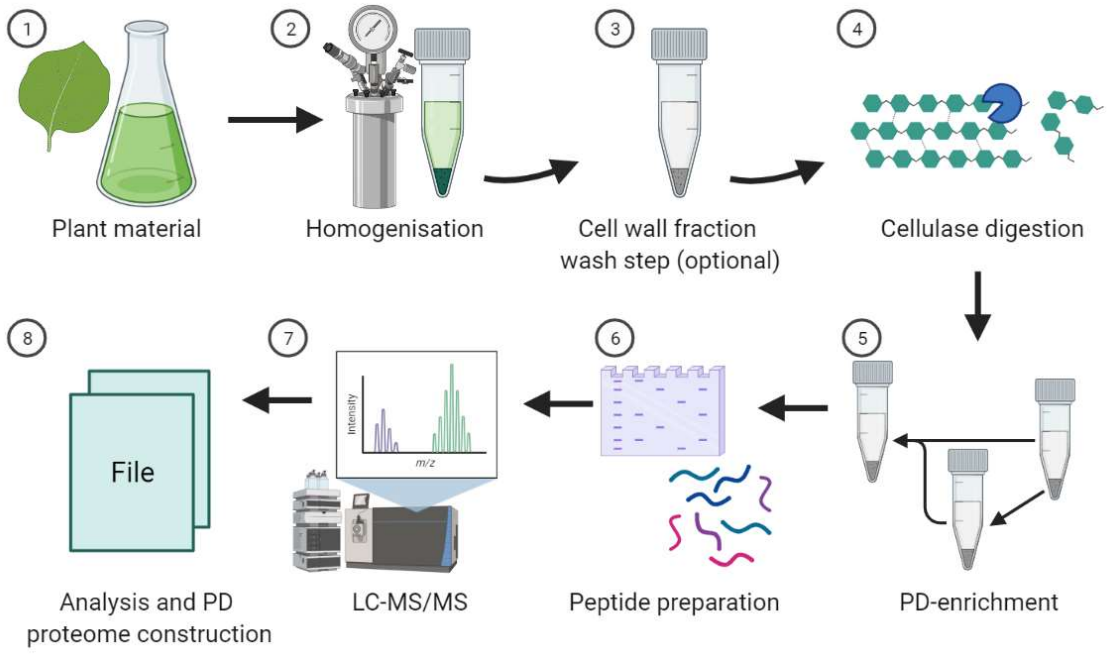

Figure 1.10 Preparation of experimentally determined PD proteomes. (1) The starting material for PD proteomes is generally suspension cultured cells (Fernandez-Calvino et al., 2011; Leijon et al., 2018; Brault et al., 2019). Park et al. (2017) used leaf tissue as the starting material. (2) Plant material is homogenised in a cell wall extraction buffer in the presence of protease inhibitors; high pressure homogenisation is the most common method employed. The pellet formed after centrifugation is considered the cell wall enriched fraction (CEF). (3) CEF may be washed in buffer several times. (4) CEF is digested with cellulase in the presence of protease inhibitors. (5) The digestion reaction is centrifuged, and the supernatant and pellet separated. The pellet is washed in digestion buffer and centrifuged. The supernatant is mixed and ultracentrifuged. The resulting pellet is considered the PD-enriched fraction (PEF). (6) Preparation of peptides differ from study to study but may involve solubilisation of peptides with Laemmli buffer, clean up with SDS-PAGE and gel extraction and then trypsin digestion. (7) Peptide sequences are determined using Liquid Chromatography with tandem mass spectrometry (LC-MS-MS). (8) Data are processed to form a list of proteins that are present in the PEF. The diagram was created with BioRender.com.

Despite the technical challenge of high throughput identification of PD proteins, such tools have been used to identify candidates for further characterisation. Localisation of protein fusions using confocal and/or FRET-FLIM (Förster resonance energy transfer/ Fluorescence lifetime imaging) assays has experimentally confirmed PD association for around 60 proteins in *Arabidopsis* (See Supplementary material 1 for references*)*. These verified PD proteins represent a broad suite of enzymatic and signalling activities associated with PD domains and their regulation, including callose synthesis, binding and degradation and PM-associated receptors involved in signalling. This accrued collection of verified PD genes is now substantial and could act as a guide to help identify further candidate genes from the PD proteome pools. In the following section, protein activities are discussed in relation to PD regulation.

1.6 The regulation of plasmodesmata and symplasmic transport

1.6.1 Callose-dependent regulation of plasmodesmata

The most characterised model of regulation of symplasmic transport is the control of callose turnover at PD. Callose-associated regulation of PD has been described in a wide range of developmental processes (Hong et al., 2001; Saatian et al., 2018) and responses to biotic (Caillaud et al., 2014; Cui and Lee, 2016b; Liu et al., 2020a) and abiotic stimuli (Sivaguru et al., 2000; Ueki and Citovsky, 2005; Piršelová et al., 2012; Müller et al., 2015). CalS and BGs are the only known enzymatic factors capable of directly altering callose deposition in plants (Amsbury et al., 2018). These activities are encoded by large families of proteins, with members targeting PD membranes. Disruption of genes encoding PD proteins from these families can have profound effects on development. Ectopic expression of *CalS3* or function-limiting mutation of *CalS10* causes changes in the amounts of callose to be deposited at PD (Vatén et al., 2011). This leads to altered mobility of the cell-fate determining transcription factor SHR in the root tip leading to growth defects (Vatén et al., 2011; Saatian et al., 2018). Loss of function mutation in CalS10, also known as *chorus* leads to abnormal clustering of stomata dues to increased mobility of the stomatal cell fate- transcription factor SPEECHLESS (SPCH) (Chen et al., 2009; Simmons and Bergmann, 2016).

Altering the expression of *PDBGs* also influences symplasmic transport. PDBGs display an N-terminal signal peptide (SP), a glycosyl hydrolase activity domain and many also contain a callose-binding X8 domain and a C-terminal glycosylphosphatidylinositol (GPI) anchor

(Gaudioso-Pedraza and Benitez-Alfonso, 2014). Silencing of a tobacco BG leads to an increase in callose accumulation which consequently reduced the symplasmic transport of tobacco mosaic virus movement protein (TMV-MP) (Iglesias and Meins Jr, 2000). Similarly, knocking out the PD specific BG *AtBG_pap* in *Arabidopsis* leads to increased callose accumulation coupled with a reduction in symplasmic movement of cytosolic GFP (Levy et al., 2007). A further 3 PD-specific BGs are known in *Arabidopsis* named PDBG1, PDBG2 and PDBG3. Knocking out these genes is also linked with callose accumulation, reduction in symplasmic transport and in the case of *pdbg1* and *pdbg2,* linked with altering lateral root patterning (Benitez-Alfonso et al., 2013). No glycosyltransferases have been discovered in plants, which in fungi are known to be able to modify β-1,3-glucan *in situ* (Aimanianda et al., 2017). Although not directly linked with enzymatic synthesis/degradation, another family of proteins, PD-localised Callose Binding proteins (PDCBs), are known to interact with callose. As PDBGs, PDCBs are a family of proteins displaying an N-terminal signal peptide, a carbohydrate X8 domain (also known as CBM43) and a C-terminal GPI anchor that lacks enzymatic activity (Simpson et al., 2009). Over expression of *PDCB1* causes an accumulation of callose and significantly reduces PD permeability (Williamson et al., 2001; Simpson et al., 2009). Overexpression of *PDCB1* leads to phenotypic defects in shoot and root growth (Benitez-Alfonso et al., 2013). These phenotypes suggest that PDCBs have a role in callose regulation although the mechanism of this is unknown.

1.6.2 Callose-independent regulation of plasmodesmata

The PD membranous domains can influence the structure of the CS and thereby regulate passive symplasmic transport in callose-dependent and -independent fashions. Indirectly, changes in the PM lipid composition may indirectly control symplasmic transport by recruiting callose-modifying factors to PD (Zhang et al., 2017; Grison et al., 2019; Liu et al., 2020a). For example, osmotic stress-induced lipid modification by a phospholipase D is required for the transient PD localisation of CYS-RICH RECEPTOR-LIKE KINASE 2 (CRK2) which triggers callose accumulation (Hunter et al., 2019). Changes in symplasmic permeability are also associated to changes in PD structure. Specifically, *phloem unloading modulator* (*plm*), is affected in the synthesis of sphingolipids in the ER leading to a reduction in ER-PM tethering and an increase in the frequency of Type I PD (PD without visible CS) (Yan et al., 2019). As a result, enhanced symplasmic transport was observed at the interface between the phloem pole pericycle and endodermal cells. Recent work also demonstrated that aberrations in PM-DT tethering in a triple *syt* mutant (*syt1,5,7*) lead to

changes in PD structure and supressed cell-cell trafficking of *Youcai mosaic virus* movement protein (Ishikawa et al., 2020). It remains to be seen whether plants can modulate PM-ER tethering dynamically to regulate transport through the CS.

Passive PD transport can also be regulated by affecting the frequency and gross morphology of PD. The density of primary PD formed during cell division is influenced by cell expansion where the same amount of PD are spread over a larger surface area (Faulkner, 2018). Secondary PD that are inserted into the cell wall post cytokinesis are not only enable symplasmic transport between neighbouring tissue types but also add transport capacity between cells with existing primary PD connections. During mesophyll development, intercellular spaces develop that sever old primary PD connections with neighbouring cells (Roberts et al., 2001). To account for this, new secondary PD are created. Secondary PD frequently have a branched morphology and are thought to arise from twinning of primary PD (Faulkner et al., 2008). Other conformations (e.g., H shaped) has also been observed by electron-microscopy. Parallel to this, existing primary PD may also adopt branched morphologies although the physical and molecular mechanism involved in branching or twinning are unknown (Burch-Smith et al., 2011b).

Modelling suggests that the shift to branched morphology could help to maintain symplasmic flux at low PD densities (Deinum et al., 2019). This study also suggests that the distribution of PD and changes in cell wall thickness could determine symplasmic transport. In the model, clustering of PD at pit field reduced flux relative to a more even PD distribution. On the other hand, to achieve the same permeability values, the model predicts that thicker cell walls require longer PD and a central PD cavity. Beside passive diffusive transport, substances over the SEL can be translocated by interacting with intracellular factors (selective transport). This is exemplified using KNOTTED1 (KN1, named SHOOTMERISTEMLESS, STM in *Arabidopsis*), which is a non-cell autonomous transcription factor that move in the shoot meristem (Kim et al., 2005). A system was designed to achieve mobility of the cell-autonomous factor GLABROUS1 by fusing the protein to the KN1 homeodomain. The fusion protein was expressed in the mesophyll of *gl1* (a mutant lacking trichomes), and this was sufficient to complement the glabrous phenotype due to movement of GL1-KN1 movement from the mesophyll to the epidermis. Mutagenesis and screening of this complemented line identified a chaperonin CCT8 which interacts with KN1 to facilitate its movement between the leaf cell layers (Xu et al., 2011). The model proposed suggests that CCT8 participates in the folding/unfolding of KN1 after translocation. There is evidence that suggest other modes of transport via PD such as the

unidirectional symplasmic transport observed into tobacco trichomes (Christensen et al., 2009) but these pathways are poorly understood.

1.6.3 Signalling pathways regulating symplasmic transport

This section will focus on signalling mechanisms that are relevant to root development and responses to abiotic stress. Signalling networks in plants are complex and highly integrated with one another. Many well established signalling pathways influence symplasmic transport likely mediated by interactions with the wide range of receptor like proteins (RLP) and RLK that target to PD (Supplementary material 1). These proteins may be recruited by the specific PD lipid composition or by forming homo- and hetero dimers with PD proteins (Li et al., 2021). PD receptor genes integrate a range of native and foreign signals diffusing in the apoplast and the symplast with the regulation of intercellular transport (Han and Kim, 2016). Receptor like proteins containing the DOMAIN OF UNKNOWN FUNCTION 26 (DUF26) are particularly associated with PD function; namely the PLASMODESMATA-LOCALISED PROTEINS (PDLPs) and CYSTEINE-RICH RLK (CRKs). These classes of proteins are only found in land plants (Vaattovaara et al., 2019).

PDLPs are associated with regulation of callose (likely by controlling CalS activity) in root and shoot response to a wide range of developmental and environmental cues (Caillaud et al., 2014; Cui and Lee, 2016b; Liu et al., 2020a). An example of this is the role PDLP5 plays in the establishment of symplasmic domains during lateral root development (Sager et al., 2020). Early in lateral root primordia formation, auxin induced-PDLP5 accumulation triggers callose deposition in the overlying endodermal tissue which may function to restrict cell-fate determining factors to move between the now separated symplasmic domains. Subsequently, auxin-dependent cell wall separation permanently severs any symplasmic ties between the founder cells in the xylem pole pericycle with the endodermis. CRKs contain a double DUF26 domain in the extracellular portion of the protein (Vaattovaara et al., 2019). CRK2 was found to transiently localise to PD under osmotic stress and this correlated with callose induction (Hunter et al., 2019). RLKs are known to have high ligand specificity but the exact ligands of PDLPs and CRK2 are not known (Vu et al., 2020). Reactive oxygen species (ROS) generation play a key role in signal transduction of both PDLPs and CRK2. CRK2 phosphorylates the RESPIRATORY BURST OXIDASE HOMOLOG D (RBOHD) which is required to trigger ROS signalling (Kimura et al., 2020). RBOHD- activity during light stress increases PD pore size and symplasmic

transport of the small fluorescent symplasmic tracer carboxyfluorescein and this activity was dependent on PDLP1 and PDLP5 (Fichman et al., 2021). It is unclear how this finding relates to previous work that has correlated PDLP5 induction with callose deposition by CalS1 (Cui and Lee, 2016b). Callose induction in response to pathogens was found to be dependent on salicylic acid production; a hormone with strong links to ROS signalling (Herrera-Vásquez et al., 2015; Cui and Lee, 2016a).

ROS were first identified as regulators of symplasmic transport during the screening for *gfp-arrested trafficking* mutants (Benitez-Alfonso et al., 2009). One such mutant, *gfp-arrested trafficking 1* (*gat1*), which encodes for thioredoxin m3 expressed in non-green plastids, displayed an increase in the accumulation of ROS, ectopic callose deposition and reduction in symplasmic transport of GFP. Chemical treatments that cause ROS accumulation such as application of paraquat or hydrogen peroxide also led to restricted movement of GFP although this effect appears to be doses dependent (Benitez-Alfonso et al., 2009).

Besides ROS, the phytohormone ABA emerges as another important regulator of symplasmic transport (Benitez-Alfonso (2019). ABA is often considered the 'stress' hormone as it regulates responses to many biotic and abiotic stimuli (Nakashima and Yamaguchi-Shinozaki, 2013). Hybrid aspen (*Populus tremula x tremuloides*) with a knockout in a critical ABA signalling gene, *aba- insensitive 1* (*abi1*), was unable to form dormant shoot buds as characteristic in over-wintering deciduous trees (Tylewicz et al., 2018). Analysis of the mutant indicates defects in the induction of callose which is required to block growth promoting factors from accessing the bud during dormancy. Overexpressing a PDLP protein was able to induce sufficient callose to supress this phenotype. After the risks of winter damage have subsided, bud dormancy must be broken which involves a different class of phytohormone: gibberellic acids. Chilling of dormant buds triggers the expression of genes involved in the synthesis of gibberellic acids (Rinne et al., 2011). Gibberellic acids subsequently trigger BGs to break down callose thus restoring symplasmic transport of growth-promoting factors. Exogenous ABA has been demonstrated to reduce PD aperture and symplasmic transport of the symplasmic reporter Dendra2 in the model moss *Physcomitrella patens (Kitagawa et al., 2019).* Overexpression of positive regulators of ABA signalling in *P. patens, SUCROSE NON-FERMENTING 1-RELATED PROTEIN KINASE 2* and *PpABI 3* also lead to decreased symplasmic movement of Dendra2 (Tomoi et al., 2020)

Another important signal in the regulation of symplasmic transport are sugars. TARGET OF RAPAMYCIN (TOR) is a highly conserved protein kinase involved in the glucose sensing pathway (McCready et al., 2020). TOR is emerging as a major signalling hub for the integration of developmental and environmental signals (McCready et al., 2020). In *A. thaliana*, TOR integrates sugar signalling with ethylene, BR and auxin responses during embryogenesis, germination, meristem development and post embryonic development (Mishra et al., 2009; Zhang et al., 2016; Brunkard et al., 2020; McCready et al., 2020; Fu et al., 2021). In plants, TOR forms a complex (TORC1) with REGULATORY-ASSOCIATED PROTEIN OF TOR (RAPTOR) and LETHAL WITH SEC THIRTEEN 8 (LST8). Dimerisation of TOR is promoted by R2TP-TTT; a complex formed by the proteins Pontin/RuvBL1, Reptin/RuvBL2, Spaghetti/Tah1Telo2, Telo2-interacting protein 1, and Telo2-interacting protein 2 (Pacheco et al., 2021). R2TP-TTT act as an energy sensor that acts upstream of TOR. When ATP is abundant, dimeric TORC1 can phosphorylate targets that modulate gene expression and cell development. Reducing the expression of or knocking out genes relating to the TORC1 and R2TP-TTT complexes, specifically *reptin1* (also known as *ise 4*) and *LST8* lead to increased symplasmic movement tested using the 10-kDa fluorescein isothiocyanate-dextran (FITC-dextran) (Brunkard et al., 2020). Pharmacological suppression of ATP production by oxidative phosphorylation of glucose also lead to increased symplasmic transport of FITC-dextran while exogenous glucose application reduced it. These findings all point to sugar signalling negatively regulating symplasmic transport via TOR although the exact mechanisms underlying this regulation are unclear. The increased symplasmic transport of *reptin1* coincided with increased expression of *PDLP5* (Brunkard et al., 2020) which may mean that this response is linked with ROS signalling as described earlier in this section (Brunkard et al., 2020; Fichman et al., 2021).

1.7 PD regulation of mobile signals: new target to modify root responses to nutrient availability and water stress.

Symplasmic transport of signals is critically important in plant development and physiology but relatively little is known about its role in coordinating plant responses to nutrient and water availability. PD facilitates the movement of RNAs, proteins, sugars and hormones thus likely it functions in controlling the distribution of signals that trigger stress responses. Table 1-1 summarizes the information on mobile factors found to depend on plasmodesmata regulation. Several of these factors coordinate plant development but

also participate in the response to biotic and abiotic stresses. Recently, computational modelling of auxin distribution in roots was performed with and without considering symplasmic transport (Mellor et al., 2020). The inclusion of symplasmic transport of auxin created a better agreement with experimental auxin distributions derived from microscopy of plants expressing the auxin sensor DII-VENUS (Brunoud et al., 2012; Mellor et al., 2020). The models suggest that symplasmic transport play a significant role in auxin transport between the outer root tissues, where auxin levels are high, and deeper root tissues. This finding supports earlier works that present experimental evidence indicating that when symplasmic transport is affected, auxin gradients are modified leading to developmental phenotypes such as in phototropism or lateral root development (Guseman et al., 2010; Rutschow et al., 2011; Maule et al., 2013; Han et al., 2014; Chapman et al., 2019; Gao et al., 2020). The potential significance of symplasmic transport on auxin distribution is discussed in a recent review by Paterlini (2020) who comments that such transport complements and does not supersede, the established mechanisms of apoplastic auxin transport.

Auxin signalling in root development is intertwined with other signalling pathways involving sugar signalling, BR, ABA, cytokinin and ethylene (Rock and Sun, 2005; Bishopp et al., 2011; Liu et al., 2017b). Evidence of interplay between symplasmic transport and these other signalling pathways is emerging (Ormenese et al., 2006; Han and Kim, 2016; Benitez-Alfonso, 2019). For example, transport of ^{14}C-labeled cytokinin in the shoots was found to be reduced when plants ectopically accumulates callose at PD caused by expression of inducible *cals3m* (*iCals3m*) under the ALTERED PHLOEM DEVELOPMENT (APL) promoter (*pAPL::XVE*>>cals3m) (Bishopp et al., 2011). *iCals3m* contains two mutations leading to a hyperactive CALS3 enzyme (Yadav et al., 2014). Constructs has been designed to induce this protein in different cell types using an estradiol inducible system (XVE) and cell-specific promoters such as *APL* (which drives expression to the phloem poles). These tools have been transformative in the investigations into the role of symplasmic transport in the transport of cytokinin, auxin and other symplasmically mobile signalling factors.

RNA and proteins are perhaps the best example of symplasmically mobile signalling factors. Their shape and size impede diffusion via the cell wall. Proteomic analysis of heterografts between different Cucurbitaceae species and of the tissues involved in parasitic symbiosis between *Arabidopsis* and *Cuscuta australis* (dodder) demonstrate that a considerable portion of a plant's proteome is mobile (Gierth et al., 2005; Hu et al., 2016;

Xu et al., 2018). An archetypal example of symplasmic signalling via cell-to-cell mobile proteins in root development is SHR. SHR is a GRAS-family transcription factor (TF) that is translated in the stele and moves to the QC and endodermis (Koizumi and Gallagher, 2013). SHR interacts with SCARECROW (SCR) in the QC and endodermis to promote the expression of factors (TFs and mirRNAs) that control asymmetric cell divisions and the patterning of vasculature, endodermal and cortical root cell layers (Carlsbecker et al., 2010; Wu et al., 2014; Kim et al., 2020). The movement of both SHR and its negative regulator, mirR165/6, are regulated by callose deposition at PD (Vatén et al., 2011). Heterologous expression of SHR disrupts miRNA behaviour leading to aberrant tissue patterning (Wu et al., 2014).

There are several other examples where symplasmic movement of TFs is essential for proper root tissue patterning such as WUSCHEL RELATED HOMEOBOX 5 (WOX5) and TARGET OF MONOPTEROS 7 (TMO7) (Pi et al., 2015; Lu et al., 2018). TMO7 is associated with the establishment of the hypophysis during embryonic root development. TMO7 fused to a triple GFP tag prevent symplasmic movement and was found to be expressed in root meristematic and lateral root cap cells around the QC but, in contrast to its native version or from TMO7-1xGFP, it was largely excluded from the QC itself and columella cells (Lu et al., 2018). Movement of TMO7 was restricted in the callose over-expressing line *cals3*-2d providing further evidence that TMO7 is non-cell autonomous. The authors of this finding were able to pinpoint two domains of TMO7 that can bestow mobility to cell autonomous factors (Lu et al., 2018).

Grafting experiments combined with transcriptomics have demonstrated that a high proportion of RNAs, both coding and non-coding, are transported long distance (Gierth et al., 2005; Buhtz et al., 2008; Thieme et al., 2015). Long distance movement of RNAs from shoot to root is considered to be via the phloem (Buhtz et al., 2008). In grafts between ecotypes of *A. thaliana*, approximately 20% of mRNAs were found to be graft transmissible (Thieme et al., 2015). The mobile transcriptome was shown to be significantly modulated under nitrogen or phosphate limiting conditions which suggests that mRNA might be acting as long-range signals or effectors under these conditions (Thieme et al., 2015). A feature, a modified base 5-methylcytosine, essential for the systemic movement of many mobile mRNAs was recently discovered (Yang et al., 2019). For example, the mobility of the T*RANSLATIONALLY CONTROLLED TUMOR PROTEIN 1* transcript, which functions in the promotion of root growth, was found dependent on the presence of this feature. Currently, this is the only example where an mRNA has been

demonstrated to function at a distance from their site of transcription (Yang et al., 2019). Long distance signalling of non-coding RNAs has also been described. Mobile miRNAs have been linked with various responses, including the promotion of flowering in *Solanum tuberosum* (Martin et al., 2009) and with low phosphate response (Melnyk et al., 2011; Skopelitis et al., 2018). The movement of miRNA appears to be directional and regulated. Skopelitis et al. (2018) used a system in which plants with ubiquitous expression of GFP were transformed with an artificial miRNA (miRGFP) designed to silence GFP in different tissues (driven by cell specific promoters). They found that miRGFP expressed in the phloem companion cells was able to silence GFP expression in ground tissue, but miRNA expressed in the ground tissue was unable to silence phloem GFP expression. This demonstrated that the movement miRNA can be unidirectional but the mechanisms for this directionality are unknown. Transport of miRNAs via PD may play a role in the regulation of Pi responses by modulation of miR399 transport (Reagan and Burch-Smith, 2020).

Evidence points to the fact that specific abiotic stresses can influence PD and symplasmic transport of mobile proteins/ RNA and hormones acting in the control of plant development. Changes in callose or symplasmic transport have been correlated with developmental responses to a wide variety of substances including calcium, aluminium, phosphate, cobalt, nickel and zinc (Peterson and Rauser, 1979; Sivaguru et al., 2000; Müller et al., 2015; Shikanai et al., 2020). In contrast, there are no reports of whether macronutrients nitrate or potassium are associated with changes in symplasmic transport. A pertinent question to consider is how such a system of regulated symplasmic transport fits within the wider regulatory pathways that govern responses to abiotic conditions. PD straddle the domains of the cell wall, PM, ER and cytosol and are the gate keepers that regulate symplasmic flux. These attributes give PD a unique platform to serve as a signalling hub. Indeed, PD regulation is integrated in a broader signalling apparatus that encompasses the whole cell. Recently, a pathway dubbed organelle-nucleus-PD signalling (ONPS) has been proposed tying the regulation of symplasmic transport to the metabolic and signalling pathways occurring in the mitochondria, chloroplasts and the nucleus (Azim and Burch-Smith, 2020). This pathway deserves some introduction as it offers a glimpse into how the regulation of symplasmic transport might control responses to abiotic stress.

The majority of chloroplast and mitochondrial genes are encoded in the nuclear genome and therefore the nucleus requires constant feedback from these organelles in the form of

retrograde signals. Due to the role these organelles play in cell homeostasis, these retrograde signals carry important information about the cellular states. Retrograde signals regulate the expression of a suite of nuclear encoded genes including those involved in sugar transport and stress responses. Retrograde signalling also regulates symplasmic transport. Increased PD density and symplasmic transport was observed when knocking down factors involved in the translation of chloroplast genes such as the *POLYNUCLEOTIDE PHOSPHORYLASE A* (*PNPaseA*) and *INCREASED SIZE EXCLUSION LIMIT 2* (*ISE2*) and other DEAD box RNA helicases such as *RH3* and *RH22* (Ganusova et al., 2020). This finding suggests that retrograde signalling control the nuclear expression of PD regulators which lead to the identification of the ONPS pathway. Interestingly, *ISE2*, *RH3* and other components of chloroplast and mitochondria translation machinery are differentially expressed in development and under biotic and abiotic stress (Nawaz and Kang, 2017). The mutant *rh3* in *Arabidopsis* displays increased sensitivity to cold and when exposed to 100 mM NaCl (Gu et al., 2014). *rh3* displays a wildtype phenotype when grown in 150 mM mannitol indicating that salinity response is not related to water potential. *rh3* mutant has reduced levels of ABA linked with down regulation of nuclear encoded genes involved in ABA synthesis (Lee et al., 2013). Since ABA participates in the regulation of PD communication (Benitez-Alfonso, 2019) is tempting to hypothesise a role for ONPS in this response. Retrograde signalling has also been shown to regulate iron homeostasis (Balparda et al., 2020) and, perhaps, other nutrients. The accumulation of SA, which is partially synthesised in chloroplasts, and ROS is also regulated by retrograde signalling, and both are linked with the regulation of symplasmic transport and root development (Benitez-Alfonso et al., 2009; Patterson et al., 2015; Cui and Lee, 2016a; Wang et al., 2020). To summarise, there is a possible role for ONPS and other pathways regulating PD in the root responses to nutrient and water availability however, this has not been yet investigated.

1.8 Aims and objectives

Examples have been given in this introduction of links between regulated symplasmic transport with root development and responses to abiotic stress. However, our understanding of these pathways is fragmented and is likely to be just a small snapshot of the true nature of these interactions. More broadly, our understanding of how PD function is limited. Only a small fraction of proteins identified in PD proteomes have been experimentally checked for PD localisation and many have had little to no functional characterisation (Supplementary material 1). Identifying proteins with links between symplasmic transport and specific responses to environmental cues is further hampered by the difficult nature of isolating clean PD fractions for proteomic analysis.

The aim of my work was to fill these gaps in knowledge by designing new tools to improve PD protein identification and to address the effect of PD modifications in root development. Abiotic conditions that regulate or are regulated by symplasmic signalling pathways were identified using bioinformatics approaches and symplasmic connectivity was experimentally tested in these conditions. Candidate PD proteins and a mobile factor involved in the regulation of root development were identified and used to dissect the role of PD in the root responses to abiotic conditions.

The specific aims of this project were to:

1. Develop bioinformatics tools for the *in silico* screen of PD proteins and their regulation in response to macronutrient and water availability.
2. Determine the influence of macronutrient and water availability in the regulation of symplasmic transport.
3. Determine the effect of manipulating callose at PD on the regulation of RSA in response to abiotic conditions.
4. Identify novel proteins that regulate symplasmic signalling during the root response to water and macronutrient availability.

Chapter 2 Materials and Methods

2.1 Plant materials and methods

2.1.1 Plant materials

The origin of plant materials used in this thesis are listed in Table 2.1. Seeds of *A. thaliana* were surface sterilised in 70% ethanol for 10 minutes which was replaced with 100% ethanol. Ethanol was immediately aspirated, and seeds were left to dry on sterile filter paper. Seeds were plated individually onto growth media. Media used in this study were based on '*Arabidopsis thaliana* Salts Media' (ATS) (Wilson et al., 1990) and ½ Murashige and Skoog (MS) (Murashige and Skoog, 1962). ATS- and ½ MS-based media were developed with changes in specific nutrients. See Table 2-2 and Table 2-3 for specific composition of each medium used in this study. Media water potential was approximated by summing estimated solute potential of each component of the media. Published data was used to extrapolate solute potential of agar (Ghashghaie et al., 1991), sucrose (Michel, 1972), PEG (MW8000) (Gopal and Iwama, 2007) and mannitol (Michel, 1983). Water potential of all other media components was estimated using the Van 't Hoff equation with the assumption of ideal solution behaviour. In subsequent chapters, figures legends indicate whether media was supplemented with 1% (w/v) sucrose. Plates were stratified at 4°C for 4 days before being transferred to long day light conditions (22°C, 16 h day, 150 mE/m2/s).

Table 2.1 *Arabidopsis thaliana* seed lines used in this work. Notes and references are given regarding the origin of these lines. Unless references are provided, the lines were generated or first characterised during this project. References: 1- Imlau et al., 1999, 2- Levesque et al., 2006, 3-Lin and Schiefelbein, 2001, 4-Simpson et al., 2009, 5-Benitez-Alfonso et al., 2013, 6-Thomas et al., 2008, 7-Hayashi et al., 2008.

Seed stock	Related gene ID	Notes	References
Control lines			
WT (Col-0)			
WT (CR1-7,CR1-8)		WT (no mutation) isolated during CRISPR-Cas screen	
Symplasmic reporters			
pSUC2::GFP			1
pSCR::GFP			2
pGL2::GFP			3
pSUC2::GFP (*svl1*)		*pSUC2::GFP* crossed with *svl1*. Selfed to F3 and genotyped.	
Tagged lines			
p*35S*::YFP-PDCB1 (PDCB1OE)	AT5G61130		4
p35S::YFP-PDCB4 (PDCB4OE)	AT1G69295		4
p*35S*::YFP-PDBG1 (PDBG1OE)	AT3G13560		5
p35S::YFP-PDLP1 (PDLP1OE)	AT5G3980		6
p35S::YFP-SVL1	AT5G55480		
pSVL1::YFP-SVL1	AT5G55480		
Other Reporter lines			
pSVL1::GUS	AT5G55480		7
Knock out/reduced expression lines			
pdcb4 (CR1-5, CR1-7, CR3-4, CR3-7, CR1-5, CR12-2, CR12-9)	AT1G69295	T2 CRISPR lines genotyped to confirm mutation.	
pdbg1	AT3G13560	SAIL_389_H11 (NASC)	
svl1	AT5G55480	SALK_064539 (NASC)	
svl1 pdbg1		F3 genotyped	

Table 2-2 Composition of ATS-based growth media

ATS-based media	
Common to all ATS-based media:	
2 mM $MgSO_4$	0mM K+ ATS
50 mM Fe-EDTA	5 mM $NaNO_3$
70 µM H_3BO3	2.5 mM NaH_2PO_4 (adjusted to pH 5.5)
14 µM $MnCl_2$	2 mM $Ca(NO_3)_2$
0.5 µM $CuSO_4$	0 mM Pi ATS
1 µM $ZnSO_4$	5 mM KNO_3
0.2 µM $NaMoO_4$	2 mM $Ca(NO_3)_2$
10 µM NaCl	2.5 mM KCl
0.01 µM CoCl	
0.8% (w/v) agar (A7921, Sigma)	3% PEG ATS
ATS (control)	5 mM KNO_3
5 mM KNO_3	2.5 mM KH_2PO_4 (adjusted to pH 5.5)
2.5 mM KH_2PO_4 (adjusted to pH 5.5)	2 mM $Ca(NO_3)_2$
2 mM $Ca(NO_3)_2$	3% (w/v) PEG MW 8000
	2 mM $Ca(NO_3)_2$
0.1 mM NO_3^- ATS	3% (w/v) PEG MW 8000
5 mM KCl	75 mM NaCl ATS
2.5 mM KH_2PO_4 (adjusted to pH 5.5)	5 mM KNO_3
0.05 mM $Ca(NO_3)_2$	2.5 mM KH_2PO_4 (adjusted to pH 5.5)
	2 mM $Ca(NO_3)_2$
	75 mM NaCl

Table 2-3 Composition of ½ MS-based media

1/2MS-based media	
Common to all 1/2MS-based media:	0.1 mM Pi 1/2MS
10% MS micronutrient solution (M0529, Sigma)	1 mM KNO3
1.5 mM CaCl2	100 µM KH_2PO_4
0.75 mM $MgSO_4$	0.5 mM KCL
pH adjusted to pH 5.7 with KOH	
0.8% (w/v) agar (A7921, Sigma)	
	2.5 mM Pi 1/2MS
1/2MS (control)	1 mM KNO3
1 mM KNO3	2.5 mM KH_2PO_4
624 µM KH_2PO_4	
	20 µM K+ 1/2MS
0.1 mM NO3- 1/2MS	15 µM KNO3
0.1 mM KNO3	1 mM NaNO3
624 µM KH_2PO_4	624 µM NaH_2PO_4
0.9 mM KCL	
	3% PEG 1/2MS
5 mM NO3- 1/2MS	1 mM KNO3
5 mM KNO3	624 µM KH_2PO_4
624 µM KH_2PO_4	3% PEG 8000
400 mM mannitol 1/2MS	
1 mM KNO3	
624 µM KH_2PO_4	
400 mM mannitol	

2.1.2 Agrobacterium mediated transformation of *A. thaliana*

Agrobacterium tumefaciens carrying the vectors containing the phosphinothricin (PPT) resistance cassette (see section 2.5.5 for more details) were used to transform Col-0 plants via the floral-dip method as described before (Clough and Bent, 1998). T1 transformants were selected by screening resistant plants to treatment with 10 µg/ml PPT (45520, Sigma). Resistant plants were transferred to soil and selfed to at least T2.

2.1.3 Generation of double mutant or reporter *A. thaliana* lines via crossing

A. thaliana flower buds on the acceptor plant (just before they open) were selected for crossing. Under a dissection microscope, fine tweezers were used to remove the calyx and petals. Flowers were then emasculated by the removal of stamen taking care not to damage or transfer pollen to the stigma. After 24 hours, donor stamen was detached and lightly rubbed against undamaged stigmata to transfer pollen. Siliques were left to develop and bagged before shattering. Plants were selfed to F2 generation and genotyped. Double homozygous plants were selfed to F3.

2.2 Bioinformatics

2.2.1 Candidate PD protein pipeline

PD proteomic data for *A. thaliana*, *Nicotiana benthamiana* and *Populus trichocarpa* were retrieved from their original publications (Fernandez-Calvino et al., 2011; Park et al., 2017b; Leijon et al., 2018; Brault et al., 2019) and subfamilies annotated based on PANTHER16 (Mi et al., 2021). A comprehensive list of known PD proteins in *A. thaliana* was assembled by identifying published reports of tagged proteins displaying characteristic punctate co-localisation with aniline blue via confocal microscopy or clear PD localisation via immunogold labelling with electron microscopy (Supplementary material 1). The proteomes and list of known PD proteins were incorporated into a pipeline using a custom-built R script (https://github.com/PhilPlantMan/PIP1). Instructions on how to use the pipeline are included in the GitHub repository along with instructions on how to customise pipeline parameters depending on user requirements. Necessary databases including the PD proteomes used here are packaged with the script.

The script dependencies include the R library 'biomartr' (Drost and Paszkowski, 2017). Protein features were predicted using the R library 'ragp' (Dragićević et al., 2020). This tool uses SignalP (Emanuelsson et al., 2007; Almagro Armenteros et al., 2019) and Phobius (Käll et al., 2007) to predict possession of a SP and PredGPI (Pierleoni et al., 2008) and NetGPI (Gíslason et al., 2019) to predict possession of a GPI anchor. The tool ragp was also used to predict subcellular localisation via TargetP (Almagro Armenteros et al., 2019). Genes were classified as having a GPI anchor and/or SP if at least one tool returned true for that feature. TM domains prediction was acquired from the ENSEMBL database annotation via the R package 'biomartr' using TMHMM (Krogh et al., 2001). Predictions

for N-myristoylation, S-farnesylation, S-geranylgeranylation, S-palmitoylation and S-nitrosylation were made using tools available by the Cuckoo workgroup (Xue et al., 2010; Xie et al., 2016; Ning et al., 2020). For protein feature enrichment analysis, the tools described above were used to predict features for the whole *A. thaliana* genome (Araport11). Fisher's exact test was used to determine statistical significance (cut-off provided in figure legends). To be fully pipeline-compatible for proteome input or to generate candidate gene output, the species must be listed in both Ensembl Plant databases (used by biomartr to retrieve sequence information) and in PANTHER16 (used to retrieve subfamily annotation) (Drost and Paszkowski, 2017; Howe et al., 2020; Mi et al., 2021). Currently, there are 22 compatible plant species (Supplementary material 2). For non-compatible species, such as *N. benthamiana*, *Arabidopsis* orthologues can be used. This enables integration of the PD proteome of Park et al. (2017) in the pipeline.

Lists of genes were compared by drawing a Venn or Euler diagram using the R library 'eulerr'. The significance of the overlap between candidate lists and proteomes was determined using bootstrap analysis as follows. Sets of genes the same length as a candidate list and a proteome were randomly sampled from Araport11. The overlap in genes between the samples was recorded and repeated for n cycles (n = 10,000). Probability (p) was calculated as the proportion of cycles that attained an overlap at least as large as was observed between the candidate list and the proteome. The size of the overlap by chance was given as the median overlap in random samples over n cycles. Overrepresentation analysis was performed in R using pairwise comparisons using Fisher's exact test. Multiple testing was corrected by Holm's Step-Down Procedure unless otherwise stated in the figure legend.

2.2.2 Co-expression analysis between candidate genes and known PD genes

The gene correlation dataset 'Ath-u.c1-0' was downloaded from the ATTEDII database (Obayashi et al., 2018). Optimal gene order and the corresponding dendrograms were computed using hierarchical clustering. The dendrogram was cut at an optimised height (h = 16) that gave a sufficient number/size of clusters (k = 151). These processes were performed in base R. Enrichment of genes within clusters from candidate lists and verified genes were determined using pairwise comparisons with Fisher's exact test ($p<0.05$, holm-adjusted) via the R library 'rcompanion '. For network analysis, pairwise correlation data were compiled and exported for *A. thaliana* PD candidates using R. The network of <1000

genes (nodes) and <300,000 interactions (edges) was fed into Cytoscape (Shannon *et al.,* 2003) with correlation set as the edge attribute.

2.2.3 Microarray expression analysis

Publicly available microarray data for *A. thaliana* were independently analysed by this author and Dr Sam Amsbury for a subset of conditions. This was also performed in *M. truncatula* by Liam German. Details about the conditions and source of microarray experiments are listed in Supplementary material 3. Microarray datasets were downloaded from EBI ArrayExpress. For each experiment, expression data were normalised using the robust multi-array average (RMA) method and $\log_2$ transformed with the R package 'oligo' (Carvalho and Irizarry, 2010). Principal component analysis was used to identify and exclude outlier arrays and experiments with insufficient biological replicates. Genes with low levels of expression were filtered out. A design matrix was constructed for each experiment and a linear model applied using the R package 'limma' (Ritchie et al., 2015). Differential expression of genes and a multiple comparison correction were determined using empirical bayes statistics via the package 'limma' and the results filtered by gene IDs. Heatmaps were constructed using the R package 'ComplexHeatmap' (Gu et al., 2016).

2.2.4 Determination of differential enrichment of metabolites between plant lines

Metabolic profiles were received that contained a list of metabolites with normalised mass spectrometry reads for each biological sample. Metabolic profiles of different plant lines were analysed by partial least squares discriminant analysis (PLS-DA) using MetaboAnalyst4 (Chong et al., 2019). One of the outputs of MetaboAnalyst4 is a 3D-component analysis that plots each biological sample on axes relating to the 3 components which account for most of the variation in the data. Another output of MetaboAnalyst4 is a weighted sum of absolute regression coefficients of the most important component. This gives the relative contribution of each metabolite to the total variation and can be used to establish the most important metabolic features. Enriched metabolites were fed into a 'smart table' on the online platform Plant Metabolic Network 15 (Hawkins et al., 2021). Using this tool, statistical enrichment of metabolic pathways was determined by Fisher's exact test. Pathways that contained only 1 metabolite of interest were excluded. Only 1 pathway was included for those pathways where the same set metabolites of interest were represented.

2.2.5 Peptide sequence alignment and phylogenetic analysis

Peptide sequences of related proteins were downloaded from The *Arabidopsis* Information Resource (TAIR). Sequences were aligned using the MUSCLE algorithm using default parameters using UGENE (Okonechnikov et al., 2012). The alignment file generated was used to build a phylogenetic tree using the PHYLIP neighbour joining method using default parameters via UGENE. Screengrabs of the resulting tree and the original alignment were pasted together using generic image editing software.

2.3 Microscopy techniques

2.3.1 Confocal and epifluorescence microscopy

Confocal microscopy was performed with a LSM800 (Zeiss, Germany) upright microscope. Pinhole size was set first set 1 airy unit (unless otherwise stated) and adjusted to ensure optical slices were the same thickness between channels. Specific laser and detection settings for every fluorochrome used in this study are described in Table 2-4. For determining symplasmic movement of GFP within symplasmic reporters, seedlings were mounted in 100 µg/ml propidium iodine solution (PI, P4864, Sigma) used as counterstaining. Primary roots were imaged by confocal microscopy ensuring that the optical plain was focused onto the centre of root. Seedlings were discarded if substantial damage was apparent from internalisation of PI stain. For colocalisation with aniline blue assays, cotyledons or hypocotyls of plants expressing fluorescently tagged proteins were excised and mounted onto microscope slides in aniline blue fluorochrome solution (33 µg/ml aniline blue fluorochrome (100-1, Biosupplies, Australia), 0.1 M K_3PO_4 pH 12.0). Samples were imaged by confocal microscopy using a 405 nm laser. Growth conditions and age of plants are described in figure legends. Epifluorescence microscopy was performed with BH2 (Olympus) fitted with a QIMAGING camera (Canada).

Table 2-4 Confocal microscope settings for each fluorochrome used in this study.

Fluorochrome	**Laser**	**Detector used**	**Detection range (nm)**
GFP	Argon 488 nm	Spectral imager	508-570
YFP	Argon 488 nm	Spectral imager	508-570
mCherry	DPSS 561 nm	PMT	580 - 695
Propidium iodide (PI)	DPSS 561 nm	PMT	595-735
Aniline blue (AB)	Diode 405 nm	Spectral imager	428-500

2.3.2 Transmission light microscopy

Samples to be imaged were mounted in water on glass slides with a coverslip. Slides were imaged on a Axio microscope (Zeiss, Germany) with or without differential interference contrast microscopy (DIC, see figure legends).

2.3.3 Dye-loading symplasmic transport assay

Seedlings 7 days post germination (dpg) were mounted in water onto glass lights with a cover slip covering the entirety of the root. 10µl pipette tips were trimmed and preloaded with 500 µg/ml 5-Carboxyfluorescein diacetate (CFDA, C4916, Sigma) solution (from 5 mg/ml in acetone stock) with the solution kept in place by surface tension. One cotyledon was excised, and the remaining petiole was quickly inserted into the narrow end of the tip to minimise an air bubble forming in the vasculature. The tip was secured to the slide by Blu Tack®. The slide was tilted so the tip was elevated relative to the root between imaging. Root tips were imaged under an epifluorescence microscopy at several timepoint over the course of an hour.

2.3.4 Histological analysis of promotor activity

Seeds expressing β-glucuronidase (GUS) the SVL1 promoter (Hayashi et al., 2008) were grown for 8 days on 0.1 mM and 9 mM nitrate ATS with and with 1% sucrose (4 treatments in total). Seedlings were harvested into ice-cold 90% acetone. Samples were vacuum infiltrated (200 mbar for this and subsequent infiltration steps) for 10 minutes at room temperature. The pressure was equalised, and samples were fixed at room temperature for a further 20 minutes. The acetone solution was aspirated and replaced with assay buffer (100 mM phosphate buffered saline (PBS) pH7, 0.5 mM potassium ferrocyanide, 0.1 mM potassium ferricyanide, 10 mM EDTA, 0.1% (v/v) Triton X-100). Samples were vacuum infiltrated in assay buffer until bubbles started to form in the solution. The pressure was equalised. The assay solution was aspirated and replaced with ice-cold X-gluc solution (assay solution, 0.25 mg/ml 5-Bromo-4-chloro-3-indolyl-β-D-glucuronide (B4527, Sigma). Two cycles of vacuum infiltration and pressure equalisation were performed. Samples were incubated at 37°C for 3 hours or until the blue colour develops. The X-gluc solution was removed and samples were sequentially incubated in 20%, 35% and 50% ethanol at room temperature with 30 minute incubations between each step. Samples were stored in 70% ethanol at 4°C until imaged. The ethanol was gradually replaced with water in 10% decrements with 10 minutes incubations between each step. Samples were

mounted on glass slides and imagined on a microscope with (Axio, Zeiss, Germany) using DIC.

2.4 Image analysis

2.4.1 Quantification of GFP diffusion in root tips

Confocal images of roots expressing symplasmic reporters and stained with PI were analysed in a novel image analysis pipeline. Profiles of fluorescence were determined using line and profiling tools in ImageJ combined into a custom ImageJ plugin (Supplementary material 4). Lateral profiles were taken across the transition zone. Rootward profiles started from the basal/apical meristem transition zone ending 150 µm towards the root tip. The ImageJ plugin outputs a comma separated value (CSV) file for each image. A directory was made containing all the CSVs for each treatment/profile type. A custom python script was developed that aggregates and plots the profiles (Supplementary material 5). The script is pointed to the directories to be analysed. If normalisation is set to true, the script scales the range in fluorescence between 0 and 1. Fluorescence across each lateral profile was binned (bins = 100, aggregated by mean) to compensate for small differences in root width. Fluorescence profiles of at least 6 plants per treatment were aggregated by calculating the mean (±SD) for each binned position along the profile and plotted.

2.4.2 Semi-quantification of fluorescence in the root

Seedlings mounted on glass slides in 10 µg/ml PI. Roots were imaged in the elongation zone using an LSM 800 upright confocal microscope (Zeiss, Germany) ensuring the focus achieved an optical slice through the centre of the root. The same imaging conditions were maintained for all samples. Images were processed in ImageJ. The PI channel was used as a guide to draw a rectangular region of interest (ROI) over the length of the stele within the elongation zone. The mean fluorescence of the ROI in the YFP channel was measured. The sample size of each treatment was 3. ANOVA with Tukey post hoc test was performed to determine statistical differences in between treatments.

2.5 Molecular biology techniques

2.5.1 Standard PCR

Standard PCR was performed using DreamTaq according to the manufacturer's instructions (Thermofisher, USA) in 20 µl reactions with 200 µM dNTPs and 1 µM forward and reverse primers. See Table 2-5 for thermocycler settings. Primer pairs, annealing temperatures and product length are listed in Supplementary material 6.

Table 2-5 Standard PCR thermocycler conditions

Temperature (°C)	**Time (min)**	**Cycles**
95	2	1
95	0.5	25-30
60-65	0.5	
72	1 min/kb	
72	10 minutes	1
	Hold at 10°C	

2.5.2 RT-PCR conditions

Leaves were excised and sealed in separate 1.5 ml microcentrifuge tubes and immediately submersed in liquid N_2. Samples were removed from liquid N_2 and ground with micro pestles in 1x RNA Protection Reagent from the Monarch® Total RNA Miniprep Kit (NEB BioLabs, USA). This kit was used in subsequent RNA extraction steps according to manufacturer's instructions. RNA concentration was measured using a spectrophotometer (Nanodrop 1000, Thermofisher, USA). RNA concentration was equalised to the lowest RNA concentration with nuclease free water. cDNA was generated using QuantiTect Reverse Transcription Kit (Qiagen, Germany) according to manufacturer's instructions. RT-PCR was performed as described in the 'Standard PCR' method described above using 25 amplification cycles. RT-PCR primers and annealing temperatures are listed in Supplementary material 6.

2.5.3 Agarose gel-electrophoresis

DNA was resolved on 1% agarose gel (1% (w/v) agarose; 1X tris-acetate EDTA buffer; 1x Midori green; Nippon-Japan) at 90 V. Gels were imaged on a GBox transilluminator (SynGene , UK).

2.5.4 *Arabidopsis thaliana* DNA extraction

Plant material was harvested into 1.5 microcentrifuge tubes on ice. While on ice, 200 µl of extraction buffer (200 mM Tris-HCl pH7.5, 250 mM NaCl, 25 mM EDTA, 0.5% (w/v) SDS) was added. Tissue was ground in the tube with a clean micropestle. All remaining steps were performed at room temperature. Samples were centrifuged for 5 min at 13,500 rpm. The supernatant was transferred to a clean Eppendorf containing 200 µl of isopropanol. Tubes were transferred to -20 °C for a minimum of 2 hours and centrifuged for 5 min at 13,500 rpm. Supernatant was replaced with 500 µl of 70% (v/v) ethanol and inverted several times. Samples were centrifuged for 5 min at 13,500 rpm. The supernatant was aspirated, and the pellets were lightly covered with tissue paper and allowed to dry overnight. The DNA was resuspended in 200 µl of molecular-grade water (W4502, Sigma).

2.5.5 Targeting mutations to native *PDCB4* using CRISPR-Cas9

CRISPR-Cas9 targets were generated using the web-tool ChopChop (Labun et al., 2019). The most likely sites that non homologous end joining (NHEJ) will cause a mutation are 3-6 bp upstream from the protospacer adjacent motif (PAM) (Fauser et al., 2014). Restriction enzyme binding sites within this region were listed for the 50 highest ranked candidate targets (ranked by ChopChop predicted CRISPR-Cas9 efficiency) using SnapGene software (USA). Of the 50 targets, 9 contained at least one restriction binding site within the mutation zone. For each enzyme represented, restriction fragment length polymorphism (RFLP) patterns were predicted *in silico* using SnapGene for a single digestion of a 1300 bp amplicon of *PDCB4* (See Supplementary material 6 for primer sequences). The predicted RFLP pattern was used to select one target based on the ease at which the different fragments would be resolved via gel electrophoresis. The target chosen contained a BstY1 site within the mutation zone. A plant transformation T-DNA plasmid (pDE-Cas9) harbouring the CRISPR-Cas9-related machinery and the single guide RNA (sgRNA) specific for the PDCB4 target were generated following the protocol described in Fauser et al. (2014). The protospacer oligos designed for the PDCB4 target are listed in Supplementary material 6. The process is outlined in Figure 2.1. The

transformation plasmid pDE-Cas9 was transformed in *A. tumefaciens* by electroporation via a MicroPulser (BioRad, USA) according to the manufacturer's instructions. Colony PCR was performed as described by Fauser et al. (2014). *A. thaliana* Col-0 plants were transfected via floral dip and selected using PPT (see section 2.1.2). Resistant plants were transferred to soil and selfed to T2. To screen T2 lines that had lost the Cas9/PPT resistance cassette, seeds were germinated on ATS + 1% (w/v) sucrose + 10 µg/ml PPT. After 7 days, visibly stunted seedlings were transferred to ATS + 1% (w/v) sucrose + 2 mM glutamine. These 'PPT-rescued' seedlings were allowed to recover for 5 days before being transferred to soil. Plants were genotyped using primers SS42 and M13 as described in Fauser et al. (2014) to ensure that the plants do not contain the Cas9 cassette. To screen for plants with probable mutation, gDNA of each plant was extracted from the leaves and a 1300 bp portion of *PDCB4* was amplified by PCR. The PCR product was digested with BstY1 (NEB, USA) in a 15 µl reaction with NEBuffer 2.1 at 60 °C for 15 minutes as described in the manufacturer's instructions. The digests were resolved via gel electrophoresis. Lines with fragments with a length of 315 and 1015 were deemed likely to have a desired mutation. The 1300 bp *PDCB4* fragment associated with these lines was sent to GATC (LightRun) for Sanger sequencing using the forward primer the fragment was generated with.

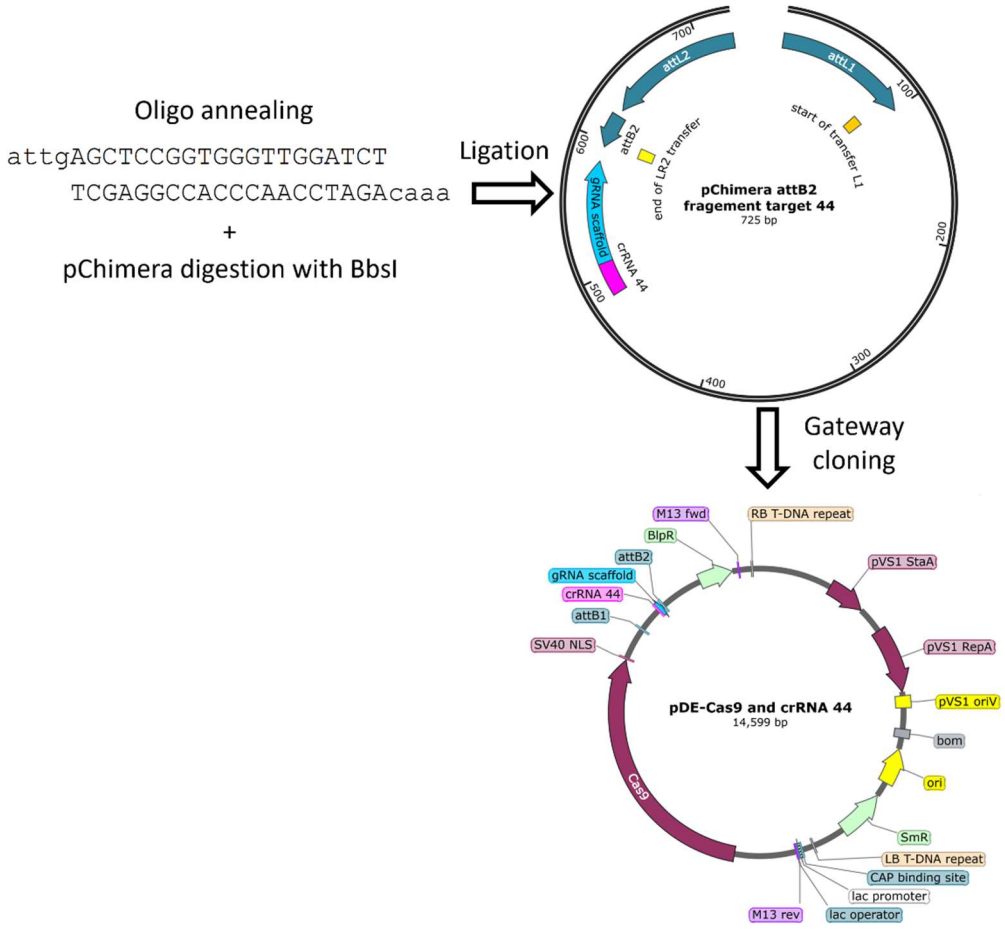

Figure 2.1 Generation of the T-DNA plant transformation plasmid harbouring Cas9 machinery and single guide RNA specific to PDCB4. The protocol is described in (Fauser et al., 2014).

2.6 Phenotyping *A. thaliana* seedlings

2.6.1 Root architecture trait determination

A. thaliana seeds were sown onto agar-based media in 2 horizontal lines of 15 seeds on clear, vented 120 mm^2 plates (Greiner, Austria). At specified time points, plates were imaged on a flatbed scanner (Perfection V370, Epsom). Images were used to reconstruct root architectures in a semi-automated fashion using RootNav (Pound et al., 2013). RootNav Viewer was used to export raw root length and tortuosity data. A custom python script (Supplementary material 7) was made that processed these data to produce primary root length, total lateral root length, lateral root number and emerged lateral root density. Pairwise comparisons between lines/treatments were made by ANOVA with Tukey post hoc test.

2.6.2 Root meristem size determination

A. thaliana seeds were sown onto agar-based media for 4 days. Seedlings were transferred onto slides and mounted in 1% (w/v) PI. Roots were imaged by confocal microscopy. The distance and cortical cell count between the TZ and QC were taken as measurements of meristem size as performed by Ubeda-Tomás et al. (2009). Pairwise comparisons between lines/treatments were made by ANOVA with Dunnett's post hoc test.

2.6.3 Stomatal density determination

True leaves were excised and cleared in 70% ethanol at 50°C for 1 hour. The ethanol was replaced with PBS and stored at 4°C for a short amount of time until required. Leaves were mounted onto glass slides and imaged on a microscope (Axioscope, Zeiss, Germany) using DIC. Stomata were counted on 4 random 0.25 mm^2 areas of each leaf. 5 leaves from independent plants were measured for each treatment. Pairwise comparisons between lines/treatments were made by ANOVA with Tukey post hoc test.

2.6.4 Cell wall glycome profiling

Roots and shoots (from 8 dpg seedlings) were pooled separately and quickly submersed in liquid N_2 to minimise further changes to cell wall composition. Plant material was freeze dried overnight. Alcohol Insoluble Residue (AIR) and cell wall extracts were prepared as described by Cornuault et al. (2018) with the exception that the first extraction with distilled water was not performed as this part of the protocol was deemed unnecessary. Extracts at varying dilutions with PBS (1:1, 1:5, 1:25) were used to coat enzyme-linked immunosorbent assay (ELISA) plates overnight at 4°C ensuring that there are two coated wells for each line and antibody used plus two extra wells for a negative antibody control. In total 39 antibodies for different cell wall epitopes (described at PlantProbes, UK) were used. Plates were washed by inverting the plate and flicking out the content, briefly submerged in lukewarm-cold water, followed by water flicked out. This wash step was repeated 3 times, rotated in the hand 180° and repeated a further 3 times. Plates were thoroughly dried by hitting against a stack of blotting paper. Plates were then blocked in 5% milk/PBS for 1 hour at room temperature. Plates were washed and dried as above. Plates were incubated in 1° antibody (1:10 antibody: 5% milk/PBS) for 1 hour and room temperature and washed then dried as before. Plates were incubated in 2° antibody (used 1:1000 HRP anti-mouse conjugate: 5% milk/PBS) for 1 hour at RT then washed and dried as before. The signal/ binding was revealed by adding 150 µl of substrate (0.1 M sodium

acetate buffer, pH 6, 1% tetramethyl benzidine, 0.006% H_2O_2) per well. The reaction was stopped by addition of 40 µl 2.5 M H_2SO_4 to each well. The absorbance of each well was read at 450 nm using a plate reader (Multiskan, Thermo Scientific).

2.6.5 Statistical analysis: Pairwise comparisons

Pairwise comparisons of parametric data were determined by ANOVA with Tukey post hoc test. Pairwise comparisons of non-parametric data were determined by Kruskal–Wallis with Dunn post hoc. Tests performed in python were using the 'Statsmodels' module (Seabold and Perktold, 2010). Pairwise comparisons in python were converted to a letter-based representation by a custom python tool based on Piepho (2004). The tool can be accessed from https://github.com/PhilPlantMan/Python-pairwise-comparison-letter-generator. In R, pairwise comparisons were made using the libraries 'rcompanion' and 'multcompView' (Graves et al., 2015; Mangiafico, 2018).

Chapter 3 PIP1: A comparative meta-proteomic analysis pipeline for identification of plasmodesmata associated proteins

3.1 Summary

Proteomic isolation and sequencing of PD enriched plasma membrane fractions have been achieved in few model species including *Arabidopsis thaliana*, *Nicotiana benthamiana* and *Populus trichocarpa* (poplar) (Fernandez-Calvino et al., 2011; Park et al., 2017b; Leijon et al., 2018; Brault et al., 2019). Studies of proteins identified in these screens have improved our understanding of how PD function and the conditions affecting their regulation. For example, Brault et al. (2019) identified several MCTPs in their *Arabidopsis* PD proteome and studied these using a combination of electron microscopy, mutational studies and heterologous expression in yeast. The researchers determined that MCTPs tether the ER to the plasma membrane PM at PD and are required for their functioning in symplasmic transport. Experimental determination of PD proteomes has mainly been performed on cell cultures, which do not reflect the complex spatial and temporal dynamic nature of PD during plant development and in response to the environment. Even in this simplified system, PD fractions are often contaminated with non-PD structures such as the PM, cell walls and the ER (Brault et al., 2019). Inclusion of non-PD cellular domains within PD proteomes introduces proteins that have no specific association with PD such as AT5G59700 identified in the proteome of Fernandez-Calvino et al. (2011) which show uniform PM-distribution (instead of a punctate PM distribution characteristic of PD) when studied using confocal microscopy of *A. thaliana* leaves expressing a fluorescently tagged-fusion (Fernandez-Calvino et al., 2011). These non-PD proteins dilute the PD proteome and make it more difficult and resource intensive for workers to identify true PD proteins.

This chapter introduces the first publicly available tool to generate *in silico* PD proteomes in a species of interest. This resource aims to overcome some of the limitations that restrict the identification of new PD proteins in species where experimental data is not available. This R-based tool is named Plasmodesmata *in silico* Proteome 1 (PIP1). PIP1 is in the public domain and is able to integrate experimentally determined PD proteomes to aid the identification of new PD proteins in a variety of plant species (Kirk et al., 2022). In brief, PIP1 pulls all genes from an online database (PANTHER16) that encode proteins belonging to families or subfamilies represented in experimentally determined proteomes. The genes identified are then categorised according to the number of times in which the protein families/subfamilies they encode appear in PD proteomes and whether they contain features found here to be overrepresented in proteins with confirmed PD localisation.

These features are the presence of an SP, transmembrane domains (TM, which binds the protein to the membrane) or GPI anchor. Various tools exist to predict whether a protein contains a SP (Käll et al., 2007; Owji et al., 2018; Almagro Armenteros et al., 2019) or a TMs (Krogh et al., 2001 ; Gee et al., 2018). Translated proteins able to undergo GPI modification contain a conserved C-terminal 25-30 amino acid GPI attachment signal that can be predicted based on amino acid sequence (Pierleoni et al., 2008; Zavaliev et al., 2016; Gíslason et al., 2019). GPI anchors can specifically target proteins to PD and known PD proteins that have a GPI include PDBGs and PDCBs (Levy et al., 2007; Simpson et al., 2009; Zavaliev et al., 2016). GPI can be cleaved allowing the protein to move in the apoplast untethered (Schindelman et al., 2001).

PIP1 was used to screen for novel PD-localising proteins in *A. thaliana* and *M. truncatula*. Co-expression analysis suggests that many PD proteins and candidates interact at the transcriptional level which may extend to functional and direct interactions between PD proteins. Geno ontogeny (GO) term over representation analysis and expression analysis highlighted biotic and abiotic conditions that caused differential expression of a wide range of known PD proteins and proteins which have not been previously associated with symplasmic transport like GALACTURONOSYL-TRANSFERASE 4 (GAUT4); a gene involved in pectin biosynthesis (Lund et al., 2020).

To summarise, PIP1 is able to predict PD proteins for species where experimental proteomic information is not available and help to prioritise the validation of targets identified in experimental proteomes. PIP1 is publicly accessible (https://github.com/PhilPlantMan/PIP1) and can be easily modified by the user to add new sequenced proteomes and/or experimentally verified genes thus will serve as a long-lasting resource for the plant community. Candidates generated by PIP1, and conditions highlighted in this chapter form the basis to subsequent chapters that look to characterise how abiotic conditions affect symplasmic transport and which factors are involved in these processes.

3.2 Results

3.2.1 Design of a pipeline to screen candidate PD proteins in multiple plant species.

Meta analysis of different PD proteomic studies has the potential to separate proteins with real PD association from those that originate from contamination. PD proteomic data was extracted from the literature and relates to the species *Arabidopsis thaliana* (Fernandez-Calvino et al., 2011; Brault et al., 2019), *Nicotiana benthamiana* (Park et al., 2017b) and *Populus trichocarpa* (Leijon et al., 2018). As this data is derived from multiple species it cannot by compared on a gene-level basis. PANTHER is a platform that uses a combination of manual curation and homology to assign genes to a family, a subfamily and to GO terms (Mi et al., 2021). Comparison of PANTHER subfamilies identified in the different proteomes unveiled a large overlap: between 38-80% of families and 25-57% of subfamilies represented in at least one other proteome (Figure 3.1). It is likely that the occurrence of a family or subfamily in multiple PD proteomes is a function of how likely those groups contain bona fide PD proteins and therefore could be used as a method to filter a collection of proteins and narrow down candidates. There is less functional disparity between subfamily members relative to members of a family therefore subfamily membership was deemed a more appropriate attribute to grade candidate PD proteins by. A pipeline was developed that, for a given species genome, extracts all members of subfamilies represented in PD proteomes (Figure 3.2).

Genes are classified by the number of proteomes the subfamily appears in and whether they encode proteins that contain features enriched in experimentally verified PD proteins. The protein features used in the pipeline were selected from predictions in the 62 *A. thaliana* proteins that have published PD localisation (see Supplementary material 1 for lists of genes with references). Publicly available tools were used to predict 8 types of protein feature for the whole *A. thaliana* genome: SP, TM, GPI, N-myristoylation, S-farnesylation, S-geranylgeranylation, S-palmitoylation and S-nitrosylation. Overrepresentation analysis was performed comparing features present in verified PD genes in comparison to the wider genome. PD-localised proteins were found to be overrepresented with GPI anchors, SP and TM domains and, to lower level of significance, s-geranylgeranylation and s-palmitoylation (Figure 3.3). The combination of either the presence of a SP, GPI or TM domain returned the highest proportion of verified PD proteins thus was implemented in the pipeline to classify candidate PD proteins.

This pipeline can be applied to most species that are listed in PANTHER16 (see Supplementary material 2 for a list of compatible species). For a given species, the pipeline identifies all proteins that are present in a subfamily represented in any PD proteome, categorises the protein by whether the subfamily is present in one or multiple PD proteomes and then further classifies candidates based on whether the protein is predicted to have at least 1 feature that is greatly over represented in verified PD proteins (SP, GPI or TM). As a result, the pipeline outputs 4 lists of genes: PIP-A are genes of subfamilies present in more than one PD proteome containing either a SP, GPI or TM domains; PIP-B are also present in multiple proteomes but lacking distinctive membrane localising features, PIP-C and PIP-D are genes in subfamilies found in a single proteome either with (PIP-C) or without (PIP-D) any predicted SP, GPI or TM features. An automated version of the PIPI pipeline was implemented in R. PIPI is flexible and proteomes can be added or removed at will. PIPI can be set to pull proteins for a given species based on family or subfamily representation in PD proteomes and determines orthologues of verified PD genes (provided as a user-editable spreadsheet) for a given species. Users are also prompted to set the minimum number of PD proteomes required to classify candidates as PIP-A or PIP-B; in this chapter, the minimum number is set as the default (≥2). PIPI also annotates genes with other useful information including how many proteomes the subfamily appears in (counts), how many times the subfamily appears in PD proteomes (sum), the size of the family and the size of the subfamily. Users can also provide gene data such as transcriptomes (in a spreadsheet format) which PIPI will cross-reference with the pipeline outputs.

To demonstrate its functionality, PIPI was used to generate candidates for various species. The output is summarised in Table 3.1. For *A. thaliana*, the *in silico* proteome (the aggregation of PD candidate lists) is presented in Supplementary material 8 and contains 64% of the genes known to localise at PD (Supplementary material 1). PIP-A (subfamilies present in multiple proteomes and displaying predicted membrane targeting features) is most likely to contain PD localised proteins but PIP-B and PIP-C cannot be discarded. For *Arabidopsis*, 9.2% of PIP-A proteins (generated based on subfamilies) have already been verified to be PD proteins. For PIP-B and PIP-C, 0.5% and 2.1% of these proteins have already been verified as PD proteins respectively. PIP-D did not contain any verified genes suggesting this list may contain a high proportion of contaminants. PIP-B contained one verified gene suggesting that PD proteins might have alternative targeting signals not predicted by the available bioinformatics tools.

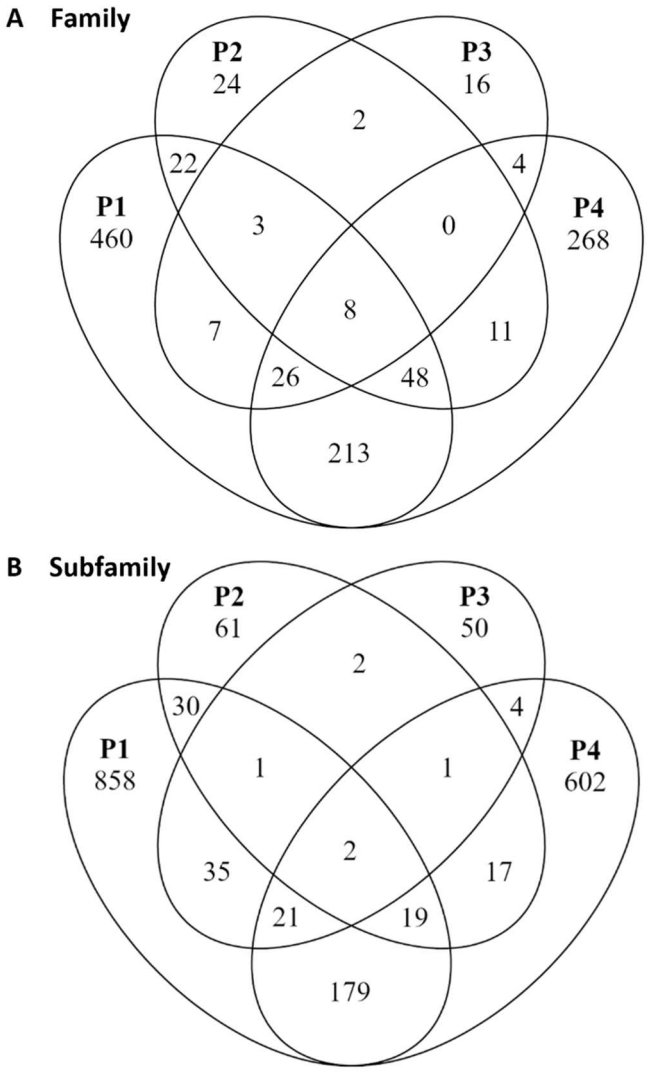

Figure 3.1 Publicly available PD proteomes overlap considerably in family and subfamily composition. Venn diagrams of (A) family and (B) subfamilies represented in experimentally determined PD proteomes (P1: Fernandez-Calvino et al., 2011, P2: Park et al, 2017, P3: Brault et al., 2019 and P4: Leijon et al., 2018). PANTHER16 was used to annotate subfamily identity.

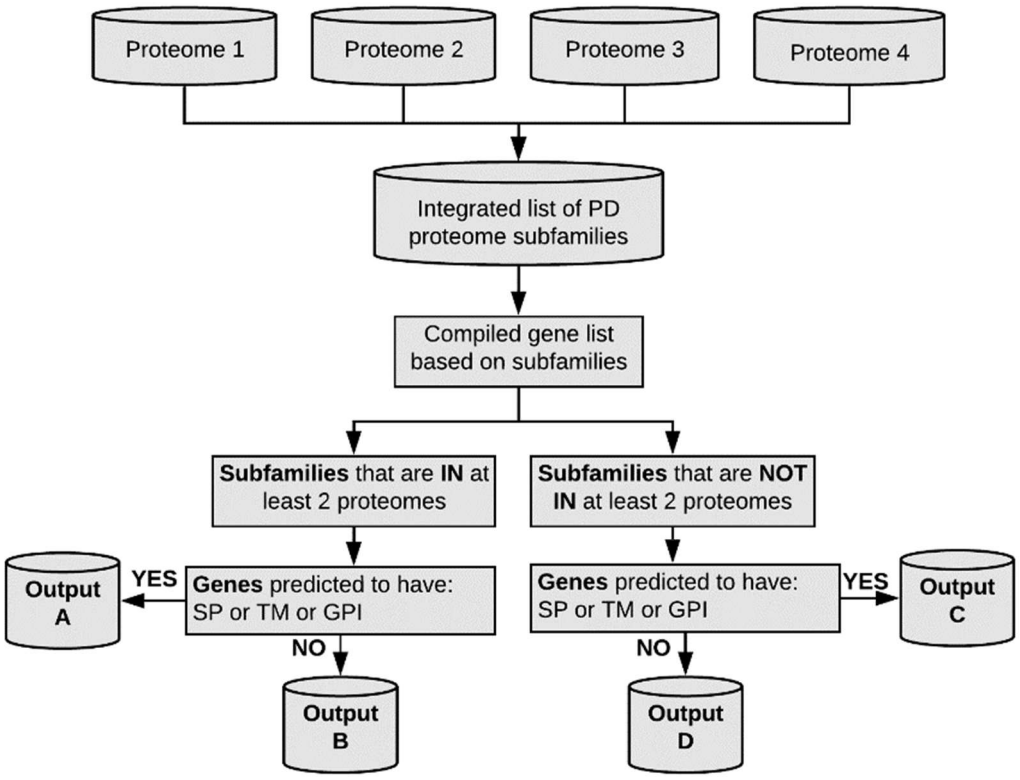

Figure 3.2 Schematic used by PIP1 to generate and classify candidate PD proteome. 4 proteome databases have been determined experimentally by Fernandez-Calvino et al. (2011); Park et al. (2017); Brault et al. (2019) and Leijon et al. (2018). A list was compiled of subfamilies of proteins identified in the different experimental proteome databases using PANTHER16. Genes belonging to these subfamilies were extracted for the target plant species. Genes were classified by whether its subfamily was present in at least two PD experimental proteomes or just one. Further classification was based on whether genes were predicted to have a signal peptide (SP), transmembrane domain (TM) or glycophosphatidylinositol anchor (GPI) as these features are enriched in verified PD genes (Figure 3.3). As a result, 4 list of genes were obtained (PIPA-D) representing the predicted PD proteome for the target plant. An automated version of this pipeline was implemented in R and is named Plasmodesmata *in silico* Proteome 1 (PIP1).

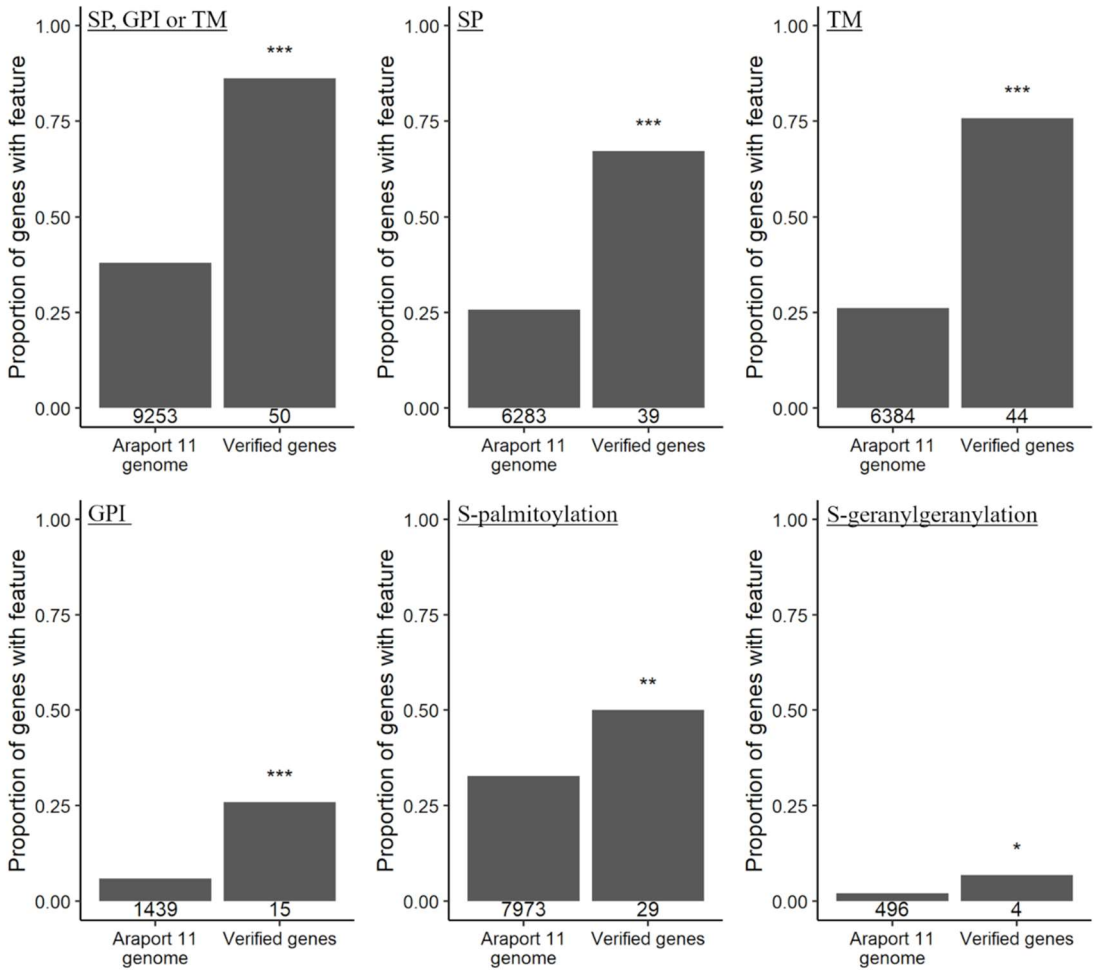

Figure 3.3 Verified PD proteins are over represented in features relating to secretion and membrane targeting. Publicly available protein prediction tools were applied to peptide sequences encoded by the whole *A. thaliana* genome. The proportion of verified PD genes with signal peptide (SP), glycophosphatidylinositol anchor (GPI), transmembrane domain (TM), s-palmitoylation or s-geranylgeranylation was compared against the wider genome (Fisher's exact test, *: $p \leq 0.05$, **: $p \leq 0.01$, ***: $p \leq 0.001$). The number of proteins that are predicted to have the given feature are displayed underneath each column. Other protein features listed in the materials and methods were not found to be significantly overrepresented in verified PD proteins (not shown). The specific s-palmitoylation prediction is 'cluster C' predicted using GPS-Palm (Ning et al., 2020). The specific S-geranylgeranylation prediction is 'cccxc' predicted using GPS-Palm (Xie et al., 2016). See materials and methods for further details.

Table 3.1 PD candidate protein counts generated by PIP1 for a subset of available species. PIP1 was used to generate candidate PD proteins for 3 dicot species (*A. thaliana, M. truncatula, P. trichocarpa, L. lycopersicum*) and a monocot species (*T. aestivum*). Candidates are separated into lists (PIPA-D) based on whether the protein is predicted to have a SP, GPI or TM (lists A and C) and whether the subfamily is represented in 1 (lists C and D) or ≥2 (list A and B) PD proteomes. See Supplementary material 2 for a list of all compatible species.

PD candidate lists	PIP-A	PIP-B	PIP-C	PIP-D
SP, GPI or TM?	Yes	No	Yes	No
Num. PD proteomes	≥2	≥2	1	1
Arabidopsis thaliana	206	208	751	1117
Medicago truncatula	219	244	799	1106
Populus trichocarpa (poplar)	358	299	1124	1706
Solanum lycopersicum	133	134	455	710
Triticum aestivum	329	272	1206	1668

3.2.2 PIP1-generated *in silico* proteomes align with experimentally determined proteomes.

Comparing an experimentally determined PD proteome with an *in silico* proteome was used to validate PIP1. All candidate PD genes lists generated for poplar exhibited a larger overlap with the experimentally determined PD proteome reported by Leijon et al. (2018) than what would be expected by chance (Figure 3.4 A). 1032 out of 1148 genes/proteins identified in the PD-enriched fraction of poplar cell cultures were identified as candidates by PIP1 (Figure 3.5). The 116 proteins present in the experimental proteome but not in the candidate lists correspond with subfamilies not annotated in the PANTHER16 database.

The *in silico* PD proteome of poplar contains 3 times as many proteins as the experimentally determined proteome. The overlap of PIP-A (the priority list) and PIP-B with the experimentally determined proteome is between 45-50%; an overlap 19x and 15x larger than what would be expected by chance respectively (Figure 3.4 A). The strength of PIP1 to generate candidate PD proteins can be simulated by excluding the poplar PD

proteome from PIPI and then comparing the resulting candidate PD proteins to the poplar PD proteome. It is worth noting that given the few proteomes available, eliminating one from the pipeline would be expected to diminish its predictive value considerably. Nevertheless, the overlap between PIP-A and PIP-B generated by this 'abridged' pipeline and the experimental PD proteome remains highly significant; 19x and 8x larger than would be expected by chance respectively (Figure 3.4 B). The size of the overlap aligned with the classification order (PIP-A,B,C,D) where PIP-A has the largest overlap proportionally and list PIP-D the least when all available proteomes are used and when the poplar proteome is excluded.

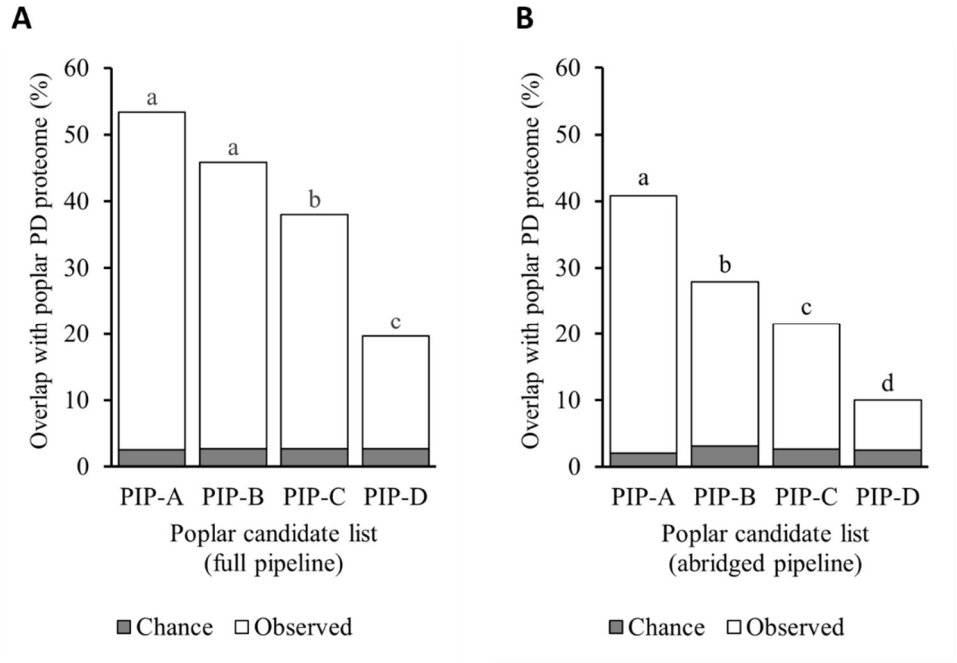

Figure 3.4 Overlap between *in silico* and experimentally determined proteome is dependent on candidate list classification. Poplar candidate PD genes lists (PIP-A,B,C,D) were generated using (A) the full pipeline using all available PD proteomes and (B) abridged PD candidate pipeline that omitted the poplar PD proteome (Leijon et al., 2018) as an input. The size of the overlap for gene lists with the PD proteome by chance was determined by bootstrap sampling of the whole poplar genome (10,000 cycles, median % overlap given). Pairwise comparisons between observed overlaps of candidate lists and PD proteomes were made with Fisher's exact test ($p>0.05$, holm adjusted, bars with differing letters are significantly different).

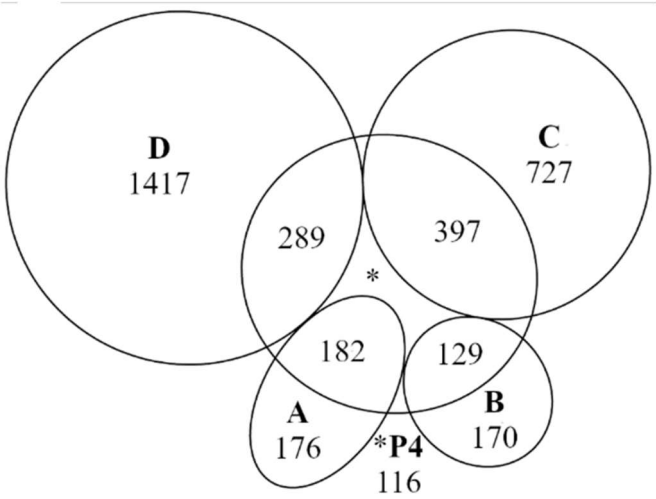

Figure 3.5 PIP1 expands the number of PD candidates for species with an existing experimentally determined PD proteome. Euler diagram shows that PD candidate proteins for poplar (PIP-A to PIP-D) overlap considerably with the experimentally determined proteome (P4, Leijon et al., 2018). * 116 proteins in P4 are excluded from PD candidate lists because they are not annotated within PANTHER16 subfamilies. See (Figure 3.4) for a comparison between candidate lists and the experimentally determined PD proteome when P4 is excluded from the pipeline.

3.2.3 *Arabidopsis* PD candidate lists are over represented in stress-related GO terms, mobile proteins and mobile transcripts

GO analysis was performed on candidate PD proteins generated for *A. thaliana*. The online PANTHER GO over representation analysis tool was used to search for under and over represented GO terms relating to 'Cellular components' and 'Biological processes' in PD candidates. PIP-C and PIP-D were excluded from this analysis to improve the quality of candidates as these lists (when generated for poplar) overlap significantly less with PD experimental proteomes than PIP-A and PIP-B (Figure 3.5). Cellular component GO terms were grouped into 14 groups based on general cellular domain (Figure 3.6). Fold enrichment of GO terms within cellular domains shared the same general behaviour. Cellular domains that were enriched in PD candidates includes cell wall, PD, PM, extracellular region and vesicle and endomembrane related domains. Cellular domains that were under represented in PD candidates were all intracellular domains included nucleus-, plastid- and cytosolic- related domains. There are more biological process GO terms than cellular component GO terms and only those GO terms that were enriched in

PD candidates are presented (Figure 3.7). Biological process GO terms that are enriched in PD candidates were grouped into 7 groups. 17 of the 46 over represented GO terms relate to a stress or other stimulus response. Between 15%-25% of candidates have GO terms relating to protein modification and metabolic processes.

It is possible that mobile proteins may have been sampled in proteomic studies whilst in transition through PD. To test whether mobile proteins could form a component of *in silico* proteomes, *Arabidopsis* candidate PD proteins were cross-referenced against a mobile proteome identified in *Cuscuta australis* (dodder) parasitising *A. thaliana* (Liu et al., 2020b). This was done by adding the supplemental data from the publication to the 'Cross reference with' directory in PIP1. Mobile proteins were found to be over represented in all candidate lists but PIP-B had the largest over representation (20.2%) when compared against random genome samples. The overlap is over 10x greater than would be expected by chance. Matching genes between candidate lists and the mobile proteome are listed annotated Supplementary material 8. To determine the representation of mobile transcripts in the *in silico* proteome, *Arabidopsis* candidate PD proteins were cross-referenced against graft-transmissible (mobile) transcripts identified by Thieme et al. (2015). Mobile transcripts were over represented in all candidate lists with overlaps between 3-4x greater than what would be expected by chance when compared against random genome samples. Matching genes between the *Arabidopsis in silico* PD proteome and Thieme et al. (2015) mobile transcripts are annotated in Supplementary material 8.

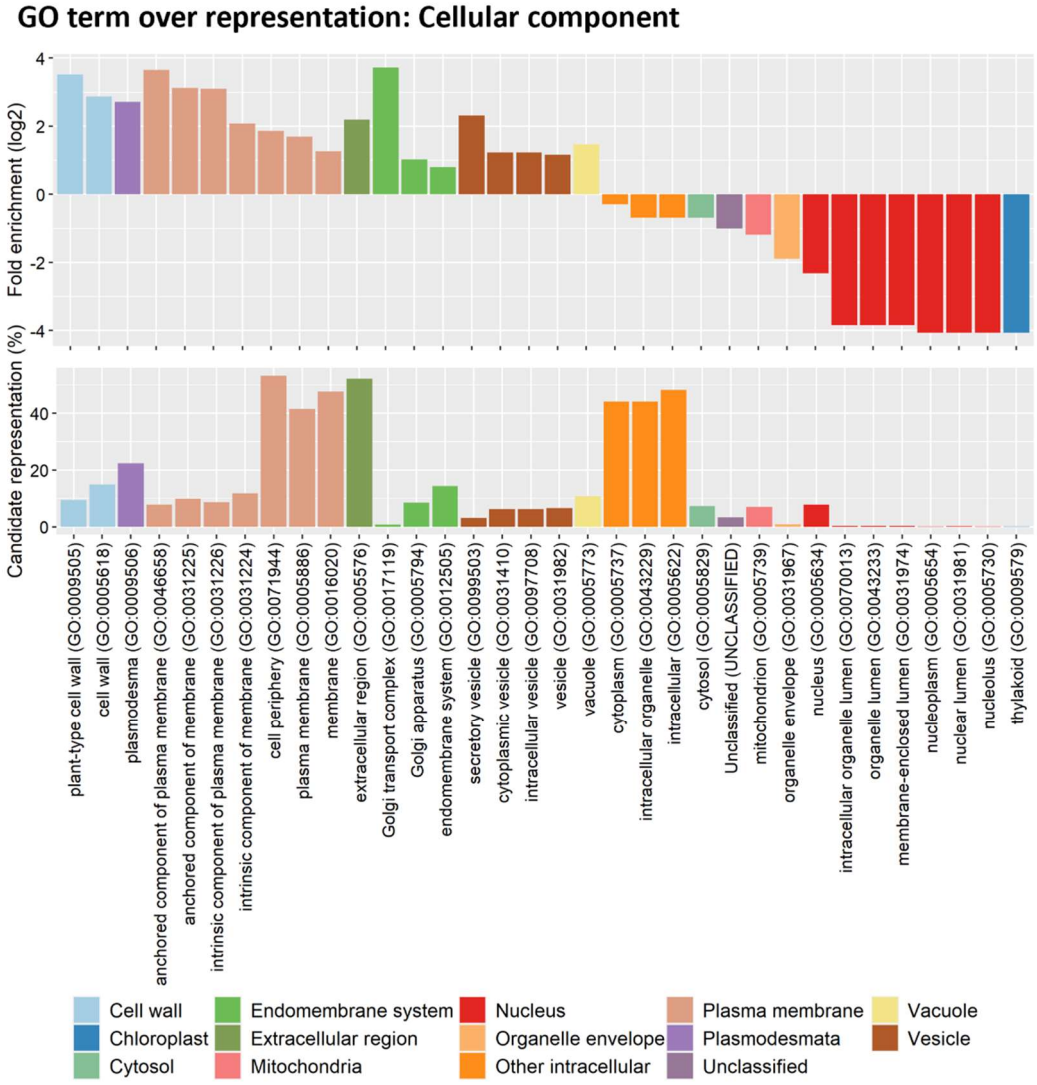

Figure 3.6 PD candidates are overrepresented in cellular component GO terms relating to extracellular domains and secretory pathways and underrepresented in those relating to intracellular compartments and cytoplasm. Gene ontogeny (GO) term over representation analysis was performed on *A. thaliana* candidate PD lists A and B (aggregated) using the online PANTHER16 gene list analysis tools. Significantly over- or under- represented GO terms were identified by Fisher's exact test ($p>0.05$, Bonferroni adjusted). Output from the tool was formatted and graphed in python using Matplotlib (Hunter, 2007). Fold enrichment (log2) is the representation of that GO term relative to chance. Candidate representation is the proportion of candidate genes that are annotated with that GO term.

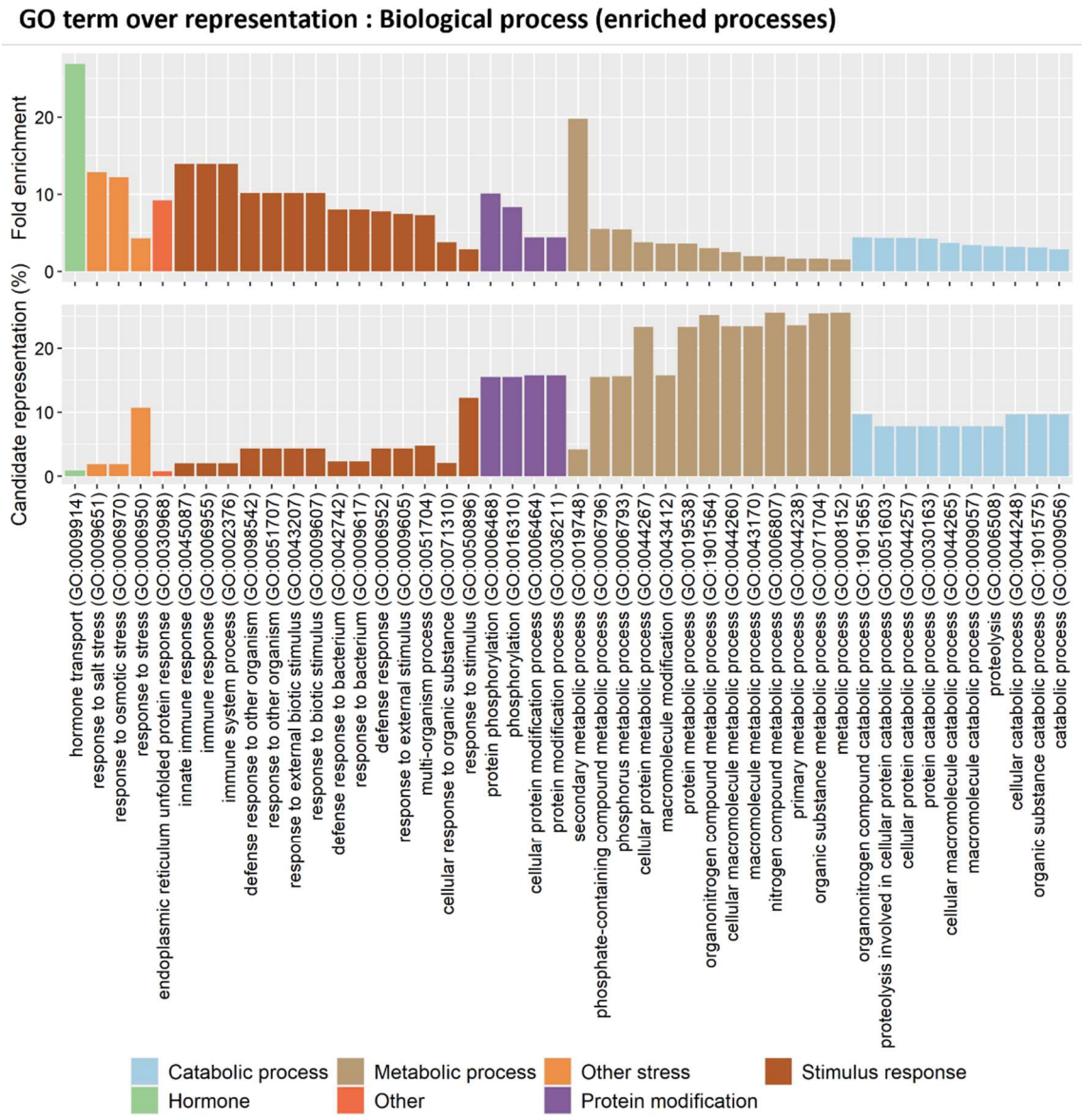

Figure 3.7 Biological process GO terms overrepresented in PD candidates include those relating to hormone signalling, response to stimuli and protein modification. Gene ontogeny (GO) term over representation analysis was performed on *A. thaliana* candidate PD lists A and B (aggregated) using the online PANTHER16 gene list analysis tools. Significantly over- or under- represented GO terms were identified by Fisher's exact test ($p>0.05$, Bonferroni adjusted). Output from the tool was formatted and graphed in python using Matplotlib (Hunter, 2007). Fold enrichment (log2) is the representation of that GO term relative to chance. Candidate representation is the proportion of candidate genes that are annotated with that GO term.

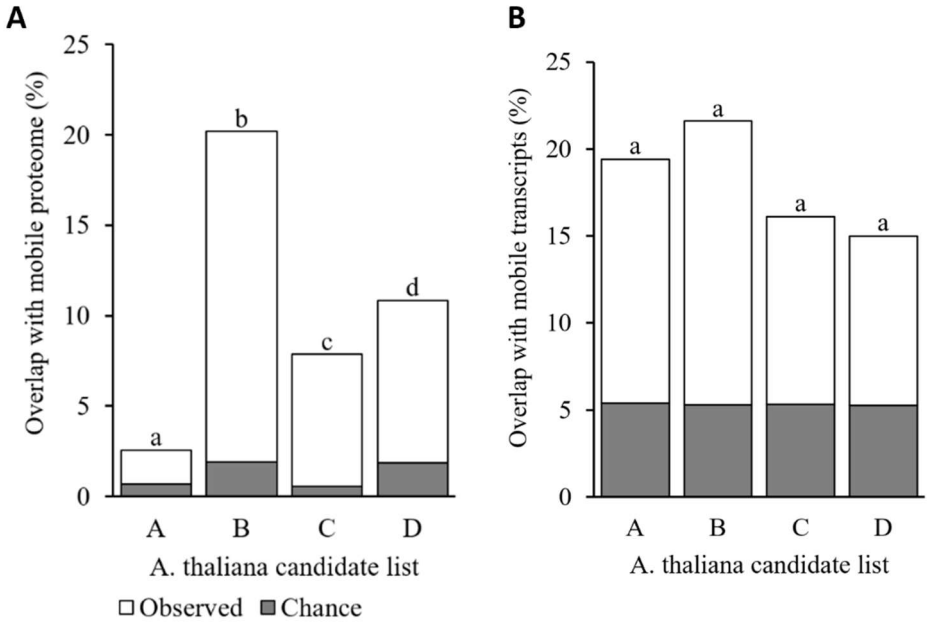

Figure 3.8 *A. thaliana* PD candidate lists are overrepresented in mobile proteins and mobile transcripts. *A. thaliana* candidate proteome lists were compared to (A) mobile proteins identified in Cuscuta parasitising *A. thaliana* (Liu et al., 2020) (mobile proteome) and (B) graft-transmissible transcripts (mobile transcripts) (Thieme et al., 2015). The size of the overlap for gene lists with the mobile proteome/mobile transcripts by chance was determined by bootstrap sampling of the whole genome (10,000 cycles, median % overlap given). Pairwise comparisons between observed overlaps of candidate lists and PD proteomes were made with Fisher's exact test ($p>0.05$, holm adjusted, bars with differing letters are significantly different).

3.2.4 Integrated meta-analysis of transcriptome and proteome data reveal interactomes and conditions regulating symplasmic transport

Co-expression analysis may highlight functional relationships between PD proteins at a transcriptional level which could help to screen for PD proteins. To assess the viability of this approach, 215 publicly available *Arabidopsis* microarray experiments were analysed. This analysis involved normalising the raw microarray data, filtering out low quality data and fitting linear models to the data to generate lists of differentially expressed (DE) genes (transcriptomes, see Supplementary material 3 for details about transcriptomes used). The transcriptomes were cross referenced against the list of verified PD proteins in *A. thaliana* and presented as a heatmap showing the transcriptional profile against a wide range of treatments (Figure 3.9). This heatmap demonstrates that many biotic and abiotic

treatments including cold, desiccation, drought, hypoxia, NaCl, and wounding may cause differential expression of PD factors.

Pearson correlation analysis was performed on the transcriptomes to determine pairwise correlation coefficients of expression between all verified PD genes (Figure 3.10). Genes were ordered by seriation to reveal at least 3 distinct clusters of known PD proteins that share a high degree of correlation in gene expression. To improve the resolution, ATTEDII data for *A. thaliana* was acquired which integrates many hundreds of transcriptomic experiments including microarray and RNA-seq datasets for 18,957 genes (Obayashi et al., 2018). ATTED-II data for all available genes were compiled and ordered by hierarchical clustering. The resulting dendrogram was cut into an optimised number of clusters (k = 151) derived by cutting the dendrogram at an arbitrary height (h = 16). Setting the height to 15 lead to far too small clusters to be able to perform meaningful statistical analysis on. Setting the height to 17 leads to a small number of large clusters that had insufficient resolution required to see meaningful transcriptional relationships within clusters.

For each cluster, over-representation analysis of specific gene/protein sets was performed. The gene/protein sets used were PIP-A, B,C,D, subfamilies present in verified PD proteins and the wider set of available genes in ATTEDII (the full transcript population). Two clusters were found to be significantly overrepresented (relative to the wider ATTED-II gene set) in genes that are in the same subfamily as PD-verified genes: cluster 87 and cluster 100 (Figure 3.11 A, B). One hypothesis is that candidate proteins in these clusters may be more likely to participate in PD regulation and thereby localise at PD. 11 genes from list A and 18 from list C were found in cluster 87 along with known PD proteins such as the PDBG, BG_PPAP. Cluster 100 contained 16 genes from list C and 3 genes from list A along with known PD proteins such as PDCB1, PDCB3, PDLP2 and PDLP3. Both PDLP3, BG_PPAP and PDCB1,3 proteins are related to callose regulation thus candidate genes in these clusters might potentially have a cell wall function. Genes involved in cellulose/hemicellulose modifications (such as COBL7), pectin biosynthesis and esterification (e.g. GAUT4), extensins, expansins and arabinogalactan proteins were identified in the clusters and in List A/C (Park et al., 2017b; Li et al., 2019; Li et al., 2022).

The expression of PD-candidates in clusters 87 and 100 in publicly available microarrays are presented (Figure 3.11 C). Gene expression of known PD proteins was compared across a wide range of treatments including biotic treatments such as bacterial infection and abiotic treatments such as exposure to osmotic challenge and differences in nutrient

concentrations. Due to figure size constraints, only expression data for cluster 87 and cluster 100 pertaining to osmotic stress is shown in Fig. 3.11. Most of these treatments caused strong negative differential expression of genes in these clusters including PDCB1, PDCB3 and BG_PPAP. Specific treatments that elicited a reduction in expression of these genes included withholding water for several days (e.g. E-MTAB-3044, (Zhang et al., 2014a) and transferring seedlings to plates with a reduced water potential from dissolved polyethylene glycol (E-GEOD-35258, (Bhaskara et al., 2012).

1


Material
Agrobacterium
Cold
aba1 mutant
abi1 mutant
axr1 mutant
max4 mutant
Dessication
Drought
flg22
H2O2
H2O2 (dark)
Hypoxia
Light
Light (relative to dark)
NaCl
Low nitrate
Ozone
Low pH
PEG
Phosphate resupply
Phosphate deficient
Photoperiod
High selenate
Sucrose
Nitrate deficient/sucrose
Temp
Wounding
SP
GPI
TM
Verified PD localisation
Other
TRUE
hypocotyl
inflorescence
leaf
root
seedling
shoot
siliques
logFC

Figure 3.9 Verified PD proteins are differentially expressed under a wide range of biotic and abiotic conditions. Differential expression (log_2FC, ranges from blue: downregulated to red: upregulated in relation to control) of verified PD proteins determined using public microarrays transcriptomes. Columns labels bottom = ArrayExpress accession codes followed by a reference number. See Supplementary material 3 for further information. (left) Rows are grouped by cluster and then (dendrogram) ordered by hierarchical clustering. (right) Gene ID and properties. Asterisks in cells denote predictions on membrane targeting features (e.g. is predicted to have a SP). SP = Signal peptide, GPI = glycophosphatidylinositol anchor, TM = transmembrane domain. Cell colour above each column = plant material sampled.

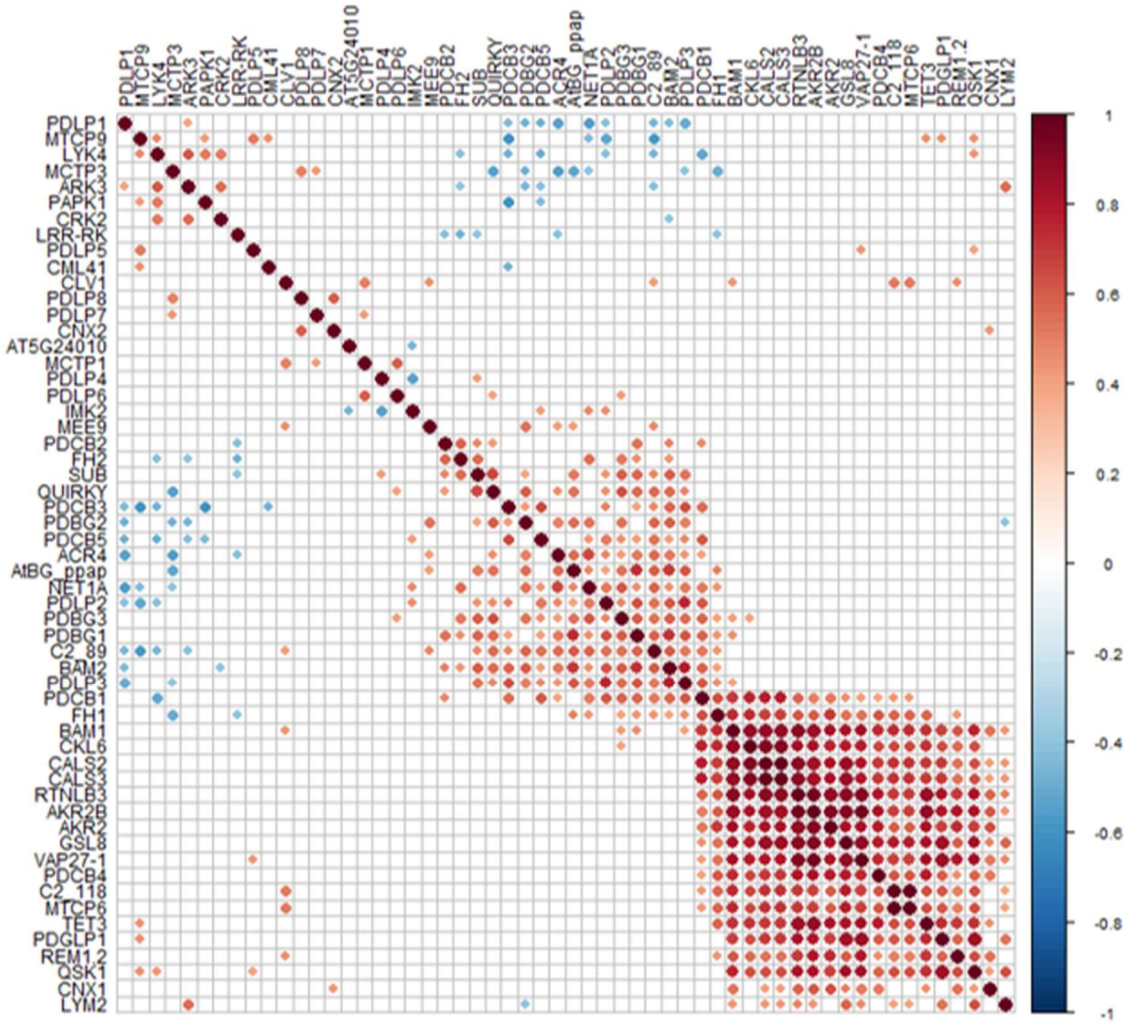

Figure 3.10 Expression analysis reveals distinct clusters of gene expression correlation between known PD genes. Differential expression (DE) between treatment and control were determined for abiotic and biotic related transcriptomes (215 microarrays). Pearson correlation analysis was performed on DE datasets to determine correlation coefficients of expression between all known PD genes. Colour intensity and the size of the circles are proportional to the correlation coefficients. Blank squares represent a non-significant correlation (FDR-corrected Pearson's r, $p \leq 0.05$). Gene order was determined by the rank-two ellipse method via the 'seriation' package in R (Hahsler et al., 2018). Correlation matrix was plotted using 'corrplot' package in R.

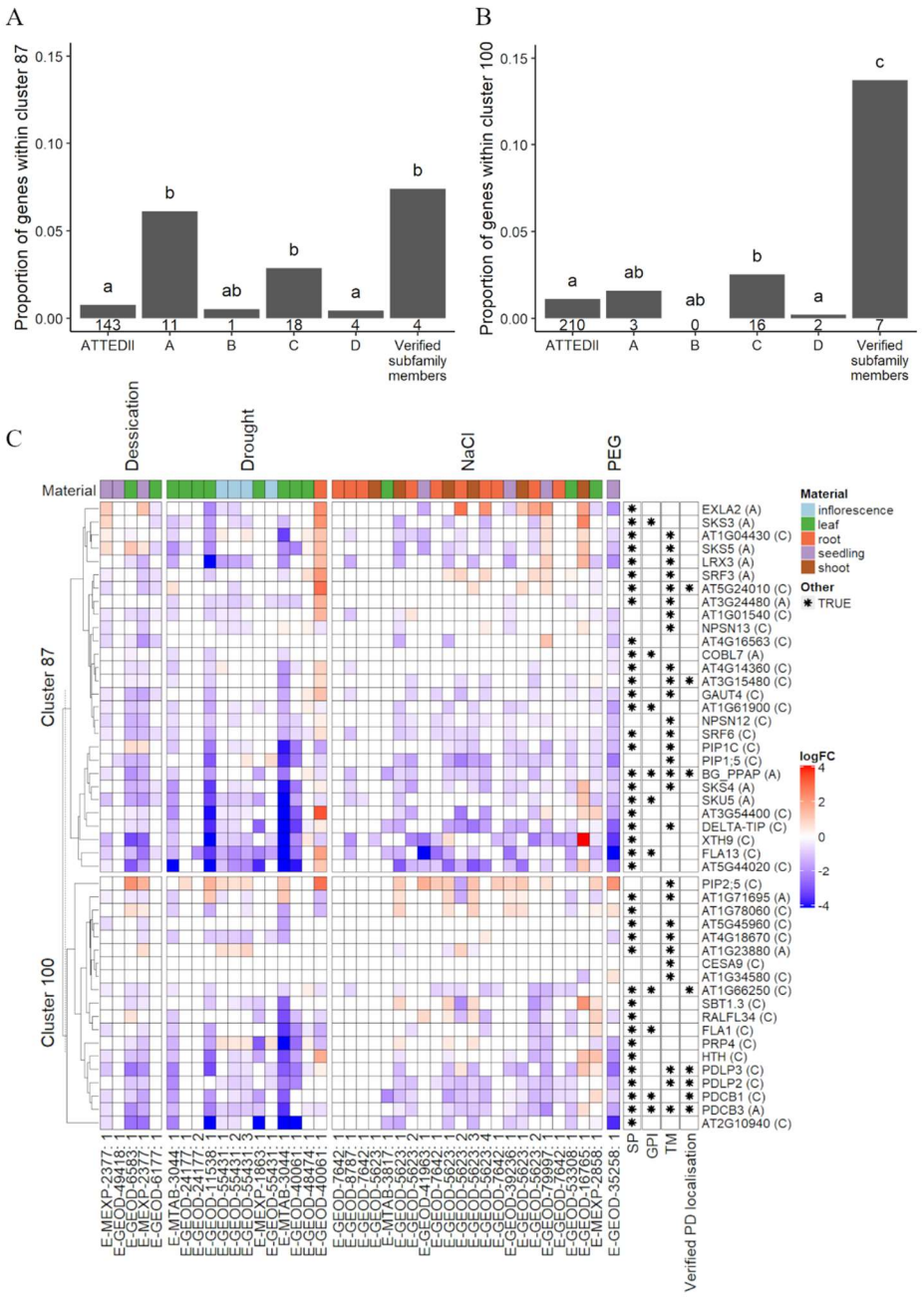

Figure 3.11 Candidate PD protein screening based on whole genome co-expression cluster analysis. *A. thaliana* co-expression data from ATTEDII were subset into clusters based on hierarchical clustering (k = 151). Representation analysis of the total ATTEDII database, candidate lists A-D and verified PD subfamilies was performed on each cluster; (A) cluster 87 and (B) cluster 100 show significant over representation in verified subfamily members. Number underneath each bar = number of genes within that cluster. Bars with differing letters above are significantly different (Fisher's exact test, Holm corrected, $p \leq 0.05$). (C) Differential expression (log2FC, ranges from blue: downregulated to red: upregulated in relation to control) of genes in clusters 87 and 100 (only list PIP-A,C and verified genes are shown) determined using public microarrays from experiments pertaining to osmotic

stress. Columns labels bottom = ArrayExpress accession codes followed by a reference number. See Supplementary material 3 for further information. (left) Rows are grouped by cluster and then (dendrogram) ordered by hierarchical clustering. (right) Gene ID and properties. Asterisks in cells denote predictions on membrane targeting features (e.g. is predicted to have a SP). SP = Signal peptide, GPI = glycophosphatidylinositol anchor, TM = transmembrane domain. Cell colour above each column = plant material sampled.

3.2.5 Validation of the pipeline for the identification of novel plasmodesmata proteins in *Medicago truncatula*

One of the advantages PIP1 is that it can be applied to species for which an experimentally determined PD proteome is not publicly available (such as *M. truncatula*). To demonstrate the use of the pipeline in the identification of novel PD proteins, the pipeline was used to generate *M. truncatula* orthologues of verified PD proteins in *A. thaliana* based on PANTHER16 family membership. Of particular interest to the Benitez-Alfonso group are the family of callose degrading enzymes (beta-1,3 glucanases), which were outputted by the pipeline. A recent study of this family of proteins revealed that MtBG2 (MTR_3g083580) is PD localised and was induced early in Medicago roots infected with the nitrogen-fixing bacteria rhizobia (Gaudioso-Pedraza et al., 2018). This author found that hairy root cultures of *M. truncatula* with constitutive expression of MtBG2 driven by the *UBIQUITIN* (*UBI*) promotor (via transformation with *Agrobacterium rhizogenes* containing *pUBI::MtBG2*) led to an increase in the number of nodule organs formed to host the bacteria (Figure 3.12 B:E). To verify the role of MtBG2 in the regulation of symplasmic transport, Medicago roots expressing GFP under the epidermal *EXPA* promotor (*pEXPA::GFP*) were transformed with a *pUBI::MtBG2* construct. The symplasmic reporter *pEXPA::GFP* was also transformed with *cals3m* (a mutated version of CALS3 that induced callose deposition) driven by the epidermal *ETHYLENE RESPONSE FACTOR REQUIRED FOR NODULATION 1* (*ERN1*) promotor (Vatén et al., 2011; Cerri et al., 2012). Roots were imaged by confocal microscopy and GFP diffusion profiles generated using a custom ImageJ plugin (Supplementary material 4). In roots transformed with control vectors, GFP expression was found in the epidermis but also diffused into the cortical tissue. Ectopic expression of MtBG2 lead to increase in GFP transport into deeper tissues whereas cals3m reduced it.

Next, an *in silico* proteome for *M. truncatula* were generated using PIP1 (Supplementary material 9). PIP-A and PIP-C comprised 1018 genes belonging to subfamilies represented

in at least one experimental proteome and displaying membrane targeting features (SP, GPI or TM). These lists include *M. truncatula* orthologues of *A. thaliana* PD genes such as members of the CALS, PDCB, PDBG and PDLP families. Besides MtBG2, the SUPER NUMERIC NODULE RECEPTOR (SUNN, Crook et al., 2016) was found to regulate rhizobia infection and the response to nitrate thus we used these conditions to screen the PIP1 proteome lists. Published microarrays data from early rhizobia inoculation, various nitrate concentrations and nodulating roots were re-analysed (by Liam German). A cluster containing MtBG2 and SUNN was identified comprising 70 genes from list A and C (Figure 3.12). This includes members of the receptor-like kinase PDLP family and other candidates involved in callose regulation. PD-localisation was confirmed (by Rocio Gaudioso-Pedraza) for one of these candidates (MTR_1g073320) (Gaudioso-Pedraza, 2017) indicating that the integrated metanalysis of PD proteomes and transcriptomes is a valid approach for identifying novel PD components in this legume plant species for which no experimental PD proteome exists.

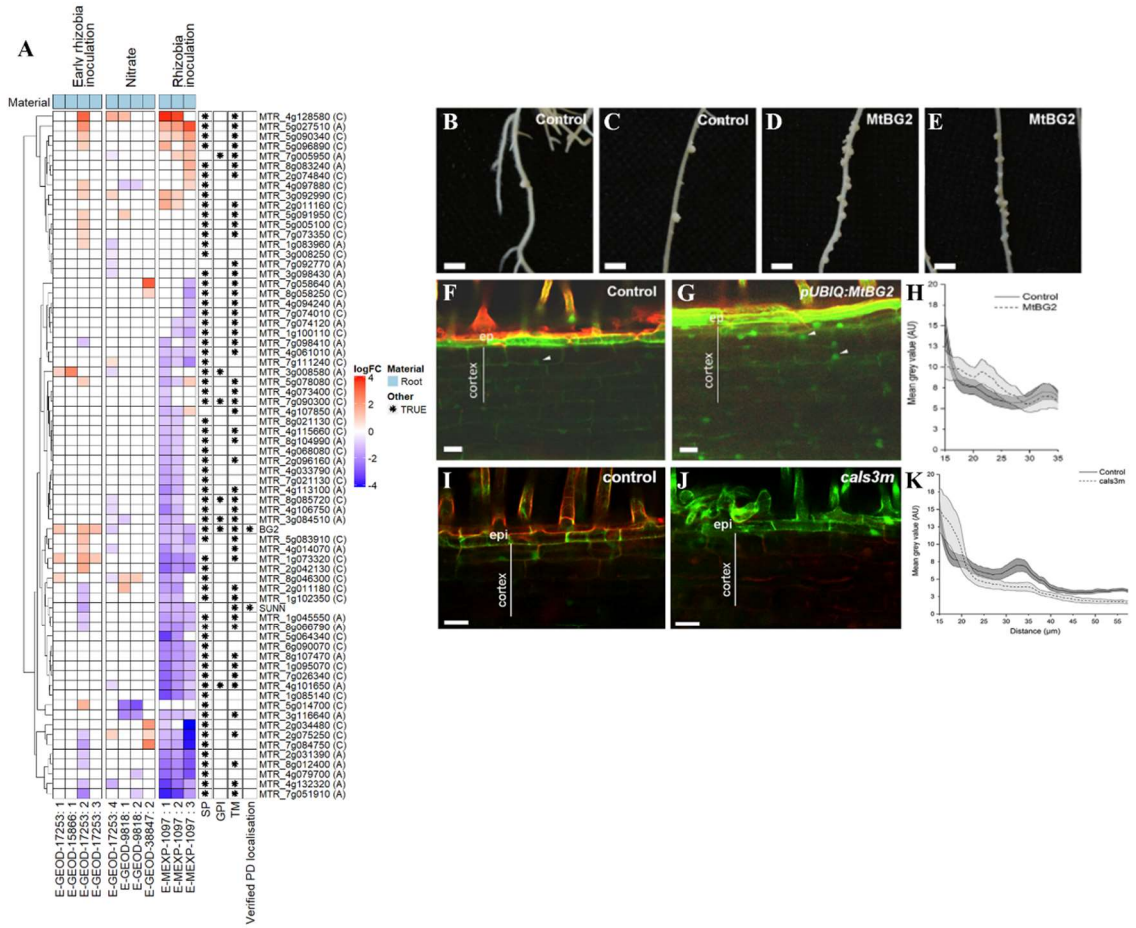

Figure 3.12 MtBG2 and *Medicago truncatula* PD candidates are differentially expressed in response to rhizobia inoculation. MtBG2 regulates nodule count and symplasmic transport. (A) Gene expression analysis of *M. truncatula* PD candidates (PIP-A and PIP-C) and verified PD genes. Differential gene expression (log_2FC) was determined using public microarray data of experiments relating to nitrate and rhizobia inoculation in root tissue. Columns labels bottom= ArrayExpress accession codes followed by a reference number. See Supplementary material 3 for further information. (left dendrogram) Rows are ordered by hierarchical clustering with empty rows removed. Asterisks in cells denote that gene has a membrane targeting feature or are verified. SP = Signal peptide, GPI = glycophosphatidylinositol anchor, TM = transmembrane domain. (B:E) M. truncatula roots without (control) or with constitutive expression of MtBG2 (*pUBI::MtBG2*) 15 days post infection with *Sinorhizobium meliloti*. (F:K) A stable *M. truncatula* line expressing a mobile GFP under the control of the epidermis-specific promoter (*pEXPA::GFP*). This line was used to generate transgenic roots co-expressing a (F, I) control empty vector, (G) *pUBI::MtBG2* or (J) *pERN1::calsm*. Roots were imaged 5 dpi with rhizobia using confocal microscopy. Counterstaining with propidium iodide reveals the epidermal cell layer in red.

GFP fluorescence (green) is expressed in the root epidermis, but it is also detected in cortical tissues presumably due to symplasmic diffusion. (H, K) Quantification of the GFP signal (using ImageJ mean grey values as a.u.) in cortical cell layers (x axis represents distance from the epidermis) in three independent biological replicas and in a region of interest 55mm wide (n > 5). The grey area above and below the mean (continuous line for control; discontinuous line for MtBG2 and *calsm*) shows SEs. Notice that mean values in MtBG2 are above control and in *calsm* values are below the control, indicating increase and decrease in GFP diffusion, respectively. Data presented in panel A was produced in collaboration with Liam German. Data presented in panels B:K were generated by this author and are published in Gaudioso-Pedraza et al. (2018).

3.3 Discussion

In summary, the pipeline described in this chapter identifies all members of subfamilies represented in experimental PD proteomes and categorises them based on two attributes: 1) the number of proteomes that identify the same protein subfamily (or family depending on how the pipeline is initialised) and 2) whether the proteins encode features (SP, TM or GPI) associated with membrane targeting. These features were significantly over-represented in verified PD located proteins reported in the literature. The output of PIPI is dubbed the *in silico* proteome. This approach was validated in poplar where all *in silico* proteomes overlapped significantly with the experimentally determined poplar PD proteome. The extend of the overlap correlated well with our classification, showing PIP-A the largest overlap and PIP-D the lowest. Analysis of the *in silico* proteome of *Arabidopsis* revealed an overrepresentation of GO terms relating to abiotic and biotic stresses. This aligns well with the described function of known PD proteins in the response to external stimuli. For example, callose synthases and PDLPs are described to regulate the response to pathogen attack (Lee et al., 2011; Caillaud et al., 2014; Cui and Lee, 2016a). PIP-B had a large overlap with the mobile proteome determined in dodder parasitising *Arabidopsis* (Liu et al., 2020b). PIP-B also exhibited a large representation of transcripts identified to move in the graft interface between different *Arabidopsis* ecotypes (Thieme et al., 2015).

In addition to PIPI, transcriptomic data was used to identify factors with transcriptional interactions to experimentally verified PD proteins that could be used to dissect the underlying molecular mechanisms. Two transcriptomic clusters in *Arabidopsis* were found

overrepresented in genes encoding verified PD proteins and also contained a larger number of genes identified in PIP-A and PIP-C. Most of the genes in these transcriptomic clusters were down regulated in transcriptomes responding to elevated sodium chloride, drought and other osmotic stressors. The validity of the pipeline for prediction in species with no sequenced experimental PD proteome was tested in *M. truncatula*. Transcriptomic analysis was performed on PIP-A and PIP-C and two known PD genes identified in this plant (MtBG2 and SUNN). This analysis revealed a cluster of genes which exhibited differential expression in response to rhizobia inoculation. This led to the discovery of MTR_1g073320, a member of the PDLP family that localise at PD (Gaudioso-Pedraza, 2017) and that transcriptomically correlates with MtBG2.

3.3.1 Limitations and mitigation of risks to consider when using PIP1

PIP1 is easy-to-use and users can add new PD proteomes and known PD proteins to increase its predictive capacity. PIP1 outputs well annotated lists that identify genes of interest for a wide variety of applications. This tool could be used to analyse proteomes for different conditions or to cross reference PIP1 lists against published transcriptomes, other proteomes or curated gene lists. For all species, including those for which experimentally determined PD proteomes exist, PIP1 expands the number of candidates and classifies them to discriminate which proteins are more likely to be bona fide PD proteins or which are more likely to be contaminants. When PIP1 is applied to identify candidates in *A. thaliana*, GO terms represented in the list corelates with those identified in verified PD proteins. This result suggests that PIP1 intrinsically excludes proteins that are not expected to associate with PD such as those that are linked with the nuclear lumen. For species for which no experimental proteome exists, PIP1 can create a PD proteome *in silico* with far less resources than required to create one experimentally. However, despite the advantages of PIP-1, users should be aware of their limitations.

PIP1 usage is limited to plant species and subfamilies annotated in both PANTHER16 and Ensembl Plant databases but these databases are continuously being updated with new and updated UniProt Reference Proteomes (Drost and Paszkowski, 2017; Howe et al., 2020; Mi et al., 2021). Currently, PIP1 allows the generation of *in silico* candidate PD proteomes for 22 species. Of these, 19 are angiosperms (5 monocots, 13 dicots and *Amborella trichopoda*). Lycophytes, bryophytes and algae are represented only by single species (*Selaginella moellendorffii*, *Physcomitrella patens* and *Chlamydomonas reinhardtii*, respectively). While these 22 species represent the majority of the most widely studied

plant species, including major crops such as *Zea mays, Triticum aestivum* and *Solanum tuberosum*, PIP1 will be of little use to those interested in non-supported species. PIP1 relies on annotation within the PANTHER database and therefore shares limitations associated with the platform. For the 40 reference plant genomes included in PANTHER16, family/subfamily annotation coverage for each gene is between 60-95% depending on species (Mi et al., 2021). For *A. thaliana* and poplar, the coverage is at 89% and 81% respectively. As a result of lack of coverage, 116 poplar proteins identified in the experimentally determined proteome, are not included in the PIP1 derived *in silico* proteomes. A limitation of this study is that the inputted experimental proteomes are from 3 dicot species. Due to family/subfamily conservation, it is logical to assume that PIP1 have less power when predicting proteomes of monocots and non-angiosperms. An analysis on the PANTHER16 database reveals that only 34% of wheat subfamilies are present in *A. thaliana* thus the pipeline is effectively blind to a considerable proportion of the wheat genome. It is unknown to what extend the composition of PD differs between monocots and dicots. Differences in cell walls composition, for example, might suggest that a different cast of factors are required to maintain and regulate PD (Calderan-Rodrigues et al., 2019). To overcome this issue, new PD proteomes need to be sequenced and more PD proteins identified in monocots and non-angiosperm species. During finalisation of this thesis, 3 new PD proteomes have been published; one for *Arabidopsis thaliana* and two for the bryophyte *Physcomitrella patens* (Gombos et al., 2022; Johnston et al., 2022). Inclusion of these new proteomes are likely to improve the quality of *in silico* proteomes generated by PIP1. The implications for release of the first comprehensive PD proteomes for a non-dicotyledonous plant are explored in the Discussion chapter.

PIP1 also carries over limitations from its underlying PD proteomes such as only proteins that are expressed in cell culture are more likely to be sampled. Of the 61 currently verified *Arabidopsis* PD proteins, 40.1% are not represented at a gene level in PD proteomes. This non-representation drops to 36.1% and 13.1% on a subfamily and family level respectively. By default, PIP1 uses subfamily identity to pull proteins for the chosen species. The *Arabidopsis in silico* proteome based on subfamily identify BAM1 and CALNEXIN2 (CNX2), which are not present in any of the experimental proteomes but localised at PD in independent studies (Fernandez-Calvino et al., 2011; Liu et al., 2017a; Rosas-Diaz et al., 2018; Brault et al., 2019). Pulling factors based on subfamily members overcomes some of the sampling bias inherent in PD proteome determination. PIP1 can be instructed to pull proteins based on family identity which would increase the representation of known PD

proteins at the cost of increasing potential contaminants and inflating the combined size of the *in silico* proteome. In *Arabidopsis*, the size of the *in silico* proteome (excluding PIP-D) increases from 1,165 (based on subfamily identity) to 5,737 when based on family identity (approximately 15% of the genome). Given the size of this candidate list, pulling proteins based on families may not be appropriate for screening but might be useful when creating co-expression interactomes to look for conditions likely affecting PD.

Prioritising candidates based on the number of PD proteomes in which their subfamily appear has advantages and disadvantages. One might expect that ubiquitous and well conserved PD proteins would appear in multiple proteomes. This expectation would rank PIP-A and PIP-B candidates above PIP-C and PIP-D. Consistent with this hypothesis, poplar PIP-A overlaps more than 50% with the experimental proteome whereas PIP-C overlaps is less than 40%. PIP-B was found to have the largest overlap proportionally to the mobile proteome, recently reported in dodder parasitising *A. thaliana* (Liu et al., 2020). PIP- B candidates should not be disregarded however as this list is likely to include proteins with unusual membrane targeting mechanisms or with features poorly predicted by the available platforms. This is the case for REMORIN2, for example, which localises to PD independent of the secretory pathway and lacks a predicted SP, GPI or TM (Reymond et al., 1996; Gronnier et al., 2017; Huang et al., 2019). Another PIPI limitation is that there is a bias as larger subfamilies are more likely to be sampled in PD proteomes. To help the user mitigate this issue, PIPI annotates all candidate proteins with information on how large the subfamily is.

Contaminating proteins are included in experimentally determined proteomes thus remain likely present in the *in silico* proteomes. PIP-D contains proteins identified in only one proteome and no-membrane targeting features, thus it is likely that PIP-D has a high proportion of contaminating proteins. In our study, none of *Arabidopsis* PIPI-D predicted genes were confirmed to locate to PD and there is relatively poor overlap between this list and the poplar experimental proteome. Excluding this list from the *in silico* proteome should facilitate the screen for 'real' PD genes. Despite these limitations, the pipeline offers a significant improvement to relying on experimentally determined PD proteomes alone.

3.3.2 Expression cluster analysis of the *in silico* PD proteome identifies PD proteins and conditions potentially associated with PD regulation

Classifying candidates as PIP-A, B, C, D and other annotations made by PIPI can help in prioritising candidates of interest. Presented here is an additional process that can be applied to further screen PIPI-derived candidates based on co-expression analysis. Co-expression analysis has been used extensively to identify putative gene interactions that are subsequently confirmed experimentally (Serin et al., 2016; Yao et al., 2018; Zhu et al., 2020b). Co-expression analysis of known *A. thaliana* PD genes revealed emergent patterns, suggesting that PD genes/proteins may interact at a transcriptional level. The significance of the two co-expression clusters overrepresented in genes from the same subfamilies as known PD genes requires further attention. For example, cluster 100 contains known PD proteins PDCB1, PDCB3, PDLP2 and PDLP3 as well as 22 candidate PD proteins. These clusters may represent transcriptional networks and hint at possible interactions between these genes/proteins, thus hold high potential to be mechanistically relevant. PDCBs and PDLPs have both been linked to the regulation of callose at PD (Simpson et al., 2009; Lee et al., 2011) but their genetic interaction has not been previously reported. Further work is needed to confirm this putative genetic interaction and establish whether it extends to a functional interaction. One way that this could be achieved is to determine PD-callose in single and combinations of double/triple/quadruple knock out mutants of *pdlp3, pdlp2, pdcb1 and pdcb3* to test for a functional interaction between these factors.

Candidates identified in these clusters may have a higher likelihood of being 'real' PD proteins given they are co-regulated with known PD genes and are thus more likely to also participate in PD regulation. Candidates that associate with the cell wall are particularly attractive given the role cell wall components play in the regulation of PD (Amsbury et al., 2018). For example, GAUT4 and XTH9 both appear in cluster 87. GAUT4 and XTH9 are involved in pectin and xyloglucan biosynthesis respectively (Hyodo et al., 2003; Lund et al., 2020). The clusters also contain proteins not directly associated with the cell walls such as the SKU5 family of proteins. SKU5, is an inactive multi-copper oxidase with a signalling function to modify cell walls and root development in response to abiotic stress conditions (Sedbrook et al., 2002). SKU5 has been shown to localise to the bulk PM (Sedbrook et al., 2002), however SKU5 and SKU5-SIMILAR, (SKSs) have been identified in multiple PD proteomes. Overexpression of a native SKU5-like protein in *Gossypium*

hirsutum has been recently shown to promote callose deposition during pollen tube development (Li et al., 2020c) which highlights a potential role for SKU5-like proteins in the PD regulation via callose. Further work is required to examine whether these candidate proteins are real PD proteins and whether their transcriptional relationships to known PD proteins is functional.

One of the benefits of PIP1 is that it can generate candidates for species for which experimentally determined PD proteomes do not exist such as *M. truncatula*. At the start of this work, SUNN (Crook et al., 2016) was the only confirmed PD protein in *M. truncatula* linked to both nitrogen uptake and rhizobia symbiosis. More recent work from the lab using qRT-PCR and GUS expression analysis identified MtBG2, a PD-located protein that is regulated in response to rhizobia infection (Gaudioso-Pedraza et al., 2018). Further analysis using a transgenic line showed that ectopic *MtBG2* increased symplasmic transport between the epidermis and underlying tissues and that this regulation affects the number of nodules formed in *M. truncatula* – rhizobia interaction. To identify new candidates involved in this pathway, cluster analysis was performed to determine co-expression between MtBG2, SUNN and candidate PD genes extracted from list A and C of the *in silico* proteome. This approach identified MTR_1g073320, a member of the PDLP family which also localises at PD (Gaudioso-Pedraza, 2017). Members of this family in *Arabidopsis* have shown to regulate symplasmic transport by upregulating expression of *CALS* in response to pathogen attack and during lateral root development to alter auxin distribution (Caillaud et al., 2014; Liu et al., 2020a; Sager et al., 2020). The identification of this gene further supports the validity of using PIP1 to generate candidate PD genes even for species for which no experimental PD proteome exists.

The generation of candidate PD genes not only enables target gene selection but, in combination with transcriptomics, can reveal conditions that regulate PD genes. Many of the biological process GO terms that are over represented in *A. thaliana* PD candidates relate to responses to stimuli including stress. This is reflected in the expression analysis of candidate and known PD genes in a wide range of conditions. In almost all abiotic conditions tested, there were a suite of known PD proteins and candidates that were both positively and negatively differentially expressed, reflecting the dynamic nature of PD. Drought, osmotic challenge and elevated salinity strongly affected the expression of genes in clusters 87 and 100. During the development of this PhD, these conditions were confirmed to regulate PD by this (see Chapters 4-6) and other authors (Grison et al., 2019; Hunter et al., 2019). Treatments such as low nitrate, hypoxia, reduced media pH causing

differential expression in known PD proteins. Altered concentrations of macro nutrients including nitrate and phosphate and water stress conditions will be explored in subsequent chapters to dissect their role in the regulation of PD proteins and symplasmic transport.

Chapter 4 Root system architecture and symplasmic transport in responses to micronutrient availability, osmotic challenge and elevated NaCl

4.1 Summary

A growing body of work now exists that has established a link between PD proteins, symplasmic transport and responses to abiotic conditions (Müller et al., 2015; Grison et al., 2019; Hunter et al., 2019). However, only a small collection of abiotic conditions and responses to those conditions have been directly linked with PD proteins or the regulation of PD transport. In Chapter 3, known and candidate PD genes were found to be differentially expressed under a wide range of abiotic conditions. This finding warrants further investigation as it might point to novel mechanisms of how plants control responses to challenging external conditions. Adaptation of root system architecture are recognised as an important class of responses to nutrient availability, water availability and salinity (Roycewicz and Malamy, 2012; Kellermeier et al., 2013; Uga et al., 2013; Kellermeier et al., 2014; Hunter et al., 2019). Given that the regulation of PD is involved in response to low Pi, osmotic challenge and elevated NaCl, it is highly plausible that regulation of PD transport is also involved in the regulation of responses to other abiotic conditions. As regulation of root system architecture are important responses to abiotic conditions, it is also plausible that the regulation of PD transport is regulating these responses.

The aim of this chapter is to explore the role of PD have in regulating root responses to a range of abiotic conditions; specifically low concentrations of nitrate, potassium, and inorganic phosphate (Pi), exogenous polyethylene glycol (PEG, reduces substrate water potential) and increased salinity. The hypothesis to test is that changes in the expression of PD genes drive changes in symplasmic transport and signalling leading to growth phenotypes. First, nutrients and osmotic conditions leading to changes in root architecture in our growth conditions were identified, before testing the effects in symplasmic transport. Experimentally, seedlings were scored for primary and lateral root length phenotypes, primary root tortuosity, lateral root number and lateral root density comparing control conditions to low nutrient, reduced water availability and elevated salinity conditions. Conditions that elicited phenotypic responses were then tested for their effect in symplasmic transport using GFP-based symplasmic reporter systems. Alongside the widely used *pSUC2::GFP* reporter system (Benitez-Alfonso et al., 2009; Vatén et al., 2011; Benitez-Alfonso et al., 2013; Grison et al., 2019; Kirk et al., 2022) which drives GFP expression via a phloem-specific promoter, the novel *pSCR::GFP* and *pGLABRA2*::GFP (*pGL2::GFP*) reporter systems were used. In these reporters GFP

expression is driven by an endodermal- and a epidermal- specific promotor, respectively, which allows for the movement of GFP to be determined from different tissue types and in the retrograde direction relative to phloem unloading of GFP in the *pSUC2::GFP* reporter (Lin and Schiefelbein, 2001; Levesque et al., 2006).

The main findings of this chapter are that low nitrate led to a reduction in primary root length that correlated with reduced bi-directional flux of GFP; the first account of changes in symplasmic transport in this type of treatment that was supported by observations with all 3 symplasmic reporter systems. Another finding is that GFP flux is altered in response to much weaker osmotic stresses than have been previously reported. This reduced flux correlates with reduced primary root length and increased tortuosity.

4.2 Results

4.2.1 Primary and lateral root growth is affected by the concentration of primary macronutrients, changes in water potential and salinity.

As a preliminary screen for potential effects in symplasmic transport, root phenotypes of *Arabidopsis* seedlings exposed to abiotic conditions were determined. Wildtype *Arabidopsis* plants were grown in ATS media (Wilson et al., 1990) and modified ATS media (which differs in the composition of one nutrient or compound; see Materials and Methods) without exogenous sucrose. The control (full) ATS media contains 9 mM nitrate , 2.5 mM Pi, 7.5 mM K^+, 0% polyethylene glycol (PEG), 10 µM NaCl and a full complement of micronutrients. Modified ATS treatments developed to dissect responses to low concentrations of macronutrients were media that contained 0.1 mM nitrate, 0 mM K+ or 0 mM Pi. Modified ATS treatments developed to dissect responses to elevated osmotic challenge and salt stress were 3% PEG and 75 mM NaCl. The predicted water potential of the media relating to osmotic challenge and salt stress are presented in Table 4-1.

At 4 and 7 dpg, primary root length, primary root tortuosity (the Euclidean distance from the hypocotyl root junction to the primary root tip over the primary root length), total lateral root length, lateral root number and lateral root density (number of emerged lateral roots per mm of primary root length) were determined (Figure 4.1, Figure 4.3). At 4 and 7 dpg, primary root length was significantly shorter in 0.1 mM nitrate, 0 mM K+, 3% PEG and 75 mM NaCl relative to control conditions but was not altered in 0 mM Pi (Figure 4.1 a, b). Primary root tortuosity at 4 dpg appeared reduced in 0 mM K+ and 3% PEG but

differences were not distinguishable at 7dpg (Figure 4.1 D,E). At 7dpg, primary root tortuosity is significantly increased in 75 mM NaCl. Primary root length is determined by the rate of cell division and growth of the root apical meristem (RAM). To verify if differences in primary root length are reflected in differences in the RAM, 4 days old seedlings grown in control and treatment conditions were stained with propidium iodide and imaged under a confocal microscope. The distance and the number of cells between the quiescent centre (QC) and the transition zone (TZ) were measured using ImageJ (Figure 4.2). These data are considered preliminary as this experiment was not repeated. No significant differences were observed in either parameter measured between control and treatment conditions. To determine the effects of changing conditions, seeds were germinated on ATS media and grown for 4 days after which they were transferred to treatment plates. Root phenotypes were determined 3 day post transfer (dpt). Significant reductions in primary root length were observed in 3% PEG or 75 mM NaCl (Figure 4.1 C). Although not significant, the median primary root length was also reduced in plants transferred to 0.1 mM nitrate and 0 mM K+. Primary root tortuosity is highest in plants transferred onto 75 mM NaCl although the difference was not statistically significant (Figure 4.1 F).

Table 4-1 Estimated water potential of media used in this study. Media water potential (Ψ) was approximated by summing the estimated solute potential of each media component as described in Materials and Methods.

ATS + 0.8% agar Ψ (MPa)			**1/2 MS + 0.8% agar Ψ (MPa)**		
	0% sucrose	1% sucrose		0% sucrose	1% sucrose
Control	-0.66	-0.73	Control	-0.71	-0.78
3% PEG (Mr 8000)	-1.35	-1.42	3% PEG (Mr 8000)	-1.33	-1.40
75 mM NaCl	-1.53	-1.60	400 mM mannitol	-2.37	-2.44

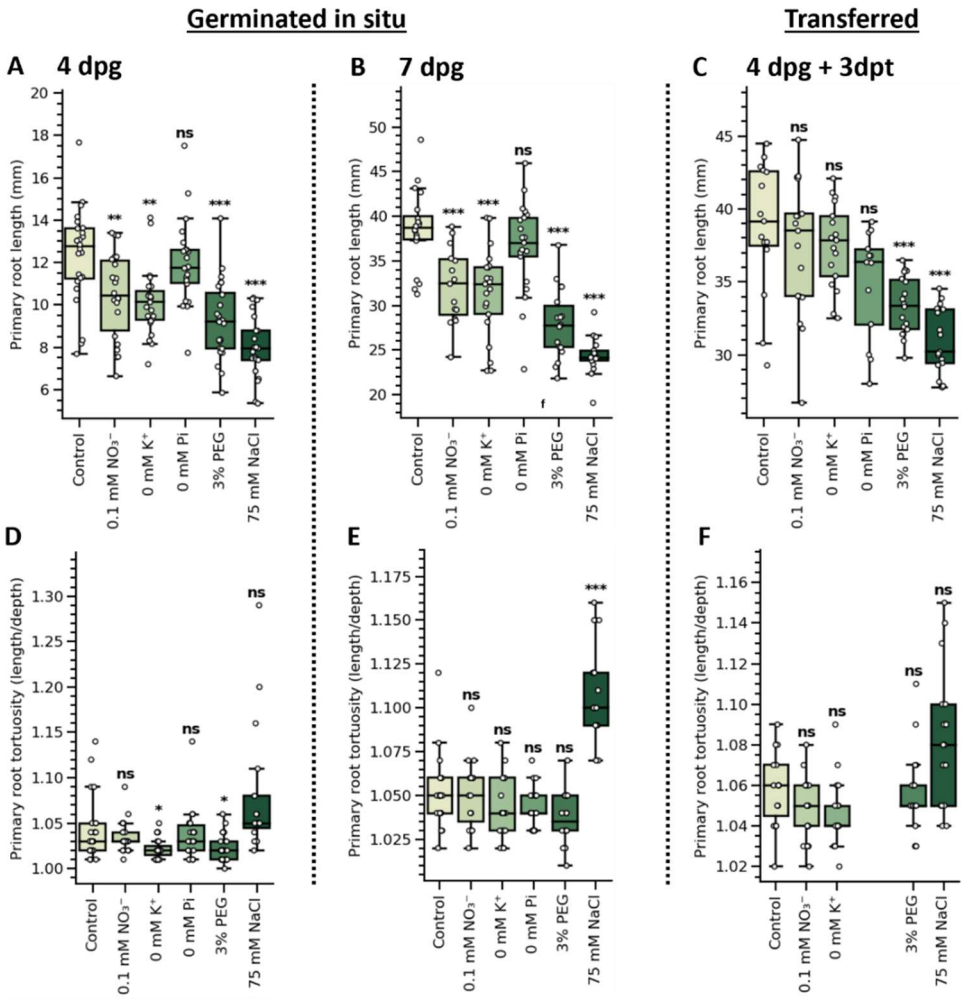

Figure 4.1 Primary root length and tortuosity is modified in seedlings germinated in different concentrations of nitrate, Pi, K+, PEG and NaCl. Seedlings were grown in ATS (0% sucrose, 9 mM NO_3, 7.5 mM K+, 2.5 mM Pi, 0% PEG, 10 µM NaCl) or in the modified testing conditions: 0.1mM NO_3, 0mM K+, 0mM Pi, 3% PEG or 75mM NaCl as described in Material and Methods. (C,F) For transfer experiments, seeds were germinated in ATS for 4 days and transferred to either fresh media (control) or ATS with the different concentrations of N, Pi, K+, PEG and NaCl. Primary root length and tortuosity were measured (A,D) 4 days and (B,E) 7 days post germination. (C,F) For transferred plants, primary root length and tortuosity were measured 3 days post transfer. Pairwise significance testing was performed on treatments relative to Control by one-way ANOVA (Dunnett's post hoc test, N≥13, ns: not significant, **: $0.001<p \leq 0.01$, ***: $p \leq 0.001$, see Material and Methods for more details of statistical analyses).

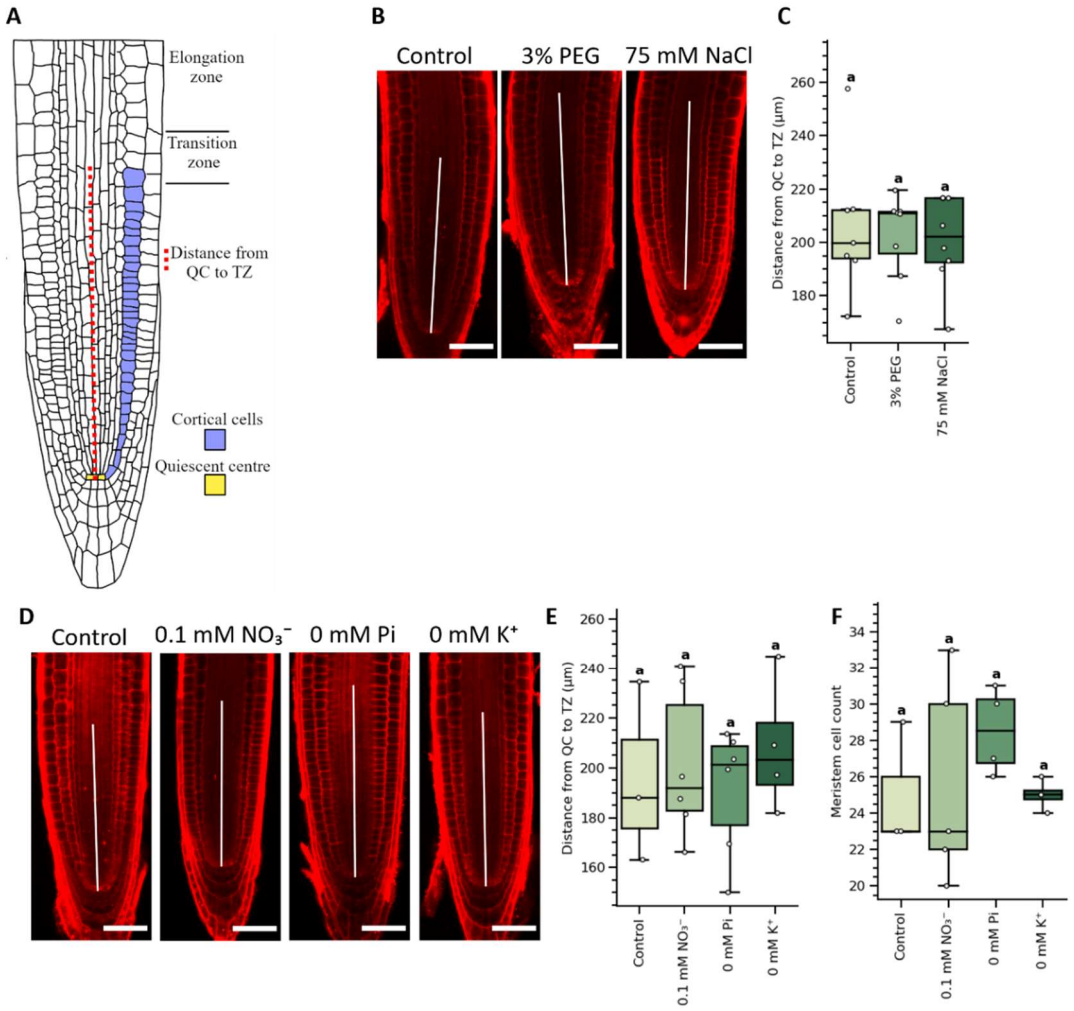

Figure 4.2 Meristem size and cell number in low nutrient and water availability. (A) Meristem size was determined as the distance and number of cortical cells between the transition zone (TZ) and the quiescent centre (QC). 4-days old *A. thaliana* roots grown on ATS (0% sucrose, 9 mM NO_3, 7.5 mM K+, 2.5 mM Pi, 0% PEG, 10 µM NaCl) or in the modified testing conditions: 0.1mM NO_3, 0mM K+, 0mM Pi, 3% PEG or 75mM NaCl, were stained with 1% propidium iodide (PI). (A, D) Representative images of root tips imaged by confocal microscopy (red: PI) are shown. (B,E) Distance from the quiescent centre (QC) to the transition zone (TZ, determined as the region where cell division ends and start to elongate in cortical cell files). (C) Number of meristem cells counted from the QC to the TZ. No significant difference was noted in this small sample number. Pairwise significance testing was performed on treatments relative to Control by one-way ANOVA (Dunnett's post hoc test, N≥7, ns: not significant). Scale bar = 100 µm

A significant difference in lateral root development was observed when plants were germinated *in situ* on control and 75mM NaCl treatment media where total lateral root length and number of lateral roots were reduced (Figure 4.3). Relative to control conditions, plants grown *in situ* on 3% PEG also displayed a slight reduction in these parameters although it was not statistically significant. Lateral root development was not significant altered in any other treatment condition at this time-point (7 dpg). When plants are grown in control conditions and then transferred into treatment or control conditions (transfer experiments), total lateral root length was found reduced in 75mM NaCl but not in any of the other treatment condition.

To summarise, strong effects in primary root length, primary root tortuosity and total lateral root length were observed in plants germinated in elevated salinity/NaCl although these were not translated in differences in meristem size at 4 dpg. Low nitrate, no addition of K and 3% PEG also reduced primary root length and have milder effects in primary root tortuosity but these conditions do not appear to significantly affect lateral roots at 7dpg. Roots grown in media without exogenous Pi resembled control in our conditions.

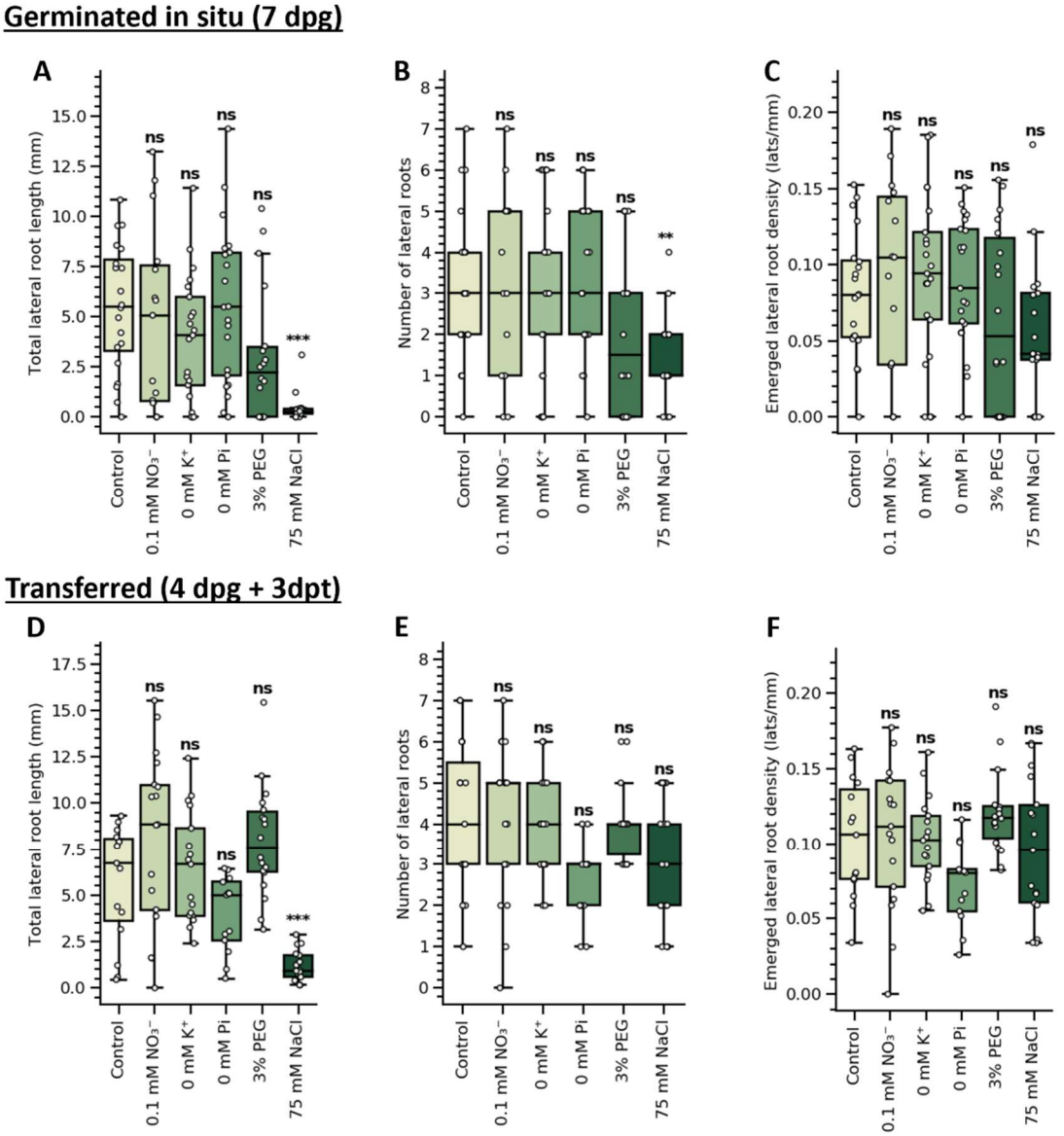

Figure 4.3 Lateral root changes in seedlings germinated in different concentrations of nitrate, Pi, K+, PEG and NaCl. Seedlings were grown in ATS (0% sucrose, 9 mM nitrate, 7.5 mM K+, 2.5 mM Pi, 0% PEG, 10 µM NaCl) or in the modified testing conditions: 0.1 mM nitrate, 0 mM K+, 0 mM Pi, 3% PEG or 75 mM NaCl as described in Material and Methods. Total lateral root length, lateral root number and emerged lateral root density were calculated (A-C) 7 days post germination in seedlings directly grown in the different media or (D-F) 3 days post transfer for seedlings germinated in ATS for 4 days before being transferred to the different media. Pairwise significance testing was performed on treatments relative to Control by one-way ANOVA (Dunnett's post hoc test, N≥13, ns: not significant, **: $0.001 < p \leq 0.01$, ***: $p \leq 0.001$, see Material and Methods for more details of statistical analyses). Total lateral root length and number but not density is significantly reduced in 75 mM NaCl.

4.2.2 Addition of sucrose affects the root response to primary nutrients, to osmotic changes and high salt.

Experiments described in 4.2.1 were done without the addition of sucrose, partially to simulate normal growing conditions and promote normal physiological responses. However, sucrose is routinely added to the growth media in root phenotyping experiments (Xu et al., 2013) and therefore phenotyping experiments were repeated in media with 1% sucrose. Plants were grown in ATS and modified-ATS (as described above) supplemented with 1% sucrose. In parallel, plants were also grown in ½ MS and modified MS media; another common media system employed in phenotyping root morphology (Saucedo et al., 2012; Zheng et al., 2016; Li et al., 2020a). MS media used here contained 1 mM nitrate, 624 µM Pi, 1.6 mM K^+, 0% PEG and a full complement of micronutrients. The modified MS treatments developed here differ from MS in only one component each (see Materials and Methods) giving rise to media with 5 mM nitrate, 0.1 mM nitrate, 20 µm K+, 2.5 mM Pi, 0.1 mM Pi and 3% PEG.

Primary root length, primary root tortuosity, total lateral root length, lateral root number and lateral root density were determined after the treatments described above. WT plants grown in 0 mM Pi (ATS) displayed a significantly larger primary root length at 3 dpg (Figure 4.4 A) relative to control. Primary root length was significantly reduced in 0 mM K+ and 3% PEG. No change in primary root length was observed in 0.1 mM nitrate. These phenotypes were still observed at 6 dpg (Figure 4.4 B). Primary root tortuosity was reduced in plants grown in 0.1 mM nitrate, 0 mM K+, 0mM Pi and 3% PEG after 6 dpg (Figure 4.4 C,D). Changes in primary root length of WT plants grown in ½ MS based media for 4 dpg and then transferred to treatments were apparent after different lengths of time after transfer (Figure 4.5). At 1 dpt, primary root length was increased in 2.5 mM Pi. At 3 dpt, additionally, primary root length was reduced in 3% PEG. At 7 dpt, primary root length was reduced in 0.1 mM Pi and 0.1 mM nitrate. No primary root tortuosity phenotypes were evident until 7 dpt where 0.1 mM nitrate caused a significant increase in this phenotype. Changes in primary root length at 7 dpt were reflected in total lateral root length with an increase in length in 2.5 mM Pi and reductions in length in 3% PEG, 0.1 mM Pi and 0.1 mM nitrate (Figure 4.6 A). Lateral root number was reduced in 3% PEG, 0.1 mM Pi and 0.1 mM nitrate (Figure 4.6 B). No change in lateral root number was observed in 2.5 mM Pi and subsequently this treatment experienced a reduction in emerged lateral root density,

likely due to an increase in primary root length (Figure 4.6 C). No changes in emerged lateral root density were observed in response to the other treatments.

In summary, the phenotypes observed in the presence of sucrose were different to those where no exogenous sucrose was supplied. Relative to growth in control media, primary root length under 0.1 mM nitrate when supplemented with sucrose was not significantly different. However, without sucrose the relative primary root length was reduced in 0.1 mM nitrate. Likewise, relative primary root length under 0 mM Pi with supplemented sucrose was significantly increased but not significantly different without supplemental sucrose. With sucrose, primary root tortuosity was reduced in 0.1 mM nitrate, 0 mM K+, 0mM Pi and 3% PEG but with exogenous sucrose, no significant differences were observed in any of these treatments.

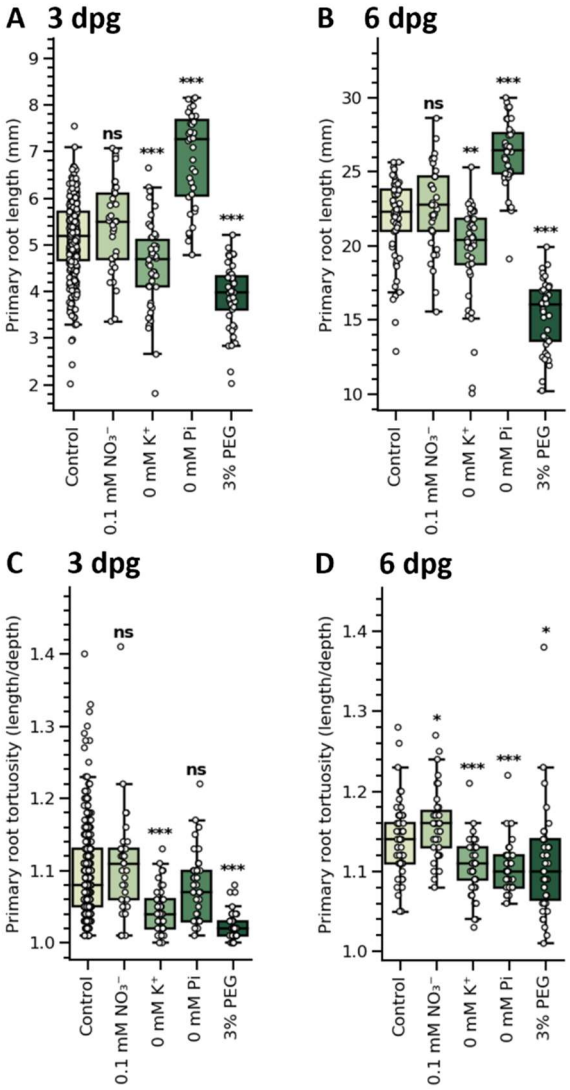

Figure 4.4 Addition of sucrose modify primary root responses to nitrate, Pi, K+ and PEG. Seedlings were grown in ATS plates 1% sucrose or in the modified testing conditions: 0.1mM nitrate, 0 mM K+, 0 mM Pi, 3% PEG as described in the Material and Methods. Control media contained 9 mM NO_3, 7.5 mM K+, 2.5 mM Pi and 0% PEG. Primary root length and tortuosity were measured (A,C) 3 days and (B,D) 6 days (B, D) post germination. Pairwise significance testing was performed on treatments relative to control by one-way ANOVA (Dunnett's post hoc test, N≥35, ns: not significant, *: 0.01 < p ≤ 0.05, **: 0.001<p ≤ 0.01, ***: p ≤ 0.001, see Material and Methods for more details of statistical analyses).

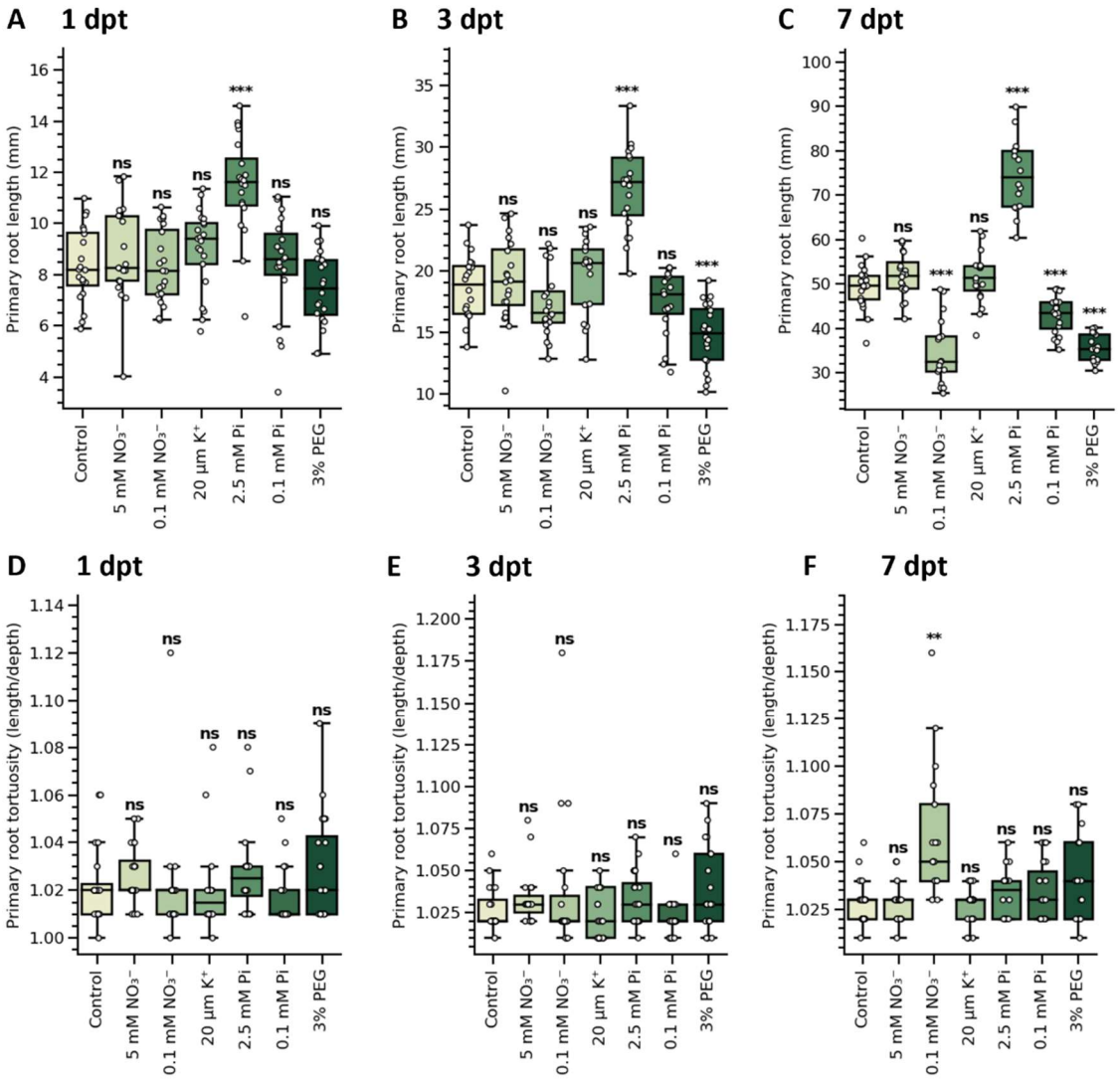

Figure 4.5 Primary root responses after transfer to nitrate, Pi, K+ and PEG in the presence of exogenous sucrose. Plants were first grown in ½ MS (1% sucrose, 9 mM nitrate, 1 mM Pi, 10 mM K+, 0% PEG) for 3 days before transfer to fresh plates of the same media (Control) or to plates with different concentrations nitrate, Pi, K+, or PEG as indicated in the figure. Primary root length and tortuosity were measured at (A,D) 1, (B, E) 3 and (C, F) 7 days post transfer. Pairwise significance testing was performed on treatments relative to Control by one-way ANOVA (Dunnett's post hoc test, N≥16, ns: not significant, **: 0.001<p ≤ 0.01, ***: p ≤ 0.001, see Material and Methods for more details of statistical analyses).

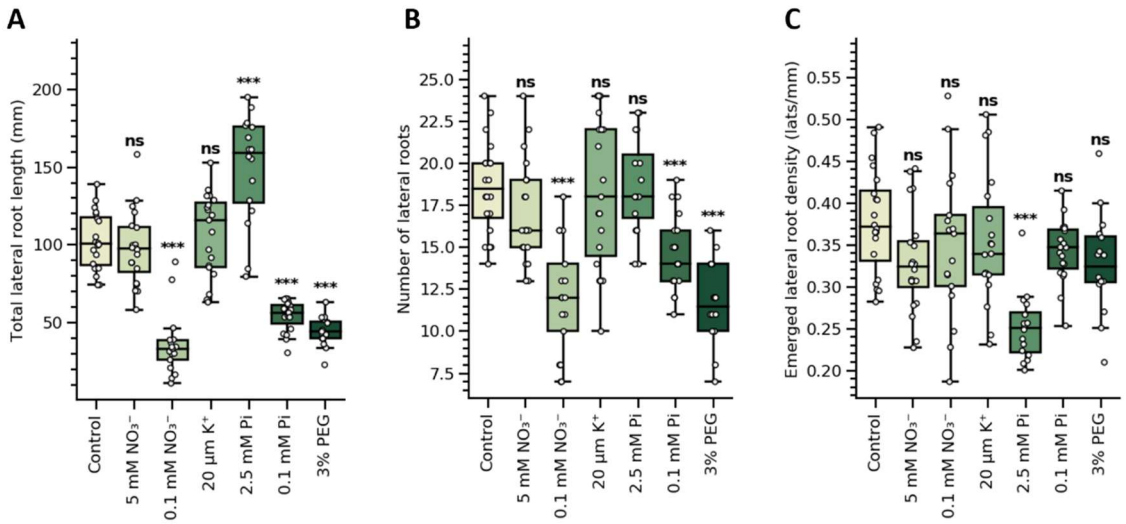

Figure 4.6 Lateral root responses after transfer to different concentration of nitrate, Pi, K+, or PEG in the presence of exogenous sucrose. Plants were germinated and grown for 3 days on ½ MS (1% sucrose, 9 mM nitrate, 1 mM Pi, 10 mM K+, 0% PEG) and transferred to fresh plates of the same media (Control) or containing the concentrations of nitrate, Pi, K+, or PEG indicated in the figure. (A) Total lateral root length, (B) number of lateral roots and (C) emerged lateral root density were measured at 7 days post transfer. Pairwise significance testing was performed on treatments relative to Control by one-way ANOVA (Dunnett's post hoc test, N≥16, ns: not significant, ***: $p \leq 0.001$, see Material and Methods for more details of statistical analyses).

4.2.3 Symplasmic transport studies using GFP reporters in response to depleted macronutrients

In sections 4.2.1 and 4.2.2, conditions affecting root development were identified. To evaluate the effect of these conditions on symplasmic transport, seedlings expressing GFP under the phloem specific promoter of *pSUC2::GFP* were used. *pSUC2* drives GFP expression to the phloem companion cells from where it can diffuse via PD into neighbouring tissues (Figure 4.7 A). *pSUC2::GFP* seeds were germinated in ATS, 0% sucrose media and exposed permanently (germinated *in situ*) or transiently (transfer experiments) to the same treatment conditions in the root phenotyping experiments described above. Root tips were imaged under a epifluorescence or confocal microscope and GFP profiles determined via ImageJ as described in Material and Methods.

GFP profiles for seedlings grown in control, 0.1mM nitrate, 0 mM Pi and 0 mM K^+ after 3 days post germination were generated (Figure 4.7). Plants on 0.1 mM nitrate (ATS, 0% sucrose) show a distribution of fluorescence that is more restricted to the stele within the TZ of primary roots relative to control as shown in representative images (Figure 4.7 B). To generate the aggregated profiles of multiple plants (henceforth referred to as fluorescence profiles), fluorescence is scaled (min-max normalised) to control for differences in absolute expression between biological replicates and treatments. The area of lateral profiles that equate to the centre of expression show similar levels of relative expression between 0.1 mM nitrate and control. Moving away from the centre of expression, relative fluorescence decreases to a larger extend in plants grown in 0.1 mM nitrate and there is less fluorescence in the epidermis (Figure 4.7 C).

For rootward fluorescence profiles, levels of relative fluorescence decrease more rapidly in 0.1 mM nitrate (Figure 4.7 D). Over a length of 50 µm from the TZ/proliferation zone (PZ) boundary towards to root tip, relative fluorescence had dropped under 6% in control conditions but over 20% in 0.1 mM nitrate (Figure 4.7 D). Relative fluorescence drops much less slowly over the next 100 µm and relative fluorescence at 150 µm from the apical/basal meristem junction is similar between 0.1 mM nitrate and control (Figure 4.7 D). Lateral profiles of fluorescence in plants grown in 0 mM Pi show higher levels of fluorescence in the epidermis (Figure 4.7 E). No obvious differences in lateral GFP distribution were observed under 0 mM K+ (Figure 4.7 G). No obvious differences in rootward distribution of GFP were observed for plants grown in 0 mM Pi or 0 mM K+ (Figure 4.7 F,H).

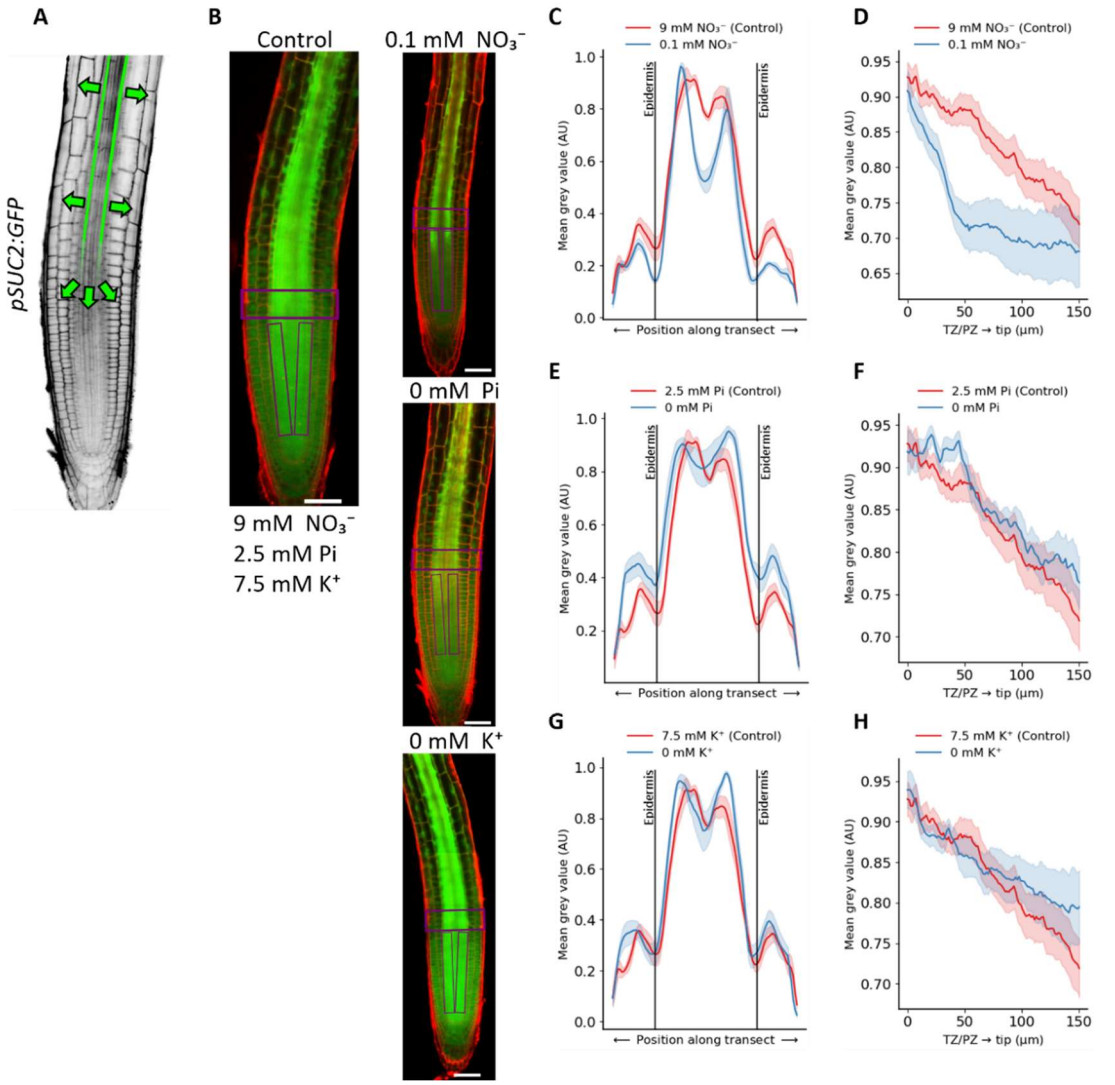

Figure 4.7 Symplasmic GFP distribution in root tips is reduced under low N conditions but not significantly affected by absence of Pi or K+. *A. thaliana* plants expressing *pSUC2::GFP* were grown on ATS (0% sucrose) for 3 days post germination. GFP expression (green) was visualised in root tips counterstained with propidium iodide (red) using a confocal microscope as described in Materials and Methods. (A) Diagram shows that transcriptional expression of GFP is restricted to the phloem companion cells in the root meristem of *A. thaliana*. Arrows represent direction of GFP diffusion. (B) Representative confocal images of root tips in control or in media with either 0.1mM nitrate, 0 mM Pi or 0 mM K^+. Purple boxes highlight area used to build fluorescence profiles. Scale bar = 100 µm. (C, E, G) Lateral GFP fluorescence profiles calculated using mean grey values (au) across the transition zone as shown in a. (D,F,H) Rootward GFP fluorescence profiles calculated using mean grey values (au) starting from the transition zone and ending 150 µm towards the root tip as shown in a. (C:H) Trace = Mean ± SE GFP fluorescence from N>6 plants.

To verify the results and test connectivity between different cell layers, two independent reporters were used. *pSCR* restricts expression to the endodermis and endodermis/cortex initials (Koizumi and Gallagher, 2013). *pGL2* restricts expression in the root to atrichoblast cells in the epidermis (Masucci et al., 1996). The expression of GFP under the *pSCR* reporter system is represented in Figure 4.8 A. Plants expressing *pSCR::GFP* were grown on control or 0.1 mM nitrate media. No major differences in the expression of GFP was apparent between these conditions. Relatively less GFP was observed in the epidermis and cortex in 0.1 mM nitrate. This is also reflected in the aggregated profiles of multiple plants where it is clear there is less fluorescence in the outer tissues relative to more central tissues (Figure 4.8 C). No differences in GFP distribution under 0.1 mM nitrate were observed in central tissues (from endodermis-endodermis). The expression of GFP under the *pGL2* reporter system is depicted in (Figure 4.8 D). Plants grown on 0.1 mM nitrate displayed moderately less GFP expression than under control conditions (Figure 4.8 E). Lateral profiles show a reduced distribution of GFP towards the centre in plants grown in 0.1 mM nitrate whereas under control conditions, GFP fluorescence is as high centrally as it is in the source tissue (Figure 4.8 F). No differences in GFP expression or distribution were observed in plants expressing *pGL2::GFP* in 0 mM Pi or 0 mM K^+ (Figure 4.9).

In summary, GFP signal in roots of symplasmic reporters diminishes the further away from the centre of expression it is measured. This is particularly evident under 0.1 mM nitrate as a reduction in lateral movement of GFP was observed in the *pSUC2*, *pGL2* and *pSCR* symplasmic reporters. Moreover, a steeper decline in rootward GFP signal was observed under 0.1 mM nitrate using the *pSUC2* promotor. An increase of lateral movement of GFP was observed in plants grown in 0 mM Pi using the *pSUC2* system but no difference in rootward GFP profile was observed. GFP fluorescence profiles of roots grown in 0 mM Pi or 0 mM K+ using the *pSCR* or *pGL2* system were not discernibly different from those grown under control conditions.

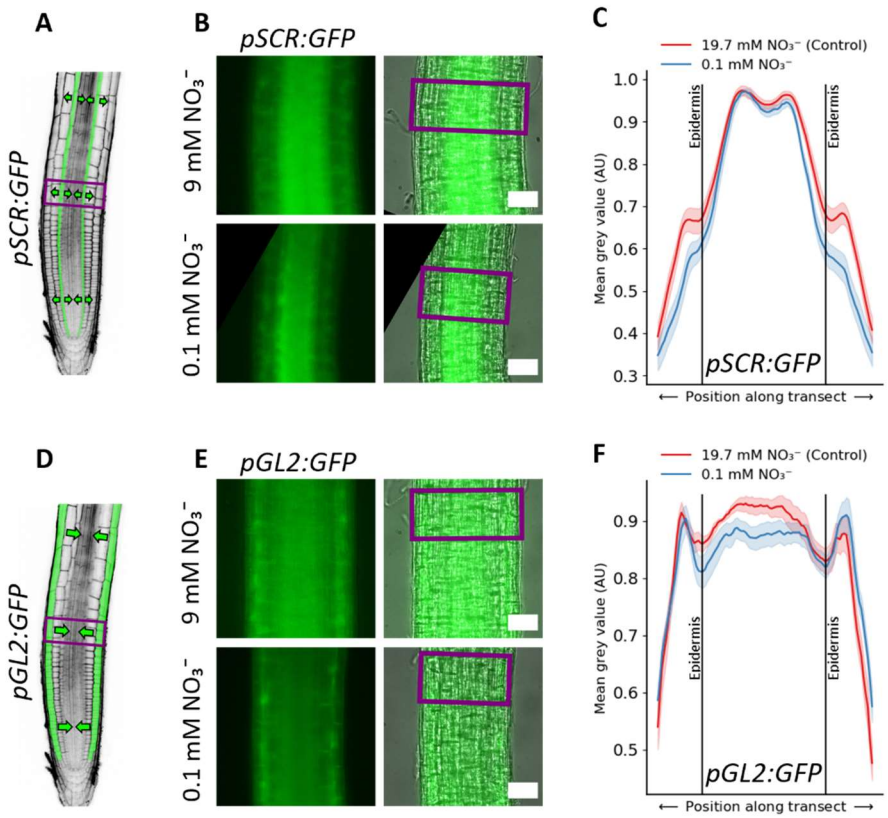

Figure 4.8 Low nitrate reduces symplasmic GFP transport across different cell layers in the root tip. Plants expressing GFP under the control of either the endodermal promoter *pSCR* or the epidermal promoter *pGL2* were grown on control (9 mM nitrate 1/2 MS, 1% sucrose) or 0.1 mM nitrate media (1/2 MS modified to 0.1 mM nitrate). Primary roots were imaged using an epifluorescence microscope at 7 dpg. (A,D) Diagrams showing tissue expression pattern of *pSCR*2::GFP and *pGL2::GFP*, respectively, with arrows representing direction of GFP diffusion that can be inferred from assay. Area of root used for lateral GFP measurement is highlighted by the purple box. (B, E) Representative images of an area within the transition zone for each treatment (left: GFP, right: merged with transmitted light). Scale bar = 100 µm. (C, F) Aggregated lateral GFP fluorescence profiles calculated using mean grey values (au) in the area highlighted in A-C. Mean ± SE lateral GFP fluorescence profile of N > 6.

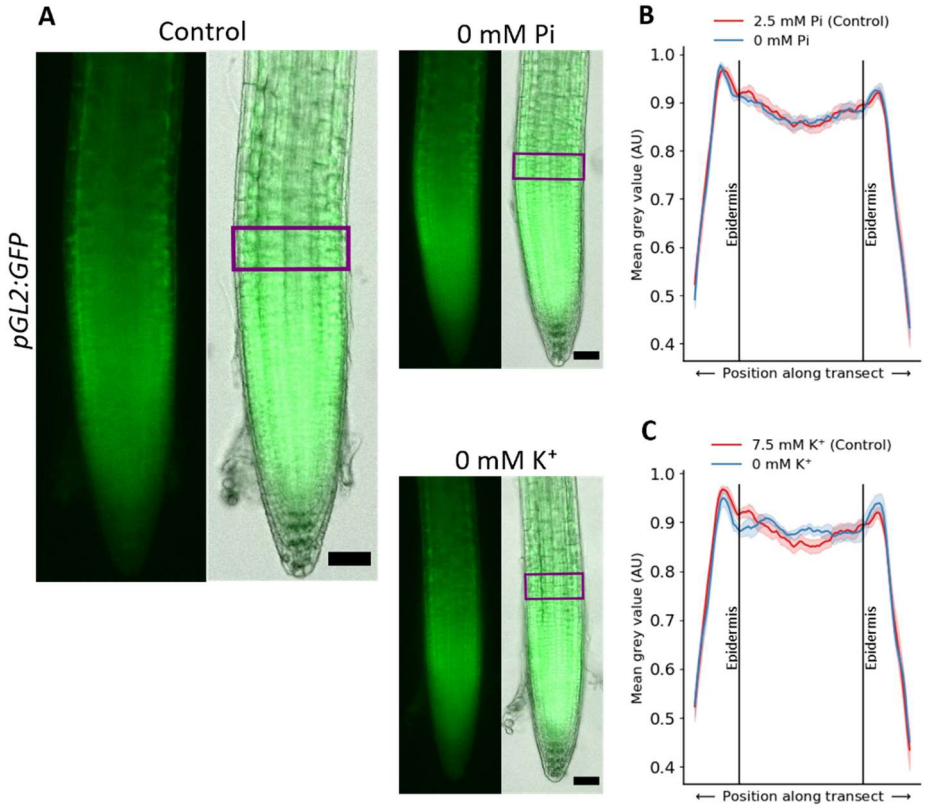

Figure 4.9 Absence of Pi or K+ does not change GFP distribution in *pGL2::GFP* root tips. Plants expressing the epidermal reporter *pGL2::GFP* were grown on control (ATS media, 2.5 mM Pi, 7.5 mM K^+), 0 mM Pi ATS or 0 mM K^+ media. Primary roots were imaged using an epifluorescence microscope at 5 dpg. (A) Representative images of root tips for each treatment (left: GFP, right: merged with transmitted light). Area of root used for lateral GFP measurement is highlighted by the purple box. (B, C) Aggregated lateral GFP fluorescence profiles calculated using mean grey values (au) in the area highlighted in **a**. Mean ± SE lateral GFP fluorescence profile of N > 6.

4.2.4 Symplasmic transport studies using GFP reporters in response to changes in water potential and salinity.

Distribution of *pSUC2::GFP* was studied to determine the effect of PEG and NaCl on symplasmic communication. Plant growth conditions matched those described for root morphology phenotyping above. Plants grown directly in 3% PEG for 4 dpg did not exhibit any noticeable changes in lateral distribution of GFP from the stele in the TZ of primary roots relative to control condition (Figure 4.10 A,B). For rootward fluorescence profiles, levels of fluorescence decreased more rapidly in 3% PEG between 0 µm - 75 µm from the TZ/PZ boundary towards to root tip, remain stable for approximately 50 µm and then

increase whereas as relative fluorescence steadily decreases across this distance (Figure 4.10 A,C). Expression of *pSUC2*::GFP is suppressed in plants grown directly in 75 mM NaCl for 4 dpg (Figure 4.10 A). Differences in expression are controlled for by min-max normalisation after which lateral fluorescence profiles of control and 75 mM NaCl closely align (Figure 4.10). Relative GFP distribution in the rootward direction is more constricted in 75 mM NaCl (Figure 4.10 A,C). This is apparent in rootward scaled fluorescence profiles, particularly between 50 µm - 150 µm away from the apical/basal meristem junction towards the tip where relative fluorescence drops over 13% in 75 mM NaCl and less than 2% in control conditions.

For transfer experiments, seedlings were grown on control media and transferred to control, 3% PEG or 75 mM NaCl for 24 hours before imaging (Figure 4.10 D-F). No differences in GFP distribution were observed 24 hours after transfer from control to 3% PEG conditions (Figure 4.10 E, F). GFP fluorescence was diminished in plants transferred to 75 mM NaCl (Figure 4.10 D). Lateral profiles of normalised fluorescence between plants transferred to 75 mM NaCl show that there is relatively higher fluorescence in the region of the epidermis (Figure 4.10 E). Relative GFP distribution in the rootward direction is modestly more constricted in plants transferred to 75 mM NaCl (Figure 4.10 F). Over the length of 150 µm from the apical/basal meristem junction towards the tip, relative fluorescence decreases 8% in control plants and 11% in plants transferred to 75 mM NaCl.

To verify the effect of changes in water potential on symplasmic transport, plants were transferred to 400 mM mannitol, which reduces the water potential from approximately -0.71 MPa to -2.37 MPa (Table 4-1). Seedlings on mannitol exhibit major changes in GFP distribution in the root tip 16 hours after transfer (Figure 4.11). The amount of GFP present in the epidermis and cortex is clearly reduced in the representative image of a plant transferred to 400 mM mannitol relative to the control (Figure 4.11 A). This effect is reflected in the aggregated lateral root profile (Figure 4.11 B). GFP distribution in the rootward direction in control plants is consistent with above and decreases steadily over 150 µm from near the TZ towards the tip, reducing 26% over this distance (Figure 4.11 A, C). Conversely, GFP distribution in the rootward direction in plants transferred to 400 mM mannitol increased over 150 µm from near the TZ towards the tip, with fluorescence increasing 35% over this distance. Tissue damage is also highlighted by cellularisation of PI stain in the elongation zone of plants transferred to 400 mM mannitol (Figure 4.11 A).

GFP distribution when expressed under the epidermal promoter *pGL2* was also assessed in 3% PEG and 75 mM NaCl (Figure 4.12). Reduced lateral distribution of GFP towards the centre of roots was observed in plants grown in 3% PEG along the apical meristem and to a less degree along the TZ (Figure 4.12 B, C). No clear differences in lateral GFP diffusion were observed along the elongation zone of plants grown in 3% PEG. GFP expression was also reduced in 75 mM NaCl relative to the control (Figure 4.12 A). In this condition, relative lateral distribution of GFP towards the centre was reduced in the TZ and to a lesser extent the EZ. No discernable differences in lateral distribution of GFP were apparent at the TZ in plants grown in 75 mM NaCl.

In summary, rootward diffusion of GFP from the stele in the *pSUC2* symplasmic reporter was restricted when plants were grown under mild osmotic challenge (3% PEG) and elevated NaCl. Rootward diffusion of GFP from the stele was also reduced when plants were transferred to elevated NaCl but not mild osmotic challenge. Under more severe osmotic challenge (400 mM mannitol), lateral diffusion of GFP from the stele towards the epidermis was highly constricted but rootward diffusion was increased. Reduced lateral diffusion of GFP from the epidermis towards the stele was evident under mild osmotic challenge and elevated NaCl using the *pGL2* symplasmic reporter.

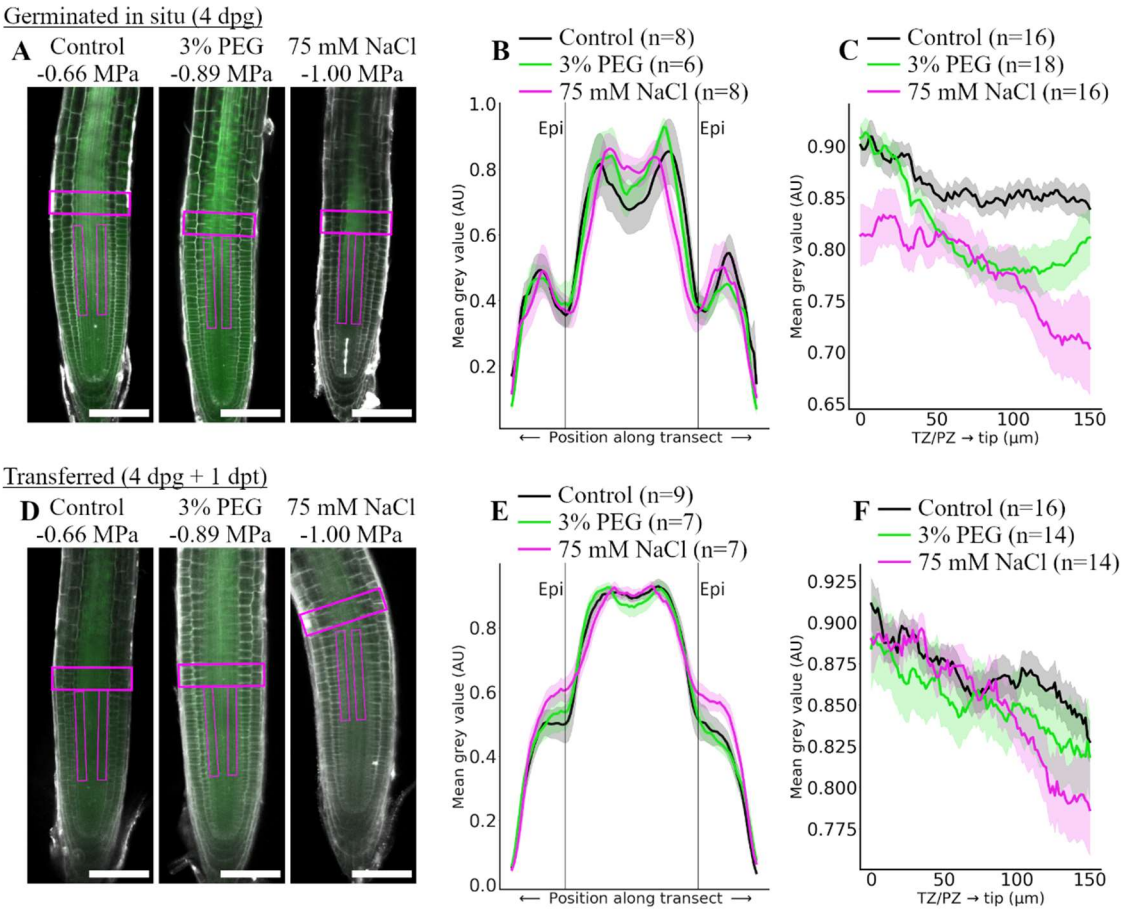

Figure 4.10 GFP diffusion in the root meristem of *Arabidopsis thaliana* is restricted in 3% PEG and 75 mM sodium chloride. (A) Seeds expressing *pSUC2::GFP* were grown on ATS control media, ATS supplemented with 3% polyethylene glycol (PEG) or with 75 mM NaCl. Roots were collected at 4 days post-germination (4 dpg) and counterstained with propidium iodide (PI). Images were sequentially collected at 561 nm (PI shown in grey) and 488 nm (green: GFP). Estimated water potential (MPa, see Table 4-1) is labelled on top of the representative pictures. (B,C) Transects highlighted by magenta boxes in A were used to determine GFP fluorescence profiles using mean grey values (AU: arbitrary units). (B) shows transects across the transition zone (TZ) while (C) shows transects rootward starting from the transition/proliferation zone (TZ/PZ) towards the root tip. (D-F) Similar experiments were carried out with seedlings germinated on ATS media and transferred for 1 day (1 dpt) to 3% PEG or 75 mM NaCl. Scale bar = 100 µm. Charts show traces representing aggregate min-max normalised GFP fluorescence along the transect (mean ± SE). Transects (n, stated in the key) are from (B,E) a separate plant or (C,F a maximum of two from one plant. This figure was also published in Kirk et al. (2022).

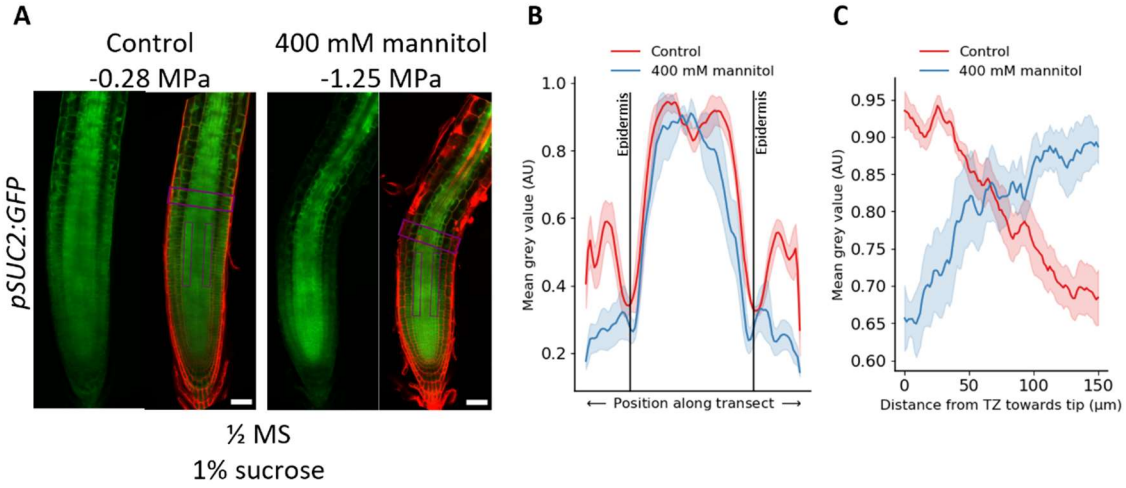

Figure 4.11 Addition of mannitol significantly alters GFP distribution supporting the role of water potential. After 6 days post germination in 1/2 MS + 1% sucrose, plants were transferred to control (1/2 MS + 1% sucrose) or mannitol treatment (1/2 MS + 1% sucrose +400 mM mannitol). GFP diffusion was determined by confocal microscopy 16 hours post transfer. (A) Representative confocal images of root tips for each treatment (red: PI, green: GFP), purple boxes highlight area used to build fluorescence profiles. The osmotic potential in these conditions is shown on the top. Scale bar = 50 µm. (B) Lateral GFP fluorescence profiles calculated using mean grey values (au) across the transition zone. (C) Rootward GFP fluorescence profiles calculated using mean grey values (au) starting from the basal/apical meristem transition zone ending 150 µm towards the root tip. (c-h) Trace = Mean ± SE scaled GFP fluorescence from N>3 plants. These data were also published in Grison et al. (2019).

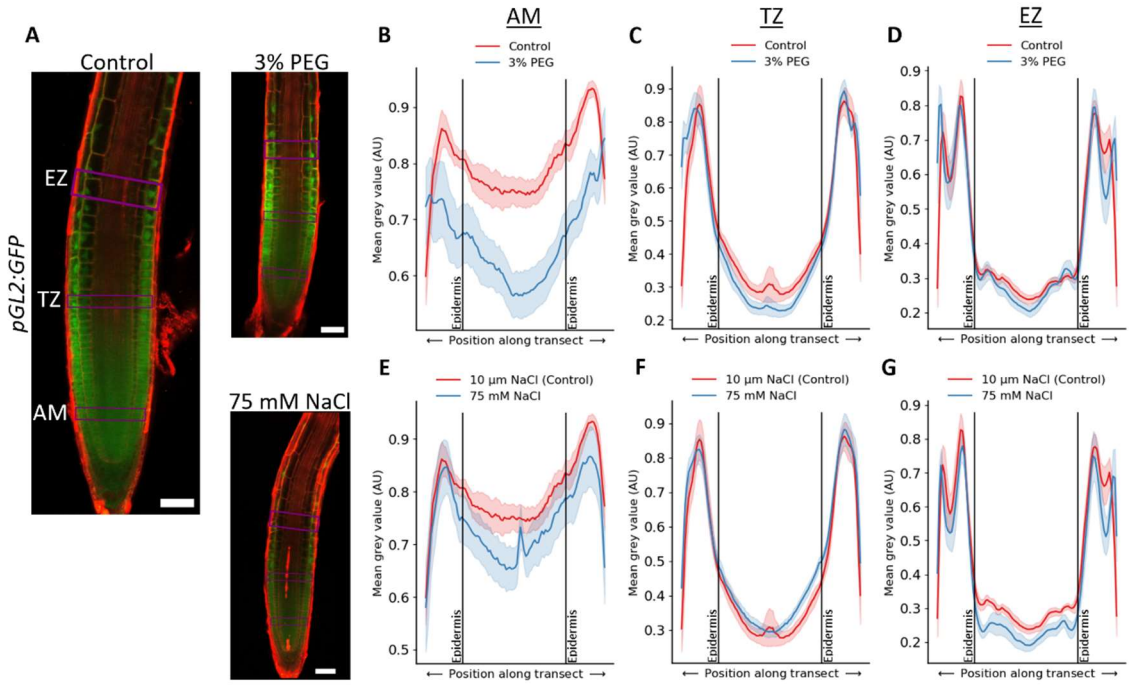

Figure 4.12 Lateral distribution of GFP from the epidermis into the internal root tissues is reduced in 3% PEG and in 75 mM NaCl. *A. thaliana* plants expressing the epidermal reporter *pGL2::GFP* were grown on ATS (0% sucrose) or ATS supplemented with (B-D) 3% PEG or (E-G) 75 mM NaCl. Primary roots were counterstained with PI (red) 4 dpg and analysed for GFP (green) fluorescence using confocal microscopy. (A) Representative confocal images of root tips for each treatment. Area of root used for lateral GFP measurements is highlighted in purple (AM: apical meristem, TZ: transition zone, EZ: elongation zone). Scale bar = 100 µm. (B-G) Lateral GFP fluorescence profiles calculated using mean grey values (au) in the areas highlighted in A. Traces = Mean ± SE lateral GFP fluorescence profile of N > 6.

4.3 Discussion

4.3.1 Root system architecture adapts to substrate water potential and nutrient composition and is modulated by sucrose

Plant root morphology shows a remarkable plasticity tuned by physiological- and environmental-borne cues (Williamson et al., 2001; Vidal et al., 2010; Zheng et al., 2016; Gupta et al., 2020; Ribba et al., 2020). Establishing a link between PD regulation and root morphological responses to nutrient and water availability requires an assessment of what the normal root responses are. In plants grown directly in ATS-based media, reduction in primary root growth was evident in low nitrate and low potassium. Root responses to soil

nitrate conditions are relatively well described and display remarkable complexity that is dependent on local supply and systemic demand (Jobbagy and Jackson, 2001; Linkohr et al., 2002; Miller and Cramer, 2005). Root morphological changes under low potassium have not received as much attention as those under low nitrate or phosphate, however *A. thaliana* ecotype-dependent root phenotypes to low potassium media equivalent to that used in this study has been reported (Kellermeier et al., 2013). The authors showed that the ecotype Columbia (Col-0), which was used in this study, was found to promote lateral root proliferation at the expense of the primary root which is consistent with data presented here. The mechanism by which primary root length was reduced under low nitrate and low K+ could not be deduced. The lack of significant differences in root meristem length or cell count under these treatments relative to control conditions suggests that it may not be morphological changes in the structure of the root meristem that was the cause. However, meristem measurements need to be repeated before this can be confirmed. Low phosphate conditions did not reduce primary root length and increase lateral root proliferation as had been reported previously (Abel, 2011; Péret et al., 2011). Measurements of lateral root morphology were taken during early development (7 dpg) which may not have been enough time for sufficient growth to have taken place for phenotypic assessment. Therefore, caution should be taken before too much significance is attributed to this result.

Recent work to dissect the role in symplasmic transport have used reasonably strong concentrations of the osmotic stressors mannitol (400 mM) and NaCl (150 mM) that have been shown to cause significant levels of cell damage (Grison et al., 2019; Hunter et al., 2019). Cellular damage is a response to strong salt and osmotic stress that can be caused by programmed cell death (Li et al., 2007; Duan et al., 2010) but the severity of this response could mask more subtle responses in root physiology and morphology. Here, efforts were made to use concentrations of PEG and NaCl that caused less cellular damage. Concentrations of PEG and NaCl were sufficient to reduce root growth whether grown *in situ* or transferred into these conditions which is consistent with other reports (Mira et al., 2017; Brunkard and Zambryski, 2019; Han et al., 2019; Hunter et al., 2019; Zhang et al., 2021b). The reason for this supressed growth could be a consequence of resource allocation shifted to adapting to osmotic stress such as the accumulation of osmolytes to rebalance internal/external water potentials (Gurrieri et al., 2020). Tortuosity is increased in plants grown in elevated NaCl. Modulation of root tortuosity has been interpreted as adapting root morphology to improve anchorage and resource prospecting (Popova et al.,

2016). Plants may increase tortuosity in elevated NaCl to find areas of the substrate with lower levels of NaCl.

An area of debate in the field is whether it is appropriate to routinely include sucrose in growth media (Roycewicz and Malamy, 2012; Xu et al., 2013). Exogenous sucrose is applied as it not only speeds up growth but also makes root phenotypes more consistent and not fully dependent on light conditions for growth (Xu et al., 2013). However, sucrose is a carbon source for growing tissues and a signalling factor linked with regulating a multitude of responses including responses to phosphate and lateral root development (Teng et al., 2005; Lei et al., 2011; Roycewicz and Malamy, 2012; Li et al., 2020a). To complicate matters further, many verified, and candidate PD genes identified in Chapter 3 are differentially expressed in sucrose. To account for divergence in approaches in the literature, roots were also phenotyped with exogenous sucrose as well. Most phenotypes were consistent between the absence and application of exogenous sucrose however there were exceptions. The addition of sucrose to ATS media caused a different response of primary root length in plants germinated in 0.1 mM nitrate and 0 mM Pi. Primary root lengths were not significantly different and increased respectively in those conditions. The modulation of low Pi phenotypes is unsurprising as sucrose is a known regulator of responses to low Pi (Lei et al., 2011). The influence of sucrose on primary root length in low nitrate may be due to interactions between N and C partitioning; mechanisms that overlap considerably (Gutiérrez et al., 2007; Shaw and Cheung, 2018).

4.3.2 Symplasmic communication is reduced in low nitrate conditions.

Establishing a link between symplasmic transport regulation with responses to nitrate and phosphate opens new avenues of discovery in uncovering how plants adapt to nutrient availability. Low nitrate strongly affected the distribution of GFP in plants expressing *pSUC2::GFP*. This change in distribution can most likely be attributed to reduced flux of GFP through PD both laterally and rootward from the phloem companion cells in root tips. This finding is supported by the use of a novel endodermal symplasmic reporter, where plants expressing *pSCR::GFP* also exhibited less GFP fluorescence in the epidermis under low nitrate. PD flux can be bi-directional (Kitagawa et al., 2019) and the symplasmic reporter system *pGL2::GFP* has enabled GFP flux to be measured from epidermis towards the centre of roots; akin to the *pEXPA::GFP* reporter system in *Medicago truncatula* (Figure 3.12, Gaudioso-Pedraza et al., 2018). Plants expressing *pGL2::GFP* displayed a reduced accumulation of GFP in more central tissues in low nitrate. Taken together, these data

suggest that symplasmic flux of GFP is reduced from the epidermis towards the phloem, from the phloem towards the epidermis and from the phloem towards the root tip. These are first reports of low nitrate affecting symplasmic transport.

The lateral distribution of GFP in *pSUC2::GFP* plants grown in low Pi contrasts with that of plants grown in low nitrate. GFP fluorescence was higher in epidermal tissues suggesting that lateral flux of GFP from the phloem is increased in this condition. No differences in GFP distribution were observed in this condition using other symplasmic reporters. Low phosphate has been previously linked with reductions in symplasmic transport due to Fe-dependent callose accumulation that correlates with reductions in root growth (Müller et al., 2015). That study a used a similar media system and the same reporter system, but a key difference was that they grew plants on control media for 4 days after which they were transferred to the treatment. Fluorescence was measured 2 days after transfer into low Pi media. This is a distinctly different context as this constriction in symplasmic transport under low Pi reported by Müller et al. (2015) is a response to environmental change and not to a static condition as used in this study. This result not only highlights the dynamic nature of regulated symplasmic transport, but it also underlines the challenge in interpreting observed differences in symplasmic movement using GFP reporter systems. This approach offers only a crude snapshot in time of the state of symplasmic transport in which it is also essential to consider the life history of the plant.

There is another important consideration when using GFP based reporter systems. In the SEL model of PD transport, the pore aperture dictates the size of molecules that can pass though (Wolf et al., 1989). GFP is 27 KDa with a Stokes radius of 2.8 nm (Terry et al., 1995) and the presence or absence of changes in the flux of GFP does not mean that the flux of smaller or bigger molecules is similarly affected. There are size-independent mechanisms by which PD are more- or less- permeable to specific factors. For example, it is thought that CHAPERONIN CONTAINING TCP1 8 binds to non-cell autonomous proteins such as native KN1 and viral movement proteins in the process of folding and unfolding proteins to allow PD to be traversed (Fichtenbauer et al., 2012; Reagan and Burch-Smith, 2020). Therefore, the use of symplasmic reporter systems offers only a restricted view of the state of cell-to-cell transport. Nevertheless, reductions in symplasmic transport observed under low nitrate aligned well with reductions in primary root growth, suggesting that alterations of PD are responsible for the root phenotypes. Reduced sink strength of roots with reduced growth could account for at least some reduction in phloem unloading, and consequently, reduced movement of GFP out of the phloem under the *pSUC2* reporter. To

test this hypothesis, future work should establish whether reduced symplastic transport is a general response to conditions that reduce root growth.

Even if reduced symplasmic transport is a direct consequence of sink strength, changes in cellular connectively are likely to affect the movement of non- cell autonomous signalling factors, such as WOX5, which control root development and therefore changes in symplasmic connectivity could control root development. Indeed, WOX5 expression is regulated by a mobile signal, CLE40 which is perceived by the ARABIDOPSIS CRINKLY4 and CLV1 complex (Berckmans et al., 2020). It is unlikely to be a coincidence that these receptors localise at PD (Stahl et al., 2013) and therefore it is likely that PD play a role in the regulation of WOX5-dependent regulation of the root meristem. Other mobile CLE factors and RNA also have links with low N signalling (Thieme et al., 2015; Okamoto et al., 2016) and therefore it is not unreasonable to consider possible PD-dependent regulation of mobile signals that control responses to low N. However, more work is required to determine which signals, if any, are being regulated changes in PD permeability under these conditions.

4.3.3 Osmotic and salinity stresses play a role on PD regulation.

Water stress is becoming increasingly problematic in agriculture and improving our understanding of plant responses to it have been highlighted as a goal to improving food security (IPCC, 2014; Gupta et al., 2020). There is a growing understanding that PD play an important role in the responses to water stress (Benitez-Alfonso, 2019; Grison et al., 2019; Hunter et al., 2019).

No change in lateral GFP distribution was detected in plants grown *in situ* on elevated NaCl using the *pSUC2* reporter system but there were increases in the amount of relative fluorescence in epidermal cells of plants transferred to elevated NaCl. This could be attributed to transient increases in symplasmic transport, perhaps as an early adaptation to changes in substrate water potential. Regardless of whether plants were grown directly or transferred to elevated NaCl, a steeper gradient of GFP distribution was observed in the rootward direction indicating a restriction of rootward movement of GFP. Changes in symplasmic transport in elevated NaCl correlate with increased root tortuosity and decreased root length.

The pattern of GFP distribution in plants transferred to elevated NaCl was reversed in plants transferred to a relatively severe osmotic stress of 400 mM mannitol where

reduction in lateral movement and increases in rootward movement of GFP were observed. Reduced rootward distribution of GFP was also evident in plants grown directly on media containing the weaker osmotic stress 3% PEG but not in plants transferred to this condition. These observations of osmotic stress increasing or decreasing symplasmic transport is also reflected in other reports (Oparka and Prior, 1992; Schulz, 1995; Grison et al., 2019). This suggests that symplasmic connectivity during osmotic stress is context specific which depends on the severity and the duration of the stress. Physiological factors such as the plants age, health and whether it has been previously exposed to these stressors could also affect the symplasmic response to osmotic- and salt stress which are interactions that have not been previously investigated.

One hypothesis for the changes in symplasmic connectivity in the root tip during salt and osmotic stress is to regulate the movement of signalling factors. Considering that GFP is a macromolecular factor, the differential permeability of this factor suggests that movement of macromolecular signals could be the target of any such regulation. There are few examples in the literature of osmotic and salt stress specific mobile macromolecular signals. However, one factor, CLE25 is expressed in roots suffering water stress and interacts with PD-localising BAM proteins to initiate stomatal closure (Rosas-Diaz et al., 2018; Takahashi et al., 2018). CLE25 also interacts with BAMs to regulate protophloem development in roots which makes it a candidate for the regulation of root morphology during salt and osmotic stress observed in this study (Hu et al., 2022).

Recent works have shed light on how symplasmic transport may be regulated under osmotic challenge. When plants were transferred to media containing concentrations of mannitol that double the water potential of the media, two receptor-like kinases (RLKs), QSK1 (Qian Shou kinase 1) and IMK2 (Inflorescence Meristem Kinase 2) were found to transiently localise to PD. Mutant *qsk1* plants exhibited increased callose and showed changes in lateral root patterning (Grison et al., 2019). The cysteine-rich receptor kinase CRK2 also transiently localises at PD under osmotic stress (150 mM NaCl) and is required for callose deposition under these conditions potentially through direct interaction with callose synthases (Hunter et al., 2019). CRK2 was also shown to play a key role in germination and root length regulation under elevated NaCl highlighting the importance of callose regulation under salinity stress. In the work presented here changes in symplasmic transport were observed in osmotic conditions that are at least 60% less severe than those used in Grison et al. (2019) and Hunter et al. (2019). These changes in symplasmic transport within root meristems correlates with changes in root morphology

but more work is required to determine whether this link is causative. Bioinformatics presented in Chapter 3 highlight many known, and candidate PD genes are differentially expressed in response to drought, salt and osmotic stress. To date, only a handful of PD factors have been directly implicated in plant responses to abiotic stress. Undoubtedly there is much more to be discovered about the role PD proteins play in the regulation of responses to abiotic stress. In the next chapter, the molecular components of the mechanism underlying PD regulation during abiotic stress response is further investigated.

Chapter 5 Responses to low water availability and elevated salt are regulated by PLASMODESMATA CALLOSE-BINDING PROTEIN 4

5.1 Summary

Regulation of PD transport is emerging as a significant regulator of root responses to abiotic conditions but our knowledge so far is restricted to responses linked with low phosphate and severe osmotic stress (Müller et al., 2015; Grison et al., 2019; Hunter et al., 2019). Very little is known about PD regulation in response to nutrient and water availability or how this regulation is linked to changes in root system architecture. One of the key mechanisms underlying PD regulation is via reversible deposition of callose in the cell wall surrounding PD (Amsbury et al., 2018). Callose, is synthesised *in situ* by CalSs and hydrolysed by PDBGs. Other PD-localised proteins can contribute to the homeostasis of PD callose including PDCBs and PDLPs. PDCB proteins have an N-terminal signal peptide, a carbohydrate X8 domain predicted to bind callose and a C-terminal GPI anchor (Simpson et al., 2009). Of the 11 proteins in this family, only 3 members (PDCB1, 2, 3) have been characterised, but PD localisation was confirmed for 2 more members (PDCB4 and PDCB5) (Simpson et al., 2009; Benitez-Alfonso et al., 2013). The mechanism of how PDCBs influence the levels of PD callose is not known. On the other hand, PDLPs which are receptor-like kinases are known to modulate *CalS* expression or activity in response to a wide range of developmental and environmental cues (Caillaud et al., 2014; Cui and Lee, 2016b; Liu et al., 2020a). The role of PD callose in root responses to nitrate, potassium and mild osmotic challenge have not been investigated. In Chapter 4, it was established that root architectural responses to low nitrate and mild osmotic challenge correlate with changes in the symplasmic flux of GFP in root tips. The aim of this chapter is to determine whether there is a causative link between changes in root architecture and changes in PD callose and to identify PD proteins that may be involved in this regulation.

This was achieved by characterising metabolic profiles and phenotyping plants with contrasting levels of PD callose. The lines chosen for this study included plants expressing *p35S::PDBG1-GFP* (PDBG1OE), *p35S::PDLP1-GFP* (PDLP1OE), *p35S::PDCB4-GFP* (PDCB4OE) and *pdbg1*. The choice of these lines was based on previous reports indicating differences in PD callose relative to WT. PDLP1OE increases PD callose and impair symplasmic movement in *Arabidopsis* (Thomas et al., 2008; Caillaud et al., 2014).. PDBG1OE lead to enhanced degradation thus reduced levels of PD callose leading to increased symplasmic transport (Benitez-Alfonso et al., 2013). It was reported that PDBG1OE displays reduced lateral root density whereas the knockout mutant *pdbg1* displays high levels of callose in the stele and an increased lateral root density. Despite

lacking a known enzymatic function, overexpression of PDCB1 causes an accumulation of callose and significantly reduces PD permeability (Williamson et al., 2001; Simpson et al., 2009). Like *pdbg1*, the increased callose in PDCB1OE is associated with increased lateral root density (Benitez-Alfonso et al., 2013). Early work described in this chapter identified that PDCB4 is highly upregulated in roots under abiotic (especially osmotic) stress, thus for phenotyping responses PDCB4OE was analysed instead of PDCB1OE.

Our results suggest that lines with contrasting levels of PD callose have differential enrichment of metabolic pathways related to abiotic stress including ABA accumulation, metabolites related to photorespiration and to glucosinolate biosynthesis. Phenotypic differences in root development were also detected when comparing lines affected in callose regulation (PDBG1OE, PDLP1OE, PDCB4OE and *pdbg1*). PDCB4 was identified as a strong candidate to regulate root response to osmotic conditions, thus a novel *pdcb4* KO line was generated using CRISPR Cas9. Mutants roots showed reduced sensitivity to PEG treatment.

5.2 Results

5.2.1 Altering the expression of genes controlling PD callose affects the accumulation of metabolites involved in photorespiration, ABA and glucosinolate production

The metabolomic profile of plants can change dramatically under different abiotic conditions including under different availability of nitrate, phosphate and potassium as well as under salt- and drought-stress (Chandna et al., 2013; Balazadeh et al., 2014; Sung et al., 2015; Meng et al., 2019). In Chapter 3 it was established that many PD proteins and candidate PD proteins are differentially expressed under abiotic conditions. Identifying metabolites with differential enrichment in plants with altered expression of known PD regulators could help to link PD regulation with specific abiotic responses. Metabolic profiling of roots dissected from WT and constitutively expressing *YFP-PDCB1*, *YFP-PDBG1* and the knockout mutants *pdbg1* and *pdbg2* was performed by the industrial partner BASF. The outcome of this work was a compiled list of metabolites with relative concentrations for each plant line. This list was analysed here by partial least squares discriminant analysis (PLS-DA) (Figure 5.1). The top 3 components of the PLS-DA were used to build a 3-D component analysis (Figure 5.1 a). Independent biological samples largely clustered according to genotype. The weighted sum of absolute regression coefficients of the most

important PLS-DA component gave the relative measure of metabolites between lines. In roots, the top 20 most important metabolic features included ABA, glycolate, glucosinolates, sucrose, myo-inositol and raffinose (Figure 5.1 b). PDCBlOE, PDBGlOE, *pdbg1* and *pdbg2* all displayed higher levels of ABA in relation to wildtype. Over represented metabolic pathways within the top most differentially enriched metabolites were determined using the online tool Plant Metabolic Network 15 (Hawkins et al., 2021). Metabolic pathways that are over represented are stachyose biosynthesis, photorespiration, amino acid biosynthesis and glucosinolate biosynthesis (Table 5-1). In summary, metabolomics of plant roots with altered expression of genes controlling PD callose were found to contain higher levels of ABA and differential enrichment in sugar and glucosinolate biosynthesis and in metabolic pathways associated with photorespiration.

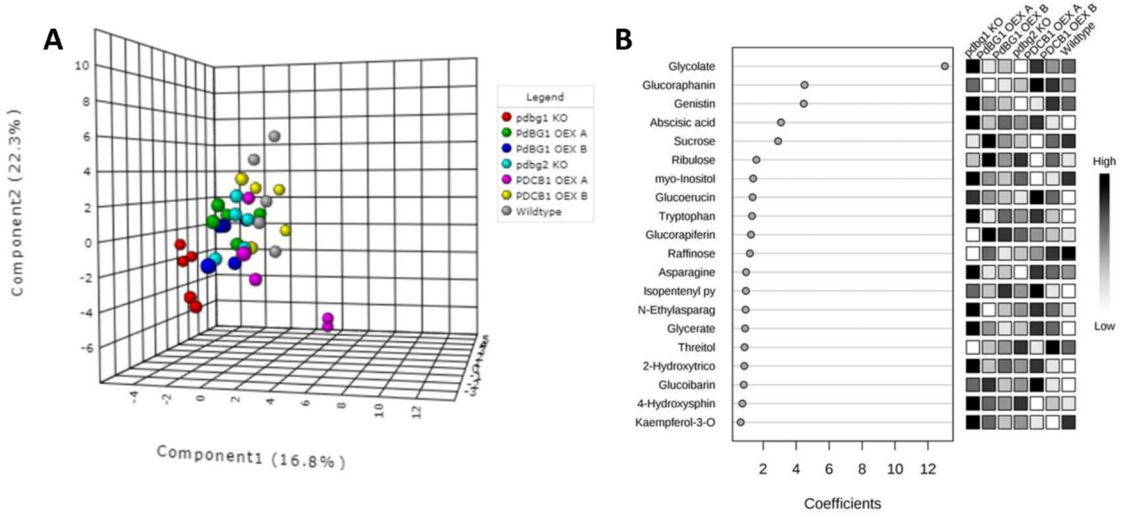

Figure 5.1 Lines affected in callose synthesis or degradation display differences in the root metabolome. Roots and shoots from 9 dpg seedlings were collected by Dr Ambra de Simone. Mass spectroscopy was performed, and relative compound concentrations were determined by BASF-Plant Sciences. The profiles obtained for WT, *pdbg1, pdbg2* and independent lines of PDBG1 OE and PDCB1 OE were compared. Partial least squares discriminant analysis (PLS-DA) using default parameters is presented. (A) 3-D principal component analysis (PCA) of metabolomic profiles, displaying PC1, PC2 and PC3. Each data point presents a pooled biological sample. (B) 'Important features' determined on the weighted sum of absolute regression coefficients (coefficients) of PC1 for root and shoot isolated material. Statistical analysis was performed using MetaboAnalyst 4.0 (Chong et al., 2019).

Table 5-1 Metabolic pathways overrepresented in the root tissue metabolome of *pdbg1*, *pdbg2*, PDBG1OE and PDCB1OE relative to WT. Statistical enrichment of metabolic pathways listed in Figure 5.1b were determined by Fisher's exact test via Plant Metabolic Network 15 (Hawkins et al., 2021).

Enriched pathway	p value	Compound
Stachyose biosynthesis	0.01	raffinose
		myo-inositol
		sucrose
Photorespiration	0.01	(R)-glycerate
		glycolate
Amino Acid Biosynthesis	0.03	L-asparagine
		(R)-glycerate
		L-tryptophan
Glucosinolate Biosynthesis	0.06	L-tryptophan
		glucoraphanin
		glucoibarin

5.2.2 PDCB4 localises to PD and is differentially expressed in response to salt and water stress

Chapter 4 revealed that osmotic stressors, specifically PEG treatment and elevated concentrations of NaCl caused major effects in plant phenotypes and symplasmic transport. To identify new PD proteins involved in the root response to osmotic stresses, candidate lists PIP-A and PIP-C from the *in silico* proteome (described in Chapter 3) were scored according to how many times they appeared to be differentially expressed in transcriptomes pertaining to osmotic stresses. The top 20 genes are presented in Figure 5.2 A. There is consistent differential expression for each gene across the 42 transcriptomes analysed. The only verified PD genes differentially regulated in this list are from the PDCB family. *PDCB3* was found to be consistently down regulated in response to salt and osmotic stress in root and shoot tissue. *PDCB4*, was upregulated in shoot and root tissue in response to drought, PEG and salt. To confirm PDCB4 localisation, PDCB4OE plants (carrying an internal GFP fusion) were imaged by confocal microscopy after staining with aniline blue to detect callose. A clear co-localisation with callose deposits was present in a characteristic punctate pattern reminiscent of PD localisation (Figure 5.2 B).

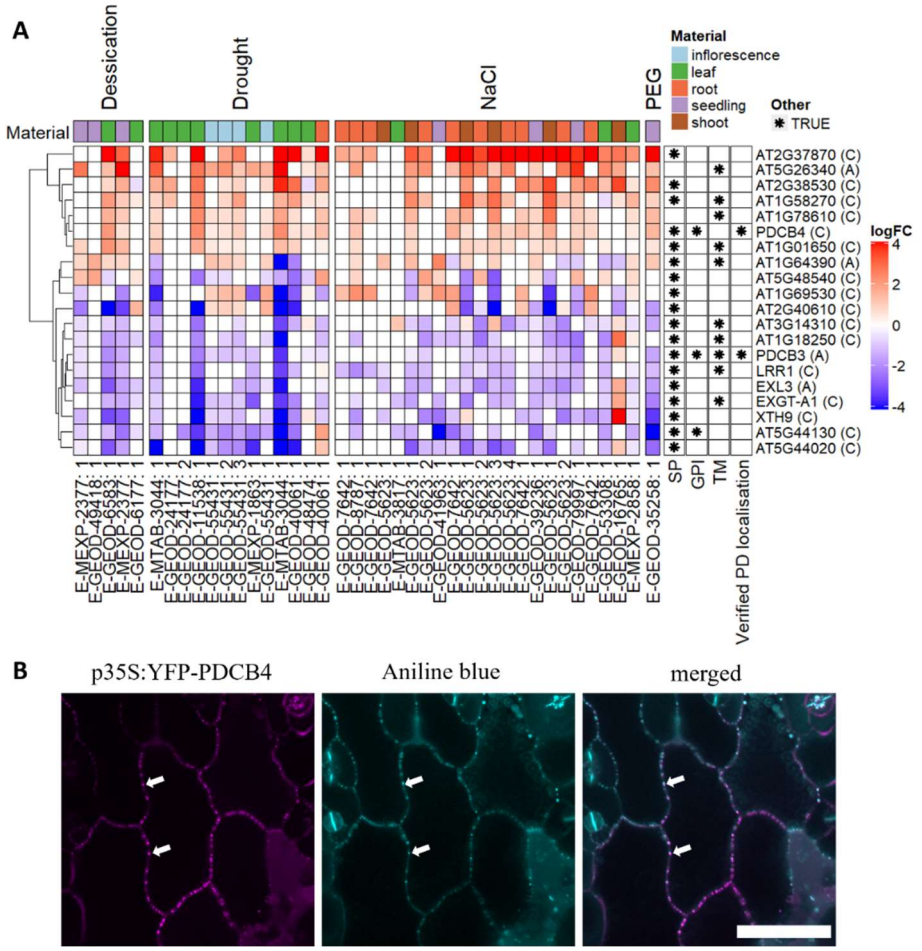

Figure 5.2 PDCB4 is upregulated under osmotic challenge and localises to PD. (A) Gene expression analysis of 20 PD candidate PD genes from PIP-A and PIP-C (see Chapter 3) that are differentially expressed in a number of osmotic stress transcriptomes. Column labels = ArrayExpress accession codes followed by a reference number. See Supplementary material 3 for more information on array description. Rows are labelled by gene symbol followed by the candidate list membership in brackets. Row order was determined by hierarchical clustering, denoted by the dendrogram. Asterisks in cells denote that the protein has a given property (e.g. is predicted to have a SP). SP = Signal peptide, GPI = glycophosphatidylinositol anchor, TM = transmembrane domain. Cell colour above each column = plant material sampled. (B) Abaxial cotyledon epidermis of transgenic 7 days old *p35S::YFP-PDCB4* seedlings were imaged using a confocal microscope. Plants were counterstained with aniline blue fluorochrome. Channels were collected sequentially with excitation laser 488 nm (magenta - YFP-PDCB4) and 405 nm (aniline blue shown in cyan). Co-localisation events are highlighted with arrows. Scale bar = 50 µm.

5.2.3 Ectopic expression of PDCB4, PDLP1 and PDBG1 alters primary and lateral root responses to N, P, K, NaCl and PEG treatment

PDCB4 was regulated in response to abiotic stresses and the metabolome of callose modifiers also indicates potential changes in the accumulation of metabolites acting in stress response. To determine if changes in the transcriptome and metabolome correlate with changes in the root response to abiotic stress, phenotyping was performed on transgenic plants overexpressing *YFP-PDLP*, *YFP-PDBGI* and *YFP-PDCB4* driven by the 35S promoter (over expression lines, OE). OE lines were grown on control, low nitrate, low potassium, low phosphate, 75 mM NaCl and 3% PEG. Root responses were phenotypically analysed by measuring primary root length, tortuosity, number of lateral roots, emerged lateral root density and total lateral root length. A summary of phenotypes between replicates is presented in Table 5-2 which shows that phenotyping results were largely consistent between replicates. Representative replicates are presented in Figures 5.3 - 5.5.

At 7 dpg in ATS-based media, primary root length was significantly shorter than WT in PDBGlOE and PDLPlOE in all conditions tested except 75 mM NaCl where the differences were not significant (Figure 5.3 A). Roots in PDCB4OE, on the other hand, were not significantly different from WT except in 0 mM K+ where they appear shorter. WT roots grown in 3% PEG and 75 mM NaCl were significantly shorter in relation to control media, displaying a 36% and 48% reduction in median primary root length respectively. The same trend was observed for PDBGlOE and PDLPlOE although differences were not statistically significant in all replicates (Table 5-2). Primary root length in PDCB4OE was also reduced by 41% in 75 mM NaCl but not significantly reduced in 3% PEG (the median primary root length increased slightly). Primary root tortuosity was also measured in all lines in the different media and in relation to WT. Primary root tortuosity is slightly reduced in WT grown in low K+, low phosphate and 3% PEG in relation to control media but increased in 75 mM NaCl. In control media, PDBGlOE's primary root tortuosity was slightly reduced in relation to WT, but no significant differences were observed in PDLPlOE or PDCB4OE. As in WT, primary root tortuosity increased in all transgenic lines grown in 75 mM NaCl (Figure 5.3).

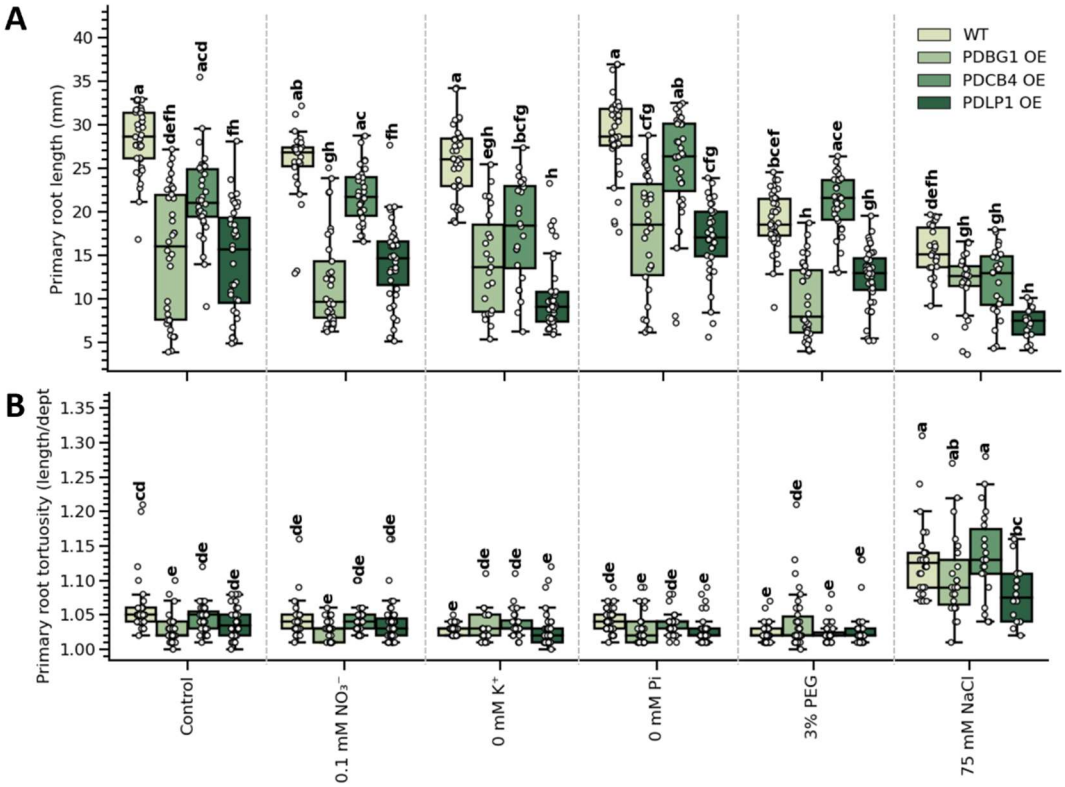

Figure 5.3 Plants ectopically expressing PDBG1, PDLP1 or PDCB4 under the 35S promoter display primary root developmental phenotypes in control and 3% PEG media. (A) Primary root length and (B) primary root tortuosity were measured 7 days post germination (dpg) in control (ATS 0% sucrose) and abiotic treatment media (0.1 mM nitrate, 0 mM K+, 0 mM Pi, 3% PEG and 75mM NaCl). Pairwise significance testing was performed by one-way ANOVA (Tukey post hoc test, N≥30, bars that do not share a letter are significantly different).

Emerged lateral root number, emerged lateral root density and total lateral root length (total lateral root length) were also scored in WT and transgenic grown in the different media (Figure 5.4). WT seedlings had significantly fewer lateral roots in 3% PEG and 75 mM NaCl relative to control medium but no consistent significant differences were observed in low nitrate, low potassium or low phosphate conditions (Table 5-2, Figure 5.4 A). Emerged lateral root density was reduced in WT only under 75 mM NaCl. Total lateral root length was reduced in WT grown in 3% PEG and 75 mM NaCl conditions (Table 5-2, Figure 5.4 B,C). A significant reduction in lateral root number, emerged lateral root density and total lateral root length was quantified in PDBG1OE and PDLP1OE in all conditions probably linked to the reduction in primary root length (Figure 5.4 A-C). A different phenotype was observed for PDCB4OE. The number of lateral roots in PDCB4OE

were similar to WT in all media but significantly reduced in 75 mM NaCl. PDCB4OE did not display a reduction in lateral root number in response to 3% PEG. Emerged lateral root density did not change but total lateral root length was reduced in PDCB4OE in comparison to WT grown in control medium (Figure 5.4 B,C). In contrast to WT, total lateral root length in PDCB4OE was not significantly different in control vs 3% PEG, but both emerged lateral root density and total lateral root length were reduced in 75 mM NaCl (Figure 5.4 B,C).

The phenotype of PDBGlOE is somewhat unexpected as it behaves similar to PDLPlOE. To further investigate the role of callose degradation in root response to the abiotic treatments, the phenotype of a knockout *pdbg1* mutant was also tested in the different media and compared to wildtype. As for the transgenic lines, *pdbg1* seedlings were grown in control, low nitrate, low potassium, low phosphate, 75 mM NaCl and 3% PEG for 7 days and primary root length, primary root tortuosity, lateral root number, emerged lateral root density and total lateral root length was calculated and compared to control. When grown in ATS-based media (0% sucrose), *pdbg1* had longer primary root length, increased lateral root number and total lateral root length in relation to WT whereas primary root tortuosity and emerged lateral root density were not significantly different (Figure 5.5). In this experiment and in response to 0.1 mM nitrate, 0 mM K+, 3% PEG and 75 mM NaCl, both *pdbg1* and WT showed reduced primary root length relative to control conditions. There was no significant difference in WT primary root length in 0 mM Pi but *pdbg1* primary root length was significantly reduced in this condition. Since primary root length was significantly increased in *pdbg1* in control conditions, the reductions in the different treatment media were significantly steeper in the mutant in relation to WT. Primary root tortuosity, in both WT and *pdbg1*, was only increased by 75 mM NaCl but the effect is more prominent in *pdbg1* (Figure 5.5 A). A reduction in lateral root number was found in *pdbg1* grown in all treatments in relation to control whereas WT only show a significant difference in 3% PEG and 75 mM NaCl. Like WT, emerged lateral root density was significantly reduced in *pdbg1* grown in 75 mM NaCl, but the mutant also shows a significant reduction in 0 mM phosphate and 3% PEG which do not affect the WT (Figure 5.5 D). In the conditions of this experiment, total lateral root length was not significantly different in WT grown in the different conditions whereas this parameter was reduced in *pdbg1* grown in all low nitrate, low potassium, low phosphate, 75 mM NaCl and 3% PEG in relation to control medium (Figure 5.5 E).

To summarise, the results show that ectopically expressing proteins involved in callose metabolism at PD leads to defects in root growth (PR and LR development) in control conditions. In terms of primary root length, all transgenic lines respond to low nitrate, phosphate and potassium in similar fashion to WT. At 7 dpg, PDLP1OE and PDBG1OE transgenic developed no lateral roots thus it was not possible to assess the effects of treatments on lateral root development. In 3% PEG and 75mM NaCl, PDBG1OE and PDLP1OE do not experience a significant reduction in primary root length different to the WT but, the effect might be missed because these transgenic lines developed significantly shorter roots in control media. Interestingly, the phenotypes are somewhat different in PDCB4OE: primary and lateral root development are not severely affected in control media (compared to WT) but the transgenic response to 3% PEG appears impaired. PDCB4OE's primary root length, LR or total lateral root length were not significantly reduced in 3% PEG like WT whereas the behaviour in high salinity resembled WT. Regarding *pdbg1*, increased primary root length and lateral root number and length were observed in control media relative to WT. This is consistent with the observed reduction in primary root length observed for PDBG1OE. Relative to the phenotypes in control conditions, primary root length, lateral root number and lateral root length of *pdbg1* decrease under low nitrate, low potassium, low phosphate, 3% PEG and 75 mM NaCl.

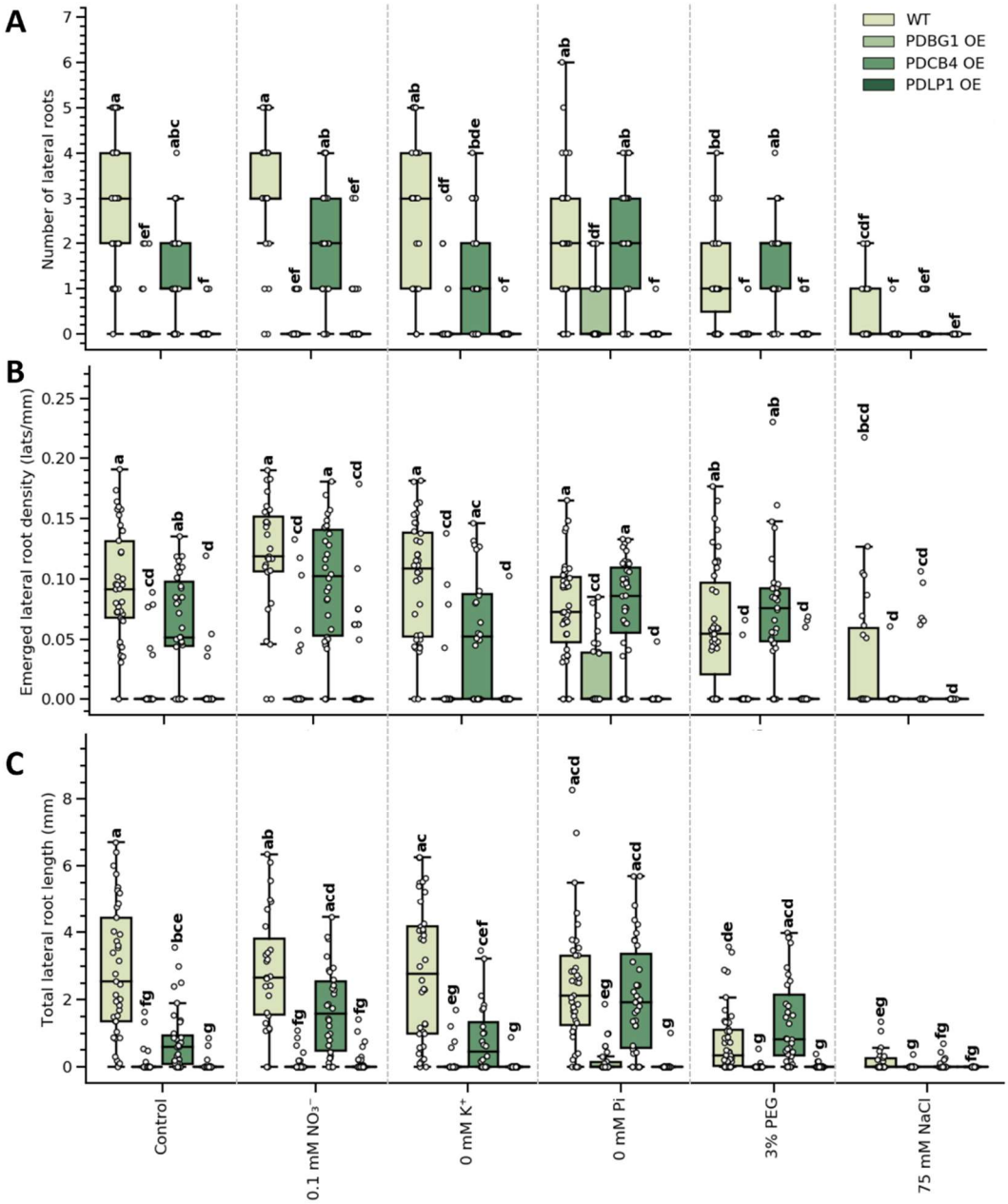

Figure 5.4 Plants ectopically expressing *PDBG1*, *PDLP1* or *PDCB4* under the 35S promotor are defective in lateral root development. (A) Number of lateral roots, (B) emerged lateral root density and (C) total lateral root length were measured at 7 days post germination (dpg) in control (ATS 0% sucrose) and abiotic treatment media (0.1 mM nitrate, 0 mM K+, 0 mM Pi, 3% PEG and 75mM NaCl). Pairwise significance testing was performed by one-way ANOVA (Tukey post hoc test, N≥30, bars that do not share a letter are significantly different).

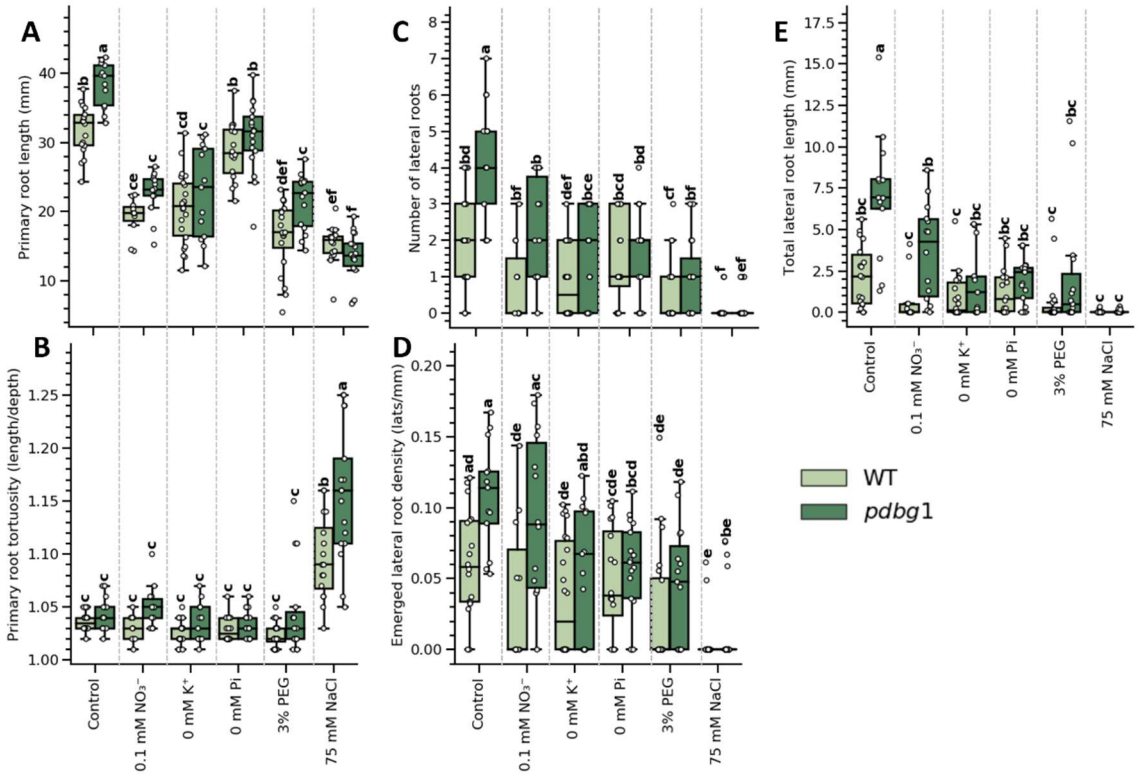

Figure 5.5 *pdbg1* display a primary root and lateral root phenotype in control and during abiotic response. (A) Primary root length, (B) primary root tortuosity, (C) number of lateral roots, (D) emerged lateral root density and (E) total lateral root length were measured at 7 days post germination (dpg) in control (ATS 0% sucrose) and abiotic treatment media (0.1 mM nitrate, 0 mM K+, 0 mM Pi, 3% PEG and 75mM NaCl). Pairwise significance testing was performed by one-way ANOVA (Tukey post hoc test, N≥30, bars that do not share a letter are significantly different).

Table 5-2 Summary of primary root length, tortuosity, lateral root number, density and total length root phenotypes recorded for WT, PDBG1OE, PDCB4OE, PDLP1OE and *pdbg1*. Plants were grown on ATS based media. Phenotypes were determined at 7 days post germination. Statistical differences between lines were determined using ANOVA, Tukey post hoc ($p < 0.05$). Each symbol in the table refers to a different experimental replicate. In control media, statistical differences between each line and WT are represented by an arrow indicating whether the line exhibited a phenotype larger (↑) or smaller (↓) or not different (–) relative to WT. In other media, arrows indicate whether the phenotype is larger, smaller or not different to the control media phenotype of that line.

Primary root length	Control	0.1 mM NO3-	0 mM K	0 mM Pi	3% PEG	75 mM NaCl
WT		– ↓ ↓	– ↓ ↓	– – ↓	↓ ↓ ↓	↓ ↓ ↓
PDBG1OE	↓	–	–	–	–	–
PDCB4OE	– ↑	–	–	–	–	↓
PDLP1OE	↓ –	– ↓	– ↓	– –	– ↓	– ↓
pdbg1	↑ –	↓	↓	↓	↓	↓

Primary root tortuosity	Control	0.1 mM NO3-	0 mM K	0 mM Pi	3% PEG	75 mM NaCl
WT		– –	↓ –	– –	↓ –	↑ ↑
PDBG1OE	↓	–	–	–	–	↑
PDCB4OE	–	–	–	–	–	↑
PDLP1OE	– –	– –	– –	– –	– –	↑ ↑
pdbg1	– –	–	–	–	–	↑

Lateral root number	Control	0.1 mM NO3-	0 mM K	0 mM Pi	3% PEG	75 mM NaCl
WT		– – –	– ↓ –	– – –	↓ ↓ ↓	↓ ↓ ↓
PDBG1OE	↓	–	–	–	–	–
PDCB4OE	–	–	–	–	–	↓
PDLP1OE	↓ ↓	– –	– –	– –	– –	– –
pdbg1	↑	↓	↓	↓	↓	↓

Emerged lateral root den.	Control	0.1 mM NO3-	0 mM K	0 mM Pi	3% PEG	75 mM NaCl
WT		– – –	– – –	– – –	– – –	↓ ↓ ↓
PDBG1OE	↓	–	–	–	–	–
PDCB4OE	–	–	–	–	–	↓
PDLP1OE	↓ –	– –	– –	– –	– –	– –
pdbg1	– –	–	–	↓	↓	↓

Total lateral root length	Control	0.1 mM NO3-	0 mM K	0 mM Pi	3% PEG	75 mM NaCl
WT		– – –	– – –	– – –	↓ ↓ –	↓ ↓ –
PDBG1OE	↓	–	–	–	–	–
PDCB4OE	↓	–	–	–	–	↓
PDLP1OE	↓	– –	– –	– –	– –	– –
pdbg1	↑ –	↓	↓	↓	↓	↓

5.2.4 *pdcb4* CRISPR/Cas9 lines display a frameshift mutation and reduced RNA expression

PDCB4 OE primary root length was similar to WT in control media, but this line did not display the significant reduction in root length observed for WT in PEG and NaCl (Table 5.2). Moreover, PDCB4 is located at PD and upregulated under osmotic stress (Figure 5.2). This result suggests that PDCB4 expression might be necessary to regulate callose, symplasmic transport and root responses to osmotic stress. To verify this hypothesis, it was necessary to analyse a *pdcb4* knockout line. As these mutants were not available in stock centres a CRISPR/Cas9 strategy was designed to knockout PDCB4 by error prone non homologous end joining (NHEJ). The proto-spacer was designed to cause a frame shift mutation within a conserved region of the X8 domain in *PDCB4* (Figure 5.6) with the most likely position of the mutation falling within a BstYI restriction site (aiding the screening for mutations). After Agrobacterium-mediated transformation by floral dip, T0 seeds were screened by PPT resistance to identify Cas9 positive plants. Next, T1 plants were screened for the loss of PPT resistance which co-segregates with the Cas9 cassette. This was done with a novel PPT rescue screen based on the phenotypic differences between PPT-susceptible and resistant plants (Figure 5.7 A). PPT-susceptible plants were transferred to plates containing glutamine to rescue their growth. Although the parents of these seeds expressed Cas9/sgRNA template, not all seedlings will contain the desired mutation. To screen for mutations, PCR/Restriction Enzyme (PCR/RE) analysis was performed. As the CRISPR/Cas9 mutation was designed to fall within 1 of the two BstYI sites within a fragment of PDCB4, the resulting PCR/RE pattern was used to screen for probable mutations (Figure 5.7 B).

Lines carrying potential mutations were sequenced and aligned against the proto-spacer to check for mutations. Several lines had the desirable frameshift mutation including lines CR1-5, CR3-7 and CR12-9 (Figure 5.7 C). CR1-5 displays a single thymine insertion at position 146 of the coding sequence. This causes a frameshift mutation starting with an amino acid change in the proceeding codon (Q50P) and a premature stop codon a further 9 amino acids downstream. CR3-7 and CR12-9 both display a guanine insertion in position 146 of the coding sequence causing a I49S mutation leading to the same premature stop codon described for CR1-5. RT-PCR was performed, and all three lines appear to be knocked-out or knocked down at a transcriptional level (Figure 5.7 D) with ACTIN2

(housekeeping gene) and PDCB4OE used as controls. To summarise, CRIPR Cas9 was used to generate three independent mutant lines of *pdcb4*.

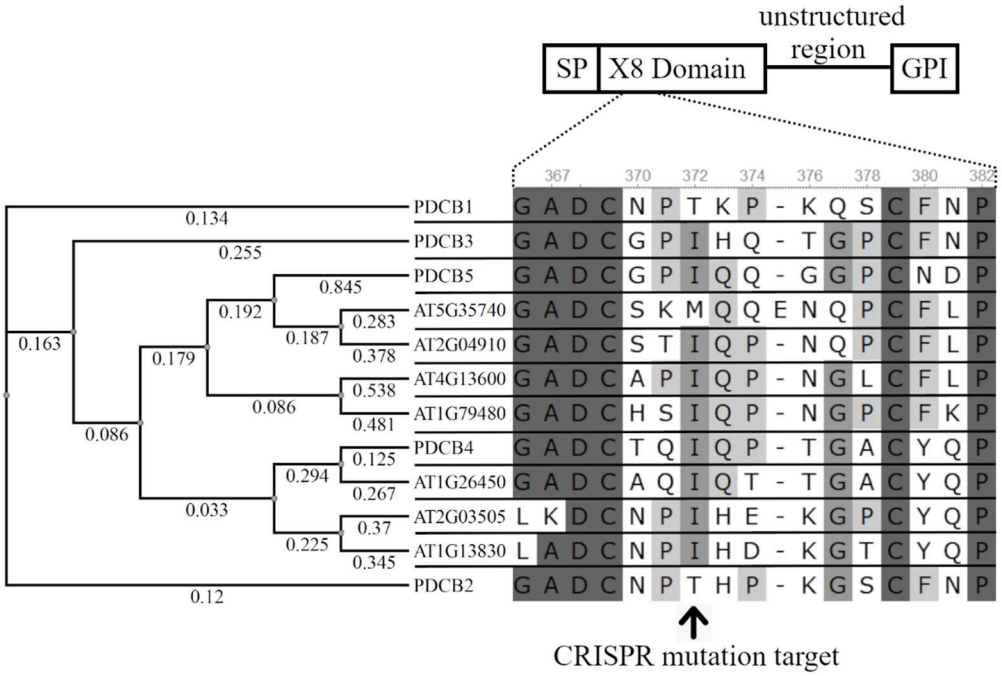

Figure 5.6 X8 domains in PDCB family member share a high degree of sequence similarity. The X8 domain in *PDCB4* was targeted for mutation using CRISPR/Cas9. (left) Phylogeny of PDCB members based on peptide sequences. The tree was built in UGENE using the PHYLIP algorithm using default settings. Branch distance is displayed below each branch. (top) schematic of the domain structure of PDCB family members. (right) A region of the X8 domain peptide sequence aligned in UGENE using the algorithm MUSCLE using default settings. The arrow indicates the location of the CRISPR target site for mutating *PDCB4* with error prone non homologous end joining.

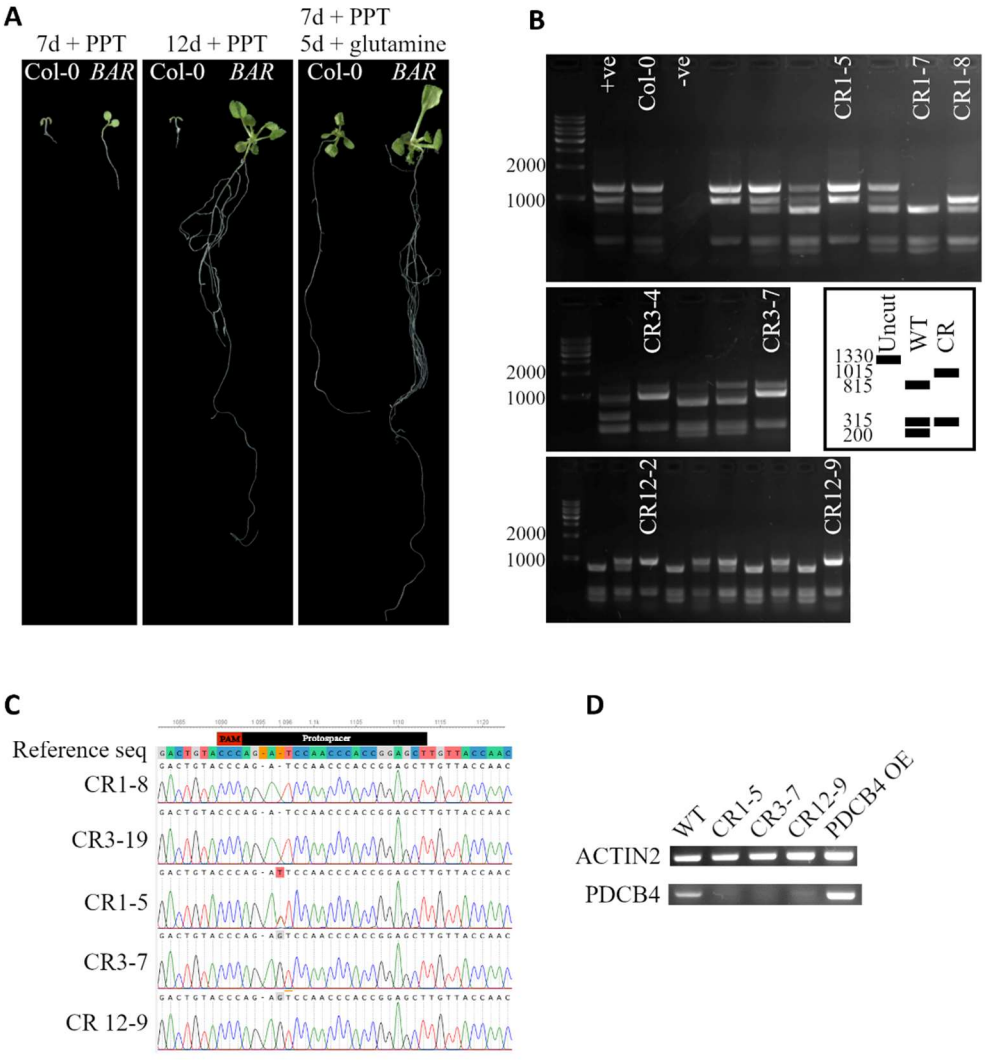

Figure 5.7 PDCB4 CRISPR/Cas mutants display a frameshift and reduce RNA expression. CRISPR knockout mutants of *pdcb4* were screened using a combination of novel phosphinothricin (PPT) rescue, PCR/Restriction Enzyme (PCR/RE) analysis and sequencing. (A) To segregate out Cas9 and marker genes (BAR: PPT resistance cassette) from the genome, T1 seeds were grown on plants containing 10 µg/ml PPT. After 7 days, PPT-susceptible plants were transferred to plates containing 2 mM glutamine. After 5 days, rescued plants were transferred to soil. The error prone non homologous end joining (NHEJ) mutation site was designed to be in a BstYI site in *PDCB4*. (B) *PDCB4* of CRISPR lines (CR...) was amplified by PCR from gDNA and digested with BstYI. (inset) BstYI restriction pattern for uncut PCR product, WT and a successful mutation in the target BstY1 site. (C) Sanger sequencing of CRISPR lines in the region around the target within *PDCB4*. Mutations in individual lines are highlighted. (D) RT-PCR of WT, CRISPR lines and *p35S::YFP-PDCB4* (PDCB4OE) for *ACTIN2* and *PDCB4* after 25 cycles.

5.2.5 Phenotypic analysis indicates that responses to 3% PEG is impaired in *pdcb4* CRISPR/Cas mutants.

To establish whether PDCB4 is involved in root responses to abiotic stress, confirmed mutant CR1-5 and two other probable mutants CR3-4 and CR12-2 (according to PCR/RE analysis Figure 5.7 B) were grown alongside WT and a control sibling line CR1-7. CR1-7 does not appear to have a PDCB4 mutation according to PCR/RE analysis but underwent the same transformation and treatments as the CRISPR-Cas mutants thus was selected as the most appropriate wildtype control. PDCB4 was regulated by osmotic stressors (Figure 5.1) and PDCB4OE show a differential response to wildtype in PEG (Figure 5.2, 5.3) thus focus was placed on conditions that affect plant water potential (3% PEG and 75 mM NaCl) and K (which affects the response to water stresses). *pdcb4* plants were grown for 7 dpg on ATS- based control, 0mM K, 3% PEG and 75 mM NaCl media. WT and CR1-7 behaved similarly in terms of primary root length, LR number, emerged lateral root density and total lateral root length both showing a reduction in all parameters in 3% PEG and 75 mM NaCl (Figure 5.8). CR3-4 and CR1-5, but not CR12-2, exhibited a longer primary root length than WT and the control line CR1-7 in control media. In 3% PEG, CR3-4, CR1-5 and CR12-2 did not exhibit a reduction in primary root length relative to control conditions as exhibited by WT and the control line CR1-7. Primary root length was significantly reduced in CR3-4, CR1-5 and CR12-2, but remain larger than WT and CR1-7, in 75 mM NaCl relative to control conditions. CR1-5 and CR3-4 but not CR12-2 have significantly more lateral roots than WT and the control line CR1-7 in control and 3% PEG (Figure 5.9 A).

There was only a slight decrease in the number of lateral roots in CR1-5, CR3-4 and CR12-2 when grown in control conditions and 3% PEG. This reduction is only significant for CR3-4. The number of lateral roots was significantly reduced when grown in 75 mM NaCl relative to control conditions in all lines. CR1-5 had significantly more lateral roots than the control lines, WT and CR1-7, in this condition. Emerged lateral root density in CR1-5, CR3-4 and CR12-2 were not significantly reduced in 3% PEG or 75 mM NaCl, unlike WT and CR1-7 (Figure 5.9 B). Total lateral root length was increased in CR3-4 in control conditions and 3% PEG relative to WT and CR1-7 (Figure 5.9 c). In PEG, WT and *pdbg4* mutants show a mild but not significant reduction in total lateral root length. Total lateral root length is not significantly different between *pdcb4* mutants and controls in 75 mM NaCl (Figure 5.9 B).

In summary, the data show that mutations in PDCB4 lead to reduced response to the osmoticum PEG suggesting a role for PDCB4 in the regulation of plant responses to reduced water potential caused by osmotic stress. Regulation of stomata is an essential response to osmotic stress and YFP-PDCB4 is expressed in stomata when driven by the constitutive promoter (Figure 5.10 A). Leaf stomatal density was measured at 10 dpg in CR1-7, CR1-5 and CR3-4 seedlings grown on ATS- based (0% sucrose) control or 3% PEG media. Stomatal density was significantly increased in CR1-5 and CR3-4 when comparing control and 3% PEG media but remained constant in CR1-7 (WT) (Figure 5.10 B). This result supports a role for PDCB4 in osmotic stress responses in both shoots and roots however this experiment must be repeated.

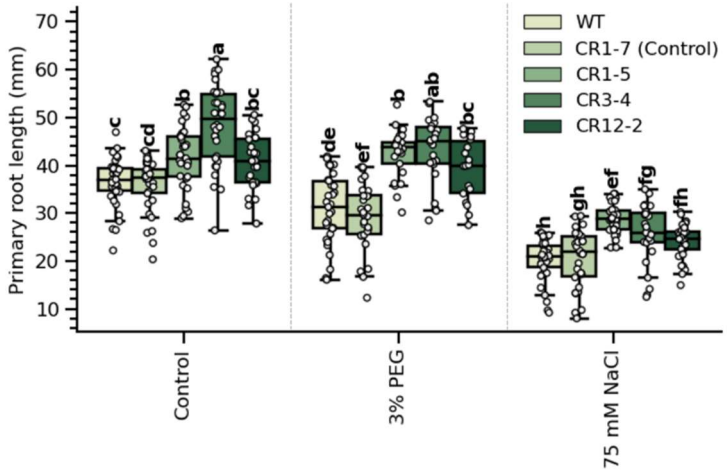

Figure 5.8 CRISPR *pdcb4* mutants have longer primary roots and are less sensitive to 3% PEG. Primary root was measured at 7 days post germination (dpg) in control (ATS 0% sucrose) and treatment media (0 mM K, 3% PEG and 75mM NaCl). Pairwise significance testing was performed by one-way ANOVA (Tukey post hoc test, N≥18, bars that do not share a letter are significantly different). CR1-7 lacks the CRISPR mutation based on PCR/RE analysis (Figure 5.7 B) and is included as a wildtype control for the CRISPR mutants.

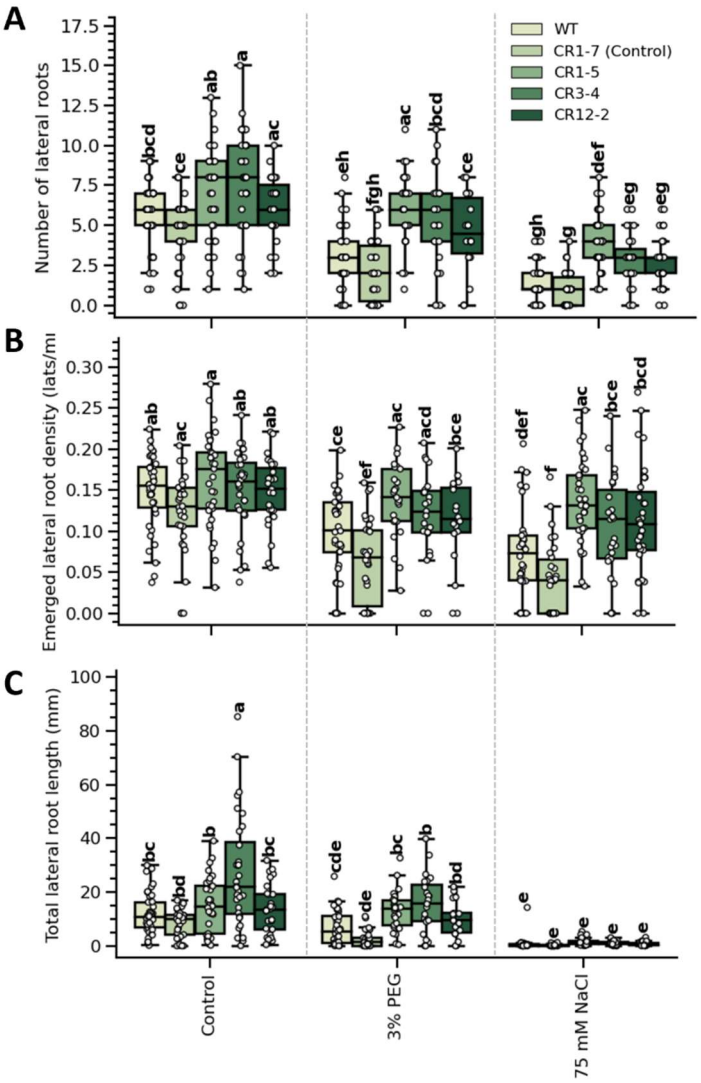

Figure 5.9 Lateral root phenotype in CRISPR *pdcb4* mutants is less sensitive to 3% PEG and 75 mM NaCl treatment. (A) Number of lateral roots, (B) emerged lateral root density and (C) total lateral root length were measured at 7 days post germination (dpg) in control (ATS 0% sucrose) and treatment media (0 mM K, 3%PEG and 75mM NaCl). Pairwise significance testing was performed by one-way ANOVA (Tukey post hoc test, N≥18, bars that do not share a letter are significantly different).

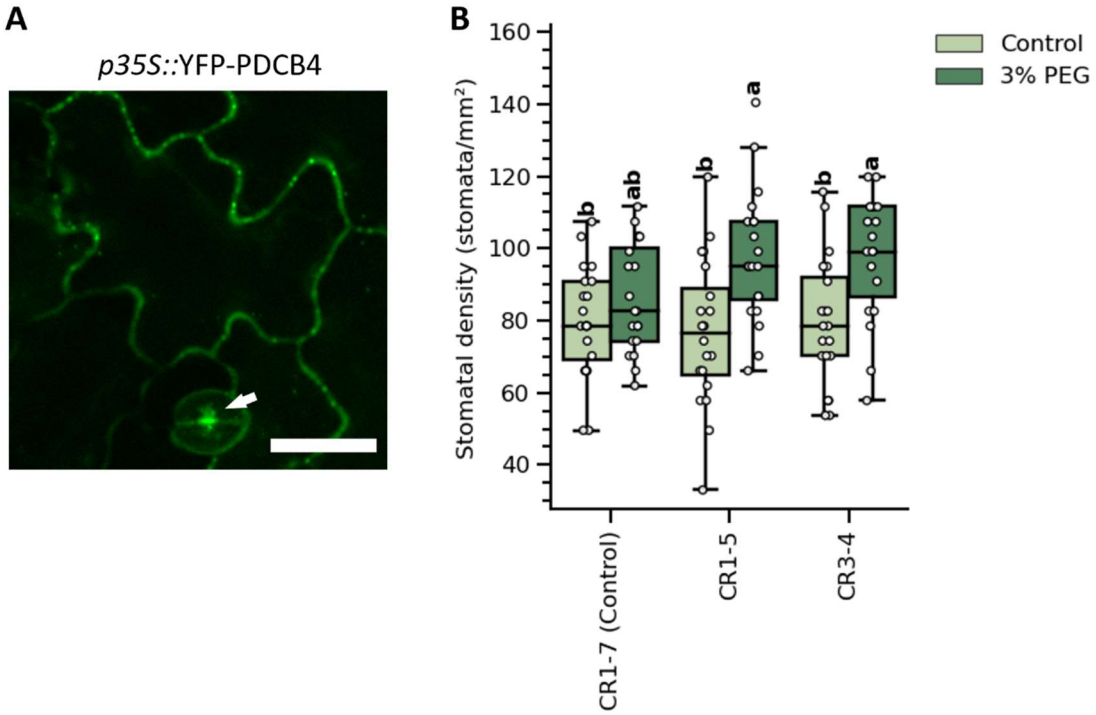

Figure 5.10 CRISPR *pdcb4* mutants display increased stomatal density in 3% PEG. (A) Constitutively expressed YFP-PDCB4 localises at stomata. Abaxial cotyledon epidermis of transgenic 7 days old *A. thaliana* seedlings expressing *p35S::YFP-PDCB4* was imaged using a confocal microscope with a 488 nm excitation laser. Arrow indicates stomatal localisation of YFP-PDCB4. Scale bar = 20 µm. (B) CRISPR *pdcb4* mutant lines (CR lines) were grown for 10 days post germination (dpg) on ATS based media with or without 3% (w/v) PEG. True leaves were imaged on a DIC microscope (Axioscope, Zeiss, Germany). Images were analysed in ImageJ and stomata number were counted in a given area. Pairwise significance testing was performed by one-way ANOVA (Tukey post hoc test, N≥19, bars that do not share a letter are significantly different). CR1-7 is included as a control wildtype.

5.2.6 Callose accumulation in response to osmotic stress may be suppressed in *pdcb4* mutants

To determine if the phenotypic differences observed in the *pdcb4* mutants were due to changes in callose regulation, aniline blue staining was performed. Primary root tips of plants grown on ATS-based media (0% sucrose) or 3% PEG media were stained and imaged under the confocal microscope. Figure 5.11 shows the results of quantifying aniline blue staining in the transect highlighted in panel A. In the control line CR1-7, there is a clear increase in aniline blue fluorescence in 3% PEG treatment in comparison to control media (Figure 5.11 B, C). Aggregated lateral fluorescence profiles (Figure 5.11 D) support this finding. The differences are much less significant in the *pdcb4* CRISPR lines CR1-5 and CR3-4. Some increase in fluorescence in 3% PEG is also evident in CR3-4 but not as strongly as in CR1-7 (Figure 5.11 H-J). In CR1-5, less fluorescence was observed in 3% PEG in relation to control media (Figure 5.11 E-G). Aniline blue staining of cotyledons did not reveal any major differences in fluorescence between CR1-7 grown in control or 3% PEG but generally there was less fluorescence in *pdcb4* mutants grown in PEG in relation to control media (Figure 5.12).

To determine if symplasmic transport is altered in *pdcb4* mutants the dye CFDA was used to measure movement through PD. CFDA becomes fluorescent when entering cells where it is metabolised into an impermeable derivative of fluorescein that can only move via PD. Plants ectopically expressing PDCB1 (known to have high callose and reduced transport) were used as positive control. CFDA was introduced into the phloem stream via the petiole of an excised cotyledon and time course pictures were taken to determine when the dye reached the root meristem and move symplasmically into the outer tissues (Figure 5.13 A, B). Aggregated fluorescence profiles obtained from transects across the EZ are presented in (Figure 5.13 D-F). Fluorescence in the CR1-7 wildtype line is detected, at about 50 AU, 30min after dye loading and this increased with time (Figure 5.13 D). Fluorescence appears somewhat restricted to the middle of the transect in PDCB1OE as expected due to the high callose deposition linked to reduced symplasmic transport (Figure 5.13 G). CR1-5, on the other hand, shows significant fluorescence 10 min after dye loading (earlier than wildtype) suggesting increase phloem or symplasmic transport (Figure 5.13 E). In comparison, for most PDCB1OE, CFDA loading ceased rapidly and before the dye had reached the root tip (Figure 5.13 G).

To summarise, our preliminary results indicates that the phenotype of the *pdcb4* CRISPR mutants and PDCB4OE in response to PEG may be related to defects in the regulation of callose deposition and symplasmic transport in the root meristem. Symplasmic assays were done in control media thus the changes in dye unloading might become more significant when the plants are grown in osmotic stress conditions. These experiments have not been repeated and therefore caution must be taken when interpreting these results.

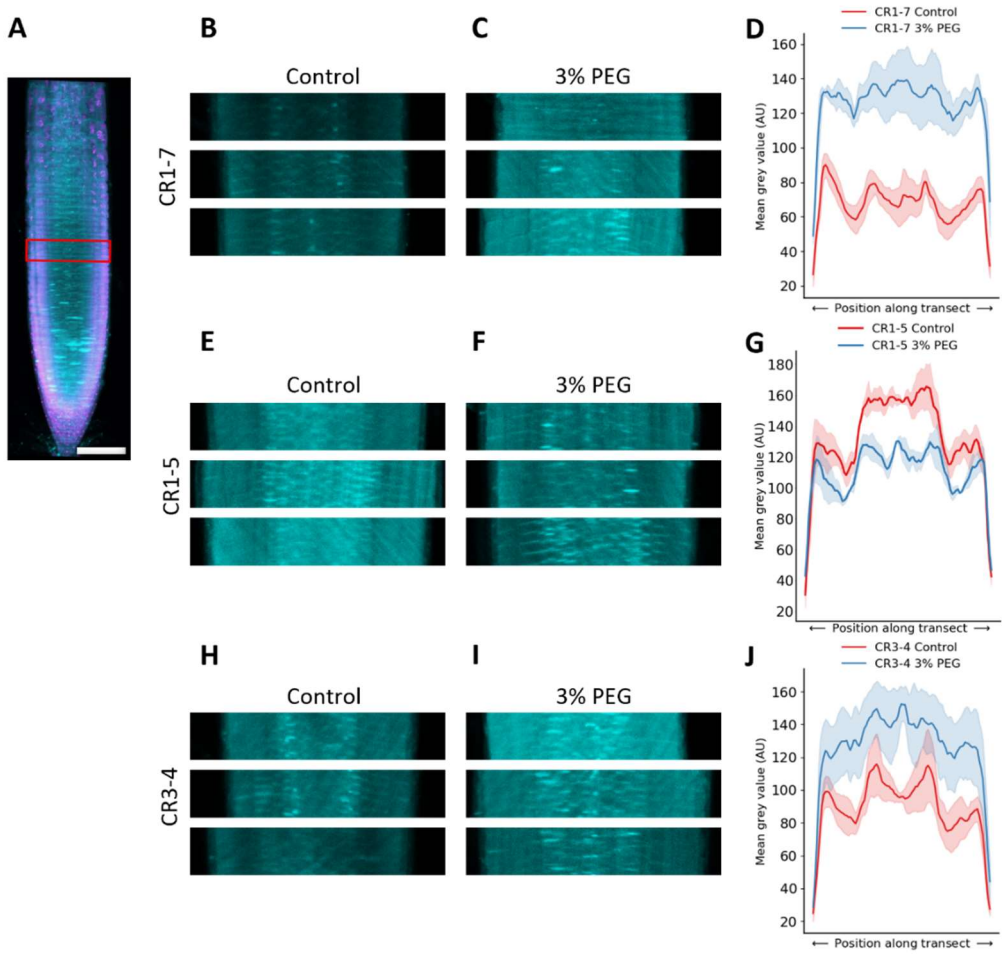

Figure 5.11 Aniline blue staining suggests that callose accumulation in response to 3% PEG is reduced in *pdcb4* mutants. CRISPR *pdcb4* mutants were grown on ATS based media with or without 3% (w/v) PEG for 7 days post germination. CR1-7 lacks the CRISPR mutation based on PCR/RE analysis (Figure 5.7 B) and is included as a control. Primary root tips were stained with aniline blue fluorochrome and imaged with a confocal microscope with a 405 nm laser. (A) Representative image with the red box indicating transect of root for lateral aniline blue fluorescence measurement (300 µm from QC). Scale bar = 100 µm.

(B,C,E,F,H,I) Aniline blue channel across transects for biological samples (n = 3). (D,G,J) Aggregated lateral aniline blue fluorescence profiles across transects (Line = mean ± SD).

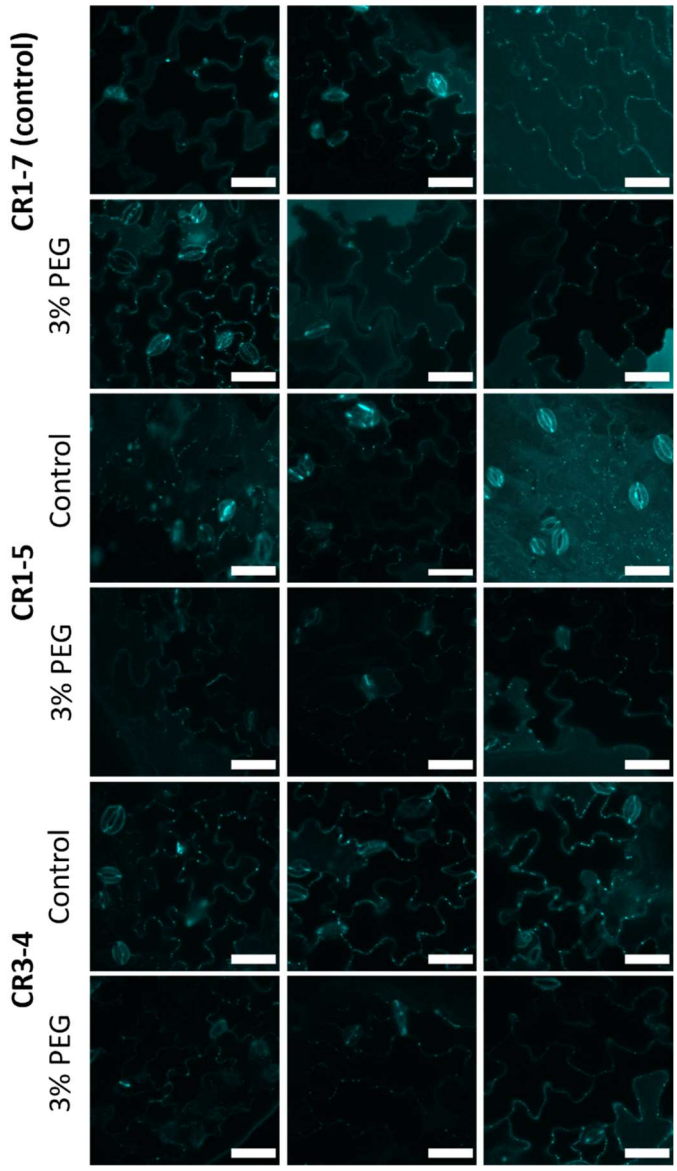

Figure 5.12 Aniline blue staining does not reveal major differences in callose deposition in cotyledons of *pdcb4* mutants. CRISPR *pdcb4* mutants (CR...) were grown on ATS based media with or without 3% (w/v) PEG for 7 days post germination. CRI-7 lacks the CRISPR mutation based on PCR/RE analysis (Figure 5.7 B) and is included as a control. Abaxial cotyledon epidermis were stained with aniline blue fluorochrome and imaged with a confocal microscope with a 405 nm laser. Scale bar = 50 μm.

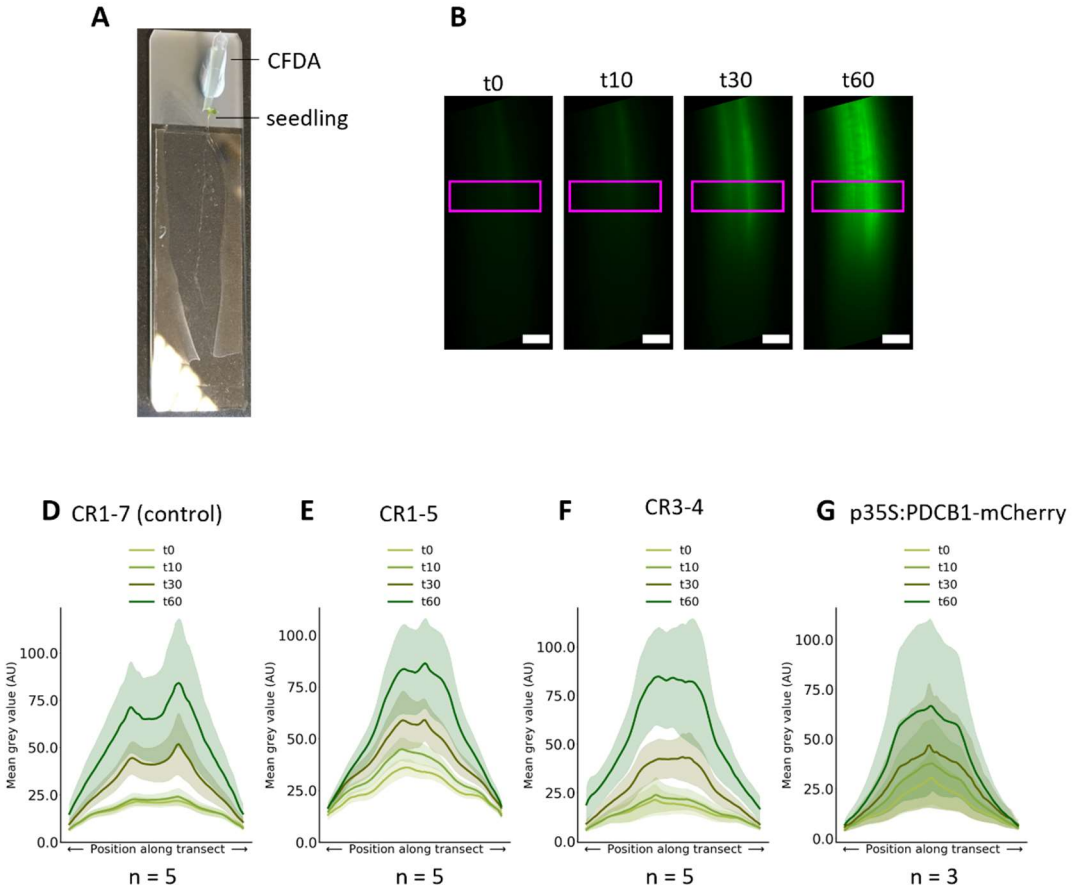

Figure 5.13 Lateral diffusion of the symplasmic dye CFDA in *pdcb4* mutants and PDCBIOE grown in control conditions. CRISPR *pdcb4* mutants (CR...) were grown on ATS based media for 7 days post germination. CRI-7 lacks the CRISPR mutation based on PCR/RE analysis (Figure 5.7 B) and is included as a control. (A) Setup for CFDA dye loading. Whole seedlings were mounted on a slide in water. 10 µl pipette tips were trimmed and loaded with 500 µg/ml CFDA. A cotyledon was excised, and the remaining petiole immediately pushed into the tip to contact the dye. The tip was secured in place with Blu Tack®. The slide was tilted so the tip was elevated relative to the root between imaging. Root tips were imaged with an epifluorescence microscope. T0 was set when the dye had reached the root tip. Root tips were imaged at 0, 10, 30 and 60 minutes after T0. (B) Representative images of root tips at different time points. Magenta box indicates transects of elongation zone where fluorescence measurements were taken. Scale bar = 50 µm. (D-G) Aggregated lateral CFDA fluorescence profiles across transects (Line = mean ± SD, n ≥ 3). This experiment has only been performed once.

5.3 Discussion

Regulation of callose at PD is integral to development and to responses to biotic and abiotic stimuli (Benitez-Alfonso et al., 2013; Maule et al., 2013; Caillaud et al., 2014; Müller et al., 2015; Cui and Lee, 2016a; Gaudioso-Pedraza et al., 2018). In this chapter, metabolic profiles and morphological phenotypes of mutant and overexpression lines affected in callose deposition at PD were determined. Building on the results presented in Chapter 3 and 4, the effect of depleted nutrients, osmotic potential and salinity were determined in *PDBG1* and *PDLP1* overexpression lines (which have decreased and increased ectopic callose accumulation, respectively) (Benitez-Alfonso et al., 2013; Caillaud et al., 2014). Both overexpression lines led to reductions in root length and lateral root proliferation when comparing to WT in all conditions tested (Figure 5.3, Figure 5.4). Unlike WT, root length and lateral root proliferation in PDBG1OE and PDLP1OE were not always reduced by PEG or NaCl treatment. Phenotypic responses to nutrients and osmolytes might have been masked as constitutive expression of these genes lead to shorter roots in normal growth conditions. What is surprising is that both increasing and decreasing callose lead to similar phenotypes thus to clarify the role of callose knock out *pdbg1* was studied. PDBG1 is expressed specifically in the root pericycle thus callose increase is restricted to this tissue. Additionally, *pdbg1* roots are longer in control, low nitrate and in mild osmotic challenge with PEG relative to WT (Figure 5.5). The latter two conditions were shown in chapter 4 to cause changes in symplasmic transport, suggesting that PDBG1 might control callose deposits to negatively regulate root growth in these conditions. Constitutive, instead of localised, callose deposition (as in PDLP1OE) causes pleiotropic effects, for example, the unloading of photoassimilates that maintain the growth of the root meristems.

Osmotic stresses cause changes in symplasmic transport and root phenotypes, and PDCB4, a protein that localises at PD, was strongly upregulated in response to various osmotic stresses (Figure 5.2). PDCB4 is proposed to bind and induce callose thus it was expected that as for PDLP1, overexpression would reduce root length. Interestingly, primary root length and lateral root proliferation was similar in PDCB4OE and WT in control conditions but unlike WT, PDCB4OE did not show a reduction in primary root length or lateral root number under PEG treatment (Figure 5.3,Figure 5.4). Using CRISPR/Cas9 NHEJ, knock out *pdcb4* mutants (PDCB4 CR) were generated and phenotypically characterised. *pdcb4* mutants were insensitive to PEG which correlates

with preliminary data that shows that these mutants have reduced callose in root tips in comparison to WT growing in these conditions (Figure 5.8, Figure 5.11). These data strengthen previous associations between osmotic stress and PD proteins and suggest that PDCB4 may play a role in regulating callose and root growth in response to this challenge. Insights into the molecular mechanism underlying the regulation of callose in response to osmotic challenges were obtained by analysing the metabolic profiling of callose mutants. Many of the topmost differentially presented metabolites in roots from transgenic lines with altered expression of genes related to callose homeostasis were linked to the osmotic stress and defence response, including ABA and glucosinolates (Figure 5.1). These results and their significance are discussed below.

5.3.1 PD associated callose regulates root response to osmotic stress and nutrient availability

In Chapter 4, it was shown that symplasmic transport is severely affected by low nitrate, PEG, salt and other osmolytes which correlated with reductions in root growth and lateral root proliferation. The experiments described here were designed to test the hypothesis that the regulation of symplasmic transport controls root development in response to nutrient availability and osmotic challenge. It was found that lines with contrasting PD-callose levels exhibit metabolic profiles differentially enriched in pathways relating to abiotic stress indicating that responses to abiotic challenge could be perturbed in these lines. The enriched pathways include photorespiration, stachyose biosynthesis and glucosinolate biosynthesis. The products of photorespiration glycolate and glycerate, which are differentially enriched in callose-modified lines, are related with heat and light stress and have been shown to have protect the photosynthetic apparatus under drought stress (Brestic et al., 1995; Guan et al., 2004; Wada et al., 2020). Compounds that have a more direct relationship with responses to osmotic stress are sucrose, myo-inositol and raffinose; compounds in the stachyose biosynthesis pathway. These compounds are osmoprotectants and osmolytes that help maintain turgor and proper protein folding under osmotic stress (Hogg et al., 2011; Kahlaoui et al., 2018; Li et al., 2020b). Other differentially presented metabolites include glucosinolates such as glucoraphanin which have been found to accumulate under drought stress in *A. thaliana* and another member of the Brassicaceae (Salehin et al., 2019; Park et al., 2021). The next stage of this work would be to profile the metabolome of these lines when subjected to abiotic challenge

such as drought to determine how their metabolomes respond relative to each other and to WT.

Artificially altering the amount of callose at PD and challenging the plants to reduced nutrient supply, osmotic challenge or elevated salt was to interrogate the relationship between symplasmic transport and root responses to abiotic conditions. Increased callose have been previously linked with reductions in primary root growth such as in gain-of-function mutants *cals3m* (Vatén et al., 2011). This phenotype is consistent with PDLP1OE which had a reduced primary root length relative to WT irrespective of growth condition. PDLP1 activates callose deposition by an unknown mechanism likely linked to a signalling pathway that activate CALSs (Caillaud et al., 2014). It is noteworthy that this phenotype was also found in PDBG1OE (ectopic expression of callose degrading enzyme) (Benitez-Alfonso et al., 2013). This finding suggests that both, positive and negative, effects in the regulation of callose metabolism (synthesis and degradation) triggers reductions in primary root length and in lateral roots number.

The similarities in root phenotypes between plants with contrasting levels of callose is also reflected in the metabolic profiles of PDBG1OE, PDCB1OE and *pdbg1*. PDBG1OE downregulates callose whereas PDCB1OE and *pdbg1* lead to higher deposition but all of these lines show an increase in ABA levels relative to WT. ABA is a major regulator of plants responses to abiotic stress. ABA has also been described to regulate callose, PD density and symplasmic transport (Tylewicz et al., 2018; Benitez-Alfonso, 2019; Kitagawa et al., 2019). Specifically, PD permeability to the movement of developmental regulators such as the florigen FT was downregulated in response to treatment with ABA and in ABA mutants (Tylewicz et al., 2018). The finding that ABA levels are elevated in lines with aberrant PD callose points to potential positive feedback loops between callose and ABA. The higher levels of ABA in these lines could also be contributing to the shorter root phenotypes supported by the finding that exogenous ABA supresses root elongation (Gazzarrini and McCourt, 2003). Crosses between the callose-related lines and mutants in ABA signalling (such as *aba insensitive 2* (*abi2*) which are insensitive ABA-dependent inhibition of root elongation (Thole et al., 2014)) could help understanding the interactions between these pathways. If the double mutant display enhanced root length, it would suggest that elevated ABA is the primary cause for the defective root length observed in callose mutants.

An alternative hypothesis to ABA-dependent root growth suppression is that callose deposition is altering PD permeability and, thereby the movement of signals that coordinate growth responses to abiotic challenge. These signals could include transcription factors, mRNAs and hormones. Transcription factors such as SHR, WOX5 and TMO7 function non-cell autonomously and are required for proper root development (Koizumi and Gallagher, 2013; Pi et al., 2015; Lu et al., 2018). Mutations in specific amino acids in TMO7 by CRISPR Cas9 leads to shorter root phenotypes (Lu et al., 2018) which are not dissimilar to those reported here for PDLP1OE. The movement of fluorescently tagged SHR and TMO7 is greatly reduced in lines with excessive PD callose (Vatén et al., 2011; Lu et al., 2018). It is conceivable, therefore, that perturbing movement of these transcription factors could be responsible for the changes in root length in these lines and form the basis for how callose-dependent regulation functions. To test this, fluorescently tagged versions of these transcription factors driven by their native promoters could be transformed into WT, PDLP1OE, PDBG1OE and *pdbg1* to study their movement in these callose altered backgrounds. The distribution of these factors could then be determined by confocal microscopy. Differential movement of these transcription factors would provide evidence of the mechanism regulating root architectural responses to water and nutrient availability.

The similarities in PDBG1OE and PDLP1OE phenotypes could be related to pleiotropic effects of constitutively expressing these genes. Future work to disentangle these effects could involve expressing PDLP1 and PDBG1 under inducible or tissue specific promoters. PDBG1 expression is restricted to the vasculature and meristematic tissues (Benitez-Alfonso et al., 2013), therefore, the phenotypes of *pdbg1* more accurately reflects what happens in nature. The increase in primary root length of *pdbg1* relative to WT in control, low nitrate and 3% PEG but not in low potassium, low phosphate or elevated NaCl suggests that PDBG1 may have a specific role in regulating root length responses in these conditions. Previous reports have linked PDBG1 function to lateral root patterning but not directly to primary root length (Benitez-Alfonso et al., 2013). Histological studies suggest that there is promotor activity in root apical meristems which supports a putative role for PDBG1 in root length regulation (Benitez-Alfonso et al., 2013). Further work will compare PDBG1 expression in control, PEG and low nitrate conditions. In Chapter 4, it was described that both PEG and low nitrate conditions lead to reductions in phloem unloading into the root tips. Given that the mutant *pdbg1* has been reported to have higher levels of callose in the stele (Benitez-Alfonso et al., 2013), it would be prudent to use the

pdbg1 x *pSUC2::GFP* line to establish whether phloem export is even further restricted under low nitrate and 3% PEG. Such a result would suggest that PDBG1 has an antagonistic role in regulating symplasmic transport under these conditions.

Here, lateral root number was increased in control conditions relative to WT as reported by Benitez-Alfonso et al. (2013). The increased number of lateral roots in *pdbg1* has been previously attributed to reduced spacing between lateral root primordia and increased callose accumulation (Benitez-Alfonso et al., 2013). *pdbg1* lateral root number was significantly reduced relative to control conditions in low nitrate and low phosphate, different to WT. This could be interpreted as an indication that PDBG1 has a role in regulating lateral root development in a context specific manner and that under low nitrate and low phosphate, PDBG1 may be involved in limiting the inhibitory effects of these conditions on lateral root development. However, this experiment should be repeated quantifying emerged and primordia lateral roots and/or, at least, 10 dpg to be able to determine the effect on primordia formation and emergence.

In summary, plants with artificially altered levels of PD callose display metabolic profiles differentially enriched in pathways relating to abiotic stress. Ectopic expression of PDLP1, reported to increase callose levels, leads to reductions in root length and lateral root proliferation. These phenotypes are also observed when PDBG1 is ectopically expressed which has reduced PD callose. These observations suggest that having tight control over PD callose turnover may be more important than absolute levels of callose. As reported elsewhere, *pdbg1* has increased lateral root proliferation supporting the role of PDBG1 as a regulator of lateral root development. Novel phenotypes are reported here, specifically that *pdbg1* displays increased primary root length in control, low nitrate and under mild osmotic challenge with PEG suggesting that PDBG1 could be a regulator of root length under these conditions. The mechanism is not known but could involve the regulation of symplasmic signals.

5.3.2 PDCB4 regulates root architecture in response to osmotic challenge

Over 20% of the *A. thaliana* genome is differentially expressed under osmotic stress conditions including a high proportion of candidate PD genes (Chapter 3) (Sharma et al., 2018). To date, two PD genes have been directly linked with responses to osmotic stress: Qiān Shǒu kinase (QSK1) and Cys-rich receptor-like kinase2 (CRK2) (Hunter et al., 2019; Silva-Sanzana et al., 2019). These genes are both receptor-like kinases involved in

signalling PD regulation. PDCB4 is a PD-localised protein (Simpson et al., 2009) encoding a predicted callose binding domain (also called CBM43 or X8). Transcriptomics suggest that PDCB4 is induced in both roots and shoots in response to osmotic challenge and PDCB4 OE does not exhibit a reduction in primary root length or lateral root number seen in WT in response to PEG treatment (Table 5-2).

To further dissect the role of PDCB4 in the osmotic stress response, knockout mutants were generated using CRISPR-Cas9. A novel approach was taken here to segregate out transgenes containing the Cas9 cassette on T1 seeds (which should already contain the desired mutations) by rescue of PPT-susceptible lines with exogenous glutamine ('PPT-rescue' system). This is required so that resulting lines only harbour the desired mutation and not marker genes or the associated genes required to cause the mutation. This approach is far less resource intensive than screening individual plants by PCR. However, new methods have since been developed for *Arabidopsis*, that supersede the method described here, based on the use of fluorescent seed coat markers (Aliaga-Franco et al., 2019). 'PPT-rescue' may remain more appropriate for species where expression of seed coat markers is not available or suitable to develop.

Primary roots of *pdcb4* CR mutants continue growing even when exposed to exogenous PEG or elevated NaCl, as a result the effects on root length were less severe than in WT. Lateral root density was also less affected in *pdcb4* exposed to PEG, supporting a role for PDCB4 in this root response to osmotic stress. Callose accumulates in roots grown in exogenous PEG, but this response is suppressed in *pdcb4* suggesting that PDCB4 may function in regulating callose levels in these conditions. A similar response was described when the mutant *qsk1* was transferred to reduced water potential media (Grison et al., 2019), which suggests QSK1 and PDCB4 may form part of the same regulatory pathway, although this needs experimentally confirmed. According to the prevailing model, this increase in callose would lead to reductions in symplasmic transport (Amsbury et al., 2018). A role for PDCB4 in negatively influencing symplasmic transport is supported by the preliminary finding that that CFDA diffusion was increased in *pdcb4* mutants; however, this experiment was conducted only once and must be repeated. The mobile fluorescein derivative of CFDA is approximately 0.5 kDa in size which is similar in size to sugars and phytohormones, but it is much smaller than mobile macromolecules such as proteins and RNAs. Determining whether movement of macromolecules is affected in *pdcb4* mutants is logically the next step to dissect the role of PDCB4 in symplasmic transport. This could be achieved by crossing *pdcb4* and GFP-based symplasmic reporter

systems such as *pSUC2::GFP* and then assessing GFP diffusion under osmotic challenge conditions.

Supporting a role for PDCB4 in the osmotic stress response, a preliminary finding was that leaf stomatal density in *pdcb4* mutants appears to increase in response to exogenous PEG. It is not known whether this increase in stomatal density is associated with an increase in the stomatal index (proportion of epidermal cells that are stomatal cells). Stomatal index was shown to be reduced in wheat under drought conditions (Quarrie and Jones, 1977) which could be attributed to the need to minimise water loss by transpiration. Surprisingly little is known about the effects of osmotic challenge on stomatal development. Seedlings grown in plates with exogenous PEG are under stable osmotic challenge and in relatively high humidity due to low rates in gaseous exchange between the outside and the inside of the plate. Higher rates of transpiration due to increased stomatal density may not be detrimental to plant growth in these conditions. Under field conditions, higher stomatal density is linked with poorer drought tolerance (Caine et al., 2019). It would be pertinent to test whether *pdcb4* mutants are more sensitive to progressive drought by withholding watering. The increase in stomatal density may be disadvantageous in these conditions particularly if the rate of transpiration results in a rate of water loss that exceeds the rate of water acquisition from the soil.

PDCB4 involvement in the regulation of stomatal density is highly speculative at this stage. However, there is a precedent linking callose regulation and stomatal development. The mutant *glucan synthase-like 8* (*gsl8*), also known as *chorus,* has less epidermal callose and exhibits abnormal clustering of stomata. GSL8 is required to restrict the movement of SPCH that is expressed in meristemoid mother cells and meristemoids that initiates stomatal cell lineage (Guseman et al., 2010). Other mobile signals are known to be important in the regulation of stomatal development and patterning including miRNAs (Zhu et al., 2020a) and peptides (Zeng et al., 2020). EPIDERMAL PATTERNING FACTORs (e.g. EPF1 and EPF2) and EPF-LIKE (e.g. EPFL9) peptides bind to ERECTA-family receptors in complex with the LR-RLK TOO MANY MOUTHS (Hara et al., 2007; Hara et al., 2009; Lee et al., 2015; Lin et al., 2017). EPF1 and EPF2 repress stomatal development. EPFL9 blocks receptor function which promotes stomatal development. EPF2 is expressed early in meristematic mother cells that express SPCH. EPF2 has been modelled to supresses stomatal development in neighbouring cells (Pillitteri and Dong, 2013), maintaining the 'one cell rule' where stomata are separated by at least 1 non-stomatal epidermal cell (Sachs, 1991). EPF1 and EPFL9 have been demonstrated to function non-cell

autonomously (Zeng et al., 2020) but is not known whether they are mobile or regulated by PD. No obvious changes in stomatal clustering were observed in *pdcb4* relative to WT suggesting that the mechanisms of maintaining the one cell rule may be intact. However, the increase in stomatal density could suggest that later in development stomatal patterning is perturbed. One avenue to explore is whether the transport of SPCH is perturbed in *pdcb4* and to analyse the phenotype in mature plants grown in drought conditions (MacAlister et al., 2007; Wright et al., 2007).

To summarise, phenotypic analysis of plants ectopically expressing *PDCB4* or *pdcb4* knockout have perturbed primary and lateral root phenotypes under osmotic challenge. This underlines the role of PDCB4 as regulator of root responses to osmotic stress. Under these conditions, callose levels do not increase in *pdcb4* plants as observed in WT plants. Encoding a callose binding domain, the mechanism of how PDCB4 regulates responses to osmotic stress is likely linked with callose regulation. Given the localisation pattern, it is likely that PDCB4 is specifically regulating PD callose although influence in other polysaccharides cannot be disregarded. Other questions remain outstanding. For example, does PDCB4 modulate the diffusion of osmotic response signals? What is the identity of these signalling molecules? More broadly, our understanding of mobile signals involved in the response to nutrient and water availability is rather limited. In the next chapter, new insights on a mobile factor involved in the root responses to nitrate availability are presented.

Chapter 6 SVL1 is a mobile signal that regulates cell walls in response to nitrate and sucrose

6.1 Summary

Chapter 4 established that differences in nutrient availability and substrate water potential are associated with differences in symplasmic transport. However, the functional significance and mechanistic causes of this regulation are not fully understood. Furthermore, conditions where PD factors have been discovered to have a role in root responses to a nutrient availability and substrate water potential are limited to osmotic stress (Grison et al., 2019; Hunter et al., 2019) and low phosphate (Müller et al., 2015). In Chapter 4, roots grown in low nitrate were shown to have a relative reduction in symplasmic transport of GFP from the stele laterally towards to epidermis and distally towards the root tip. No PD located or transported proteins have been previously associated with facilitating responses to low nitrate. Therefore, there is great potential for uncovering novel processes linking PD with this condition. Using tools presented in Chapter 3 and available literature, SHAVEN3 (SHV3) -LIKE 1 (SVL1) was selected for further characterisation as this protein was identified in the PD proteome (Fernandez-Calvino et al., 2011), has been linked with cell wall changes (Hayashi et al., 2008; Yeats et al., 2016) and its mRNA was described as mobile in response to nitrate (Thieme et al., 2015). The following introduces relevant background information about this protein.

SVL1 belongs to the glycerophosphodiester phosphodiesterase (GDPD) protein family. GDPDs catalyse the breakdown of glycerophosphoryl diesters (GPD) to glycerol 3-phosphate and their respective alcohols, and have a role in diverse physiological responses including phosphate homeostasis (Cheng et al., 2011). SHV3 and SVLs form a clade within the GDPD family containing a domain composed of two tandemly repeated GDPD-like subdomains (Hayashi et al., 2008). No GDPD activity for SHV3 was detected, in vitro, when using heterologous expression of SHV3 in *Escherichia coli* or *Pichia pastoris* (Hayashi et al., 2008; Yeats et al., 2016). This suggests that this protein does not have enzymatic activity, characteristic of other members of the GDPD family. However, considerable GDPD activity has been shown in SVL2 on several GDP substrates and therefore this activity cannot be ruled out in other GDPL proteins, including SHV3 and SVL1 (Cheng et al., 2011).

The function of SHV3 and members of SVL are not clearly understood at this time but mutant phenotypes suggest they are involved in plant development. Root hair development in *shv3, a*s the name suggests, is severely restricted which is caused by rupture of root hair cells early in development (Kuromori et al., 2006). This phenotype is

partly rescued when grown in elevated borate, linked to borate's capacity to increase pectic-crosslinking in the cell wall (Hayashi et al., 2008). *SHV3* transcripts are present in roots and shoot; including leaves, stems and siliques, but absent in flowers (Hayashi et al., 2008). In comparison to *SHV3*, *SVL1* expression has overlapping and distinct domains. Promoter SVL1-GUS activity for example is stronger in root tips and in the developing shoot. Intracellular localisation of SHV3 indicates binding to the PM. SHV3 (as SVL1) contains a predicted SP and a GPI anchor supporting their membranous localisation (Hayashi et al., 2008).

Several lines of evidence suggest that SVL1 and SHV3 might function in synergistic pathways. No strong phenotypes of *svl1* have been reported but the double mutant *shv3svl1* exhibits additional, more severe phenotypes than *shv3* (Hayashi et al., 2008). The double mutant *shv3svl1* displays ectopic lignification in hypocotyl and a 50% reduction in etiolated hypocotyl length. Stomata cells were found to be larger, and swelling was observed in the hypocotyl epidermis. These phenotypes were correlated with defects in cell wall organisation. Fourier-transform infrared spectroscopy of AIR demonstrated a severe reduction in cellulose content, increased uronic acid, a decreased amount of methyl esterification, and an almost 10 fold increase in starch when grown in exogenous sucrose (Hayashi et al., 2008). These phenotypes were sucrose dependent, and further work using a suppressor screen identified a mutation in *SUCROSE TRANSPORTER 1* (*SUC1*) that supressed the reduction in cellulose and etiolated hypocotyl length phenotypes in *shv3svl1* seedlings (Yeats et al., 2016). This report suggested that the reduction in cellulose content in *shv3svl1* is due to a reduction in cellulose synthase activity due to an increase in sucrose uptake and transport (demonstrated using the sucrose fluorescent analogue esculin). Yeats et al. (2016) propose that mutations in *SHV3* and *SVL1* cause aberrant signalling leading to hyperpolarisation of the PM, induced sucrose uptake and transport, and downstream phenotypes supporting a role in signalling.

Considering that SVL1 was identified in a PD proteome, contains protein features shared with other PD proteins, and has a role in regulating cell walls, there is potential for SVL1 to function at PD. *SVL1* transcripts were identified as graft transmissible under nitrogen limiting conditions via high throughput screening linking SVL1 with responses to low nitrogen (Thieme et al., 2015). Work presented in this chapter aimed to determine if SVL1 is PD localised, to determine whether sucrose and nitrate concentrations alter gene/protein expression and/or localisation, and to determine whether SVL1 regulates RSA, cell wall composition, and symplasmic transport. *SVL1* is co-expressed with *PDBG1*

therefore work was carried out to determine whether SVL1 interacts with PDBG1 in the regulation of PD. The results improve our understanding of the role PD plays in the nitrate and sucrose response and the potential functional links between SVL1 and PDBG1 in this process.

6.2 Results

6.2.1 SVL1 localises at the cell periphery

To characterise SVL1 intracellular localisation, fluorescent constructs were generated by Dr Yoselin Benitez Alfonso. SVL1 contains a predicted SP, tandem GDPL domains, and a GPI anchor (Figure 6.1 A). As there are signalling sequences in the N and C terminal, a YFP tag was introduced internally between the SP and the first GDPL domain (fusion named YFP-SVL1). Two constructs were designed: one driven by the constitutive CaMV *35S* promotor (*p35S*) and another under the native *SVL1* promotor (-2000 bp, *pSVL1*). Plants expressing *p35S::YFP-SVL1* were grown for 5 dpg and imaged on a confocal microscope. *p35S::YFP-SVL1* displayed clear cell periphery localisation as seen in the abaxial pavement and guard cells of cotyledons (Figure 6.1 B). A small proportion of fluorescence is also visible inside cells. In rare occasions, *p35S::YFP-SVL1* was observed forming punctate patterns at the cell periphery (Figure 6.1 B). Similarly, in root tips, most *p35S::YFP-SVL1* fluorescence is seen in the cell periphery with some internal fluorescence apparent. Expression in the root apical meristem is largely restricted to the lateral and columella root cap. Localisation of YFP-SVL1 under its native promoter (*pSVL1::YFP-SVL1*) was similar with most of fluorescence observed at the cell periphery (Figure 6.2 A). Punctate-like fluorescence was also observed at the cell periphery. These punctate-like patterns do not co-localise with the callose stain aniline blue (Figure 6.2 B). Localisation of *pSVL1::YFP-SVL1* in the root is similar to that described for *p35S::YFP-SVL1* (Figure 6.2 C). Notably, YFP-SVL1 strongly localises to trichome papillae (Figure 6.2 D).

To summarise, SVL1 is expressed in roots and shoot, predominantly in epidermal tissues, and localises at the cell membranes, sometimes forming aggregates that do not fully co-localise with callose. The results do not support PD localisation for this protein.

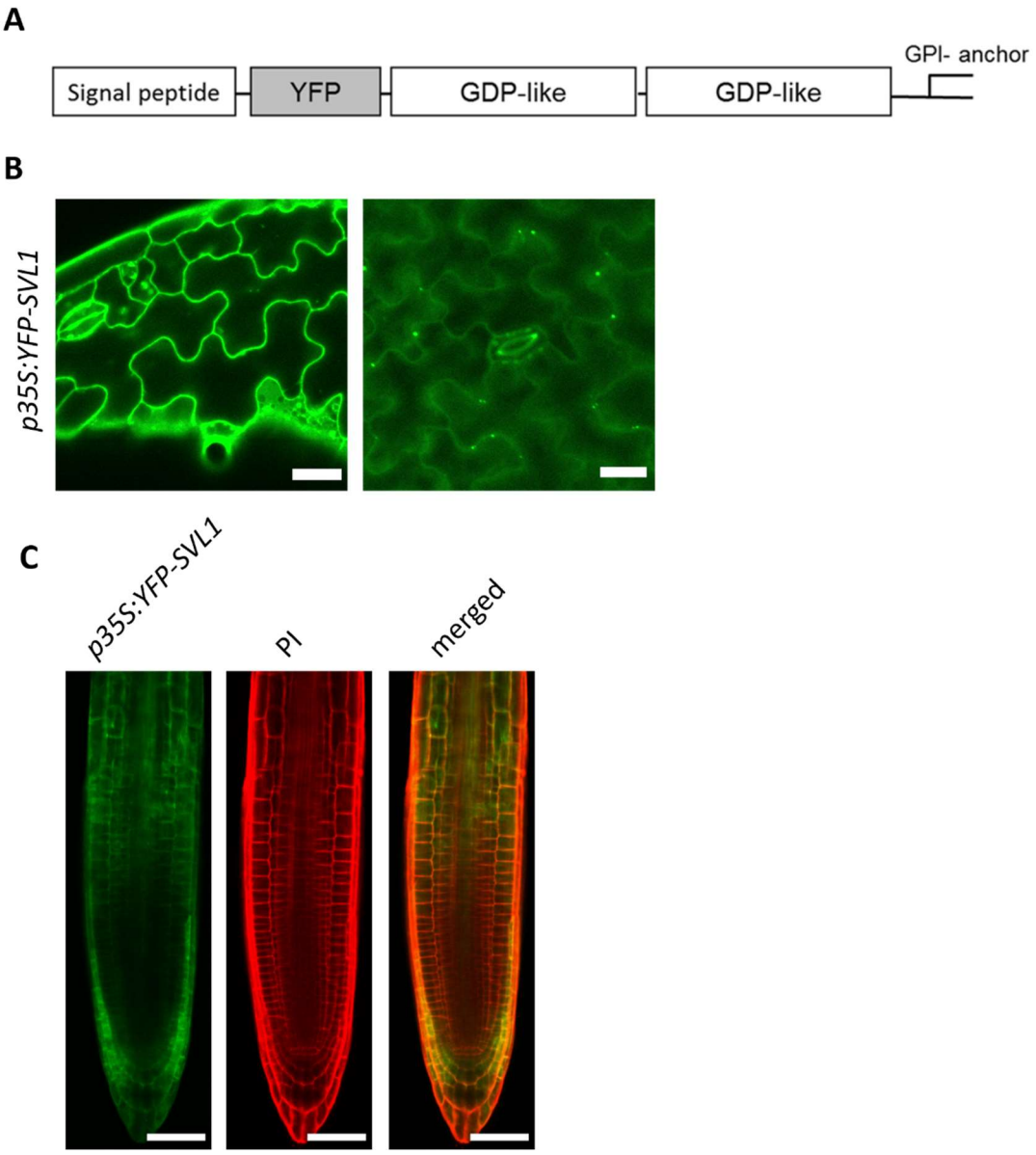

Figure 6.1 Constitutively expressed YFP-tagged SVL1 localises at the cell periphery. (A) Domain structure of YFP-SVL1. The tag was introduced downstream of a predicted signal peptide and before tandem glycerophosphoryl diester phosphodiesterase (GDP) – like domains. SVL1 is predicted to be post transcriptionally modified with a glycosylphosphatidylinositol (GPI) anchor. (B,C) Transgenic 5 days old *A. thaliana* seedlings expressing *p35S::YFP-SVL1* were imaged using a confocal microscope. (B) Abaxial cotyledon epidermis was imaged with a 488 nm laser. Scale bar = 20 µm. (C) Primary root tips were counterstained with propidium iodide (PI) and images were collected sequentially with a 488 nm (green: YFP-SVL1) and 561 nm (red: PI) laser. Scale bar = 50 µm.

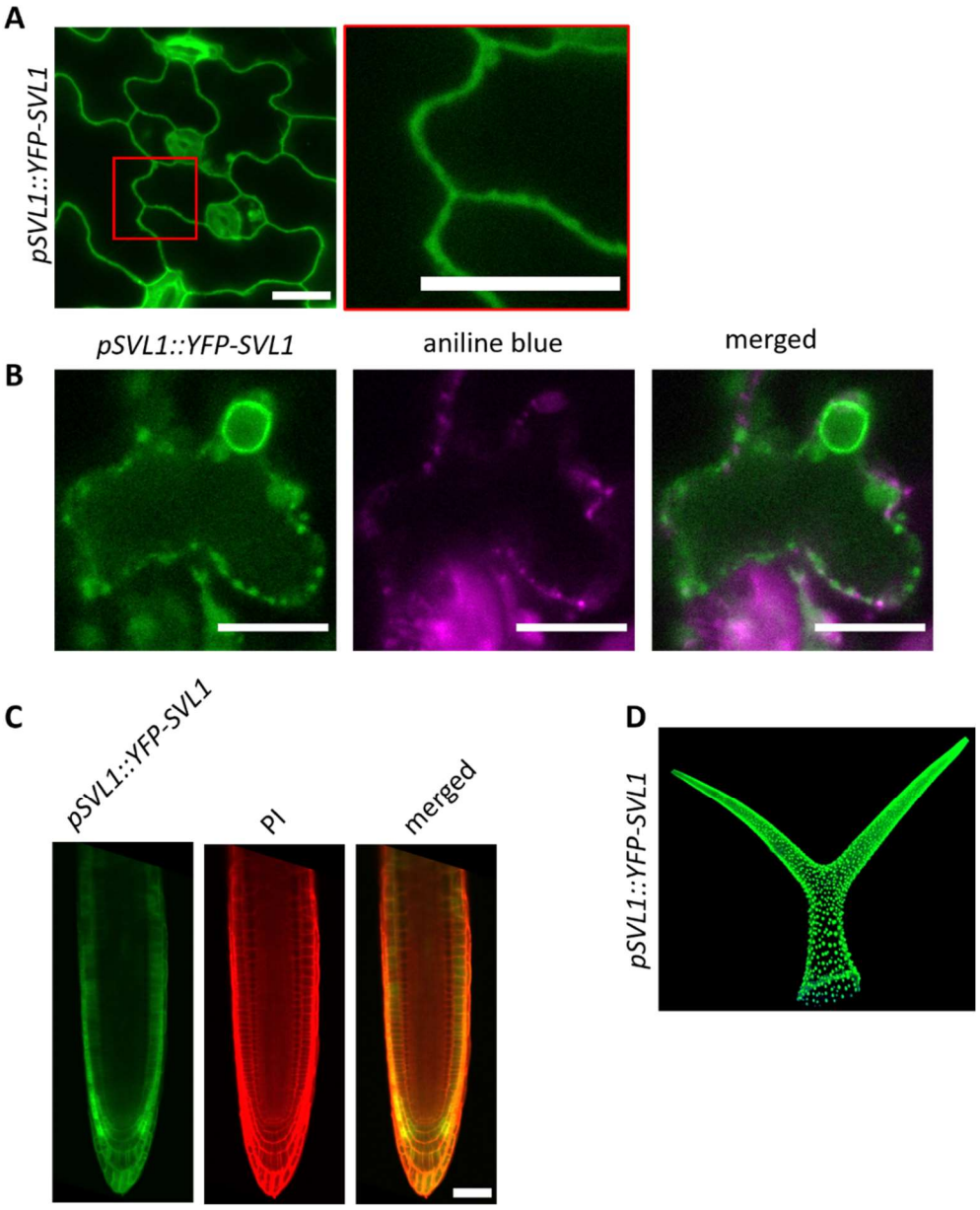

Figure 6.2 YFP-tagged SVL1 driven by its native promotor localises in shoot and root. (A-C) Transgenic 5 days old *A. thaliana* seedlings expressing *pSVL1::YFP-SVL1* were imaged using a confocal microscope. (A) Abaxial cotyledon epidermis was imaged with a 488 nm laser. (right panel) magnified portion highlighted by red box. Scale bar = 20 µm. (B) Cotyledons were counterstained with aniline blue fluorochrome to reveal callose deposits. Channels were collected sequentially with excitation laser 488 nm (green: YFP-SVL1) and 405 nm (magenta: aniline blue). Scale bar = 20 µm. (C) Primary root tips were counterstained with propidium iodide (PI) and images were collected sequentially with 488 nm (green: YFP-SVL1) and 561 nm (red: PI). Scale bar = 50 µm. (D) Trichome of 7dpg *A. thaliana* seedlings expressing *pSVL1::YFP-SVL1*; taken with assistance from Dr Fritz Kragler (Max Planck Institute of Molecular Plant Physiology, Germany).

6.2.2 Grafting demonstrates that *SVL1* transcripts are shoot-root mobile

SVL1 transcripts had been identified in the shoot-to-root mobile RNA-seq population after grafting two different ecotypes under N-limitation (Thieme et al., 2015). To confirm whether SVL1 transcripts are truly graft transmissible, Dr Lei Yang (collaborator from the Kragler group, Max Planck Institute of Molecular Plant Physiology) grafted Col-0 shoots as scions and knockout mutant *svl1* as the rootstock (written as Col-0/*svl1* in scion/rootstock format) with the junction being made across hypocotyls (Figure 6.3 A). After 10 days, scion and rootstock were sampled, and RNA extracted. RT-PCR of this tissue showed that *SVL1* transcripts were present in *svl1* root stocks that were knock out for this transcript (Figure 6.3 C). To confirm this result, *pSVL1::SVL1-YFP*/Col-0 grafts were made and the YFP signal detected by confocal microscopy. YFP fluorescence was evident in the Col-0 rootstocks demonstrating that *YFP-SVL1* transcripts can move from shoot into the root tissue even in N depleted conditions. (Figure 6.3 B). SVL1-YFP presence in the root originates from either mobile transcripts or mobile protein.

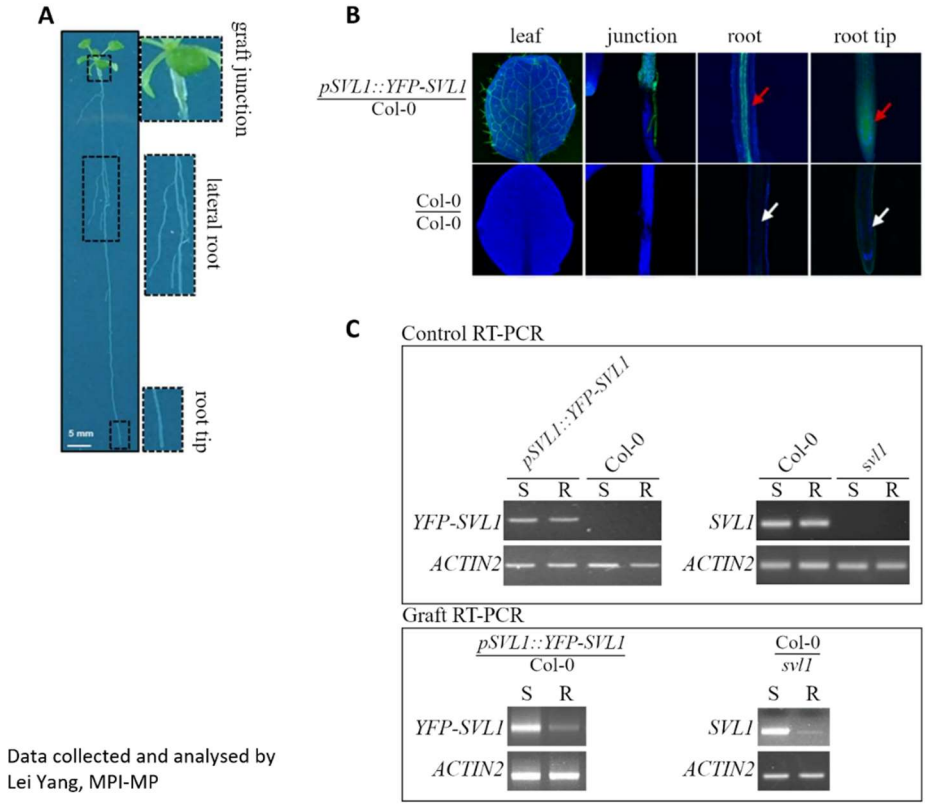

Figure 6.3 *SVL1* mRNA is shoot-root graft-transmissible. Grafting and imaging of *A. thaliana* were performed by Lei Yang as described in Yang et al. (2019). (A) Representative image of a shoot-root grafted *A. thaliana* seedling. Microtubing can be seen covering the graft junction made between hypocotyls of the scion and rootstock. (B,C) Graft combinations are written as scion/root stock. (B) Material was imaged by confocal microscopy 10 days post grafting using a 514 nm / 565 nm argon laser. Red arrows indicate scion derived YFP-SVL1 detected in Col-0 root stock (green: emission between 524 to 550 nm). No YFP signal is detected in Col-0 root stock when the scion is Col-0 (white arrows). Blue channel is autofluorescence (blue: emission between 700 to 800 nm). (C, top) Detection of *SVL1-YFP* and native *SVL1* by RT-PCR of non-grafted shoot (S) and root (R). Plants expressing *pSVL1::YFP-SVL1* and Col-0 were assayed for *SVL1-YFP* expression and knockout mutant *svl1* and Col-0 were assayed for native *SVL1* expression. (C, bottom) Detection of *SVL1-YFP* and native *SVL1* by RT-PCR in grafted tissue. Expression of the housekeeping gene *ACTIN2* was assayed in all cases as a control.

6.2.3 SVL1 expression is modulated by sucrose and nitrate

SVL1 transcripts were mobile in N limiting conditions (Thieme et al., 2015) and *shv3svl1* displayed a sucrose-dependent phenotype (Yeats et al., 2016). Sucrose is a major regulator of nitrate responses (Roycewicz and Malamy, 2012), thus the expression of *SVL1* was tested on ATS media (9 mM nitrate) and 0.1 mM nitrate-based media, with and without 1% (w/v) sucrose. Seeds expressing GUS driven by the *SVL1* promoter were obtained from the authors of Hayashi et al. (2008). Plants were fixed 8 dpg and GUS activity was assayed. Blue signal was strong after 3 hours incubation. The pattern of GUS activity was similar (but slightly different) between treatments. *SVL1* expression was strong in the root apical meristem particularly in the region surrounding the stem cell niche (Figure 6.4). GUS activity was relatively high in lateral root cap cells but considerably lower in columella cells and initials. Expression decreases distally from the stem cells. When grown in 1% sucrose, regardless of nitrate concentration, this proximal decrease in expression is less steep and extends towards and into the basal meristem. GUS reporter activity is present in early lateral root development, resembling the apical root meristem (Figure 6.4). Expression in lateral roots is not significantly affected by sucrose/nitrate treatment. Expression is low, but present, in the shoot apical meristem and hypocotyl/root junctions in all treatments (Figure 6.4).

To test for the effect of sucrose and nitrate on SVL1 protein levels, plants expressing *pSVL1::YFP-SVL1* were grown in the same sucrose and nitrate media described above and analysed by confocal microscopy at 5 dpg. When grown in the absence or presence of sucrose, YFP-SVL1 accumulates in the periphery of cotyledon pavement cells independent of nitrate concentration (Figure 6.5 A). However, YFP-SVL1 appears to aggregate in the cell periphery in cotyledons grown in 0.1 mM nitrate with 0% sucrose. In the root tip, accumulation of YFP-SVL1 was low when plants were grown in control (9 mM nitrate) when compared to low (0.1 mM) nitrate (Figure 6.5 B). YFP-SVL1 accumulation was the highest in plants grown in 0.1 mM nitrate without sucrose. This was semi-quantified for the stele region of the elongation zone of root tips which showed that YFP-SVL1 accumulation in 0.1 mM nitrate with 0% sucrose was significantly larger than in plants grown in 9 mM nitrate (Figure 6.5 B).

To summarise, *SVL1* expression was significantly higher in root tips than in other tissues. Protein accumulation appears to be regulated by nitrate and sucrose, being highest in roots grown in depleted N and no sucrose media. Note that the pattern of gene expression

and protein accumulation in the elongation zone do not overlap suggesting potential for protein movement (Figure 6.2 C, Figure 6.4).

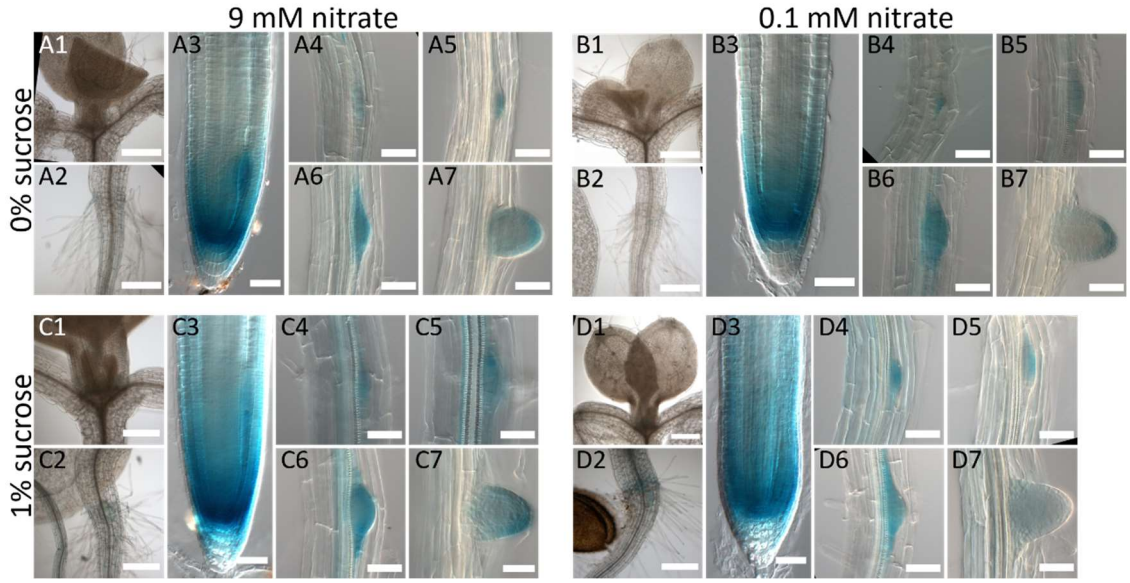

Figure 6.4 The pattern of *SVL1* gene expression in primary root tips is expanded in response to exogenous sucrose but minimally affected by nitrate concentration. Histochemical analysis of 8 day old plants expressing GUS under the *SVL1* promoter grown on ATS-based media with (A, C) 9 mM nitrate or 0.1 mM nitrate (B, D). Media was supplemented with (C,D) or without (A,B) 1% sucrose. Plants were incubated in GUS-staining buffer in the dark for 3 hours. Material was imaged on a DIC microscope (Axioscope, Zeiss). Numbers after letters refer to the organ being imaged: 1- shoot apex with first leaves emerging, scale bar = 0.5 mm; 2-hypocotyl/root junction, scale bar = 0.5 mm; 3-primary root tip; 4:7 – lateral roots at varying degrees of development, scale bar = 50 µm.

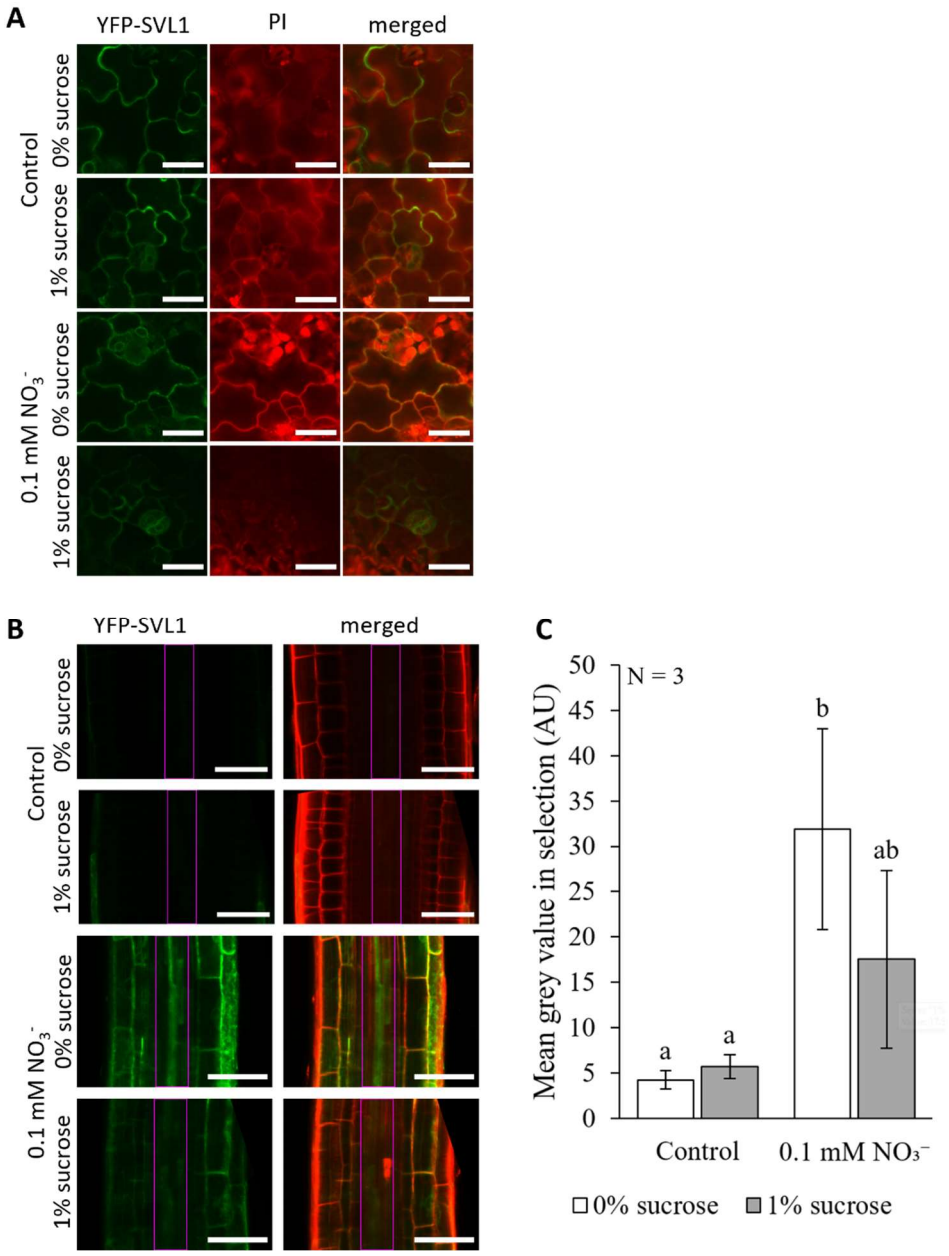

Figure 6.5 Accumulation of YFP-SVL1 in the root is dependent on nitrate concentration and exogenous sucrose. Transgenic 5 days old *A. thaliana* seedlings expressing *pSVL1::YFP-SVL1* were grown on ATS-based media in 9mM (control) and 0.1 mM nitrate and without or with 1% (w/v) added sucrose. Plants were counterstained in propidium iodide (PI) and imaged using a confocal microscope. (A, B) Images were collected sequentially with a 488 nm laser (green: YFP-SVL1) and 561 nm laser (red: PI). (A) Abaxial cotyledon epidermis, scale bar = 20 µm. (B) Primary root elongation zone, Scale bar = 50 µm. Purple box highlighted areas were used to calculate mean stele YFP-SVL1 fluorescence. (C) Mean YFP-SVL1 fluorescence in the stele of the elongation zone of primary roots. Bars with differing letters are significantly different (ANOVA, Tukey post hoc, $p < 0.05$).

6.2.4 Ectopic expression of YFP-SVL1 reduces primary root length and lateral root number in a nitrate dependent fashion.

SVL1 is expressed in the stem cells and meristem of the primary root and the extent of SVL1 accumulation seems to be regulated by sucrose and nitrate concentration. Both sucrose and N are known to regulate root growth as shown in Chapter 4 (Zhang and Forde, 2000; Roycewicz and Malamy, 2012; O'Brien et al., 2016). To test if SVL1 expression is important in this regulation, root phenotypes of *svl1* and plants expressing *p35S::YFP-SVL1* were determined in ATS (9 mM nitrate) and 0.1 mM nitrate ATS with and without 1% (w/v) sucrose. WT and seedlings expressing *pSVL1::YFP-SVL1* were used as controls. Primary root length, number of lateral roots, total lateral root length, and emerged lateral root density were measured at 8 dpg. Two replicates of this experiment are presented to portray the observed variance more accurately in phenotypes observed for these lines (Figure 6.6, Figure 6.7). A summary of phenotypes between all replicates is given in Table 6-1.

Under both sucrose treatments, WT primary root length was consistently shorter in 0.1 mM nitrate in all replicates (Figure 6.6, Figure 6.7, Table 6-1). As expected, primary root length of *pSVL1::YFP-SVL1* (in *svl1* background) was not significantly different from WT under 0% sucrose in either nitrate condition (Figure 6.6, Table 6-1). However, in one replicate at 1% sucrose, *pSVL1::YFP-SVL1* appears longer than WT, but the ratio of reduction between nitrate conditions appears consistent (Figure 6.7, Table 6-1). Primary root length of *p35S::YFP-SVL1* was significantly shorter than both WT and *pSVL1::YFP-SVL1*, when grown in control media supplemented with either 0% or 1% sucrose (Figure 6.6, Figure 6.7, Table 6-1). As for WT, *p35S::YFP-SVL1* primary root length is reduced under 0.1 mM nitrate, although no significant changes were observed relative to WT and *pSVL1::YFP-SVL1* in the same conditions (except for replicate 1 in 0% sucrose) (Figure 6.7, Table 6-1). Since the primary root is already shorter in control conditions, the result might indicate that *p35S::YFP-SVL1* primary roots are less sensitive to 0.1 mM nitrate, as the percentage of reduction is smaller than WT in this condition. *svl1* primary root phenotyping was not reproducible as reflected in all 4 replicates (Table 6-1). In 0% sucrose control media, *svl1* roots length appear shorter (replicate 2) or not significantly different than WT (Figure 6.6). Under 1% sucrose, variability was also observed between replicas. In response to low nitrate, *svl1* primary root is significantly reduced, similar to WT, in both 0 and 1% sucrose conditions (Figure 6.7).

Under both sucrose treatments, WT displayed fewer lateral roots and reduced emerged lateral root density in 0.1 mM nitrate relative to 9 mM nitrate consistent with the reduction in primary root length (Figure 6.6, Figure 6.7, Table 6-1). Neither *svl1* or *pSVL1::YFP-SVL1* consistently showed any significant difference in lateral root count or emerged lateral root density relative to WT in any nitrate/sucrose treatment. WT plants exhibited a relative reduction in lateral root length in 0.1 mM nitrate relative to 9 mM nitrate in 0% sucrose but not in 1% sucrose (Figure 6.6, Figure 6.7, Table 6-1). Lateral root length of *svl1* and *pSVL1::YFP-SVL1* was not consistently significantly different from WT in 0% sucrose in either nitrate treatment. However, under 9 mM nitrate with 1% sucrose, lateral root length was observed to be longer, shorter or unchanged relative to WT depending on replicate (Figure 6.7, Table 6-1). *p35S::YFP-SVL1* displayed fewer lateral roots, reduced emerged lateral root density, and lateral root length relative to WT in 9 mM nitrate regardless of sucrose treatment and consistent with the reduced primary root length. In 0.1 mM nitrate, primary root lengths do not differ between *p35S::YFP-SVL1* and WT in at least 3 replicates (Table 6-1). Accordingly, lateral root phenotypes are not different (Table 6-1).

To summarise, ectopic expression of YFP-SVL1 leads to severe reduction in root growth and lateral root development. Phenotypes of *svl1* are inconsistent between replicates.

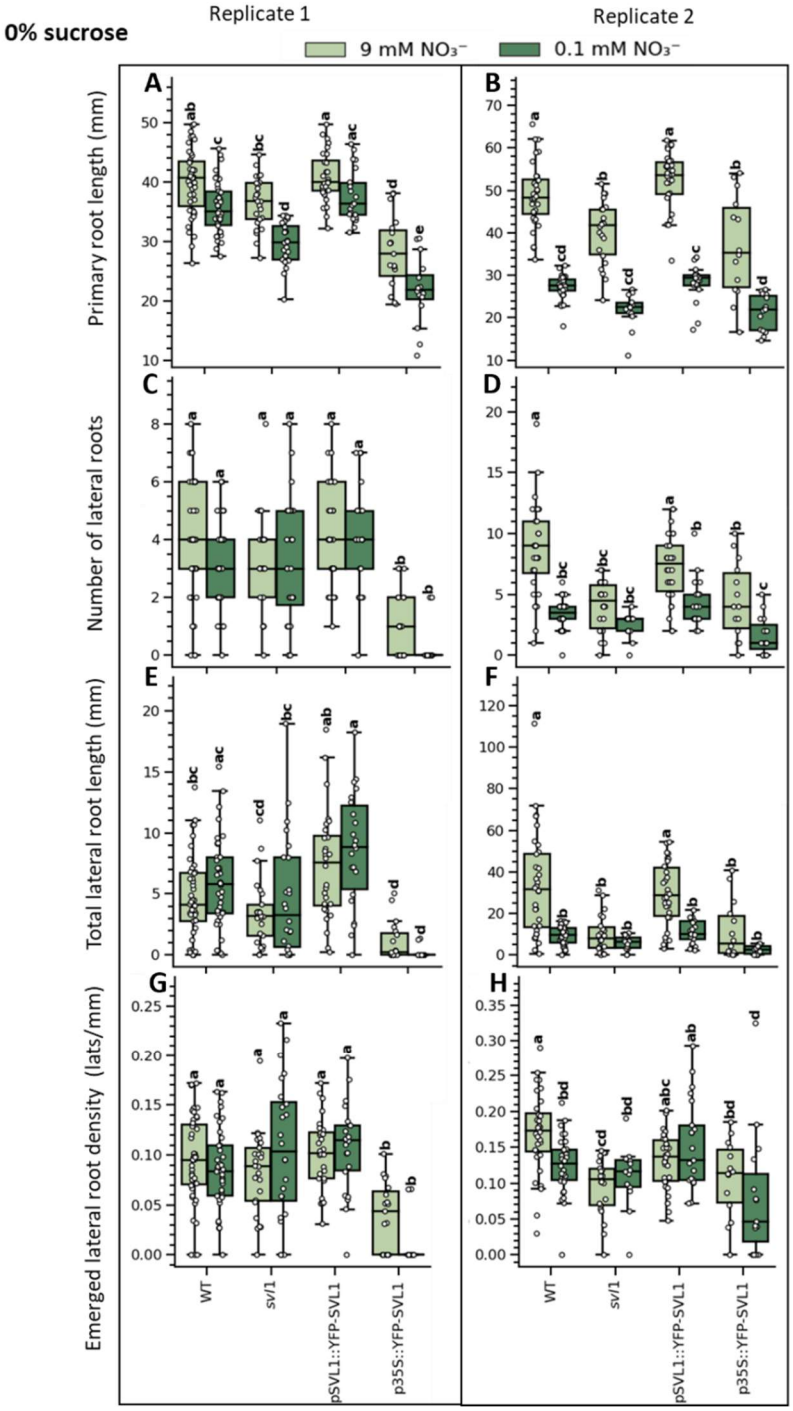

Figure 6.6 Primary and lateral root phenotyping of *svll* mutant and transgenic SVL1 lines grown on either 9 mM nitrate or 0.1 mM nitrate with 0% sucrose. (A,B) Primary root length, (C,D) number of lateral roots, (E,F) total lateral root length, and (G,H) emerged lateral root density were measured 8 days post germination (dpg). Pairwise significance testing was performed by one-way ANOVA (Tukey post hoc test, $p < 0.05$, $N \geq 20$, bars that do not share a letter are significantly different). Data from 2 representative replicates are presented. A summary of phenotypes for all replicates is presented in Table 6-1.

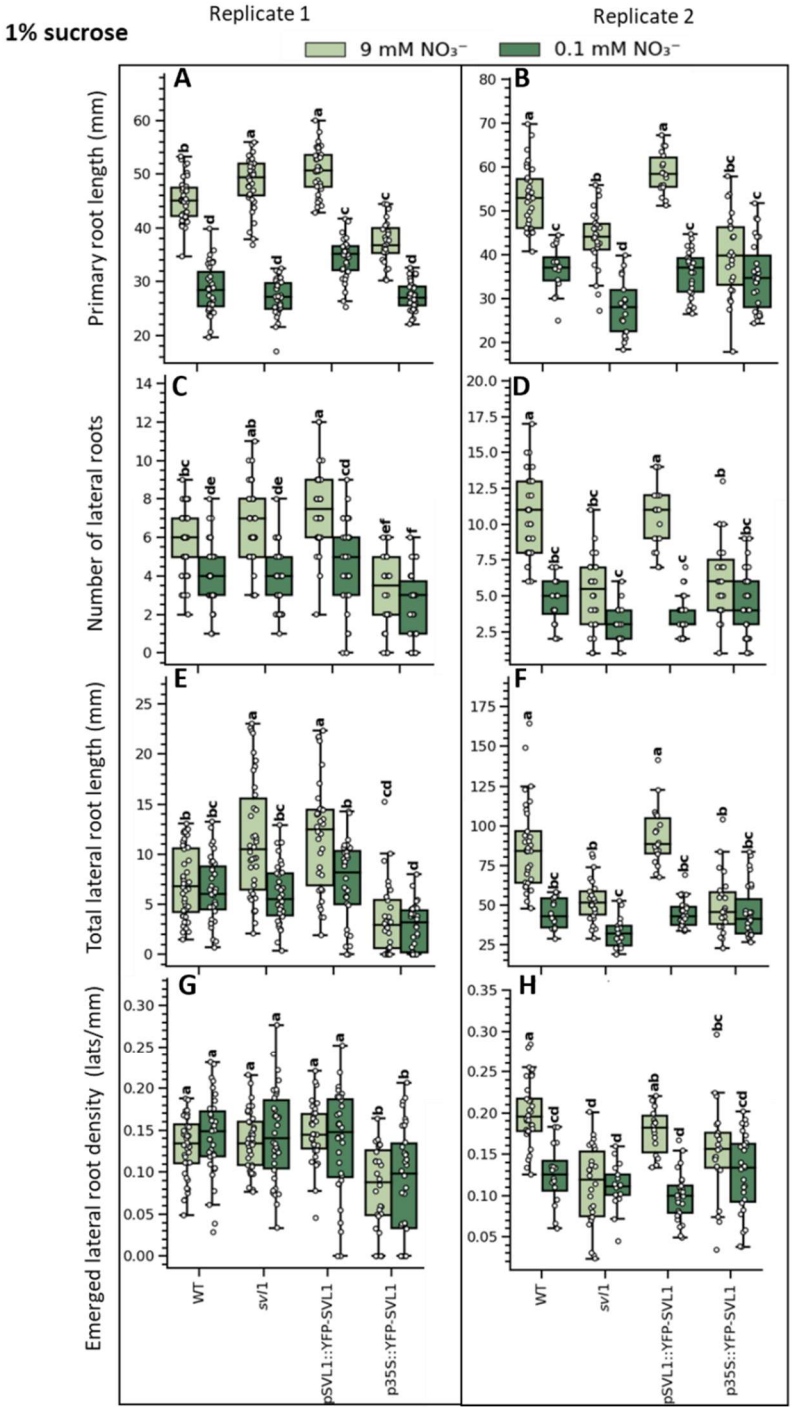

Figure 6.7 Primary and lateral root phenotyping of *svl1* mutant and transgenic SVL1 lines grown on either 9 mM nitrate or 0.1 mM nitrate with 1% sucrose. (A,B) Primary root length, (C,D) number of lateral roots, (E,F) total lateral root length, and (G,H) emerged lateral root density were measured 8 days post germination (dpg). Pairwise significance testing was performed by one-way ANOVA (Tukey post hoc test, $p < 0.05$, $N \geq 20$, bars that do not share a letter are significantly different). Data from 2 representative replicates are presented. A summary of phenotypes for all replicates is presented in Table 6-1.

Table 6-1 Summary of primary root length, lateral root number, density, and total length root phenotypes of WT, *svl1*, *pSVL1::YFP-SVL1*, *p35S::YFP-SVL1*, pdbg1 and *svll pdbg1*. Plants were grown on ATS based media. Phenotypes were determined at 7 days post germination. Statistical differences between lines were determined using ANOVA, Tukey post hoc ($p < 0.05$). Each symbol in the table refers to a different experimental replicate. In control media (9 mM nitrate), statistical differences between each line and WT are represented by an arrow indicating whether the line exhibited a phenotype larger (↑) or smaller (↓) or not different (–) relative to WT. In other media, arrows indicate whether the phenotype is larger, smaller or not different to the control media phenotype of that line.

Primary root length	0% sucrose 9 mM NO_3^-	0% sucrose 0.1 mM NO_3^-	1% sucrose 9 mM NO_3^-	1% sucrose 0.1 mM NO_3^-
WT		↓↓↓		↓↓↓
svl1	– – ↓	↓ – –	↑ ↑ ↓ ↓	– – ↓
pSVL1::YFP-SVL1	– ↓ –	– ↓ –	↑ ↓ –	↑ ↓ –
p35S::YFP-SVL1	↓ ↓ ↓	↓ ↓ –	↓ ↓ – ↓	– – ↓ –
pdbg1	– – ↓	↓ – –	↓ – – ↓	– – – –
svl1 pdbg1	– ↓ –	↓ – –	– – – –	– – – –
Lateral root number				
WT		– ↓ ↓		– ↓ ↓ ↓
svl1	– – ↓	↓ – –	– – – ↓	– – – –
pSVL1::YFP-SVL1	– ↓ –	– – –	– ↑ – –	– – –
p35S::YFP-SVL1	↓ ↓ ↓	↓ – –	↓ ↓ ↓ –	– ↓ – –
pdbg1	– – ↓	↓ – –	↓ – – ↓	– ↑ – ↓
svl1 pdbg1	– ↓ –	↓ – –	– – – –	– – – –
Total lateral root length				
WT		– ↓ ↓		– – ↓
svl1	– – ↓	– – –	↑ ↑ – ↓	– – – –
pSVL1::YFP-SVL1	– ↓ –	– – –	↑ – –	– – –
p35S::YFP-SVL1	↓ ↓ ↓	↓ – –	↓ ↓ – ↓	– ↓ – –
pdbg1	↑ – ↓	– – –	↑ ↓ – –	– – – –
svl1 pdbg1	– ↓ –	– – –	– ↑ – –	– – – –
Emerged lateral root density				
WT		↓ ↓ –		↓ – – ↓
svl1	– – ↓	– – –	– – – ↓	– – – –
pSVL1::YFP-SVL1	– – –	– – –	– – –	– – –
p35S::YFP-SVL1	↓ – ↓	↓ – –	↓ ↓ – ↓	– – – –
pdbg1	– – ↓	↑ – –	↓ – – –	– ↑ – –
svl1 pdbg1	– – –	↑ – –	– – – –	– – – –

6.2.5 *pSUC2::GFP* expression is reduced under low nitrate and unloading restricted in *svl1*.

Although differences in root growth are not clear when phenotyping the *svl1* mutant, the identification of SVL1 in the PD proteome suggests a possible involvement in the regulation of symplasmic transport. To test this, plants expressing the symplasmic reporter *pSUC2::GFP* were crossed into *svl1*. Plants expressing *pSUC2::GFP* in either a Col-0 (control) or *svl1* background were grown for 4 days on 9 mM or 0.1 mM nitrate ATS supplemented with 1% sucrose. Roots were counterstained with PI and imaged by confocal microscopy. Representative images (Figure 6.8) show GFP expression was reduced in 0.1 mM nitrate. Quantification of fluorescence in the stele region of the TZ was carried out showing that fluorescence in *pSUC2::GFP* (Col-0) is significantly higher in 9 mM nitrate (control) than 0.1 mM nitrate (Figure 6.8 B). As discussed in Chapter 4, min-max normalisation of fluorescence can control for differences in absolute expression of GFP to allow for comparisons of lateral fluorescence profiles. When comparing lateral root profiles quantified across the TZ, a high degree of overlap between Col-0 and *svl1* traces in 9 mM nitrate were observed suggesting no major differences in lateral diffusion (Figure 6.8 C). In 0.1 mM nitrate, expression levels of GFP are similar (Figure 6.8 B) and therefore normalisation was not necessary. There is a clear reduction in fluorescence towards the epidermis in *svl1* in 0.1 mM nitrate relative to Col-0 or *svl1* in 9mM nitrate suggesting a restriction in symplasmic unloading of GFP from the companion cells (where *pSUC2* is expressed) into the surrounding tissues (Figure 6.8 D). The results indicate that despite no consistency in the root length phenotype (Figure 6.7) unloading is reduced in the mutant when grown in 0.1mM nitrate and 1% sucrose.

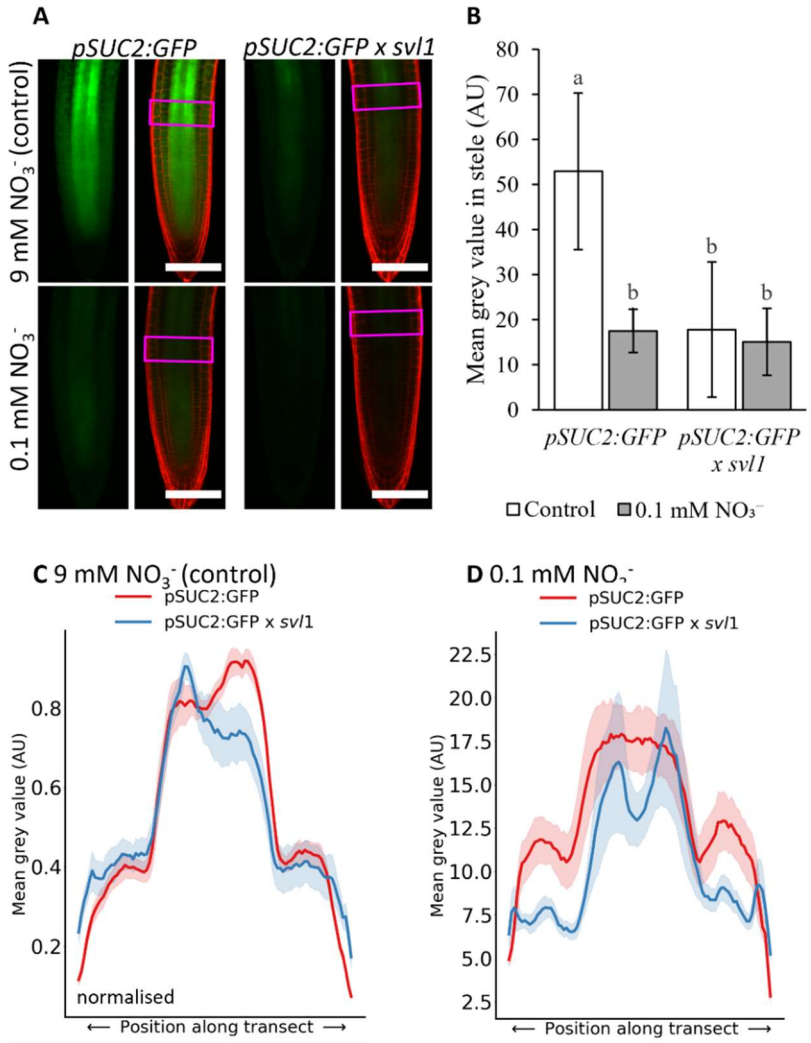

Figure 6.8 Expression of *pSUC2::GFP* is reduced in 0.1 mM nitrate and in the *svl1* background. Seeds expressing *pSUC2::GFP* in either a Col-0 or *svl1* background were grown on ATS control media (9mM nitrate) or 0.1 mM nitrate ATS media + 1% sucrose. Roots were counterstained with propidium iodide (PI) after 4 days post-germination and analysed by confocal microscopy. Images were sequentially collected at 561 nm (PI shown in red) and 488 nm (green: GFP). (A) Representative images; transects across the transition zone (TZ), highlighted by magenta boxes, were used to determine GFP fluorescence profiles using mean grey values. Scale bar = 100 µm. (B) Mean fluorescence in the stele of the TZ, calculated from the central 20% portion of the transects highlighted in A. Bars with differing letters are significantly different (ANOVA, Tukey post hoc, $p < 0.05$). (C) Lateral fluorescence profiles across the TZ in 9 mM nitrate; traces representing min-max normalised GFP fluorescence along the transect for N>6 plants (mean ± SE). (D) Lateral fluorescence profiles across the TZ in 0.1 mM nitrate; traces representing GFP fluorescence along the transect for N>6 plants (mean ± SE).

6.2.6 PDBG1 is co-regulated with SVL1 in the regulation of root growth and response to nitrate

SVL1 does not exhibit clear PD localisation but regulates symplasmic GFP trafficking in low nitrate. It is possible SVL1 acts by signalling or interacting with one or more PD components. ATTEDII provides pairwise gene expression correlation data on most genes in the *Arabidopsis* genome (Obayashi et al., 2018). A gene expression network shows potential interactions between *SVL1* and two PD-located proteins: *PDBG1*, a PD-located beta-1,3 glucanase and *PDCB1*, a callose binding domain (Figure 6.9). Like *SVL1*, *PDBG1* is expressed in the roots (Benitez-Alfonso et al., 2013). To test potential interactions between these proteins double mutant analysis was performed. *svl1* was crossed with *pdbg1* and root phenotypes were determined in the double mutant alongside WT and single *pdbg1*. Figure 6.10 and Figure 6.11 show the primary root length, lateral root number, total lateral root length, and emerged lateral root density for WT, *pdbg1,* and *svl1 pdbg1* in both control and low nitrate, and 0% and 1% sucrose. Primary root was either similar or shorter in *pdbg1* compared to WT when grown in 9 mM nitrate with 1% sucrose (Table 6-1). No significant differences are observed in primary root length between WT and *svl1 pdbg1* in either concentration of nitrate. Primary root length in 0.1 mM nitrate was significantly reduced in all genotypes in either sucrose treatment. Lateral root count of *pdbg1* was reduced relative to WT in 9 mM nitrate in 2 out of 4 replicates (coincident with primary root reduction). Regarding lateral root count in 9 mM nitrate the double mutant *svl1 pdbg1* behaves as WT. The same patterns as described for lateral root count are observed when analysing total length and density: results for *pdbg1* and *svl1 pdbg1* were not consistently different to WT under 9 mM nitrate. In 0.1 mM nitrate, *pdbg1* displays differences between replicates showing to have significantly more, fewer or similar lateral root counts to WT. Inconsistencies were also observed in lateral root length and density of *pdbg1*. The double mutant *svl1 pdbg1* did not consistently display different phenotype from WT under any treatment tested.

To summarise, SVL1 is co-expressed with PDBG1. The double mutant *svl1 pdbg1* does not show any consistent difference relative to WT between experimental replicates unlike the single mutants *svl1* and *pdbg1*.

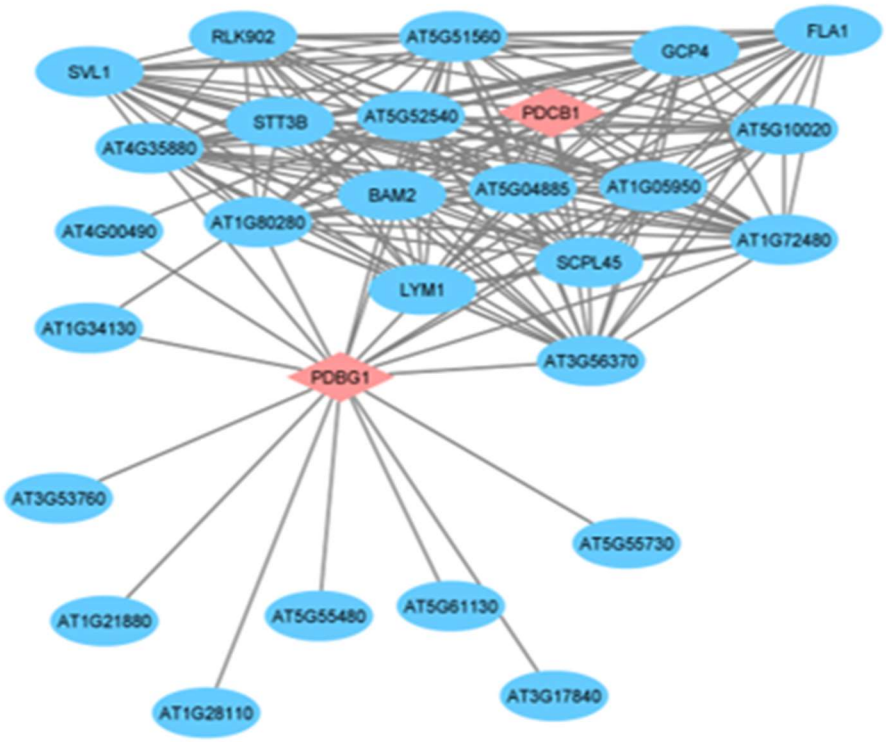

Figure 6.9 Network analysis indicates that *PDBG1* and *SVL1* expression is correlated. A gene list was generated by taking the top 20 most co-expressed genes for *PDBG1* in the ATTEDII database (Obayashi et al., 2018). An edge-node list was derived by determining pairwise correlations for each gene in the list using a custom R script which uses the ATTEDII as a lookup database. The edge-node list was analysed using Cytoscape 3.82. The layout of the network was established by removing self-loops and performing the 'perfuse force directed layout' function. Genes denoted by red diamonds are known PD proteins.

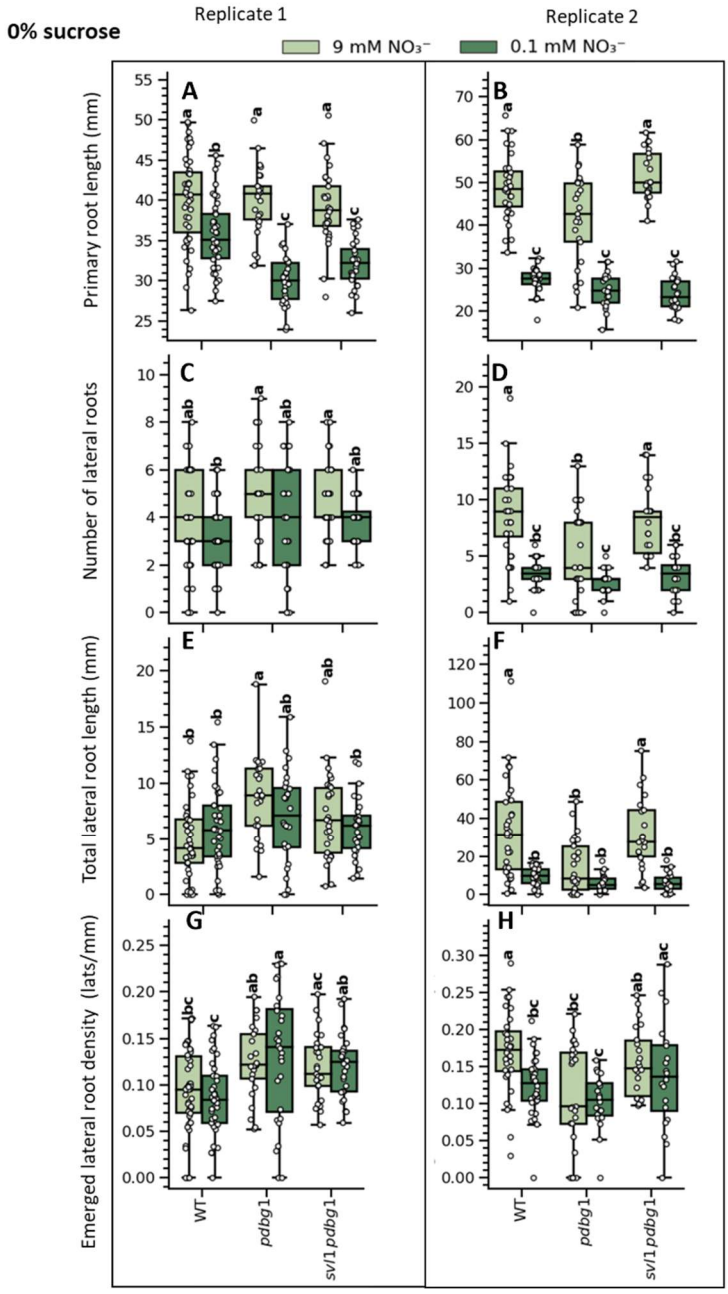

Figure 6.10 Primary and lateral root phenotyping of *pdbg1* and *svl1 pdbg1* relative to WT in 9 mM or 0.1 mM nitrate with 0% sucrose. Plants were grown on either 9 mM nitrate (unaltered ATS) or 0.1 mM nitrate (ATS-based) with 0% (w/v) sucrose. (A,B) Primary root length, (C,D) number of lateral roots, (E,F) total lateral root length, and (G,H) emerged lateral root density were measured 8 days post germination. Pairwise significance testing was performed by one-way ANOVA (Tukey post hoc test, $p<0.05$, $N\geq20$, bars that do not share a letter are significantly different). Data from 2 representative replicates are presented. A summary of phenotypes for all replicates is presented in Table 6-1.

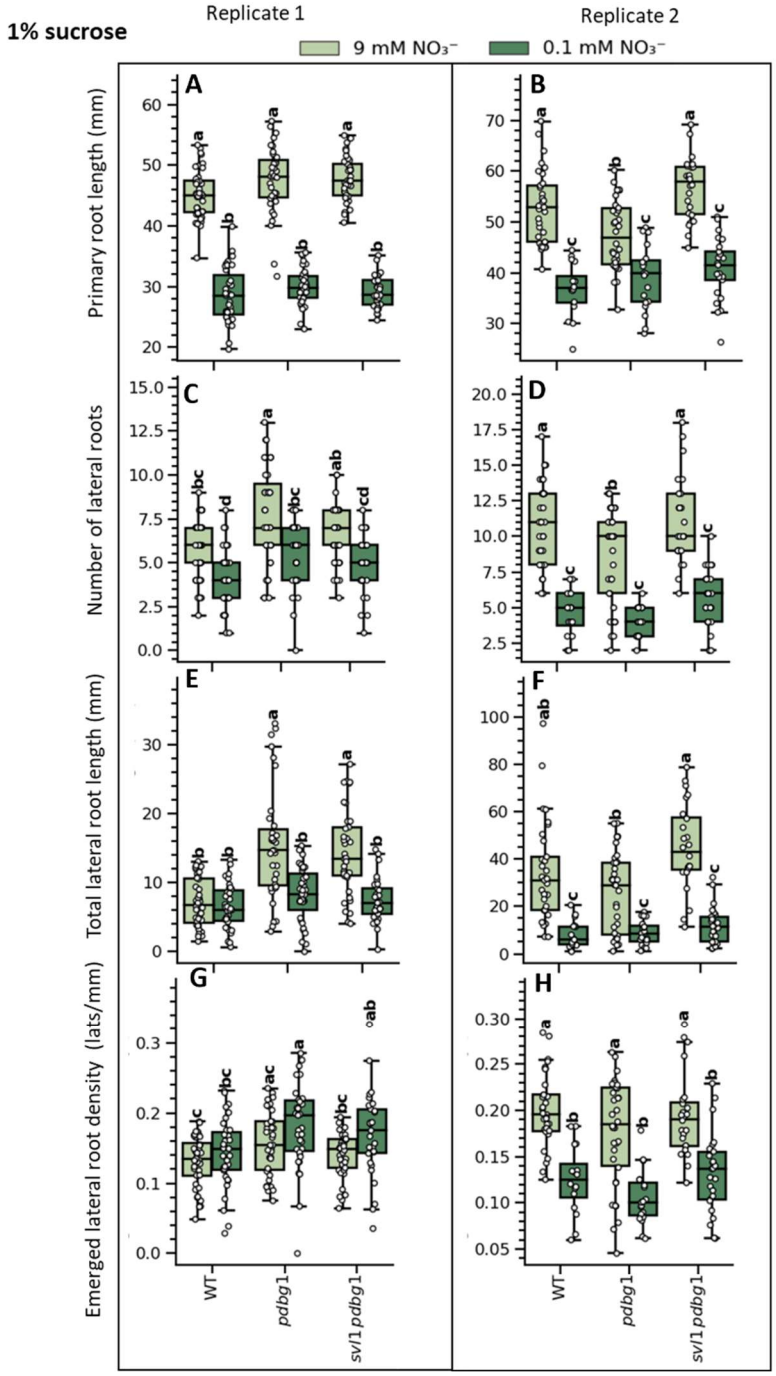

Figure 6.11 Primary and lateral root phenotyping of *pdbg1* and *svl1 pdbg1* relative to WT in 9 mM or 0.1 mM nitrate with 1% sucrose. Plants were grown on either 9 mM nitrate (unaltered ATS) or 0.1 mM nitrate (ATS-based) with 1% (w/v) sucrose. (A,B) Primary root length, (C,D) number of lateral roots, (E,F) total lateral root length, and (G,H) emerged lateral root density were measured 8 days post germination. Pairwise significance testing was performed by one-way ANOVA (Tukey post hoc test, $p<0.05$, $N\geq20$, bars that do not share a letter are significantly different). Data from 2 representative replicates are presented. A summary of phenotypes for all replicates is presented in Table 6-1.

6.2.7 SVL1 expression alters cell wall composition, and this is influenced by the expression of PDBG1

Levels of cellulose and pectin have been measured for *shv3svl1* when grown in the presence of sucrose but not the single *svl1* mutant (Hayashi et al., 2008; Yeats et al., 2016). A cell wall glycome analysis was performed on material derived from *svl1* and *p35S::YFP-SVL1* grown on 9 mM nitrate in ATS supplemented with 1% sucrose. Cell wall material from dissected roots was sequentially extracted with CDTA, KOH, and cellulase, liberating more recalcitrant cell wall material with every extraction. ELISAs were performed using monoclonal antibodies specific to cell wall epitopes. Wells subjected to the same treatment except for the addition of a primary antibody (blank) were used as a control and these showed low levels of background absorbance (Figure 6.12).

The full glycome profiling is not shown here but instead results with anti-callose (directly connected with PD regulation) and three antibodies with profiles that change in the different genotypes are presented. These antibodies are: LM5 (detects RGI pectins enriched in 1-4 beta galactan side chains), JIM7 (detects esterified HG pectins), and LM25 (detects xyloglucans). Anti-callose signal was low and no major differences were observed between WT and *svl1*. Callose content is slightly reduced in *p35S::YFP-SVL1* in the CDTA and KOH fraction although differences may not be significant (Figure 6.12). LM5 signal was strong in the CDTA fraction and the cellulase fraction whereas JIM7 signal is only detected in the CDTA fraction, consistent with the removal of esterified groups by KOH. In the CDTA fraction, both LM5 and JIM7 were strongly detected in *svl1* (+19.7%, +54.4% respectively) and reduced in *p35S::YFP-SVL1* (-15.8%, -62.4% respectively) relative to wildtype. Xyloglucans (LM25) were also detected in the CDTA and also in the KOH fraction and, as for LM5 and JIM7, increased in *svl1* (+28.5%) and were reduced (-42.1%) *p35S::YFP-SVL1* CDTA fraction.

The results suggest that pectin and xyloglucan are modified in roots by SVL1. To determine if this pattern is altered by interaction between SVL1 and PDBG1 (a modifier of callose), cell wall composition was analysed in roots dissected from *pdbg1* and *svl1 pdbg1* grown in the same conditions (Figure 6.13). Negative controls for *pdbg1* and *svl1 pdbg1* show low levels of background in all 3 fractions. There were no noticeable differences in callose signal between *pdbg1* and *svl1 pdbg1*. Interestingly, mean LM5 absorbance in the CDTA fraction (which increased in *svl1,* Figure 6.12) was lower than WT in both *pdbg1* and *svl1 pdbg1* (-50.2%, -29.6%, respectively). Mean JIM7 absorbance in the CDTA fraction was

higher in *pdbg1* relative to WT (+65.1%) but no differences were observed between *svl1 pdbg1* and WT. No major differences in LM25 absorbance are apparent between *pdbg1* and *svl1 pdbg1* with WT in any fraction (Figure 6.13).

To summarise, differences in pectin and xyloglucan composition were detected in root cell walls of *svl1* and SVL1 over-expressor. As with *svl1*, the PD mutant *pdbg1* also appears to have increased esterified pectins, but in the double mutant, *svl1 pdbg1*, these epitopes are similar to wildtype. In contrast to *svl1*, both *pdbg1* and *svl1 pdbg1* display reduced 1-4 beta galactan pectin. The results need to be confirmed by immuno-localisation studies, but it might suggest that introducing *pdbg1* mutation in the *svl1* background somewhat complements the *svl1* cell wall phenotype suggesting these proteins act in the same pathway.

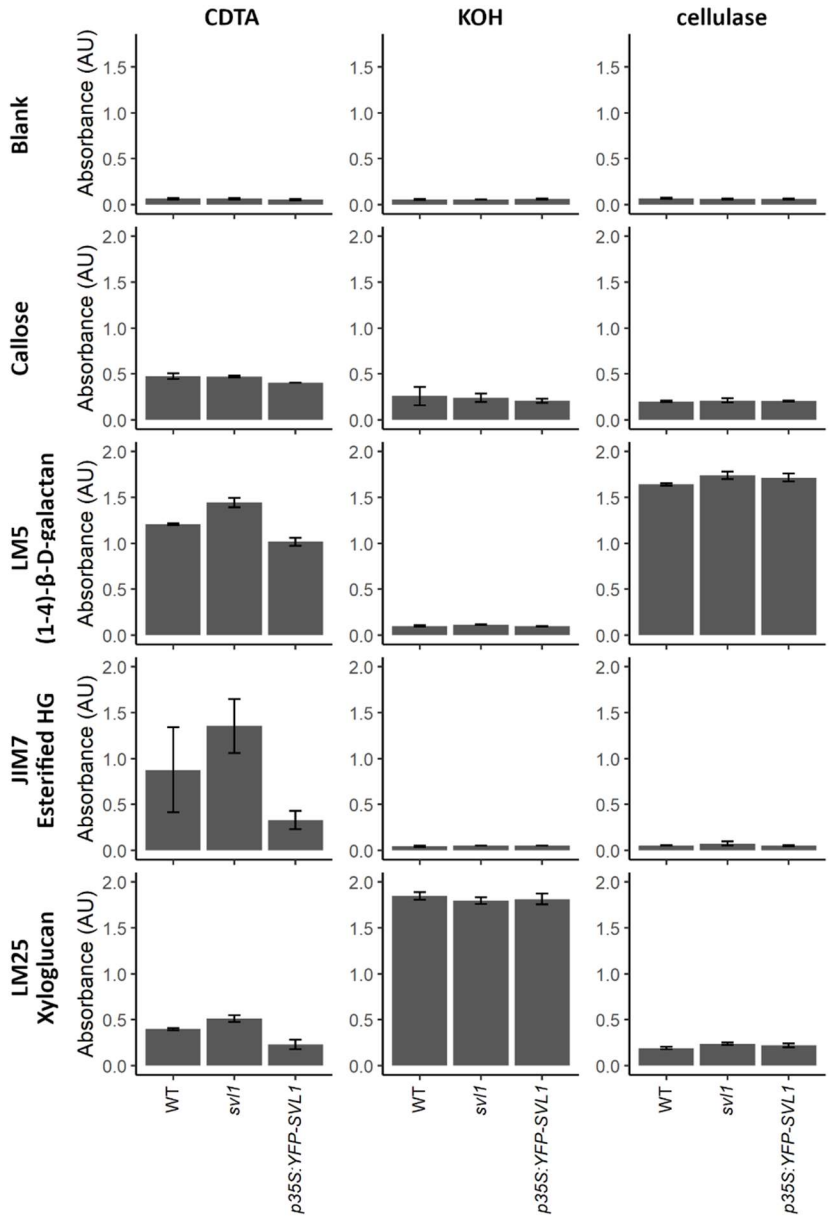

Figure 6.12 Knockout mutant *svl1* displayed increases in soluble pectins and xyloglucan in the root; a pattern that is reversed when *SVL1* is constitutively expressed. WT, *svl1* and plants expressing *p35S::YFP-SVL1* were grown on ATS with 1% (w/v) sucrose. 14 days post germination, roots from 3 biological replicates were freeze dried and cell walls were extracted as described in M&M to generate CDTA, KOH, and cellulase extracts. Extracts were analysed via ELISA-based glycome analysis with 2 technical replications. Shown here are a subset of primary antibodies used: blank (no primary antibody), anti-callose, pectin antibodies LM5 and JIM7, and xyloglucan mAb LM25. Bars represent the mean ELISA absorbance (± SD).

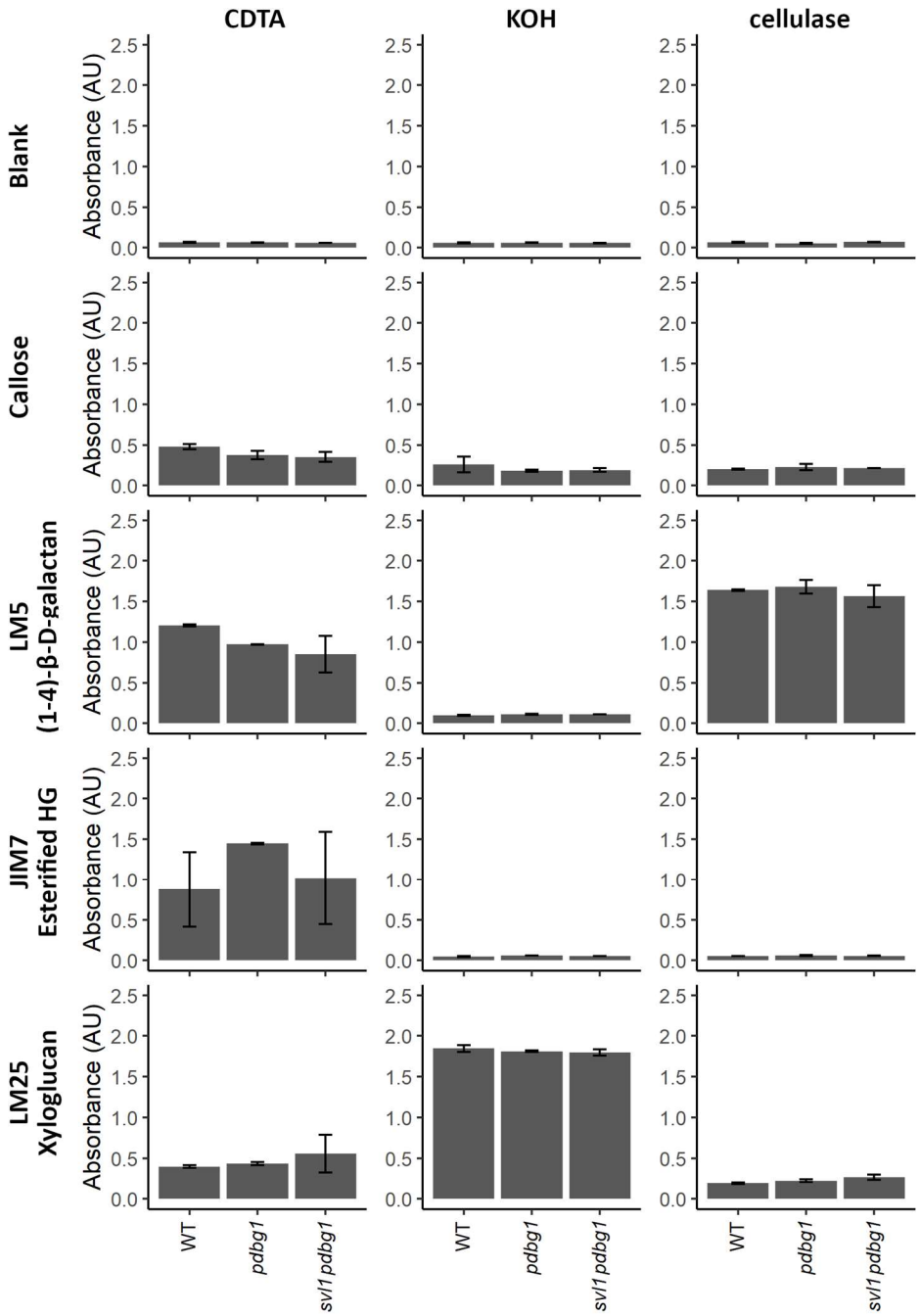

Figure 6.13 Knockout mutant cross *svl1 pdbg1* does not display any considerable changes in soluble pectins and xyloglucan in the root. WT, *pdbg1,* and *svl1 pdbg1* were grown on ATS with 1% (w/v) sucrose. 14 days post germination, roots from 3 biological replicates were freeze dried and cell wall were extracted as described in M&M to generate CDTA, KOH, and cellulase extracts. Extracts were analysed via ELISA-based glycome analysis with 2 technical replications. Shown here are a subset of primary antibodies used: blank (no primary antibody), anti-callose, pectin antibodies LM5 and JIM7, and xyloglucan mAb LM25. Bars represent the mean ELISA absorbance (± SD).

6.3 Discussion

6.3.1 SVL1 is a mobile mRNA that functions in the regulation of root growth in response to sucrose and nitrate conditions.

Changes in root system architecture in response to low nitrate correlates with changes in symplasmic transport of GFP in root tissues, as shown in chapter 4. To establish a link between the regulation of symplasmic transport and RSA in response to nitrate, the molecular factors underpinning this pathway must be identified and characterised. SVL1 was identified in the PD proteome and in the mobile transcriptome in response to low nitrate (Fernandez-Calvino et al., 2011; Thieme et al., 2015). Mutant analysis indicates this protein functions in signalling cell wall modifications (Hayashi et al., 2008) regulated by sucrose (Yeats et al., 2016). Histochemical analysis of *SVL1* promoter activity, presented here, shows strong expression in lateral and primary root meristems which is consistent with the hypothesis that SVL1 regulates RSA. There is some disparity between the data presented here and by Hayashi et al. (2008) who observed much greater promotor activity in shoots and vasculature. This is likely due to longer incubation times evidenced by what appears to be saturation of GUS in the data they presented. In the root meristem, distribution of GUS overlapped, to some degree, with YFP-SVL1 accumulation under the native promotor, although there is potential for RNA/protein mobility as protein accumulation spreads further than the promoter expression profile (Figure 6.2, Figure 6.4). In the future, YFP-SVL1 constructs can be made using cell type-specific promoters (such as p*SUC2*) to determine the domains in which SVL1 is cell-to-cell mobile. It is noteworthy that YFP-SVL1 distribution appears similar under native and constitutive promoters suggesting potential post-transcriptional regulation (Figure 6.1, Figure 6.2). Applying a proteosome inhibitor such as MG132 (Ahou et al., 2014) could test this hypothesis.

SVL1 promoter activity in the shoot was much weaker than in the root. This difference was not reflected in YFP-SVL1 protein accumulation in the shoot. The reason for this disparity is not clear and could be due to turnover rate of SVL1 transcripts or protein. Promoter activity was not strikingly different between sucrose treatments, but in primary root meristems GUS activity spread further across the meristem of plants grown in the presence of sucrose. In contrast, YFP-SVL1 accumulation in root tips was similar in the presence or absence of sucrose, demonstrating a disconnect between promotor activity and protein accumulation.

The indication that SVL1 may be involved in nitrate responses arose from the finding that scion-derived *SVL1* transcripts are able to translocate to rootstocks under N limitation, as determined by RNA-seq (Thieme et al., 2015). *SVL1* promotor expression was not different in 9 mM and 0.1 mM nitrate but there was considerable difference in YFP-SVL1 protein accumulation in roots between nitrate conditions particularly in the absence of sucrose (Figure 6.5 B,C). YFP-SVL1 accumulation was significantly higher in the stele of root tips grown in 0.1 mM nitrate relative to 9 mM nitrate. Transcript and/or protein mobility may account for the difference in protein accumulation as the work from our collaborator (Lei Yang) confirms that *SVL1* transcripts move from shoot to root during grafting. This transport is sufficient to allow for high levels of YFP-SVL1 to accumulate in the WT root stocks from YFP-SVL1-expressing scions (Figure 6.3). Detection of *SVL1* RNA in *svl1* roots suggests that the mRNA is mobile, but it does not shed light on whether the protein is also mobile. Dissecting such a question in the future could involve expressing SVL1 tagged with a trimeric GFP in specific tissues, or in the scion grafted into *svl1* rootstocks. If RNA mobility requires protein movement, no signal will be seen in the root as the the size of the trimeric GFP will restrict protein transport. If protein movement does not contribute, similar fluorescence due to mRNA movement will be detected in plants grafted with either SVL1-1XGFP or SVL1-3XGFP. SVL1 strongly localises to the cell periphery, however, on occasion, accumulation in a punctate pattern, reminiscent of PD localising proteins, was observed (Figure 6.1, Figure 6.2). This observation was not reproducible suggesting that SVL1 may transiently localise to PD, perhaps under certain, yet unknown, conditions or developmental stages. Transient PD localisation was described for other signalling proteins such as the receptor kinases QSK1 (Qian Shou kinase; AT3G02880) and IMK2 (inflorescence meristem kinase 2; AT3G51740), which accumulate at PD in response to treatment with salt or mannitol (Grison et al., 2019; Hunter et al., 2019). Since SVL1 attaches to the PM with a GPI anchor, it is very possible that, in certain conditions, this attachment is hydrolysed to release a soluble protein that accumulates and moves apoplastically to signal neighbouring tissues (Desnoyer and Palanivelu, 2020).

Nitrate- and exogenous sucrose- regulated expression and distribution of SVL1 in root meristems prompted the analysis of root phenotypes in these conditions. Regardless of sucrose treatment, primary root length was reduced at low nitrate conditions as reported in Chapter 4 and elsewhere (Araya et al., 2014). Ectopic expression of *SVL1* lead to severe reductions in primary root length, suggesting that this protein plays a role in the regulation of this phenotype. Primary root length of *svl1* was often found to be significantly

different from WT under nitrate replete and deplete conditions, but the direction of the difference (shorter or longer) was inconsistent between replicates. One explanation for this is that without SVL1, the roots lose a fine degree of control over root length regulation. SHV3 and SVL1 seems to display redundancy of function in previous research (Hayashi et al., 2008; Yeats et al., 2016), thus the response to nitrate in the double mutant should be analysed. How this fits into established mechanisms of responses to low nitrate is unclear. A significant signalling mechanism is the role NRT1.1 plays in sensing low nitrate and influencing auxin distribution to mediate downstream responses to low nitrate (Swarup et al., 2008; Krouk et al., 2010; Porco et al., 2016; Maghiaoui et al., 2020). There is no data that links SVL1 with any part of this signalling mechanism and further work should look establish links such as establishing whether *SVL1* expression is auxin- or NRT1.1-dependent.

6.3.2 SVL1 may interact with PDBG1 to target cell wall composition and regulate symplasmic unloading in the root meristem

Lack of strong evidence for PD-localisation does not rule out SVL1 from having a PD-related function. Chloroplastic and mitochondrial factors (such as GAT1) have been previously shown to alter PD transport, highlighting the broad number of signals/mechanisms affecting intercellular communication (Benitez-Alfonso et al., 2009; Burch-Smith and Zambryski, 2010). Supressed lateral movement of GFP expressed in the phloem companion cells (using the *SUC2* promoter) in root tips of *svl1* suggests a role for this protein in the regulation of PD. This may be associated with the root response to low nitrate as the restricted transport phenotype was only evident when plants were grown in this condition. The nitrate dependency correlates with SVL1 protein accumulation in the stele as the expression of YFP-SVL1 (driven by the native promoter) was found to increase under low nitrate (Figure 6.5). Given that *SVL1* transcripts are mobile under low nitrate (Thieme et al., 2015) there is also the possibility of *SVL1* distribution is being regulated by SVL1 activity in the regulation of PD.

Aside from the effect of *svl1* on symplasmic transport of GFP, the use of the *pSUC2::GFP* reporter system revealed a striking reduction of *pSUC2* expression in the *svl1* background (Figure 6.8). SUC2 is a phloem specific H+/sucrose symporter responsible for loading/unloading of sucrose in phloem companion cells (Truernit and Sauer, 1995). The influence of *svl1* on SUC2 expression is likely linked to the sucrose-dependent phenotypes described for *shv3svl1* (Yeats et al., 2016). Yeats et al. (2016) ascribes *shv3svl1* phenotypes

to hyper-accumulation of sucrose imported into roots from the media by SUC1. SUC1 and SUC2 share high sequence similarity and SUC1 expressed under a SUC2 promotor can complement *suc2* phenotypes (Sauer and Stolz, 1994; Wippel and Sauer, 2011). If the *svl1* single mutant is sufficient to hyperaccumulate sucrose, it is possible that the reduced expression of *SUC2* is due to negative feedback from increased sucrose levels.

SVL1 likely lacks GDPD activity thus it is proposed that the protein exerts its function by activating a signalling pathway that regulates cell wall composition (Yeats et al., 2016). A potential model of action for PD transport alteration by SVL1 may involve the regulation of callose deposits by modulating the activity of synthetic and/or degrading enzymes. This is plausible as a network analysis identifies PDBG1 and PDCB1 as SVL1 close neighbours suggesting co-regulated expression (Figure 6.9). Genetic interactions between SVL1 and this protein were tested using a double mutant analysis. No significantly altered root phenotypes were identified for *pdbg1* with the caveat that variations between experimental replicates were high (Table 6-1). However, there was far less inconsistency in the root phenotypes of *svl1 pdbg1* than in either of the single mutants, *pdbg1* or *svl1,* that were not significantly different from WT in most replicates. This is evidence of a genetic interaction between SVL1 and PDBG1 as the phenotypes of double mutant were not the same or additive of the phenotypes of the singles mutants.

Aside from the potential involvement of SVL1 in callose-dependent regulation via PDBG1, SVL1 may also modify PD by altering cell wall composition as reduced cellulose and pectin accumulation were described for *shv3svl1* (Hayashi et al., 2008; Yeats et al., 2016). Most differences between WT, *svl1,* and *p35S::YFP-SVL1* were observed in the cell wall CDTA soluble fraction. Specific pectin epitopes were found to be enriched in *svl1* and depleted in *p35S::YFP-SVL1*, including LM5 ((1-4)-β-D-galactan, neutral pectic side chains) and JIM7 (esterified HG) (Knox et al., 1990). Other mutants with altered cellulose production show increased levels of pectin including *trichome birefringence* (of unknown function) and *korrigan (kor*, involved in cellulose synthesis*)* (His et al., 2001; Bischoff et al., 2010). As with *svl1*, *kor* also displays higher levels of JIM7 epitope binding (His et al., 2001), suggesting a potential link between cellulose content and pectin esterification. The xyloglucan epitope LM25 (Pedersen et al., 2012) was also found enriched in the *svl1* CDTA fraction, but this finding not apparent in the monosaccharide analysis reported for *shv3svl1* (Yeats et al., 2016). Reduced LM5 and LM25 signal was observed in *p35S::YFP-SVL1* cell walls. Expressing the chickpea βI-Gal β-galactosidase (Moneo-Sánchez et al., 2020) had the same effect as ectopic SVL1 expression. The correlation between LM5 and LM25

epitope may be due to the known ability of pectin side chains to interact with xyloglucan (Cumming et al., 2005; Popper and Fry, 2008). It is possible that changes in the cellulose, pectin, and xyloglucan composition are directly causing the observed reduction in symplasmic transport in the root tips of *svll,* but very little is known about the influence of cell wall polysaccharides, other than callose, on PD function. It would be interesting to determine the symplasmic behaviour in mutants similarly displaying enrichment in these epitopes. It is also conceivable that differences in cellulose content and organisation, particularly around PD, could alter callose properties in the regulation of transport especially when considering that cellulose can interact with callose in vitro (Abou-Saleh et al., 2018).

Interestingly, cell wall analysis of *svll pdbg1* suggests an interaction between SVL1 and PDBG1 activity on cell walls. Despite being increased in both *pdbg1* and *svll* cell walls, the esterified HG epitope JIM7 do not appear different from WT in *svll pdbg1*. Similarly, LM5 and LM25 epitopes are not significantly affected in *svll pdbg1,* despite showing increased accumulation in *svll*. This suggests that the proposed coupling of LM5 and LM25 as seen in *svll*, *p35S::YFP-SVL1,* and elsewhere (Moneo-Sánchez et al., 2020) may be broken when PDBG1 activity is absent in *svll pdbg1*. This effect might be linked to PDBG1's effect on degrading callose. Callose accumulation in *pdbg1* might affect cellulose and, potentially, other polysaccharides leading to changes in cell wall structure (Abou-Saleh et al., 2018; Amsbury et al., 2018). The *svll* phenotype on cell walls might be, at least partly, linked to the activation of PDBG1, thus in its absence no modifications are observed. Tantalising evidence of a potential callose/pectin interaction is seen in HG deficient mutants, *glucuronate 4-epimerase 1* (*gae1*) and *gae6,* that display reduced callose deposition when challenged with *Botrytis cinerea* (Bethke et al., 2016). Callose-pectin interactions might also explain why *pdbg1* contains more esterified HG (JIM7).

In conclusion, there is no clear evidence of PD-localisation for SVL1 but this protein may promote symplasmic transport in the root under nitrate limiting conditions. The mechanism underlying the influence of SVL1 on symplasmic transport may be directly or indirectly linked to the suppression or remodelling of pectin and xyloglucan in the cell wall surrounding PD, or through modulating the activity of PDBG1 and/or other PD proteins. The cellulose content might be a secondary phenotype in *shv3svl1* (and *svll*), and instead sucrose accumulation might be the primary signal behind SVL1's effects on cell wall composition and symplasmic transport. The mechanism by which SVL1 affects cell walls, PD, and sucrose transport remains an open question.

Chapter 7 Discussion

7.1 Overview

Expanding our knowledge of how plants acquire and respond to nutrient availability and water stress has been highlighted as a step towards improving food security (Sharma et al., 2015). An important response to abiotic conditions in the soil is the modulation of root system architecture which can allow plants to effectively intercept resources whilst avoiding areas of the soil with suboptimal conditions such as high salt content (Li and Zhang, 2008; Dietrich et al., 2017; Ponce et al., 2017; Lombardi et al., 2021). PD proteins are known regulators of root morphology, demonstrated by the role PDLPs and PDBGs play in lateral root development via callose-dependent control of PD permeability (Benitez-Alfonso et al., 2013; Sager et al., 2020). There is an emerging body of work that is establishing a role for PD proteins and callose regulation in the regulation of responses to abiotic stresses such as low water or nutrient availability, high light, and high levels of NaCl or other toxic compounds (Piršelová et al., 2012; Müller et al., 2015; Grison et al., 2019; Hunter et al., 2019; Martínez-Barradas et al., 2019). In all these examples, only a small snapshot of the role PD play is understood and in no case do we have a complete mechanistic understanding of how or why PD are regulated. Efforts to elucidate the role PD play in specific responses are hampered by our restricted understanding of what factors associate with PD due in part to the technical constraints of PD proteomes (Brault et al., 2019; Johnston et al., 2022; Kirk et al., 2022). In this thesis PIP1, a bioinformatics tool, is presented that helps to identify PD proteins from proteomic data. Meta-transcriptomics of PD proteins was used to identify conditions that may involve regulation of PD and identify PD proteins involved in this regulation. Experiments were performed to explore the associations between abiotic conditions, root morphology and the regulation of PD.

7.2 Main findings

Plasmodesmata *In silico* Proteome 1 (PIP1) was developed to predict and rank candidate PD genes based on the frequency that protein orthologues are found in PD proteomes and whether they have features associated with known PD proteins. This tool can take proteomic data as an input from- and create *in silico* PD proteomes for-, a wide range of species. This approach was validated by using PIP1 to generate an *in silico* proteome for poplar which compared favourably with the experimentally determined poplar PD proteome reported by Leijon et al., (2018). The *in silico* proteome outputs of PIP1 were cross-referenced against a vast array of transcriptomic data to identify abiotic conditions

that cause changes in the expression of PD-related factors and, therefore, possibly in symplasmic connectivity. *Arabidopsis* candidate PD proteins were found to be differentially expressed under a wide range of abiotic conditions including cold, desiccation, drought, hypoxia, elevated NaCl, and low nitrate. Co-expression analysis revealed two clusters of genes with high correlation in gene expression that were statistically overrepresented in candidate genes and known PD genes. Genes in both clusters showed a high degree of differential expression under conditions relating to low water availability and elevated NaCl. Differentially expressed PD proteins under a given treatment may have a role in the regulation of responses to this condition.

Next, phenotypic analysis was carried out to validate abiotic conditions affecting root development and potentially PD transport. The specific abiotic conditions chosen for study are linked with low macronutrient availability (N, Pi, K^+), low water availability (exogenous PEG), and elevated NaCl as these conditions are likely to become more detrimental to global crop production due to the compounding effects of global warming and depletion of finite resources (Heffer and Prud'homme, 2016; Castrillo et al., 2017; D'Odorico et al., 2018; Rosa et al., 2020; Singh, 2021). Root morphology phenotypes were measured alongside changes in the movement of GFP using symplasmic reporters and confocal microscopy. It was discovered that symplasmic transport of GFP, driven by several different tissue-specific promotors, was altered in primary roots of plants when grown in low nitrate, low water availability, and elevated NaCl that correlated with reductions in primary root growth. To establish what PD factors could be involved in facilitating responses to osmotic challenge and elevated NaCl, transcriptomics of known and candidate PD proteins were interrogated. Gene expression of *PDCB4* was identified to respond positively to low water availability and elevated NaCl and was chosen as a target for study. Primary root length and lateral root frequency of CRISPR-Cas9 generated *pdcb4* mutants were less sensitive to osmotic stress and elevated NaCl. In primary root tips, this correlated with the preliminary finding of a reduction in callose induction in response to these treatments.

The purpose of altering symplasmic transport can be to alter the cell-to-cell transmission of signalling factors (Zhang et al., 2021a). SVL1 was viewed as a potential signalling factor linked with low N responses as its transcripts were found mobile under low N conditions (Thieme et al., 2015). SVL1 also had the potential to be a regulator of symplasmic transport as it had been identified in a PD proteome and had been reported to be related with regulating cell wall composition (Hayashi et al., 2008; Fernandez-Calvino et al., 2011; Yeats

et al., 2016). The effect of low nitrate and exogenous sucrose on protein accumulation and subcellular localisation were investigated via confocal imaging of YFP-tagged SVL1. SVL1-YFP was found to localise at the cell periphery in both the root and shoot. SLVl-YFP accumulation was promoted under low nitrate. A role for SVL1 in the regulation of root morphology, by phenotyping a *svl1* knock-out mutant and a line ectopically expressing SVL1 in response to varying nitrate and sucrose concentrations, was determined. Ectopic expression of SVL1 lead to reduced root length and lateral root proliferation but root phenotypes of *svl1* were unstable and varied highly from experiment to experiment. A potential role for SVL1 in regulating symplasmic transport was investigated by crossing *svl1* into the symplasmic reporter *pSUC2::GFP*. In the presence of sucrose, the movement of GFP from the phloem was reduced in the *svl1* background. Given the previous associations of SVL1 with cell wall composition, cell wall glycomes were constructed with cell walls extracted from *svl1* and plants ectopically expressing SVL1 using cell wall- specific antibodies. The cell wall glycome generated for *svl1* displayed increases in soluble pectins and xyloglucan in the root; a pattern that was reversed when *SVL1* was constitutively expressed. *SVL1* is co-expressed with *PDBG1*. A cross between *pdbg1* and *svl1* was made to test for an interaction between these factors for which a cell wall glycome was generated. These changes in pectin and xyloglucan determined in *svl1* appeared to be rescued in *svl1 pdbg1* for which the cell wall glycome did not appear to be noticeably different from WT.

<u>In summary the main findings of this thesis are:</u>

- PIP1 can be effectively used to identify *in silico* proteomes and conditions affecting their expression in species where experimental proteomes are not available.
- PD proteins have a pattern of co-expression that could be used to identify regulatory pathways and network interactions.
- Symplasmic communication plays a role in regulating root responses to low nitrate, reduced water available and elevated NaCl.
- Callose regulation by PDCB4 is a mechanism that mediates responses to osmotic and salinity challenge.
- Signalling mobile RNAs, such as SVL1, may regulate root growth and responses to nutrients by acting in the regulation of cell wall composition and symplasmic transport.

7.3 Discussion of Results

Central to this thesis has been the development of PIPI; a tool to generate and prioritise candidate PD proteins for a wide range of species using comparative proteomics (Kirk et al., 2022). During the compilation of this thesis and subsequent to the submission of Kirk et al. (2022), 3 new PD proteomes and a new bioinformatic technique have been developed that should be considered in the context of PIPI. Of the 3 new PD proteomes, 2 have been developed for *Physcomitrium patens* and 1 for *A. thaliana* (Gombos et al., 2022; Johnston et al., 2022). The *Arabidopsis* proteome published by Johnston et al. (2022) brings the total number of PD proteomes for this species to 3 which in future studies can be leveraged by PIPI to strengthen the predictive power of determining candidate PD proteins. This publication along with Gombos et al. (2022) have produced the first comprehensive PD proteomes for a non-flowering plant, *P. patens*. Bryophytes, which Physcomitrium is a member of, diverged from vascular plants approximately 445 million years ago (Morris et al., 2018), and, therefore, comparative proteomics between these PD proteomes and the current collection of PD proteomes could help to identify conserved PD factors in plants. 16 orthologous groups of proteins between *Arabidopsis* and *Physcomitrium* proteomes were identified demonstrating the evolutionary conservation of PD proteins (Johnston et al., 2022). This finding supports the use of PIPI to use PD proteomes from different species to generate an *in silico* PD proteome for a separate species. Future studies could use PIPI to determine whether there are other orthologous groups of proteins in common between *Physcomitrium* and the other PD proteomes published for *Arabidopsis*, poplar, and Nicotiana. This *Physcomitrium* PD proteome is a valuable missing link for PD proteomics as all the other comprehensive PD proteomic studies have been restricted to dicotyledonous angiosperms. This could be utilised to, for example, to identify PD proteins in vascular lineages not represented in in the current collection of PD proteomes such as monocots and gymnosperms.

Gombos et al. (2022) used a bioinformatic approach for PD protein classification that was distinct from that used in PIPI. The objective of their tool was to rank proteins within a PD proteome based on protein abundance and whether the proteins have features associated with their curated list of PD proteins. PIPI also categorises proteins based on whether they contain features associated with known PD genes. These approaches are

complementary as PIP1 can assimilate data from multiple sources to look for candidates in a wide range of species, whereas the approach taken by Gombos et al. (2022) is useful for drilling down into a single proteome to filter candidate genes from contaminants. The authors have also published their results to a web service that that will serve as a useful reference database for PD proteomic and localisation studies for the community. These comparative proteomics approaches, including PIP1, will continue to help identify PD proteins. As more PD proteins are discovered, the more this knowledge can be leveraged to identify other PD proteins (e.g. via identification of motifs highly correlated with PD function) and the responses that are controlled by them.

Another key goal of this thesis was to determine whether the regulation of symplasmic transport was a response to, or a regulator of, root morphological responses to abiotic conditions in the soil. Low availability of phosphate, water stress and elevated concentrations of sodium chloride and other salts are all abiotic conditions in the soil that have been linked with changes in PD or symplasmic transport (Schulz, 1995; Sivaguru et al., 2000; Müller et al., 2015; Grison et al., 2019; Hunter et al., 2019). Data presented in this thesis establish a new role for regulated PD transport in reducing symplasmic transport in response to low availability of nitrate. Further work is needed to determine whether the function of this response is to reduce movement of signalling factors, and if so, determine the identity of these factors. Work would then need to be done to establish whether these mobile factors are influencing root morphology under low nutrient and water conditions. Data presented in this thesis give fresh support to the premise that PD transport is regulated under osmotic stress and salt stress (Grison et al., 2019; Hunter et al., 2019). Furthermore, PDCB4 was established as a PD protein that is involved in regulating root morphological responses to osmotic stress and elevated salt. PDCB4 is 1 of 4 PD proteins shown to be directly linked with response to osmotic challenge and salt stress: the other 3 being the RLKs CRK2, QSK1 and IMK2 (Figure 7.1). CRK2 localises at PD in response to elevated Ca^{2+} induced under salt stress and enhances callose deposition (Hunter et al., 2019). Its effect on callose deposition may be linked to its *in vitro* ability to phosphorylate CALS1; a callose synthase linked with stress responses such as pathogen attack and wounding (Cui and Lee, 2016a). CRK2 also phosphorylates the RBOHD which is required to trigger ROS signalling (Kimura et al., 2020). The link between abiotic stress, ROS, and PD-localising RLKs extends further as light stress also leads to RBOHD-dependent ROS accumulation, which has been linked with PDLP1/5-dependent increase in symplasmic transport (Fichman et al., 2021). Like CRK2, QSK1 and IMK2 are RLKs that

can transiently localise at PD but in response to mannitol (Grison et al., 2019). Not much is known about the mechanistic function of these proteins including the identity of their targets. What is known is that QSK1 must be phosphorylated to re-localise at PD and knock-out *qsk1* has lower levels of PD callose.

The emerging picture is that osmotic stress and elevated salt lead to both reorganisation of RLKs at PD which likely trigger signalling cascades that lead to the accumulation of callose and reduced symplasmic transport. However, little is known about the downstream events that directly influence PD. PDCB4 is the only PD protein linked with responses to osmotic challenge/salt stress that is not an RLK. PDCB4 likely interacts with callose via its callose binding site (Simpson et al., 2009) and, therefore, could function downstream of CRK2, QSK1, IMK2, or PDLPs. Callose is known to regulate root morphology (Benitez-Alfonso et al., 2013; Sager et al., 2020) and, therefore, it is unsurprising that PD proteins are involved in specific responses to external stimuli that regulate root morphology. PDCB4 is not considered to have enzymatic activity and, therefore, the mode by which it influences callose accumulation is likely indirect by affecting the synthesis or degradation of callose (Amsbury et al., 2018). Preliminary evidence presented in this thesis is that PDCB4 promotes callose accumulation which could suggest that it is preventing degradation by PDBGs as previously hypothesised by Amsbury et al. (2018).Comparative proteomics and transcriptomics presented in this thesis showed that many known and candidate PD proteins are differentially expressed under both osmotic challenge and salt stress, and it is very likely that the true number of PD proteins is far larger than the 4 PD proteins currently known.

PD are emerging as important players in the regulation of responses to these conditions and it prudent to consider how such regulation could fit into the wider regulatory picture. The Organelle-Nucleus-PD (ONPS) model posited by Burch-Smith et al. (2011a) is a useful starting point as it links the critical roles retrograde signalling between chloroplast/mitochondria with the nucleus play in response to external stressors with those played by the regulation of symplasmic transport. The ONPS model is exemplified by *ISE1,* which is a mitochondrial gene, and *ISE2* and *GAT1,* which are chloroplastic genes. These genes were identified as PD-related factors from mutational screens for perturbed symplasmic transport due to changes in PD density or PD permeability (Benitez-Alfonso et al., 2009; Ganusova et al., 2020). ISE1/2 are RNA helicases, and it has been hypothesised that these genes, and others that control organelle gene expression, lead to changes in nuclear gene expression, including PD associated genes (Azim and Burch-Smith, 2020). A

central regulator of responses to salt stress and osmotic challenge is ABA (Kumar et al., 2019). The poplar ABA-insensitive mutant *abi1-1* is unable to form callose deposits at PD required to establish bud dormancy (Tylewicz et al., 2018). This finding suggests that ABA regulation works upstream from symplasmic transport regulation during establishment of bud dormancy. ABA is partially synthesised in the chloroplast and retrograde signalling between the chloroplast and nucleus has been shown to interact with ABA-dependent stomatal closure and seed germination (Tylewicz et al., 2018; Azim and Burch-Smith, 2020). The metabolome of lines with altered levels of callose were shown in this thesis to have distinct ABA levels from WT. This finding suggests that PD along with chloroplasts and the nucleus, regulate ABA levels. More work is required to understand the putative link between ONPS and ABA signalling, particularly in the context of responses to osmotic/elevated salt stress where data are lacking. It would be useful to understand whether the osmotic and salt stress induction of PDCB4 (and potentially CRK2, QSK1 and IMK2) is ABA dependent and, therefore, regulated by a potential ABA-dependent ONPS pathway.

There are at least two reasons why abiotic conditions in the root could influence symplasmic transport. The first could be linked to differences in source strength due to relative demands of the growing root meristem under different conditions. In this scenario, symplasmic transport could be tuned like a tap to control the flow of resources like sugars, amino acids, and water. The second could be to alter the transmission of non-cell autonomous signals such as phytohormones, peptides, and RNA. There is a precedent for this as Fe-dependent callose induction under Pi deficient conditions was found to reduced movement of SHR which correlated with reduced root apical meristem growth (Müller et al., 2015). Other mobile signals are linked with root responses to abiotic conditions in the root such as the production of CEPs in the root under low nitrogen that are transported to the shoot, perceived by CEP-receptors which trigger CEPD1 and CEPD2 to be transported to the root via the phloem where they activate N uptake (Ohkubo et al., 2017b; Ohkubo et al., 2021). It is possible that mobile mRNAs could also have a systemic signalling function (Thieme et al., 2015; Yang et al., 2019). The finding that SVL1 is also expressed strongly in root tissues, presented in this thesis and by Hayashi et al. (2008), could indicate that shoot derived *SVL1* transcripts boost local SVL1 translation in the root that encodes some status from the shoot (Figure 7.1).

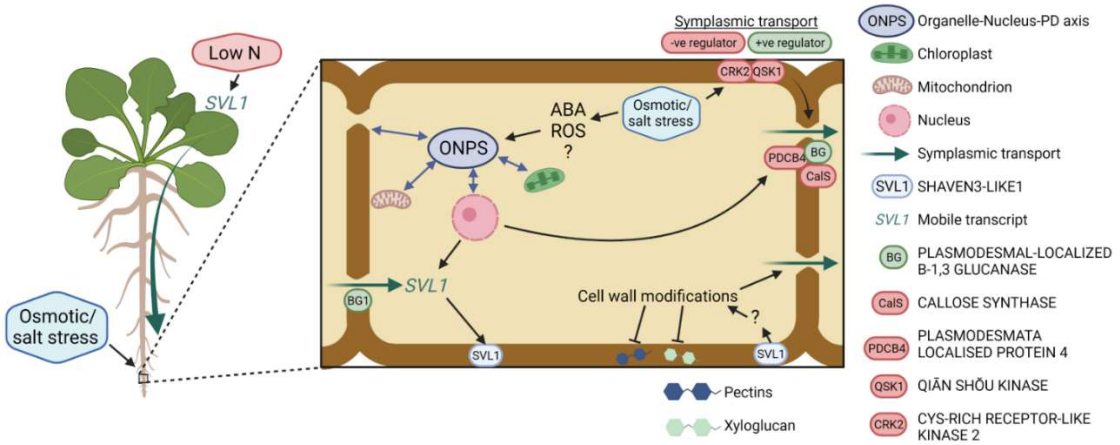

Figure 7.1 Schematic for the proposed pathway of PDCB4 and SVL1 regulation of root growth via regulation of symplasmic transport. (left) During low nitrogen (N) conditions, *SVL1* transcripts are transported from the shoot to the root symplasmically and (centre panel) translated into protein along with locally transcribed *SVL1*. The protein is secreted into the plasma membrane where it signals cell wall modifications including a reduction in pectins and xyloglucan, all required for cell growth. SVL1 also influence PD permeability and thereby the mobility of signalling factors. The mechanism of this signalling network is unknown but may involve interaction with PDBG1 which may facilitate its mobility through PD. In response to osmotic challenge and elevated salt, levels of abscisic acid (ABA) and reactive oxygen species (ROS) are elevated. ABA and ROS production may be regulated by feedback mechanisms that exist between the nucleus, PD, chloroplasts, and mitochondria that have been dubbed the organelle-nucleus-PD axis (ONPS). Under these conditions, the receptor kinases QSK1 and CRK2 localise at PD and trigger callose deposition by unknown mechanisms. Here, it is proposed that PDCB4 either antagonises PDBGs or promotes CALS activity to stimulate callose deposition. This callose deposition restricts symplasmic transport of root growth-promoting mobile signalling factors such as SHORTROOT. Proteins known to be involved in restricting and increasing symplasmic transport are coloured in red and green respectively. The diagram was created with BioRender.com.

Building on this hypothesis, the finding that over expression of SVL1 was found to restrict root length suggests SVL1 is a negative regulator of root growth. As reported here and elsewhere, low nitrate can restrict root growth (Araya et al., 2014). The purpose of such a response could be to reallocate N resources or in the reprogramming of root system architecture to better intercept nitrate in the soil elsewhere. Therefore, it is possible that the movement of SVL1 from the shoot to the root under low N is to trigger this response.

The instability in the root length phenotype in *svl1* suggests that there could be redundancy in SVL1 function, possibility from other members of the SVL3 family and that loss of SVL1 takes with it the fine control of root growth regulation. This instability in the root length phenotypes is not apparent in *svl1 pdbg1*. PDBG1, which is highly co-expressed with SVL1, is expressed in the stele and could act upstream of SVL1 and its partners. In this scenario, PDBG1 would act to increase PD transport and facilitate the movement of the mobile factors from the stele to the root tips to elicit their effects. SVL1 is a member of the glycerophosphodiester phosphodiesterase family but no enzymatic activity has been linked to this family and, instead, it is hypothesised it acts as a signalling factor (Hayashi et al., 2008; Yeats et al., 2016). Indications of the responses controlled by SVL1 are apparent in the cell wall gylcome which suggest that SVL1 negatively influences the levels of xyloglucan and pectin side chains of (1-4)-β-D-galactan and esterified homogalacturonan. Further support for PDBG1 playing an upstream role to SVL1 and its partners is that *svl1 pdbg1* cell wall glycome is contains WT levels of xyloglucan and pectic epitopes. The function of SVL1-dependent changes in cell wall composition could modulate root growth. Heterologous expression in *A. thaliana* of XTH from Capsicum annuum was found to reduce inhibition of root length to salt stress (Choi et al., 2011) demonstrating that remodelling of cell wall polysaccharides can control root growth responses. Alternatively, the putative role SVL1 in cell wall composition could underly the reduced symplasmic transport observed in *svl1*. If SVL1 is positively regulating symplasmic transport in the root, it may work antagonistically to the reduction in symplasmic transport created under low nitrate conditions. If so, SVL1 mobility could lead to a positive feedback mechanism to increase PD transport under conditions that would otherwise restrict symplasmic connectivity. The relationship between symplasmic transport and SVL1 is speculative at this time and more work is required to understand the significance of SVL1 mobility.

7.4 Conclusion and future perspectives

In conclusion, we have only begun to scratch the surface of understanding what factors are involved in facilitating PD development and function. We know even less about how these factors coordinate with one another to effect changes in PD permeability to control symplasmic transport. New tools and techniques such as PIPI are helping to unravel the mysteries of these gatekeepers of the symplasmic pathway. This thesis contributes to the growing body of work that evidences the role PD play in regulating root responses to abiotic conditions. In time, it is hoped we can garner a deep understanding of how and why PD are regulated under abiotic conditions in the soil. Eventually, it may be possible to leverage this knowledge to target PD as a strategy to improve root development and adaptive responses in adverse environments. The following are questions that arise from this thesis:

- What insights can be gained from leveraging newly available PD proteomes with PIPI? Can we identify better PD candidate proteins and circumstances where these proteins function?
- Is the underlying mechanism for reduced symplasmic transport in roots grown under low nitrate and low water conditions related to callose homeostasis? What PD proteins control this phenomenon?
- What controls the differential expression of *PDCB4* under osmotic/elevated salt stress? What other factors facilitate the role PDCB4 plays in callose accumulation in response to osmotic/elevated salt stress?
- What is the reason for regulation of symplasmic transport in response to osmotic challenge, elevated salt and low nitrate conditions? Are these changes to regulate the movement of specific signalling factors and if so, which ones?
- Can targeting specific PD factors be used to improve root morphological responses to abiotic conditions in the soil?

Bibliography

Abel, S. 2011. Phosphate sensing in root development. *Current Opinion in Plant Biology.* **14**(3), pp.303-309.

Abou-Saleh, R.H., Hernandez-Gomez, M.C., Amsbury, S., Paniagua, C., Bourdon, M., Miyashima, S., Helariutta, Y., Fuller, M., Budtova, T. and Connell, S.D. 2018. Interactions between callose and cellulose revealed through the analysis of biopolymer mixtures. *Nature Communications.* **9**(1), pp.1-13.

Ahou, A., Martignago, D., Alabdallah, O., Tavazza, R., Stano, P., Macone, A., Pivato, M., Masi, A., Rambla, J.L. and Vera-Sirera, F. 2014. A plant spermine oxidase/dehydrogenase regulated by the proteasome and polyamines. *Journal of Experimental Botany.* **65**(6), pp.1585-1603.

Aimanianda, V., Simenel, C., Garnaud, C., Clavaud, C., Tada, R., Barbin, L., Mouyna, I., Heddergott, C., Popolo, L. and Ohya, Y. 2017. The dual activity responsible for the elongation and branching of β-(1, 3)-glucan in the fungal cell wall. *American Society for Microbiology.* **8**(3), pp.e00619-00617.

Al-Ghazi, Y., Muller, B., Pinloche, S., Tranbarger, T., Nacry, P., Rossignol, M., Tardieu, F. and Doumas, P. 2003. Temporal responses of *Arabidopsis* root architecture to phosphate starvation: evidence for the involvement of auxin signalling. *Plant, Cell & Environment.* **26**(7), pp.1053-1066.

Alemán, F., Nieves-Cordones, M., Martínez, V. and Rubio, F. 2011. Root K+ acquisition in plants: the *Arabidopsis* thaliana model. *Plant and Cell Physiology.* **52**(9), pp.1603-1612.

Ali, A., Raddatz, N., Pardo, J.M. and Yun, D.J. 2021. HKT sodium and potassium transporters in *Arabidopsis* thaliana and related halophyte species. *Physiologia Plantarum.* **171**(4), pp.546-558.

Aliaga-Franco, N., Zhang, C., Presa, S., Srivastava, A.K., Granell, A., Alabadí, D., Sadanandom, A., Blázquez, M.A. and Minguet, E.G. 2019. Identification of Transgene-Free CRISPR-Edited Plants of Rice, Tomato, and *Arabidopsis* by Monitoring DsRED Fluorescence in Dry Seeds. *Frontiers in Plant Science.* **10**, p1150.

Almagro Armenteros, J.J., Tsirigos, K.D., Sønderby, C.K., Petersen, T.N., Winther, O., Brunak, S., Von Heijne, G. and Nielsen, H. 2019. SignalP 5.0 improves signal peptide predictions using deep neural networks. *Nature Biotechnology.* **37**(4), pp.420-423.

Amsbury, S., Kirk, P. and Benitez-Alfonso, Y. 2018. Emerging models on the regulation of intercellular transport by plasmodesmata-associated callose. *Journal of Experimental Botany.* **69**(1), pp.105-115.

AQUASTAT. 2021. AQUASTAT Core Database, Food and Agriculture Organization of the United Nations. [Online]. [Accessed 01/06/2021].

Araya, T., Miyamoto, M., Wibowo, J., Suzuki, A., Kojima, S., Tsuchiya, Y.N., Sawa, S., Fukuda, H., Von Wirén, N. and Takahashi, H. 2014. CLE-CLAVATA1 peptide-receptor signaling module regulates the expansion of plant root systems in a nitrogen-dependent manner. *Proceedings of the National Academy of Sciences.* **111**(5), pp.2029-2034.

Augstein, F. and Carlsbecker, A. 2018. Getting to the roots: A developmental genetic view of root anatomy and function from *Arabidopsis* to lycophytes. *Frontiers in Plant Science.* **9**, p1410.

Azevedo, C. and Saiardi, A. 2017. Eukaryotic phosphate homeostasis: the inositol pyrophosphate perspective. *Trends in Biochemical Sciences.* **42**(3), pp.219-231.

Azim, M.F. and Burch-Smith, T.M. 2020. Organelles-nucleus-plasmodesmata signaling (ONPS): an update on its roles in plant physiology, metabolism and stress responses. *Current Opinion in Plant Biology.* **58**, pp.48-59.

Balazadeh, S., Schildhauer, J., Araújo, W.L., Munné-Bosch, S., Fernie, A.R., Proost, S., Humbeck, K. and Mueller-Roeber, B. 2014. Reversal of senescence by N resupply to N-starved *Arabidopsis* thaliana: transcriptomic and metabolomic consequences. *Journal of Experimental Botany.* **65**(14), pp.3975-3992.

Balparda, M., Armas, A.M., Estavillo, G.M., Roschzttardtz, H., Pagani, M.A. and Gomez-Casati, D.F. 2020. The PAP/SAL1 retrograde signaling pathway is involved in iron homeostasis. *Plant molecular biology.* **102**(3), pp.323-337.

Barton, D.A., Cole, L., Collings, D.A., Liu, D.Y., Smith, P.M., Day, D.A. and Overall, R.L. 2011. Cell-to-cell transport via the lumen of the endoplasmic reticulum. *The Plant Journal.* **66**(5), pp.806-817.

Bayer, E., Thomas, C. and Maule, A. 2008. Symplastic domains in the *Arabidopsis* shoot apical meristem correlate with PDLP1 expression patterns. *Plant Signaling & Behavior.* **3**(10), pp.853-855.

Benitez-Alfonso, Y. 2019. The Role of Abscisic Acid in the Regulation of Plasmodesmata and Symplastic Intercellular Transport. *Plant and Cell Physiology.* **60**(4), pp.713-714.

Benitez-Alfonso, Y., Cilia, M., Roman, A.S., Thomas, C., Maule, A., Hearn, S. and Jackson, D. 2009. Control of *Arabidopsis* meristem development by thioredoxin-dependent regulation of intercellular transport. *Proceedings of the National Academy of Sciences.* **106**(9), pp.3615-3620.

Benitez-Alfonso, Y., Faulkner, C., Pendle, A., Miyashima, S., Helariutta, Y. and Maule, A. 2013. Symplastic intercellular connectivity regulates lateral root patterning. *Developmental cell.* **26**(2), pp.136-147.

Berckmans, B., Kirschner, G., Gerlitz, N., Stadler, R. and Simon, R. 2020. CLE40 Signaling Regulates Root Stem Cell Fate. *Plant Physiology.* **182**(4), pp.1776-1792.

Bertolino, L.T., Caine, R.S. and Gray, J.E. 2019. Impact of stomatal density and morphology on water-use efficiency in a changing world. *Frontiers in Plant Science.* **10**, p225.

Bethke, G., Thao, A., Xiong, G., Li, B., Soltis, N.E., Hatsugai, N., Hillmer, R.A., Katagiri, F., Kliebenstein, D.J. and Pauly, M. 2016. Pectin biosynthesis is critical for cell wall integrity and immunity in *Arabidopsis* thaliana. *The Plant Cell.* **28**(2), pp.537-556.

Bhalerao, R.P., Eklöf, J., Ljung, K., Marchant, A., Bennett, M. and Sandberg, G. 2002. Shoot-derived auxin is essential for early lateral root emergence in *Arabidopsis* seedlings. *The Plant Journal.* **29**(3), pp.325-332.

Bhaskara, G.B., Nguyen, T.T. and Verslues, P.E. 2012. Unique drought resistance functions of the highly ABA-induced clade A protein phosphatase 2Cs. *Plant Physiology.* **160**(1), pp.379-395.

Bhosale, R., Giri, J., Pandey, B.K., Giehl, R.F.H., Hartmann, A., Traini, R., Truskina, J., Leftley, N., Hanlon, M., Swarup, K., Rashed, A., Voß, U., Alonso, J., Stepanova, A., Yun, J., Ljung, K., Brown, K.M., Lynch, J.P., Dolan, L., Vernoux, T., Bishopp, A., Wells, D., Von Wirén, N., Bennett, M.J. and Swarup, R. 2018. A mechanistic framework for auxin dependent *Arabidopsis* root hair elongation to low external phosphate. *Nature Communications.* **9**(1), pp.1-9.

Bischoff, V., Nita, S., Neumetzler, L., Schindelasch, D., Urbain, A., Eshed, R., Persson, S., Delmer, D. and Scheible, W.-R. 2010. TRICHOME BIREFRINGENCE and Its Homolog AT5G01360 Encode Plant-Specific DUF231 Proteins Required for Cellulose Biosynthesis in *Arabidopsis*. *Plant Physiology.* **153**(2), pp.590-602.

Bishopp, A., Lehesranta, S., Vatén, A., Help, H., El-Showk, S., Scheres, B., Helariutta, K., Mähönen, A.P., Sakakibara, H. and Helariutta, Y. 2011. Phloem-transported cytokinin regulates polar auxin transport and maintains vascular pattern in the root meristem. *Current Biology.* **21**(11), pp.927-932.

Blum, A. and Tuberosa, R. 2018. Dehydration survival of crop plants and its measurement. *Journal of Experimental Botany.* **69**(5), pp.975-981.

Bonnemain, J.L. 1991. Recent advances in phloem transport and assimilate compartmentation=. In: *International Conference on Phloem Transport and Assimilate Compartmentation 1990: Charente, France)*: Ouest editions.

Bonser, A.M., Lynch, J. and Snapp, S. 1996. Effect of phosphorus deficiency on growth angle of basal roots in Phaseolus vulgaris. *New Phytologist.* **132**(2), pp.281-288.

Brauer, E.K., Ahsan, N., Dale, R., Kato, N., Coluccio, A.E., Piñeros, M.A., Kochian, L.V., Thelen, J.J. and Popescu, S.C. 2016. The Raf-like kinase ILK1 and the high affinity K+ transporter HAK5 are required for innate immunity and abiotic stress response. *Plant Physiology.* **171**(2), pp.1470-1484.

Brault, M.L., Petit, J.D., Immel, F., Nicolas, W.J., Glavier, M., Brocard, L., Gaston, A., Fouché, M., Hawkins, T.J., Crowet, J.M., Grison, M.S., Germain, V., Rocher,

M., Kraner, M., Alva, V., Claverol, S., Paterlini, A., Helariutta, Y., Deleu, M., Lins, L., Tilsner, J. and Bayer, E.M. 2019. Multiple C2 domains and transmembrane region proteins (MCTP s) tether membranes at plasmodesmata. *EMBO reports.* **20**(8), pe47182.

Brestic, M., Cornic, G., Freyer, M. and Baker, N. 1995. Does photorespiration protect the photosynthetic apparatus in french bean leaves from photoinhibition during drought stress? *Planta.* **196**(3).

Brunkard, J.O., Xu, M., Scarpin, M.R., Chatterjee, S., Shemyakina, E.A., Goodman, H.M. and Zambryski, P. 2020. TOR dynamically regulates plant cell-cell transport. *Proceedings of the National Academy of Sciences.* **117**(9), pp.5049-5058.

Brunkard, J.O. and Zambryski, P. 2019. Plant Cell-Cell Transport via Plasmodesmata Is Regulated by Light and the Circadian Clock. *Plant Physiology.* **181**(4), pp.1459-1467.

Brunoud, G., Wells, D.M., Oliva, M., Larrieu, A., Mirabet, V., Burrow, A.H., Beeckman, T., Kepinski, S., Traas, J. and Bennett, M.J. 2012. A novel sensor to map auxin response and distribution at high spatio-temporal resolution. *Nature.* **482**(7383), pp.103-106.

Buhtz, A., Pieritz, J., Springer, F. and Kehr, J. 2010. Phloem small RNAs, nutrient stress responses, and systemic mobility. *BMC plant biology.* **10**(1), pp.1-13.

Buhtz, A., Springer, F., Chappell, L., Baulcombe, D.C. and Kehr, J. 2008. Identification and characterization of small RNAs from the phloem of Brassica napus. *The Plant Journal.* **53**(5), pp.739-749.

Burch-Smith, T.M., Brunkard, J.O., Choi, Y.G. and Zambryski, P.C. 2011a. Organelle–nucleus cross-talk regulates plant intercellular communication via plasmodesmata. *Proceedings of the National Academy of Sciences.* **108**(51), pp.E1451-E1460.

Burch-Smith, T.M., Stonebloom, S., Xu, M. and Zambryski, P.C. 2011b. Plasmodesmata during development: re-examination of the importance of primary, secondary, and branched plasmodesmata structure versus function. *Protoplasma.* **248**(1), pp.61-74.

Burch-Smith, T.M. and Zambryski, P.C. 2010. Loss of INCREASED SIZE EXCLUSION LIMIT (ISE)1 or ISE2 increases the formation of secondary plasmodesmata. *Current Biology.* **20**(11), pp.989-993.

Caillaud, M.C., Wirthmueller, L., Sklenar, J., Findlay, K., Piquerez, S.J., Jones, A.M., Robatzek, S., Jones, J.D. and Faulkner, C. 2014. The plasmodesmal protein PDLP1 localises to haustoria-associated membranes during downy mildew infection and regulates callose deposition. *PLOS Pathogens.* **10**(10), pe1004496.

Caine, R.S., Yin, X., Sloan, J., Harrison, E.L., Mohammed, U., Fulton, T., Biswal, A.K., Dionora, J., Chater, C.C., Coe, R.A., Bandyopadhyay, A., Murchie, E.H., Swarup, R., Quick, W.P. and Gray, J.E. 2019. Rice with reduced stomatal density conserves water and has improved drought tolerance under future climate conditions. *New Phytologist.* **221**(1), pp.371-384.

Calderan-Rodrigues, M.J., Guimarães Fonseca, J., De Moraes, F.E., Vaz Setem, L., Carmanhanis Begossi, A. and Labate, C.A. 2019. Plant Cell Wall Proteomics: A Focus on Monocot Species, Brachypodium distachyon, Saccharum spp. and Oryza sativa. *International Journal of Molecular Sciences.* **20**(8), p1975.

Carlsbecker, A., Lee, J.-Y., Roberts, C.J., Dettmer, J., Lehesranta, S., Zhou, J., Lindgren, O., Moreno-Risueno, M.A., Vatén, A. and Thitamadee, S. 2010. Cell signalling by microRNA165/6 directs gene dose-dependent root cell fate. *Nature.* **465**(7296), pp.316-321.

Carvalho, B.S. and Irizarry, R.A. 2010. A framework for oligonucleotide microarray preprocessing. *Bioinformatics.* **26**(19), pp.2363-2367.

Casero, P. and Knox, J. 1995. The monoclonal antibody JIM5 indicates patterns of pectin deposition in relation to pit fields at the plasma-membrane-face of tomato pericarp cell walls. *Protoplasma.* **188**(1-2), pp.133-137.

Castrillo, G., Teixeira, P.J.P.L., Paredes, S.H., Law, T.F., de Lorenzo, L., Feltcher, M.E., Finkel, O.M., Breakfield, N.W., Mieczkowski, P. and Jones, C.D. 2017. Root microbiota drive direct integration of phosphate stress and immunity. *Nature.* **543**(7646), pp.513-518.

Cavalier, D.M., Lerouxel, O., Neumetzler, L., Yamauchi, K., Reinecke, A., Freshour, G., Zabotina, O.A., Hahn, M.G., Burgert, I. and Pauly, M. 2008. Disrupting two *Arabidopsis* thaliana xylosyltransferase genes results in plants deficient in xyloglucan, a major primary cell wall component. *The Plant Cell.* **20**(6), pp.1519-1537.

Cerri, M.R., Frances, L., Laloum, T., Auriac, M.-C., Niebel, A., Oldroyd, G.E., Barker, D.G., Fournier, J. and de Carvalho-Niebel, F. 2012. Medicago truncatula ERN transcription factors: regulatory interplay with NSP1/NSP2 GRAS factors and expression dynamics throughout rhizobial infection. *Plant Physiology.* **160**(4), pp.2155-2172.

Chandna, R., Azooz, M. and Ahmad, P. 2013. Recent advances of metabolomics to reveal plant response during salt stress. *Salt Stress in Plants.* pp.1-14.

Chapman, K., Taleski, M., Ogilvie, H.A., Imin, N. and Djordjevic, M.A. 2019. CEP–CEPR1 signalling inhibits the sucrose-dependent enhancement of lateral root growth. *Journal of Experimental Botany.* **70**(15), pp.3955-3967.

Chen, J., Liu, W., Liu, C.-M., Li, T., Liang, R.-H. and Luo, S.-J. 2015. Pectin modifications: a review. *Critical reviews in food science and nutrition.* **55**(12), pp.1684-1698.

Chen, L.-Q., Qu, X.-Q., Hou, B.-H., Sosso, D., Osorio, S., Fernie, A.R. and Frommer, W.B. 2012. Sucrose efflux mediated by SWEET proteins as a key step for phloem transport. *Science.* **335**(6065), pp.207-211.

Chen, Q.-F., Xiao, S. and Chye, M.-L. 2008. Overexpression of the *Arabidopsis* 10-kilodalton acyl-coenzyme A-binding protein ACBP6 enhances freezing tolerance. *Plant Physiology.* **148**(1), pp.304-315.

Chen, X.-Y., Liu, L., Lee, E., Han, X., Rim, Y., Chu, H., Kim, S.-W., Sack, F. and Kim, J.-Y. 2009. The *Arabidopsis* callose synthase gene GSL8 is required for cytokinesis and cell patterning. *Plant Physiology.* **150**(1), pp.105-113.

Chen, X., Yao, Q., Gao, X., Jiang, C., Harberd, N.P. and Fu, X. 2016. Shoot-to-Root Mobile Transcription Factor HY5 Coordinates Plant Carbon and Nitrogen Acquisition. *Current Biology.* **26**(5), pp.640-646.

Cheng, Y., Zhou, W., El Sheery, N.I., Peters, C., Li, M., Wang, X. and Huang, J. 2011. Characterization of the *Arabidopsis* glycerophosphodiester phosphodiesterase (GDPD) family reveals a role of the plastid-localized AtGDPD1 in maintaining cellular phosphate homeostasis under phosphate starvation. *The Plant Journal.* **66**(5), pp.781-795.

Chevalier, F., Pata, M., Nacry, P., Doumas, P. and Rossignol, M. 2003. Effects of phosphate availability on the root system architecture: large-scale analysis of the natural variation between *Arabidopsis* accessions. *Plant, Cell & Environment.* **26**(11), pp.1839-1850.

Cho, Y.-H., Sheen, J. and Yoo, S.-D. 2010. Low glucose uncouples hexokinase1-dependent sugar signaling from stress and defense hormone abscisic acid and C2H4 responses in *Arabidopsis*. *Plant Physiology.* **152**(3), pp.1180-1182.

Choi, J.Y., Seo, Y.S., Kim, S.J., Kim, W.T. and Shin, J.S. 2011. Constitutive expression of CaXTH3, a hot pepper xyloglucan endotransglucosylase/hydrolase, enhanced tolerance to salt and drought stresses without phenotypic defects in tomato plants (Solanum lycopersicum cv. Dotaerang). *Plant Cell Reports.* **30**(5), pp.867-877.

Chong, J., Wishart, D.S. and Xia, J. 2019. Using MetaboAnalyst 4.0 for comprehensive and integrative metabolomics data analysis. *Current protocols in bioinformatics.* **68**(1), pe86.

Clauw, P., Coppens, F., De Beuf, K., Dhondt, S., Van Daele, T., Maleux, K., Storme, V., Clement, L., Gonzalez, N. and Inzé, D. 2015. Leaf responses to mild drought stress in natural variants of *Arabidopsis*. *Plant Physiology.* **167**(3), pp.800-816.

Clough, S.J. and Bent, A.F. 1998. Floral dip: a simplified method for Agrobacterium-mediated transformation of *Arabidopsis* thaliana. *The plant journal.* **16**(6), pp.735-743.

Colette, A., Lu, K.-J. and Weijers, D. 2015. Building a plant: cell fate specification in the early *Arabidopsis* embryo. *Development.* **142**(3), pp.420-430.

Cordell, D., Drangert, J.-O. and White, S. 2009. The story of phosphorus: global food security and food for thought. *Global environmental change.* **19**(2), pp.292-305.

Cornuault, V., Pose, S. and Knox, J.P. 2018. Disentangling pectic homogalacturonan and rhamnogalacturonan-I polysaccharides: Evidence for sub-populations in fruit parenchyma systems. *Food Chemistry.* **246**, pp.275-285.

Cui, W. and Lee, J.-Y. 2016a. *Arabidopsis* callose synthases CalS1/8 regulate plasmodesmal permeability during stress. *Nature Plants.* **2**(5), p16034.

Cui, W. and Lee, J.-Y. 2016b. *Arabidopsis* callose synthases CalS1/8 regulate plasmodesmal permeability during stress. *Nature plants.* **2**(5), pp.1-9.

Cumming, C.M., Rizkallah, H.D., McKendrick, K.A., Abdel-Massih, R.M., Baydoun, E.A. and Brett, C.T. 2005. Biosynthesis and cell-wall deposition of a pectin–xyloglucan complex in pea. *Planta.* **222**(3), pp.546-555.

D'Odorico, P., Davis, K.F., Rosa, L., Carr, J.A., Chiarelli, D., Dell'Angelo, J., Gephart, J., MacDonald, G.K., Seekell, D.A. and Suweis, S. 2018. The global food-energy-water nexus. *Reviews of Geophysics.* **56**(3), pp.456-531.

De Schepper, V., De Swaef, T., Bauweraerts, I. and Steppe, K. 2013. Phloem transport: a review of mechanisms and controls. *Journal of Experimental Botany.* **64**(16), pp.4839-4850.

De Smet, I. 2012. Lateral root initiation: one step at a time. *New Phytologist.* **193**(4), pp.867-873.

Deak, K.I. and Malamy, J. 2005. Osmotic regulation of root system architecture. *The Plant Journal.* **43**(1), pp.17-28.

Deinum, E.E., Mulder, B.M. and Benitez-Alfonso, Y. 2019. From plasmodesma geometry to effective symplasmic permeability through biophysical modelling. *eLife.* **8**, pe49000.

Deprost, D., Yao, L., Sormani, R., Moreau, M., Leterreux, G., Nicolaï, M., Bedu, M., Robaglia, C. and Meyer, C. 2007. The *Arabidopsis* TOR kinase links plant growth, yield, stress resistance and mRNA translation. *EMBO reports.* **8**(9), pp.864-870.

Desnoyer, N. and Palanivelu, R. 2020. Bridging the GAPs in plant reproduction: a comparison of plant and animal GPI-anchored proteins. *Plant Reproduction.* **33**(3), pp.129-142.

Diao, M., Ren, S., Wang, Q., Qian, L., Shen, J., Liu, Y. and Huang, S. 2018. *Arabidopsis* formin 2 regulates cell-to-cell trafficking by capping and stabilizing actin filaments at plasmodesmata. *eLife.* **7**, pe36316.

Dietrich, D., Pang, L., Kobayashi, A., Fozard, J.A., Boudolf, V., Bhosale, R., Antoni, R., Nguyen, T., Hiratsuka, S. and Fujii, N. 2017. Root hydrotropism is controlled via a cortex-specific growth mechanism. *Nature Plants.* **3**(6), pp.1-8.

Dolan, L., Janmaat, K., Willemsen, V., Linstead, P., Poethig, S., Roberts, K. and Scheres, B. 1993. Cellular organisation of the *Arabidopsis* thaliana root. *Development.* **119**(1), pp.71-84.

Dong, J., Ma, G., Sui, L., Wei, M., Satheesh, V., Zhang, R., Ge, S., Li, J., Zhang, T.-E. and Wittwer, C. 2019. Inositol pyrophosphate InsP8 acts as an intracellular phosphate signal in *Arabidopsis*. *Molecular Plant.* **12**(11), pp.1463-1473.

Downs, J. and Jones, B. 2020. The short and intricate life of the suspensor. *Physiologia Plantarum.* **169**(1), pp.110-121.

Dragićević, M.B., Paunović, D.M., Milica, Todorović, S.I. and Simonović, A.D. 2020. ragp: Pipeline for mining of plant hydroxyproline-rich glycoproteins with implementation in R. *Glycobiology.* **30**(1), pp.19-35.

Drew, M. 1975. Comparison of the effects of a localised supply of phosphate, nitrate, ammonium and potassium on the growth of the seminal root system, and the shoot, in barley. *New Phytologist.* **75**(3), pp.479-490.

Drost, H.-G. and Paszkowski, J. 2017. Biomartr: genomic data retrieval with R. *Bioinformatics.* **33**(8), pp.1216-1217.

Du, Y. and Scheres, B. 2018. Lateral root formation and the multiple roles of auxin. *Journal of Experimental Botany.* **69**(2), pp.155-167.

Duan, Y., Zhang, W., Li, B., Wang, Y., Li, K., Han, C., Zhang, Y. and Li, X. 2010. An endoplasmic reticulum response pathway mediates programmed cell death of root tip induced by water stress in *Arabidopsis*. *New Phytologist.* **186**(3), pp.681-695.

Dubrovsky, J.G., Sauer, M., Napsucialy-Mendivil, S., Ivanchenko, M.G., Friml, J., Shishkova, S., Celenza, J. and Benková, E. 2008. Auxin acts as a local morphogenetic trigger to specify lateral root founder cells. *Proceedings of the National Academy of Sciences.* **105**(25), pp.8790-8794.

Dunbabin, V., Rengel, Z. and Diggle, A. 2004. Simulating form and function of root systems: efficiency of nitrate uptake is dependent on root system architecture and the spatial and temporal variability of nitrate supply. *Functional Ecology.* **18**(2), pp.204-211.

Durand, M., Mainson, D., Porcheron, B., Maurousset, L., Lemoine, R. and Pourtau, N. 2018. Carbon source–sink relationship in *Arabidopsis* thaliana: the role of sucrose transporters. *Planta.* **247**(3), pp.587-611.

Ehlers, K. and Kollmann, R. 2001. Primary and secondary plasmodesmata: structure, origin, and functioning. *Protoplasma.* **216**(1), pp.1-30.

El Hassouni, K., Alahmad, S., Belkadi, B., Filali-Maltouf, A., Hickey, L. and Bassi, F. 2018. Root system architecture and its association with yield under different water regimes in durum wheat. *Crop Science.* **58**(6), pp.2331-2346.

Emanuelsson, O., Brunak, S., Von Heijne, G. and Nielsen, H. 2007. Locating proteins in the cell using TargetP, SignalP and related tools. *Nature Protocols.* **2**(4), p953.

Fàbregas, N., Lozano-Elena, F., Blasco-Escámez, D., Tohge, T., Martínez-Andújar, C., Albacete, A., Osorio, S., Bustamante, M., Riechmann, J.L. and Nomura, T. 2018. Overexpression of the vascular brassinosteroid receptor BRL3 confers drought resistance without penalizing plant growth. *Nature Communications.* **9**(1), pp.1-13.

FAOSTAT. 2021. *World Food and Agriculture Statistical Yearbook.* Food and Agriculture Organization of the United Nations.

Farquharson, K.L. 2008. Phosphate-deprived roots are hypersensitive to auxin. *The Plant Cell.* **20**(12), p3183.

Faulkner, C. 2018. Plasmodesmata and the symplast. *Current Biology.* **28**(24), pp.1374-1378.

Faulkner, C., Akman, O.E., Bell, K., Jeffree, C. and Oparka, K. 2008. Peeking into pit fields: a multiple twinning model of secondary plasmodesmata formation in tobacco. *The Plant Cell.* **20**(6), pp.1504-1518.

Fauser, F., Schiml, S. and Puchta, H. 2014. Both CRISPR/C as-based nucleases and nickases can be used efficiently for genome engineering in A rabidopsis thaliana. *The Plant Journal.* **79**(2), pp.348-359.

Feng, C.z., Luo, Y.x., Wang, P.d., Gilliham, M. and Long, Y. 2021. MYB77 regulates high-affinity potassium uptake by promoting expression of HAK5. *New Phytologist.* **232**(1), pp.176-189.

Fernandez-Calvino, L., Faulkner, C., Walshaw, J., Saalbach, G., Bayer, E., Benitez-Alfonso, Y. and Maule, A. 2011. *Arabidopsis* plasmodesmal proteome. *PLOS One.* **6**(4), pe18880.

Fichman, Y., Myers, R.J., Grant, D.G. and Mittler, R. 2021. Plasmodesmata-localized proteins and ROS orchestrate light-induced rapid systemic signaling in *Arabidopsis*. *Science Signaling.* **14**(671).

Fichtenbauer, D., Xu, X.M., Jackson, D. and Kragler, F. 2012. The chaperonin CCT8 facilitates spread of tobamovirus infection. *Plant Signaling & Behavior.* **7**(3), pp.318-321.

Fischer, K., Lachner, L.A.-M., Olsen, S., Mulisch, M. and Krause, K. 2021. The enigma of interspecific plasmodesmata: insight from parasitic plants. *Frontiers in Plant Science.* **12**, p641924.

Fitzgibbon, J., Bell, K., King, E. and Oparka, K. 2010. Super-resolution imaging of plasmodesmata using three-dimensional structured illumination microscopy. *Plant Physiology.* **153**(4), pp.1453-1463.

Fu, L., Liu, Y., Qin, G., Wu, P., Zi, H., Xu, Z., Zhao, X., Wang, Y., Li, Y. and Yang, S. 2021. The TOR–EIN2 axis mediates nuclear signalling to modulate plant growth. *Nature.* **591**(7849), pp.288-292.

Ganusova, E.E., Reagan, B.C., Fernandez, J.C., Azim, M.F., Sankoh, A.F., Freeman, K.M., McCray, T.N., Patterson, K., Kim, C. and Burch-Smith, T.M. 2020. Chloroplast-to-nucleus retrograde signalling controls intercellular trafficking via plasmodesmata formation. *Philosophical Transactions of the Royal Society B.* **375**(1801), p20190408.

Gao, C., Liu, X., De Storme, N., Jensen, K.H., Xu, Q., Yang, J., Liu, X., Chen, S., Martens, H.J. and Schulz, A. 2020. Directionality of Plasmodesmata-Mediated Transport in *Arabidopsis* Leaves Supports Auxin Channeling. *Current Biology.* **30**(10), pp.1970-1977.

Gaudioso-Pedraza, R. 2017. *Callose-mediated regulation of Plasmodesmata during the establishment of Medicago Truncatula-Sinorhizobium Meliloti Symbiotic interaction*. thesis, University of Leeds.

Gaudioso-Pedraza, R., Beck, M., Frances, L., Kirk, P., Ripodas, C., Niebel, A., Oldroyd, G.E.D., Benitez-Alfonso, Y. and de Carvalho-Niebel, F. 2018. Callose-Regulated Symplastic Communication Coordinates Symbiotic Root Nodule Development. *Current Biology.* **28**(22), pp.3562-3577 e3566.

Gaudioso-Pedraza, R. and Benitez-Alfonso, Y. 2014. A phylogenetic approach to study the origin and evolution of plasmodesmata-localized glycosyl hydrolases family 17. *Frontiers in Plant Science.* **5**, p212.

Gazzarrini, S. and McCourt, P. 2003. Cross-talk in plant hormone signalling: what *Arabidopsis* mutants are telling us. *Annals of botany.* **91**(6), pp.605-612.

Gee, H.Y., Kim, J. and Lee, M.G. 2018. Unconventional secretion of transmembrane proteins. In: *Seminars in Cell & Developmental Biology*: Elsevier, pp.59-66.

Gerlitz, N., Gerum, R., Sauer, N. and Stadler, R. 2018. Photoinducible DRONPA-s: a new tool for investigating cell-cell connectivity. *The Plant Journal.* **94**(5), pp.751-766.

Ghashghaie, J., Brenckmann, F. and Saugier, B. 1991. Effects of agar concentration on water status and growth of rose plants cultured in vitro. *Physiologia Plantarum.* **82**(1), pp.73-78.

Gierth, M., Mäser, P. and Schroeder, J.I. 2005. The potassium transporter AtHAK5 functions in K+ deprivation-induced high-affinity K+ uptake and AKT1 K+ channel contribution to K+ uptake kinetics in *Arabidopsis* roots. *Plant Physiology.* **137**(3), pp.1105-1114.

Gíslason, M.H., Nielsen, H., Armenteros, J.J.A. and Johansen, A.R. 2019. Prediction of GPI-Anchored proteins with pointer neural networks. *bioRxiv.* p838680.

Gombos, S., Miras, M.M., Howe, V., Xi, L., Pottier, M., Jasemi, N.S., Schladt, M., Ejike, J.O., Neumann, U. and Hansch, S. 2022. A high confidence Physcomitrium patens plasmodesmata proteome by iterative scoring and validation reveals diversification of cell wall proteins during evolution. *bioRxiv.* p492581.

González-Guzmán, M., Apostolova, N., Bellés, J.M., Barrero, J.M., Piqueras, P., Ponce, M.R., Micol, J.L., Serrano, R. and Rodríguez, P.L. 2002. The short-chain alcohol dehydrogenase ABA2 catalyzes the conversion of xanthoxin to abscisic aldehyde. *The Plant Cell.* **14**(8), pp.1833-1846.

Goodwin, P. 1983. Molecular size limit for movement in the symplast of the Elodea leaf. *Planta.* **157**(2), pp.124-130.

Gopal, J. and Iwama, K. 2007. In vitro screening of potato against water-stress mediated through sorbitol and polyethylene glycol. *Plant Cell Reports.* **26**(5), pp.693-700.

Gou, X. 2022. A CLE–BAM–CIK signalling module controls root protophloem differentiation in *Arabidopsis*. *New Phytologist.* **233**(1), pp.282-296.

Graves, S., Piepho, H.-P., Selzer, L. and Dorai-Raj, S. 2015. *multcompView: visualizations of paired comparisons.*

Grebe, M. 2011. Unveiling the Casparian strip. *Nature.* **473**(7347), pp.294-295.

Grison, M.S., Brocard, L., Fouillen, L., Nicolas, W., Wewer, V., Dormann, P., Nacir, H., Benitez-Alfonso, Y., Claverol, S., Germain, V., Boutte, Y., Mongrand, S. and Bayer, E.M. 2015. Specific membrane lipid composition is important for plasmodesmata function in *Arabidopsis*. *The Plant Cell.* **27**(4), pp.1228-1250.

Grison, M.S., Kirk, P., Brault, M.L., Wu, X.N., Schulze, W.X., Benitez-Alfonso, Y., Immel, F. and Bayer, E.M. 2019. Plasma Membrane-Associated Receptor-like Kinases Relocalize to Plasmodesmata in Response to Osmotic Stress. *Plant Physiology.* **181**(1), pp.142-160.

Gronnier, J., Crowet, J.-M., Habenstein, B., Nasir, M.N., Bayle, V., Hosy, E., Platre, M.P., Gouguet, P., Raffaele, S., Martinez, D., Grelard, A., Loquet, A., Simon-Plas, F., Gerbeau-Pissot, P., Der, C., Bayer, E.M., Jaillais, Y., Deleu, M., Germain, V., Lins, L. and Mongrand, S. 2017. Structural basis for plant plasma membrane protein dynamics and organization into functional nanodomains. *eLife.* **6**, pe26404.

Gruber, B.D., Giehl, R.F., Friedel, S. and von Wirén, N. 2013. Plasticity of the *Arabidopsis* root system under nutrient deficiencies. *Plant Physiology.* **163**(1), pp.161-179.

Gu, L., Xu, T., Lee, K., Lee, K.H. and Kang, H. 2014. A chloroplast-localized DEAD-box RNA helicaseAtRH3 is essential for intron splicing and plays an important role in the growth and stress response in *Arabidopsis* thaliana. *Plant Physiology and Biochemistry.* **82**, pp.309-318.

Gu, Z., Eils, R. and Schlesner, M. 2016. Complex heatmaps reveal patterns and correlations in multidimensional genomic data. *Bioinformatics.* **32**(18), pp.2847-2849.

Guan, X.Q., Zhao, S.J., Li, D.Q. and Shu, H.R. 2004. Photoprotective Function of Photorespiration in Several Grapevine Cultivars Under Drought Stress. *Photosynthetica.* **42**(1), pp.31-36.

Gupta, A., Rico-Medina, A. and Caño-Delgado, A.I. 2020. The physiology of plant responses to drought. *Science.* **368**(6488), pp.266-269.

Gurrieri, L., Merico, M., Trost, P., Forlani, G. and Sparla, F. 2020. Impact of Drought on Soluble Sugars and Free Proline Content in Selected *Arabidopsis* Mutants. *Biology.* **9**(11), p367.

Guseman, J.M., Lee, J.S., Bogenschutz, N.L., Peterson, K.M., Virata, R.E., Xie, B., Kanaoka, M.M., Hong, Z. and Torii, K.U. 2010. Dysregulation of cell-to-cell connectivity and stomatal patterning by loss-of-function mutation in *Arabidopsis* chorus (glucan synthase-like 8). *Development.* **137**(10), pp.1731-1741.

Gutiérrez, R.A., Lejay, L.V., Dean, A., Chiaromonte, F., Shasha, D.E. and Coruzzi, G.M. 2007. Qualitative network models and genome-wide expression data define carbon/nitrogen-responsive molecular machines in *Arabidopsis*. *Genome biology.* **8**(1), pp.1-13.

Ham, B.-K., Chen, J., Yan, Y. and Lucas, W.J. 2018. Insights into plant phosphate sensing and signaling. *Current opinion in biotechnology.* **49**, pp.1-9.

Han, S., Jia, M.-z., Yang, J.-f. and Jiang, J. 2019. The integration of ACS2-generated ACC with GH3-mediated IAA homeostasis in NaCl-stressed primary root elongation of *Arabidopsis* seedlings. *Plant Growth Regulation.* **88**(2), pp.151-158.

Han, X., Hyun, T.K., Zhang, M., Kumar, R., Koh, E.J., Kang, B.H., Lucas, W.J. and Kim, J.Y. 2014. Auxin-callose-mediated plasmodesmal gating is essential for tropic auxin gradient formation and signaling. *Developmental cell.* **28**(2), pp.132-146.

Han, X. and Kim, J.-Y. 2016. Integrating hormone-and micromolecule-mediated signaling with plasmodesmal communication. *Molecular plant.* **9**(1), pp.46-56.

Hara, K., Kajita, R., Torii, K.U., Bergmann, D.C. and Kakimoto, T. 2007. The secretory peptide gene EPF1 enforces the stomatal one-cell-spacing rule. *Genes & development.* **21**(14), pp.1720-1725.

Hara, K., Yokoo, T., Kajita, R., Onishi, T., Yahata, S., Peterson, K.M., Torii, K.U. and Kakimoto, T. 2009. Epidermal Cell Density is Autoregulated via a Secretory Peptide, EPIDERMAL PATTERNING FACTOR 2 in *Arabidopsis* Leaves. *Plant and Cell Physiology.* **50**(6), pp.1019-1031.

Harayama, T. and Riezman, H. 2018. Understanding the diversity of membrane lipid composition. *Nature Reviews Molecular Cell Biology.* **19**(5), p281.

Harvey, C.A., Rakotobe, Z.L., Rao, N.S., Dave, R., Razafimahatratra, H., Rabarijohn, R.H., Rajaofara, H. and MacKinnon, J.L. 2014. Extreme vulnerability of smallholder farmers to agricultural risks and climate change in Madagascar. *Philosophical Transactions of the Royal Society B: Biological Sciences.* **369**(1639), p20130089.

Hawes, C., Juniper, B. and Horne, J. 1981. Low and high voltage electron microscopy of mitosis and cytokinesis in maize roots. *Planta.* **152**(5), pp.397-407.

Hawkins, C., Ginzburg, D., Zhao, K., Dwyer, W., Xue, B., Xu, A., Rice, S., Cole, B., Paley, S. and Karp, P. 2021. Plant Metabolic Network 15: A resource of genome-wide metabolism databases for 126 plants and algae. *Journal of Integrative Plant Biology.* **63**(11), pp.1888-1905.

Hayashi, S., Ishii, T., Matsunaga, T., Tominaga, R., Kuromori, T., Wada, T., Shinozaki, K. and Hirayama, T. 2008. The glycerophosphoryl diester phosphodiesterase-like proteins SHV3 and its homologs play important roles in cell wall organization. *Plant and cell physiology.* **49**(10), pp.1522-1535.

Heffer, P. and Prud'homme, M. 2016. Global nitrogen fertilizer demand and supply: Trend, current level and outlook. In: *International Nitrogen Initiative Conference. Melbourne, Australia*.

Hepler, P. 1982. Endoplasmic reticulum in the formation of the cell plate and plasmodesmata. *Protoplasma.* **111**(2), pp.121-133.

Herrera-Vásquez, A., Salinas, P. and Holuigue, L. 2015. Salicylic acid and reactive oxygen species interplay in the transcriptional control of defense genes expression. *Frontiers in Plant Science.* **6**, p171.

His, I., Driouich, A., Nicol, F., Jauneau, A. and Höfte, H. 2001. Altered pectin composition in primary cell walls of korrigan , a dwarf mutant of *Arabidopsis* deficient in a membrane-bound endo-1,4-β-glucanase. *Planta.* **212**(3), pp.348-358.

Ho, C.-H., Lin, S.-H., Hu, H.-C. and Tsay, Y.-F. 2009. CHL1 functions as a nitrate sensor in plants. *Cell.* **138**(6), pp.1184-1194.

Ho, C.-H. and Tsay, Y.-F. 2010. Nitrate, ammonium, and potassium sensing and signaling. *Current opinion in plant biology.* **13**(5), pp.604-610.

Hogg, B.V., Kacprzyk, J., Molony, E.M., O'Reilly, C., Gallagher, T.F., Gallois, P. and McCabe, P.F. 2011. An in vivo root hair assay for determining rates of apoptotic-like programmed cell death in plants. *Plant Methods.* **7**(1), p45.

Hong, Z., Delauney, A.J. and Verma, D.P.S. 2001. A cell plate–specific callose synthase and its interaction with phragmoplastin. *The Plant Cell.* **13**(4), pp.755-768.

Horie, T., Hauser, F. and Schroeder, J.I. 2009. HKT transporter-mediated salinity resistance mechanisms in *Arabidopsis* and monocot crop plants. *Trends in Plant Science.* **14**(12), pp.660-668.

Howe, K.L., Contreras-Moreira, B., Nishadi, Maslen, G., Akanni, W., Allen, J., Alvarez-Jarreta, J., Barba, M., Bolser, D.M., Cambell, L., Carbajo, M., Chakiachvili, M., Christensen, M., Cummins, C., Cuzick, A., Davis, P., Fexova, S., Gall, A., George, N., Gil, L., Gupta, P., Hammond-Kosack, K.E., Haskell, E., Hunt, S.E., Jaiswal, P., Janacek, S.H., Kersey, P.J., Langridge, N., Maheswari, U., Maurel, T., McDowall, M.D., Moore, B., Muffato, M., Naamati, G., Naithani, S., Olson, A., Papatheodorou, I., Patricio, M., Paulini, M., Pedro, H., Perry, E., Preece, J., Rosello, M., Russell, M., Sitnik, V., Staines, D.M., Stein, J., Tello-Ruiz, M.K., Trevanion, S.J., Urban, M., Wei, S., Ware, D., Williams, G., Yates, A.D. and Flicek, P. 2020. Ensembl Genomes 2020—enabling non-vertebrate genomic research. *Nucleic Acids Research.* **48**(D1), pp.D689-D695.

Hu, C., Ham, B.K., El-shabrawi, H.M., Alexander, D., Zhang, D., Ryals, J. and Lucas, W.J. 2016. Proteomics and metabolomics analyses reveal the cucurbit sieve tube system as a complex metabolic space. *The Plant Journal.* **87**(5), pp.442-454.

Hu, C., Zhu, Y., Cui, Y., Zeng, L., Li, S., Meng, F., Huang, S., Wang, W., Kui, H. and Yi, J. 2022. A CLE–BAM–CIK signalling module controls root protophloem differentiation in *Arabidopsis*. *New Phytologist.* **233**(1), pp.282-296.

Hu, Y., Omary, M., Hu, Y., Doron, O., Hoermayer, L., Chen, Q., Megides, O., Chekli, O., Ding, Z. and Friml, J. 2021. Cell kinetics of auxin transport and activity in *Arabidopsis* root growth and skewing. *Nature Communications.* **12**(1), pp.1-13.

Huang, D., Sun, Y., Ma, Z., Ke, M., Cui, Y., Chen, Z., Chen, C., Ji, C., Tran, T.M. and Yang, L. 2019. Salicylic acid-mediated plasmodesmal closure via Remorin-dependent lipid organization. *Proceedings of the National Academy of Sciences.* **116**(42), pp.21274-21284.

Hunter, J.D. 2007. Matplotlib: A 2D graphics environment. *IEEE Annals of the History of Computing.* **9**(03), pp.90-95.

Hunter, K., Kimura, S., Rokka, A., Tran, H.C., Toyota, M., Kukkonen, J.P. and Wrzaczek, M. 2019. CRK2 Enhances Salt Tolerance by Regulating Callose Deposition in Connection with PLDα1. *Plant Physiology.* **180**(4), pp.2004-2021.

Hyodo, H., Yamakawa, S., Takeda, Y., Tsuduki, M., Yokota, A., Nishitani, K. and Kohchi, T. 2003. Active gene expression of a xyloglucan endotransglucosylase/hydrolase gene, XTH9, in inflorescence apices is related to cell elongation in *Arabidopsis* thaliana. *Plant molecular biology.* **52**(2), pp.473-482.

Iglesias, V.A. and Meins Jr, F. 2000. Movement of plant viruses is delayed in a β-1, 3-glucanase-deficient mutant showing a reduced plasmodesmatal size exclusion limit and enhanced callose deposition. *The Plant Journal.* **21**(2), pp.157-166.

Iijima, M., Awala, S.K., Watanabe, Y., Kawato, Y., Fujioka, Y., Yamane, K. and Wada, K.C. 2016. Mixed cropping has the potential to enhance flood tolerance of drought-adapted grain crops. *Journal of plant physiology.* **192**, pp.21-25.

Imlau, A., Truernit, E. and Sauer, N. 1999. Cell-to-cell and long-distance trafficking of the green fluorescent protein in the phloem and symplastic unloading of the protein into sink tissues. *The Plant Cell.* **11**(3), pp.309-322.

IPCC. 2014. *Mitigation of climate change.*

Ishikawa, K., Tamura, K., Fukao, Y. and Shimada, T. 2020. Structural and functional relationships between plasmodesmata and plant endoplasmic

reticulum–plasma membrane contact sites consisting of three synaptotagmins. *New Phytologist.* **226**(3), pp.798-808.

Itaya, A., Ma, F., Qi, Y., Matsuda, Y., Zhu, Y., Liang, G. and Ding, B. 2002. Plasmodesma-mediated selective protein traffic between "symplasmically isolated" cells probed by a viral movement protein. *The Plant Cell.* **14**(9), pp.2071-2083.

Izzo, L.G. and Aronne, G. 2021. *Root Tropisms: New Insights Leading the Growth Direction of the Hidden Half*. Multidisciplinary Digital Publishing Institute.

Jain, A., Poling, M.D., Karthikeyan, A.S., Blakeslee, J.J., Peer, W.A., Titapiwatanakun, B., Murphy, A.S. and Raghothama, K.G. 2007. Differential effects of sucrose and auxin on localized phosphate deficiency-induced modulation of different traits of root system architecture in *Arabidopsis*. *Plant Physiology.* **144**(1), pp.232-247.

Janes, G., von Wangenheim, D., Cowling, S., Kerr, I., Band, L., French, A.P. and Bishopp, A. 2018. Cellular patterning of *Arabidopsis* roots under low phosphate conditions. *Frontiers in Plant Science.* **9**, p735.

Jarvis, M.C. 1984. Structure and properties of pectin gels in plant cell walls. *Plant, Cell & Environment.* **7**(3), pp.153-164.

Jobbagy, E.G. and Jackson, R.B. 2001. The distribution of soil nutrients with depth: global patterns and the imprint of plants. *Biogeochemistry.* **53**(1), pp.51-77.

Johnston, M.G., Breakspear, A., Samwald, S., Zhang, D., Papp, D., Faulkner, C. and de Keijzer, J. 2022. Comparative phyloproteomics identifies conserved plasmodesmal proteins. *bioRxiv.* p494363.

Jones-Rhoades, M.W. and Bartel, D.P. 2004. Computational identification of plant microRNAs and their targets, including a stress-induced miRNA. *Molecular cell.* **14**(6), pp.787-799.

Jung, J.-Y., Shin, R. and Schachtman, D.P. 2009. Ethylene mediates response and tolerance to potassium deprivation in *Arabidopsis*. *The Plant Cell.* **21**(2), pp.607-621.

Kahlaoui, B., Hachicha, M., Misle, E., Fidalgo, F. and Teixeira, J. 2018. Physiological and biochemical responses to the exogenous application of proline of tomato plants irrigated with saline water. *Journal of the Saudi Society of Agricultural Sciences.* **17**(1), pp.17-23.

Käll, L., Krogh, A. and Sonnhammer, E.L. 2007. Advantages of combined transmembrane topology and signal peptide prediction—the Phobius web server. *Nucleic Acids Research.* **35**(2), pp.W429-W432.

Kanno, S., Arrighi, J.-F., Chiarenza, S., Bayle, V., Berthomé, R., Peret, B., Javot, H., Delannoy, E., Marin, E. and Nakanishi, T.M. 2016. A novel role for the root cap in phosphate uptake and homeostasis. *Elife.* **5**, pe14577.

Keegstra, K., Talmadge, K.W., Bauer, W. and Albersheim, P. 1973. The structure of plant cell walls: III. A model of the walls of suspension-cultured sycamore cells based on the interconnections of the macromolecular components. *Plant Physiology.* **51**(1), pp.188-197.

Kellermeier, F., Armengaud, P., Seditas, T.J., Danku, J., Salt, D.E. and Amtmann, A. 2014. Analysis of the root system architecture of *Arabidopsis* provides a quantitative readout of crosstalk between nutritional signals. *The Plant Cell.* **26**(4), pp.1480-1496.

Kellermeier, F., Chardon, F. and Amtmann, A. 2013. Natural variation of *Arabidopsis* root architecture reveals complementing adaptive strategies to potassium starvation. *Plant Physiology.* **161**(3), pp.1421-1432.

Khan, M., Gemenet, D.C. and Villordon, A. 2016. Root system architecture and abiotic stress tolerance: current knowledge in root and tuber crops. *Frontiers in Plant Science.* **7**, p1584.

Kieffer, M., Neve, J. and Kepinski, S. 2010. Defining auxin response contexts in plant development. *Current opinion in plant biology.* **13**(1), pp.12-20.

Kim, H., Zhou, J., Kumar, D., Jang, G., Ryu, K.H., Sebastian, J., Miyashima, S., Helariutta, Y. and Lee, J.-Y. 2020. SHORTROOT-mediated intercellular signals coordinate phloem development in *Arabidopsis* roots. *The Plant Cell.* **32**(5), pp.1519-1535.

Kim, J.-Y., Rim, Y., Wang, J. and Jackson, D. 2005. A novel cell-to-cell trafficking assay indicates that the KNOX homeodomain is necessary and sufficient for intercellular protein and mRNA trafficking. *Genes & Development.* **19**(7), pp.788-793.

Kimura, S., Hunter, K., Vaahtera, L., Tran, H.C., Citterico, M., Vaattovaara, A., Rokka, A., Stolze, S.C., Harzen, A., Meißner, L., Wilkens, M.M.T., Hamann, T., Toyota, M., Nakagami, H. and Wrzaczek, M. 2020. CRK2 and C-terminal Phosphorylation of NADPH Oxidase RBOHD Regulate Reactive Oxygen Species Production in *Arabidopsis*. *The Plant Cell.* **32**(4), pp.1063-1080.

Kirk, P., Amsbury, S., German, L., Gaudioso-Pedraza, R. and Benitez-Alfonso, Y. 2022. A comparative meta-proteomic pipeline for the identification of plasmodesmata proteins and regulatory conditions in diverse plant species. *BMC biology.* **20**(1), pp.1-21.

Kitagawa, M., Tomoi, T., Fukushima, T., Sakata, Y., Sato, M., Toyooka, K., Fujita, T. and Sakakibara, H. 2019. Abscisic acid acts as a regulator of molecular trafficking through plasmodesmata in the moss Physcomitrella patens. *Plant and Cell Physiology.* **60**(4), pp.738-751.

Knox, J.P. and Benitez-Alfonso, Y. 2014. Roles and regulation of plant cell walls surrounding plasmodesmata. *Current opinion in plant biology.* **22**, pp.93-100.

Knox, J.P., Linstead, P., King, J., Cooper, C. and Roberts, K. 1990. Pectin esterification is spatially regulated both within cell walls and between developing tissues of root apices. *Planta.* **181**(4).

Knox, K., Wang, P., Kriechbaumer, V., Tilsner, J., Frigerio, L., Sparkes, I., Hawes, C. and Karl, J.O. 2015. Putting the squeeze on PDs-a role for RETICULONS in primary plasmodesmata formation. *Plant Physiology.* ppp. 00668.02015.

Kobayashi, K., Otegui, M.S., Krishnakumar, S., Mindrinos, M. and Zambryski, P. 2007. INCREASED SIZE EXCLUSION LIMIT 2 encodes a putative DEVH box RNA helicase involved in plasmodesmata function during *Arabidopsis* embryogenesis. *The Plant Cell.* **19**(6), pp.1885-1897.

Koevoets, I.T., Venema, J.H., Elzenga, J.T. and Testerink, C. 2016. Roots withstanding their environment: exploiting root system architecture responses to abiotic stress to improve crop tolerance. *Frontiers in plant science.* **7**, p1335.

Koizumi, K. and Gallagher, K.L. 2013. Identification of SHRUBBY, a SHORT-ROOT and SCARECROW interacting protein that controls root growth and radial patterning. *Development.* **140**(6), pp.1292-1300.

Kollmann, R. and Glockmann, C. 1991. Studies on graft unions. *Protoplasma.* **165**(1-3), pp.71-85.

Konstantinova, N., Korbei, B. and Luschnig, C. 2021. Auxin and Root Gravitropism: Addressing Basic Cellular Processes by Exploiting a Defined Growth Response. *International Journal of Molecular Sciences.* **22**(5), p2749.

Koornneef, M. and Meinke, D. 2010. The development of *Arabidopsis* as a model plant. *The Plant Journal.* **61**(6), pp.909-921.

Kooyers, N.J. 2015. The evolution of drought escape and avoidance in natural herbaceous populations. *Plant Science.* **234**, pp.155-162.

Krogh, A., Larsson, B., Von Heijne, G. and Sonnhammer, E.L.L. 2001. Predicting transmembrane protein topology with a hidden markov model: application to complete genomes11Edited by F. Cohen. *Journal of Molecular Biology.* **305**(3), pp.567-580.

Krouk, G., Lacombe, B., Bielach, A., Perrine-Walker, F., Malinska, K., Mounier, E., Hoyerova, K., Tillard, P., Leon, S. and Ljung, K. 2010. Nitrate-regulated auxin transport by NRT1. 1 defines a mechanism for nutrient sensing in plants. *Developmental cell.* **18**(6), pp.927-937.

Kuki, H., Yokoyama, R., Kuroha, T. and Nishitani, K. 2020. Xyloglucan is not essential for the formation and integrity of the cellulose network in the primary cell wall regenerated from *Arabidopsis* protoplasts. *Plants.* **9**(5), p629.

Kumar, M., Kesawat, M.S., Ali, A., Lee, S.-C., Gill, S.S. and Kim, H.U. 2019. Integration of abscisic acid signaling with other signaling pathways in plant stress responses and development. *Plants.* **8**(12), p592.

Kuromori, T., Wada, T., Kamiya, A., Yuguchi, M., Yokouchi, T., Imura, Y., Takabe, H., Sakurai, T., Akiyama, K. and Hirayama, T. 2006. A trial of phenome analysis using 4000 Ds-insertional mutants in gene-coding regions of *Arabidopsis*. *The Plant Journal.* **47**(4), pp.640-651.

Labun, K., Montague, T.G., Krause, M., Torres Cleuren, Y.N., Tjeldnes, H. and Valen, E. 2019. CHOPCHOP v3: expanding the CRISPR web toolbox beyond genome editing. *Nucleic Acids Research.* **47**(W1), pp.W171-W174.

Larsbrink, J., Izumi, A., Ibatullin, F.M., Nakhai, A., Gilbert, H.J., Davies, G.J. and Brumer, H. 2011. Structural and enzymatic characterization of a glycoside hydrolase family 31 α-xylosidase from Cellvibrio japonicus involved in xyloglucan saccharification. *Biochemical Journal.* **436**(3), pp.567-580.

Lee, D.-K. and Sieburth, L.E. 2010. Plasmodesmata formation: poking holes in walls with ise. *Current Biology.* **20**(11), pp.R488-R490.

Lee, J.S., Hnilova, M., Maes, M., Lin, Y.-C.L., Putarjunan, A., Han, S.-K., Avila, J. and Torii, K.U. 2015. Competitive binding of antagonistic peptides fine-tunes stomatal patterning. *Nature.* **522**(7557), pp.439-443.

Lee, J.Y., Wang, X., Cui, W., Sager, R., Modla, S., Czymmek, K., Zybaliov, B., van Wijk, K., Zhang, C., Lu, H. and Lakshmanan, V. 2011. A plasmodesmata-localized protein mediates crosstalk between cell-to-cell communication and innate immunity in *Arabidopsis*. *The Plant Cell.* **23**(9), pp.3353-3373.

Lee, K.H., Park, J., Williams, D.S., Xiong, Y., Hwang, I. and Kang, B.H. 2013. Defective chloroplast development inhibits maintenance of normal levels of abscisic acid in a mutant of the *Arabidopsis* RH 3 DEAD-box protein during early post-germination growth. *The Plant Journal.* **73**(5), pp.720-732.

Lei, M., Liu, Y., Zhang, B., Zhao, Y., Wang, X., Zhou, Y., Raghothama, K.G. and Liu, D. 2011. Genetic and genomic evidence that sucrose is a global regulator of plant responses to phosphate starvation in *Arabidopsis*. *Plant Physiology.* **156**(3), pp.1116-1130.

Leigh, R.A. and Wyn Jones, R. 1984. A hypothesis relating critical potassium concentrations for growth to the distribution and functions of this ion in the plant cell. *New Phytologist.* **97**(1), pp.1-13.

Leijon, F., Melzer, M., Zhou, Q., Srivastava, V. and Bulone, V. 2018. Proteomic analysis of plasmodesmata from populus cell suspension cultures in relation with callose biosynthesis. *Frontiers in Plant Science.* **9**, p1681.

Levesque, M.P., Vernoux, T., Busch, W., Cui, H., Wang, J.Y., Blilou, I., Hassan, H., Nakajima, K., Matsumoto, N. and Lohmann, J.U. 2006. Whole-genome analysis of the SHORT-ROOT developmental pathway in *Arabidopsis*. *PLOS Biology.* **4**(5), pe143.

Levy, A., Erlanger, M., Rosenthal, M. and Epel, B.L. 2007. A plasmodesmata-associated β-1, 3-glucanase in *Arabidopsis*. *The Plant Journal.* **49**(4), pp.669-682.

Lewis, D.R., Olex, A.L., Lundy, S.R., Turkett, W.H., Fetrow, J.S. and Muday, G.K. 2013. A kinetic analysis of the auxin transcriptome reveals cell wall remodeling proteins that modulate lateral root development in *Arabidopsis*. *The Plant Cell.* **25**(9), pp.3329-3346.

Li, H., Ma, Q., Li, H., Zhang, F., Rengel, Z. and Shen, J. 2014. Root morphological responses to localized nutrient supply differ among crop species with contrasting root traits. *Plant and Soil.* **376**(1-2), pp.151-163.

Li, J., Wang, B., Zhu, X., Li, R., Fu, J. and Cui, H. 2020a. Novel Regulators of Sugar-Mediated Lateral Root Development in *Arabidopsis* thaliana. *Genes.* **11**(11), p1257.

Li, J., Wu, W.H. and Wang, Y. 2017. Potassium channel AKT1 is involved in the auxin-mediated root growth inhibition in *Arabidopsis* response to low K+ stress. *Journal of Integrative Plant Biology.* **59**(12), pp.895-909.

Li, J.Y., Jiang, A.L. and Zhang, W. 2007. Salt stress-induced programmed cell death in rice root tip cells. *Journal of Integrative Plant Biology*. **49**(4), pp.481-486.

Li, M., Yoo, C.G., Pu, Y., Biswal, A.K., Tolbert, A.K., Mohnen, D. and Ragauskas, A.J. 2019. Downregulation of pectin biosynthesis gene GAUT4 leads to reduced ferulate and lignin-carbohydrate cross-linking in switchgrass. *Communications biology.* **2**(1), pp.1-11.

Li, T., Zhang, Y., Liu, Y., Li, X., Hao, G., Han, Q., Dirk, L.M.A., Downie, A.B., Ruan, Y.-L., Wang, J., Wang, G. and Zhao, T. 2020b. Raffinose synthase enhances drought tolerance through raffinose synthesis or galactinol hydrolysis in maize and *Arabidopsis* plants. *Journal of Biological Chemistry.* **295**(23), pp.8064-8077.

Li, X. and Zhang, W. 2008. Salt-avoidance tropism in *Arabidopsis* thaliana. *Plant signaling & behavior.* **3**(5), pp.351-353.

Li, Y., Li, L., Wang, Y., Wang, Y.-C., Wang, N.-N., Lu, R., Wu, Y.-W. and Li, X.-B. 2020c. Pollen-specific protein PSP231 activates callose synthesis to govern male gametogenesis and pollen germination. *Plant Physiology.* **184**(2), pp.1024-1041.

Li, Z., Zhou, T., Sun, P., Chen, X., Gong, L., Sun, P., Ge, S. and Liang, Y.-K. 2022. COBL9 and COBL7 synergistically regulate root hair tip growth via controlling apical cellulose deposition. *Biochemical and Biophysical Research Communications.* **596**, pp.6-13.

Li, Z.P., Paterlini, A., Glavier, M. and Bayer, E.M. 2021. Intercellular trafficking via plasmodesmata: molecular layers of complexity. *Cellular and Molecular Life Sciences.* **78**(3), pp.799-816.

Liao, H., Rubio, G., Yan, X., Cao, A., Brown, K.M. and Lynch, J.P. 2001. Effect of phosphorus availability on basal root shallowness in common bean. *Plant and Soil.* **232**(1), pp.69-79.

Liao, H., Yan, X., Rubio, G., Beebe, S.E., Blair, M.W. and Lynch, J.P. 2004. Genetic mapping of basal root gravitropism and phosphorus acquisition efficiency in common bean. *Functional Plant Biology.* **31**(10), pp.959-970.

Lin, G., Zhang, L., Han, Z., Yang, X., Liu, W., Li, E., Chang, J., Qi, Y., Shpak, E.D. and Chai, J. 2017. A receptor-like protein acts as a specificity switch for the regulation of stomatal development. *Genes & Development.* **31**(9), pp.927-938.

Lin, Y. and Schiefelbein, J. 2001. Embryonic control of epidermal cell patterning in the root and hypocotyl of *Arabidopsis*. *Development.* **128**(19), pp.3697-3705.

Linkohr, B.I., Williamson, L.C., Fitter, A.H. and Leyser, H.O. 2002. Nitrate and phosphate availability and distribution have different effects on root system architecture of *Arabidopsis*. *The Plant Journal.* **29**(6), pp.751-760.

Liu, D. 2021. Root developmental responses to phosphorus nutrition. *Journal of Integrative Plant Biology.* **63**(6), pp.1065-1090.

Liu, D.Y., Smith, P.M., Barton, D.A., Day, D.A. and Overall, R.L. 2017a. Characterisation of *Arabidopsis* calnexin 1 and calnexin 2 in the endoplasmic reticulum and at plasmodesmata. *Protoplasma.* **254**(1), pp.125-136.

Liu, J., Moore, S., Chen, C. and Lindsey, K. 2017b. Crosstalk complexities between auxin, cytokinin, and ethylene in *Arabidopsis* root development: from experiments to systems modeling, and back again. *Molecular Plant.* **10**(12), pp.1480-1496.

Liu, N.-J., Zhang, T., Liu, Z.-H., Chen, X., Guo, H.-S., Ju, B.-H., Zhang, Y.-Y., Li, G.-Z., Zhou, Q.-H. and Qin, Y.-M. 2020a. Phytosphinganine affects plasmodesmata permeability via facilitating PDLP5-stimulated callose accumulation in *Arabidopsis*. *Molecular Plant.* **13**(1), pp.128-143.

Liu, N., Shen, G., Xu, Y., Liu, H., Zhang, J., Li, S., Li, J., Zhang, C., Qi, J., Wang, L. and Wu, J. 2020b. Extensive Inter-plant Protein Transfer between Cuscuta Parasites and Their Host Plants. *Molecular Plant.* **13**(4), pp.573-585.

Lombardi, M., De Gara, L. and Loreto, F. 2021. Determinants of root system architecture for future-ready, stress-resilient crops. *Physiologia Plantarum.* **172**(4), pp.2090-2097.

López-Arredondo, D.L., Leyva-González, M.A., Alatorre-Cobos, F. and Herrera-Estrella, L. 2013. Biotechnology of nutrient uptake and assimilation in plants. *International Journal of Developmental Biology.* **57**(6-7-8), pp.595-610.

Lu, K.-J., De Rybel, B., Van Mourik, H. and Weijers, D. 2018. Regulation of intercellular TARGET OF MONOPTEROS 7 protein transport in the *Arabidopsis* root. *Development.* **145**(2), pdev152892.

Lund, C.H., Stenbæk, A., Atmodjo, M.A., Rasmussen, R.E., Moller, I.E., Erstad, S.M., Biswal, A.K., Mohnen, D., Mravec, J. and Sakuragi, Y. 2020. Pectin

synthesis and pollen tube growth in *Arabidopsis* involves three GAUT1 Golgi-anchoring proteins: GAUT5, GAUT6, and GAUT7. *Frontiers in Plant Science.* **11**, p1435.

Lynch, J.P. and Brown, K.M. 2001. Topsoil foraging–an architectural adaptation of plants to low phosphorus availability. *Plant and Soil.* **237**(2), pp.225-237.

MacAlister, C.A., Ohashi-Ito, K. and Bergmann, D.C. 2007. Transcription factor control of asymmetric cell divisions that establish the stomatal lineage. *Nature.* **445**(7127), pp.537-540.

Maghiaoui, A., Bouguyon, E., Cuesta, C., Perrine-Walker, F., Alcon, C., Krouk, G., Benková, E., Nacry, P., Gojon, A. and Bach, L. 2020. The *Arabidopsis* NRT1. 1 transceptor coordinately controls auxin biosynthesis and transport to regulate root branching in response to nitrate. *Journal of Experimental Botany.* **71**(15), pp.4480-4494.

Malamy, J.E. and Benfey, P.N. 1997. Down and out in *Arabidopsis*: the formation of lateral roots. *Trends in Plant Science.* **2**(10), pp.390-396.

Malter, D. and Wolf, S. 2011. Melon phloem-sap proteome: developmental control and response to viral infection. *Protoplasma.* **248**(1), pp.217-224.

Mangiafico, S. 2018. rcompanion: Functions to support extension education program evaluation. *R package version.* **1**(2).

Mansfield, S. and Briarty, L. 1991. Early embryogenesis in *Arabidopsis* thaliana. II. The developing embryo. *Canadian journal of botany.* **69**(3), pp.461-476.

Martignago, D., Rico-Medina, A., Blasco-Escámez, D., Fontanet-Manzaneque, J.B. and Caño-Delgado, A.I. 2020. Drought resistance by engineering plant tissue-specific responses. *Frontiers in Plant Science.* **10**, p1676.

Martin, A., Adam, H., Díaz-Mendoza, M., Żurczak, M., González-Schain, N.D. and Suárez-López, P. 2009. Graft-transmissible induction of potato tuberization by the microRNA miR172. *Development.* **136**(17), pp.2873-2881.

Martin, T., Oswald, O. and Graham, I.A. 2002. *Arabidopsis* seedling growth, storage lipid mobilization, and photosynthetic gene expression are regulated by carbon: nitrogen availability. *Plant Physiology.* **128**(2), pp.472-481.

Martínez-Barradas, V., Bernal, L., López-Baltazar, J., Coello, P., Cruz-García, F., Márquez, J. and Martínez-Barajas, E. 2019. Nutritional restriction triggers callose accumulation on the sieve plates of the funiculus of developing bean seeds. *South African Journal of Botany.* **121**, pp.549-557.

Masucci, J.D., Rerie, W.G., Foreman, D.R., Zhang, M., Galway, M.E., Marks, M.D. and Schiefelbein, J.W. 1996. The homeobox gene GLABRA2 is required for position-dependent cell differentiation in the root epidermis of *Arabidopsis* thaliana. *Development.* **122**(4), pp.1253-1260.

Maule, A., Gaudioso-Pedraza, R. and Benitez-Alfonso, Y. 2013. Callose deposition and symplastic connectivity are regulated prior to lateral root emergence. *Communicative & integrative biology.* **6**(6), pe26531.

Mbow, C., Rosenzweig, C., Barioni, L.G., Benton, T.G., Herrero, M., Krishnapillai, M., Liwenga, E., Pradhan, P., Rivera-Ferre, M.-G. and Sapkota, T. 2019. *Food security.*

McCready, K., Spencer, V. and Kim, M. 2020. The importance of TOR kinase in plant development. *Frontiers in Plant Science.* **11**, p16.

Mellor, N.L., Voß, U., Janes, G., Bennett, M.J., Wells, D.M. and Band, L.R. 2020. Auxin fluxes through plasmodesmata modify root-tip auxin distribution. *Development.* **147**(6), pdev181669.

Melnyk, C.W., Molnar, A., Bassett, A. and Baulcombe, D.C. 2011. Mobile 24 nt small RNAs direct transcriptional gene silencing in the root meristems of *Arabidopsis* thaliana. *Current Biology.* **21**(19), pp.1678-1683.

Meng, L., Zhang, T., Geng, S., Scott, P.B., Li, H. and Chen, S. 2019. Comparative proteomics and metabolomics of JAZ7-mediated drought tolerance in *Arabidopsis*. *Journal of Proteomics.* **196**, pp.81-91.

Mi, H., Ebert, D., Muruganujan, A., Mills, C., Albou, L.-P., Mushayamaha, T. and Thomas, P.D. 2021. PANTHER version 16: a revised family classification, tree-

based classification tool, enhancer regions and extensive API. *Nucleic Acids Research.* **49**(D1), pp.D394-D403.

Michel, B.E. 1972. Solute potentials of sucrose solutions. *Plant Physiology.* **50**(1), p196.

Michel, B.E. 1983. Evaluation of the water potentials of solutions of polyethylene glycol 8000 both in the absence and presence of other solutes. *Plant Physiology.* **72**(1), pp.66-70.

Miller, A. and Cramer, M. 2005. Root nitrogen acquisition and assimilation. *Plant and Soil.* **274**(1), pp.1-36.

Mira, M.M., Huang, S., Kapoor, K., Hammond, C., Hill, R.D. and Stasolla, C. 2017. Expression of *Arabidopsis* class 1 phytoglobin (AtPgb1) delays death and degradation of the root apical meristem during severe PEG-induced water deficit. *Journal of Experimental Botany.* **68**(20), pp.5653-5668.

Mishra, B.S., Singh, M., Aggrawal, P. and Laxmi, A. 2009. Glucose and auxin signaling interaction in controlling *Arabidopsis* thaliana seedlings root growth and development. *PLOS One.* **4**(2), pe4502.

Moneo-Sánchez, M., Vaquero-Rodríguez, A., Hernández-Nistal, J., Albornos, L., Knox, P., Dopico, B., Labrador, E. and Martín, I. 2020. Pectic galactan affects cell wall architecture during secondary cell wall deposition. *Planta.* **251**(5), pp.1-15.

Morris, J.L., Puttick, M.N., Clark, J.W., Edwards, D., Kenrick, P., Pressel, S., Wellman, C.H., Yang, Z., Schneider, H. and Donoghue, P.C. 2018. The timescale of early land plant evolution. *Proceedings of the National Academy of Sciences.* **115**(10), pp.E2274-E2283.

Müller, J., Toev, T., Heisters, M., Teller, J., Moore, K.L., Hause, G., Dinesh, D.C., Bürstenbinder, K. and Abel, S. 2015. Iron-dependent callose deposition adjusts root meristem maintenance to phosphate availability. *Developmental cell.* **33**(2), pp.216-230.

Murashige, T. and Skoog, F. 1962. A revised medium for rapid growth and bio assays with tobacco tissue cultures. *Physiologia Plantarum.* **15**(3), pp.473-497.

Nacry, P., Canivenc, G., Muller, B., Azmi, A., Van Onckelen, H., Rossignol, M. and Doumas, P. 2005. A role for auxin redistribution in the responses of the root system architecture to phosphate starvation in *Arabidopsis*. *Plant Physiology.* **138**(4), pp.2061-2074.

Nakashima, K. and Yamaguchi-Shinozaki, K. 2013. ABA signaling in stress-response and seed development. *Plant cell reports.* **32**(7), pp.959-970.

Nawaz, G. and Kang, H. 2017. Chloroplast-or mitochondria-targeted DEAD-box RNA helicases play essential roles in organellar RNA metabolism and abiotic stress responses. *Frontiers in Plant Science.* **8**, p871.

Nicolas, W.J., Grison, M.S., Trépout, S., Gaston, A., Fouché, M., Cordelières, F.P., Oparka, K., Tilsner, J., Brocard, L. and Bayer, E.M. 2017. Architecture and permeability of post-cytokinesis plasmodesmata lacking cytoplasmic sleeves. *Nature Plants.* **3**(7), pp.1-11.

Ning, W., Jiang, P., Guo, Y., Wang, C., Tan, X., Zhang, W., Peng, D. and Xue, Y. 2020. GPS-Palm: a deep learning-based graphic presentation system for the prediction of S-palmitoylation sites in proteins. *Briefings in Bioinformatics.* **22**(2), pp.1836-1847.

Nishitani, K. and Tominaga, R. 1992. Endo-xyloglucan transferase, a novel class of glycosyltransferase that catalyzes transfer of a segment of xyloglucan molecule to another xyloglucan molecule. *Journal of Biological Chemistry.* **267**(29), pp.21058-21064.

O'Brien, J.A., Vega, A., Bouguyon, E., Krouk, G., Gojon, A., Coruzzi, G. and Gutierrez, R.A. 2016. Nitrate Transport, Sensing, and Responses in Plants. *Molecular Plant.* **9**(6), pp.837-856.

Obayashi, T., Aoki, Y., Tadaka, S., Kagaya, Y. and Kinoshita, K. 2018. ATTED-II in 2018: A Plant Coexpression Database Based on Investigation of the Statistical Property of the Mutual Rank Index. *Plant and Cell Physiology.* **59**(1), pp.e3-e3.

Ohkubo, Y., Kuwata, K. and Matsubayashi, Y. 2021. A type 2C protein phosphatase activates high-affinity nitrate uptake by dephosphorylating NRT2. 1. *Nature Plants.* **7**(3), pp.1-7.

Ohkubo, Y., Tanaka, M., Tabata, R., Ogawa-Ohnishi, M. and Matsubayashi, Y. 2017a. Shoot-to-root mobile polypeptides involved in systemic regulation of nitrogen acquisition. *Nature Plants.* **3**(4), pp.1-6.

Ohkubo, Y., Tanaka, M., Tabata, R., Ogawa-Ohnishi, M. and Matsubayashi, Y. 2017b. Shoot-to-root mobile polypeptides involved in systemic regulation of nitrogen acquisition. *Nature Plants.* **3**(4), p17029.

Okamoto, S., Tabata, R. and Matsubayashi, Y. 2016. Long-distance peptide signaling essential for nutrient homeostasis in plants. *Current opinion in plant biology.* **34**, pp.35-40.

Okonechnikov, K., Golosova, O., Fursov, M. and Team, U. 2012. Unipro UGENE: a unified bioinformatics toolkit. *Bioinformatics.* **28**(8), pp.1166-1167.

Oparka, K.J. and Prior, D.A.M. 1992. Direct evidence for pressure-generated closure of plasmodesmata. *The Plant Journal.* **2**(5), pp.741-750.

Oparka, K.J., Roberts, A.G., Boevink, P., Santa Cruz, S., Roberts, I., Pradel, K.S., Imlau, A., Kotlizky, G., Sauer, N. and Epel, B. 1999. Simple, but not branched, plasmodesmata allow the nonspecific trafficking of proteins in developing tobacco leaves. *Cell.* **97**(6), pp.743-754.

Orfila, C. and Knox, J.P. 2000. Spatial Regulation of Pectic Polysaccharides in Relation to Pit Fields in Cell Walls of Tomato Fruit Pericarp. *Plant Physiology.* **122**(3), pp.775-782.

Ormenese, S., Bernier, G. and Périlleux, C. 2006. Cytokinin application to the shoot apical meristem of Sinapis alba enhances secondary plasmodesmata formation. *Planta.* **224**(6), pp.1481-1484.

Ostermeyer, G.P., Jensen, K.H., Franzen, A.R., Peters, W.S. and Knoblauch, M. 2021. Diversity of funnel plasmodesmata in angiosperms: the impact of geometry on plasmodesmal resistance. *bioRxiv.* p442713.

Overall, R.L. and Blackman, L.M. 1996. A model of the macromolecular structure of plasmodesmata. *Trends in Plant Science.* **1**(9), pp.307-311.

Owji, H., Nezafat, N., Negahdaripour, M., Hajiebrahimi, A. and Ghasemi, Y. 2018. A comprehensive review of signal peptides: Structure, roles, and applications. *European journal of cell biology.* **97**(6), pp.422-441.

Pacheco, J.M., Canal, M.V., Pereyra, C.M., Welchen, E., Martínez-Noël, G.M. and Estevez, J.M. 2021. The tip of the iceberg: emerging roles of TORC1, and its regulatory functions in plant cells. *Journal of Experimental Botany.* **72**(11), pp.4085-4101.

Palovaara, J., de Zeeuw, T. and Weijers, D. 2016. Tissue and organ initiation in the plant embryo: a first time for everything. *Annual Review of Cell and Developmental Biology.* **32**, pp.47-75.

Paniagua, C., Sinanaj, B. and Benitez-Alfonso, Y. 2021. Plasmodesmata and their role in the regulation of phloem unloading during fruit development. *Current opinion in plant biology.* **64**, p102145.

Parizot, B., Laplaze, L., Ricaud, L., Boucheron-Dubuisson, E., Bayle, V., Bonke, M., De Smet, I., Poethig, S.R., Helariutta, Y. and Haseloff, J. 2008. Diarch symmetry of the vascular bundle in *Arabidopsis* root encompasses the pericycle and is reflected in distich lateral root initiation. *Plant Physiology.* **146**(1), pp.140-148.

Park, J.-E., Kim, J., Purevdorj, E., Son, Y.-J., Nho, C.W. and Yoo, G. 2021. Effects of long light exposure and drought stress on plant growth and glucosinolate production in pak choi (Brassica rapa subsp. chinensis). *Food Chemistry.* **340**, p128167.

Park, J., Lee, Y., Martinoia, E. and Geisler, M. 2017a. Plant hormone transporters: what we know and what we would like to know. *Bmc Biology.* **15**(1), pp.1-15.

Park, K., Knoblauch, J., Oparka, K. and Jensen, K.H. 2019. Controlling intercellular flow through mechanosensitive plasmodesmata nanopores. *Nature Communications.* **10**(1), p3564.

Park, S.-H., Li, F., Renaud, J., Shen, W., Li, Y., Guo, L., Cui, H., Sumarah, M. and Wang, A. 2017b. NbEXPA1, an α-expansin, is plasmodesmata-specific and a novel host factor for potyviral infection. *The Plant Journal.* **92**(5), pp.846-861.

Park, S. and Harada, J.J. 2008. *Arabidopsis* embryogenesis. *Plant embryogenesis.* pp.3-16.

Park, Y.B. and Cosgrove, D.J. 2012. Changes in cell wall biomechanical properties in the xyloglucan-deficient xxt1/xxt2 mutant of *Arabidopsis*. *Plant Physiology.* **158**(1), pp.465-475.

Parris, K. 2010. Water in agriculture: Improving resource management. *Organisation for Economic Cooperation and Development. The OECD Observer.* (278), p29.

Paterlini, A. 2020. Uncharted routes: exploring the relevance of auxin movement via plasmodesmata. *Biology Open.* **9**(11), pbio055541.

Patterson, K., Walters, L., Cooper, A., Olvera, J., Rosas, M., Rasmusson, A. and Escobar, M. 2015. Nitrate-regulated glutaredoxins control *Arabidopsis* thaliana primary root growth. *Plant Physiology.* **170**(2), pp.989-999.

Pedersen, H.L., Fangel, J.U., McCleary, B., Ruzanski, C., Rydahl, M.G., Ralet, M.-C., Farkas, V., Von Schantz, L., Marcus, S.E., Andersen, M.C.F., Field, R., Ohlin, M., Knox, J.P., Clausen, M.H. and Willats, W.G.T. 2012. Versatile High Resolution Oligosaccharide Microarrays for Plant Glycobiology and Cell Wall Research*. *Journal of Biological Chemistry.* **287**(47), pp.39429-39438.

Péret, B., Clément, M., Nussaume, L. and Desnos, T. 2011. Root developmental adaptation to phosphate starvation: better safe than sorry. *Trends in Plant Science.* **16**(8), pp.442-450.

Peterson, C.A. and Rauser, W.E. 1979. Callose deposition and photoassimilate export in Phaseolus vulgaris exposed to excess cobalt, nickel, and zinc. *Plant Physiology.* **63**(6), pp.1170-1174.

Pi, L., Aichinger, E., van der Graaff, E., Llavata-Peris, C.I., Weijers, D., Hennig, L., Groot, E. and Laux, T. 2015. Organizer-derived WOX5 signal maintains root columella stem cells through chromatin-mediated repression of CDF4 expression. *Developmental cell.* **33**(5), pp.576-588.

Piepho, H.-P. 2004. An algorithm for a letter-based representation of all-pairwise comparisons. *Journal of Computational and Graphical Statistics.* **13**(2), pp.456-466.

Pierleoni, A., Martelli, P.L. and Casadio, R. 2008. PredGPI: a GPI-anchor predictor. *BMC bioinformatics.* **9**(1), p392.

Pillitteri, L.J. and Dong, J. 2013. Stomatal Development in *Arabidopsis*. *The Arabidopsis Book.* **11**, pe0162.

Piršelová, B., Mistríková, V., Libantová, J., Moravčíková, J. and Matušíková, I. 2012. Study on metal-triggered callose deposition in roots of maize and soybean. *Biologia.* **67**(4), pp.698-705.

Ponce, G., Corkidi, G., Eapen, D., Lledías, F., Cárdenas, L. and Cassab, G. 2017. Root hydrotropism and thigmotropism in *Arabidopsis* thaliana are differentially controlled by redox status. *Plant Signaling & Behavior.* **12**(4), pe1305536.

Popova, L., van Dusschoten, D., Nagel, K.A., Fiorani, F. and Mazzolai, B. 2016. Plant root tortuosity: an indicator of root path formation in soil with different composition and density. *Annals of botany.* **118**(4), pp.685-698.

Popper, Z.A. and Fry, S.C. 2008. Xyloglucan− pectin linkages are formed intra-protoplasmically, contribute to wall-assembly, and remain stable in the cell wall. *Planta.* **227**(4), pp.781-794.

Porco, S., Larrieu, A., Du, Y., Gaudinier, A., Goh, T., Swarup, K., Swarup, R., Kuempers, B., Bishopp, A. and Lavenus, J. 2016. Lateral root emergence in *Arabidopsis* is dependent on transcription factor LBD29 regulation of auxin influx carrier LAX3. *Development.* **143**(18), pp.3340-3349.

Pound, M.P., Burgess, A.J., Wilson, M.H., Atkinson, J.A., Griffiths, M., Jackson, A.S., Bulat, A., Tzimiropoulos, G., Wells, D.M. and Murchie, E.H. 2016. Deep Machine Learning provides state-of-the-art performance in image-based plant phenotyping. *bioRxiv.* p053033.

Pound, M.P., French, A.P., Atkinson, J.A., Wells, D.M., Bennett, M.J. and Pridmore, T. 2013. RootNav: navigating images of complex root architectures. *Plant Physiology.* **162**(4), pp.1802-1814.

Puga, M.I., Mateos, I., Charukesi, R., Wang, Z., Franco-Zorrilla, J.M., de Lorenzo, L., Irigoyen, M.L., Masiero, S., Bustos, R. and Rodríguez, J. 2014. SPX1 is a phosphate-dependent inhibitor of Phosphate Starvation Response 1 in *Arabidopsis*. *Proceedings of the National Academy of Sciences.* **111**(41), pp.14947-14952.

Puga, M.I., Rojas-Triana, M., de Lorenzo, L., Leyva, A., Rubio, V. and Paz-Ares, J. 2017. Novel signals in the regulation of Pi starvation responses in plants: facts and promises. *Current Opinion in Plant Biology.* **39**, pp.40-49.

Qi, W., Manfield, I.W., Muench, S.P. and Baker, A. 2017. AtSPX1 affects the AtPHR1–DNA-binding equilibrium by binding monomeric AtPHR1 in solution. *Biochemical Journal.* **474**(21), pp.3675-3687.

Quarrie, S. and Jones, H.G. 1977. Effects of abscisic acid and water stress on development and morphology of wheat. *Journal of Experimental Botany.* **28**(1), pp.192-203.

Ragel, P., Raddatz, N., Leidi, E.O., Quintero, F.J. and Pardo, J.M. 2019. Regulation of K+ nutrition in plants. *Frontiers in Plant Science.* **10**, p281.

Reagan, B.C. and Burch-Smith, T.M. 2020. Viruses Reveal the Secrets of Plasmodesmal Cell Biology. *Molecular Plant-Microbe Interactions®.* **33**(1), pp.26-39.

Remans, T., Nacry, P., Pervent, M., Filleur, S., Diatloff, E., Mounier, E., Tillard, P., Forde, B.G. and Gojon, A. 2006. The *Arabidopsis* NRT1. 1 transporter participates in the signaling pathway triggering root colonization of nitrate-rich patches. *Proceedings of the National Academy of Sciences.* **103**(50), pp.19206-19211.

Rengel, Z. and Damon, P.M. 2008. Crops and genotypes differ in efficiency of potassium uptake and use. *Physiologia Plantarum.* **133**(4), pp.624-636.

Ribba, T., Garrido-Vargas, F. and O'Brien, J.A. 2020. Auxin-mediated responses under salt stress: from developmental regulation to biotechnological applications. *Journal of Experimental Botany.* **71**(13), pp.3843-3853.

Rinne, P.L., Welling, A., Vahala, J., Ripel, L., Ruonala, R., Kangasjärvi, J. and van der Schoot, C. 2011. Chilling of dormant buds hyperinduces FLOWERING LOCUS T and recruits GA-inducible 1, 3-β-glucanases to reopen signal conduits and release dormancy in Populus. *The Plant Cell.* **23**(1), pp.130-146.

Ritchie, M.E., Phipson, B., Wu, D., Hu, Y., Law, C.W., Shi, W. and Smyth, G.K. 2015. limma powers differential expression analyses for RNA-sequencing and microarray studies. *Nucleic Acids Research.* **43**(7), pp.e47-e47.

Roberts, I., Boevink, P., Roberts, A., Sauer, N., Reichel, C. and Oparka, K. 2001. Dynamic changes in the frequency and architecture of plasmodesmata during the sink-source transition in tobacco leaves. *Protoplasma.* **218**(1), pp.31-44.

Rock, C.D. and Sun, X. 2005. Crosstalk between ABA and auxin signaling pathways in roots of *Arabidopsis* thaliana (L.) Heynh. *Planta.* **222**(1), pp.98-106.

Rodríguez-Celma, J., Ceballos-Laita, L., Grusak, M.A., Abadía, J. and López-Millán, A.-F. 2016. Plant fluid proteomics: delving into the xylem sap, phloem sap and apoplastic fluid proteomes. *Biochimica et Biophysica Acta (BBA)-Proteins and Proteomics.* **1864**(8), pp.991-1002.

Rosa, L., Chiarelli, D.D., Rulli, M.C., Dell'Angelo, J. and D'Odorico, P. 2020. Global agricultural economic water scarcity. *Science Advances.* **6**(18), peaaz6031.

Rosas-Diaz, T., Zhang, D., Fan, P., Wang, L., Ding, X., Jiang, Y., Jimenez-Gongora, T., Medina-Puche, L., Zhao, X. and Feng, Z. 2018. A virus-targeted plant receptor-like kinase promotes cell-to-cell spread of RNAi. *Proceedings of the National Academy of Sciences.* **115**(6), pp.1388-1393.

Rose, J.K., Braam, J., Fry, S.C. and Nishitani, K. 2002. The XTH family of enzymes involved in xyloglucan endotransglucosylation and endohydrolysis: current perspectives and a new unifying nomenclature. *Plant and Cell Physiology.* **43**(12), pp.1421-1435.

Ross-Elliott, T.J., Jensen, K.H., Haaning, K.S., Wager, B.M., Knoblauch, J., Howell, A.H., Mullendore, D.L., Monteith, A.G., Paultre, D., Yan, D., Otero, S., Bourdon, M., Sager, R., Lee, J.-Y., Helariutta, Y., Knoblauch, M. and Oparka, K.J. 2017. Phloem unloading in *Arabidopsis* roots is convective and regulated by the phloem-pole pericycle. *eLife.* **6**.

Rouached, H., Stefanovic, A., Secco, D., Bulak Arpat, A., Gout, E., Bligny, R. and Poirier, Y. 2011. Uncoupling phosphate deficiency from its major effects on growth and transcriptome via PHO1 expression in *Arabidopsis*. *The Plant Journal.* **65**(4), pp.557-570.

Roy, S., Watada, A.E. and Wergin, W.P. 1997. Characterization of the Cell Wall Microdomain Surrounding Plasmodesmata in Apple Fruit. *Plant Physiology.* **114**(2), pp.539-547.

Roycewicz, P. and Malamy, J.E. 2012. Dissecting the effects of nitrate, sucrose and osmotic potential on *Arabidopsis* root and shoot system growth in laboratory assays. *Philosophical Transactions of the Royal Society B: Biological Sciences.* **367**(1595), pp.1489-1500.

Roychoudhry, S., Kieffer, M., Del Bianco, M., Liao, C.-Y., Weijers, D. and Kepinski, S. 2017. The developmental and environmental regulation of gravitropic setpoint angle in *Arabidopsis* and bean. *Scientific Reports.* **7**(1), pp.1-12.

Ruan, Y.-L., Llewellyn, D.J. and Furbank, R.T. 2001. The Control of Single-Celled Cotton Fiber Elongation by Developmentally Reversible Gating of Plasmodesmata and Coordinated Expression of Sucrose and K+ Transporters and Expansin. *The Plant Cell.* **13**(1), pp.47-60.

Rutschow, H.L., Baskin, T.I. and Kramer, E.M. 2011. Regulation of solute flux through plasmodesmata in the root meristem. *Plant Physiology.* **155**(4), pp.1817-1826.

Saatian, B., Austin, R.S., Tian, G., Chen, C., Nguyen, V., Kohalmi, S.E., Geelen, D. and Cui, Y. 2018. Analysis of a novel mutant allele of GSL8 reveals its key roles in cytokinesis and symplastic trafficking in *Arabidopsis*. *BMC plant biology.* **18**(1), pp.1-17.

Sachs, T. 1991. *Pattern formation in plant tissues.* Cambridge University Press.

Sager, R., Wang, X., Hill, K., Yoo, B.-C., Caplan, J., Nedo, A., Tran, T., Bennett, M.J. and Lee, J.-Y. 2020. Auxin-dependent control of a plasmodesmal regulator creates a negative feedback loop modulating lateral root emergence. *Nature Communications.* **11**(1), pp.1-10.

Salehin, M., Li, B., Tang, M., Katz, E., Song, L., Ecker, J.R., Kliebenstein, D.J. and Estelle, M. 2019. Auxin-sensitive Aux/IAA proteins mediate drought tolerance in *Arabidopsis* by regulating glucosinolate levels. *Nature Communications.* **10**(1), pp.1-9.

Sánchez-Calderón, L., López-Bucio, J., Chacón-López, A., Cruz-Ramírez, A., Nieto-Jacobo, F., Dubrovsky, J.G. and Herrera-Estrella, L. 2005. Phosphate starvation induces a determinate developmental program in the roots of *Arabidopsis* thaliana. *Plant and Cell Physiology.* **46**(1), pp.174-184.

Sattelmacher, B. 2001. The apoplast and its significance for plant mineral nutrition. *New Phytologist.* **149**(2), pp.167-192.

Saucedo, M., Ponce, G., Campos, M.E., Eapen, D., García, E., Luján, R., Sánchez, Y. and Cassab, G.I. 2012. An altered hydrotropic response (ahr1) mutant of *Arabidopsis* recovers root hydrotropism with cytokinin. *Journal of Experimental Botany.* **63**(10), pp.3587-3601.

Sauer, N. and Stolz, J. 1994. SUC1 and SUC2: two sucrose transporters from *Arabidopsis* thaliana; expression and characterization in baker's yeast and identification of the histidine-tagged protein. *The Plant Journal.* **6**(1), pp.67-77.

Schachtman, D.P., Reid, R.J. and Ayling, S.M. 1998. Phosphorus uptake by plants: from soil to cell. *Plant Physiology.* **116**(2), pp.447-453.

Schindelman, G., Morikami, A., Jung, J., Baskin, T.I., Carpita, N.C., Derbyshire, P., McCann, M.C. and Benfey, P.N. 2001. COBRA encodes a putative GPI-anchored protein, which is polarly localized and necessary for oriented cell expansion in *Arabidopsis*. *Genes & development.* **15**(9), pp.1115-1127.

Schulz, A. 1995. Plasmodesmal widening accompanies the short-term increase in symplasmic phloem unloading in pea root tips under osmotic stress. *Protoplasma.* **188**(1-2), pp.22-37.

Seabold, S. and Perktold, J. 2010. Statsmodels: Econometric and statistical modeling with python. In: *Proceedings of the 9th Python in Science Conference*: Austin, TX, p.61.

Sedbrook, J.C., Carroll, K.L., Hung, K.F., Masson, P.H. and Somerville, C.R. 2002. The *Arabidopsis* SKU5 Gene Encodes an Extracellular Glycosyl Phosphatidylinositol–Anchored Glycoprotein Involved in Directional Root Growth. *The Plant Cell.* **14**(7), pp.1635-1648.

Serin, E.A., Nijveen, H., Hilhorst, H.W. and Ligterink, W. 2016. Learning from co-expression networks: possibilities and challenges. *Frontiers in Plant Science.* **7**, p444.

Shao, H.-B., Chu, L.-Y., Jaleel, C.A. and Zhao, C.-X. 2008. Water-deficit stress-induced anatomical changes in higher plants. *Comptes rendus biologies.* **331**(3), pp.215-225.

Sharma, B., Molden, D. and Cook, S. 2015. *Water use efficiency in agriculture: Measurement, current situation and trends.*

Sharma, R., Singh, G., Bhattacharya, S. and Singh, A. 2018. Comparative transcriptome meta-analysis of *Arabidopsis* thaliana under drought and cold stress. *PLOS ONE.* **13**(9), pe0203266.

Shaw, R. and Cheung, C.Y.M. 2018. A Dynamic Multi-Tissue Flux Balance Model Captures Carbon and Nitrogen Metabolism and Optimal Resource Partitioning During *Arabidopsis* Growth. *Frontiers in Plant Science.* **9**, p884.

Shikanai, Y., Yoshida, R., Hirano, T., Enomoto, Y., Li, B., Asada, M., Yamagami, M., Yamaguchi, K., Shigenobu, S. and Tabata, R. 2020. Callose synthesis suppresses cell death induced by low-calcium conditions in leaves. *Plant physiology.* **182**(4), pp.2199-2212.

Shin, R., Burch, A.Y., Huppert, K.A., Tiwari, S.B., Murphy, A.S., Guilfoyle, T.J. and Schachtman, D.P. 2007. The *Arabidopsis* transcription factor MYB77 modulates auxin signal transduction. *The Plant Cell.* **19**(8), pp.2440-2453.

Signora, L., De Smet, I., Foyer, C.H. and Zhang, H. 2001. ABA plays a central role in mediating the regulatory effects of nitrate on root branching in *Arabidopsis*. *The Plant Journal.* **28**(6), pp.655-662.

Silva-Sanzana, C., Estevez, J.M. and Blanco-Herrera, F. 2019. Influence of cell wall polymers and their modifying enzymes during plant-aphid interactions. *Journal of Experimental Botany.* **71**(13), pp.3854-3864.

Simmons, A.R. and Bergmann, D.C. 2016. Transcriptional control of cell fate in the stomatal lineage. *Current Opinion in Plant Biology.* **29**, pp.1-8.

Simpson, C., Thomas, C., Findlay, K., Bayer, E. and Maule, A.J. 2009. An *Arabidopsis* GPI-anchor plasmodesmal neck protein with callose binding activity and potential to regulate cell-to-cell trafficking. *The Plant Cell.* **21**(2), pp.581-594.

Sinclair, S.A., Larue, C., Bonk, L., Khan, A., Castillo-Michel, H., Stein, R.J., Grolimund, D., Begerow, D., Neumann, U. and Haydon, M.J. 2017. Etiolated seedling development requires repression of photomorphogenesis by a small cell-wall-derived dark signal. *Current Biology.* **27**(22), pp.3403-3418. e3407.

Singh, A. 2021. Soil salinization management for sustainable development: A review. *Journal of Environmental Management.* **277**, p111383.

Singh, R.K., Deshmukh, R., Muthamilarasan, M., Rani, R. and Prasad, M. 2020. Versatile roles of aquaporin in physiological processes and stress tolerance in plants. *Plant Physiology and Biochemistry.* **149**, pp.178-189.

Sivaguru, M., Fujiwara, T., Šamaj, J., Baluška, F., Yang, Z., Osawa, H., Maeda, T., Mori, T., Volkmann, D. and Matsumoto, H. 2000. Aluminum-induced 1→ 3-β-D-glucan inhibits cell-to-cell trafficking of molecules through plasmodesmata. A new mechanism of aluminum toxicity in plants. *Plant Physiology.* **124**(3), pp.991-1006.

Skopelitis, D.S., Hill, K., Klesen, S., Marco, C.F., von Born, P., Chitwood, D.H. and Timmermans, M.C.P. 2018. Gating of miRNA movement at defined cell-cell interfaces governs their impact as positional signals. *Nature Communications.* **9**(1), p3107.

Smith, F.W. and Jackson, W.A. 1987. Nitrogen enhancement of phosphate transport in roots of Zea mays L.: I. Effects of ammonium and nitrate pretreatment. *Plant Physiology.* **84**(4), pp.1314-1318.

Song, W., Xue, R., Song, Y., Bi, Y., Liang, Z., Meng, L., Dong, C., Wang, C., Liu, G. and Dong, J. 2018. Differential response of first-order lateral root elongation to low potassium involves nitric oxide in two tobacco cultivars. *Journal of Plant Growth Regulation.* **37**(1), pp.114-127.

Spiertz, J. 2009. Nitrogen, sustainable agriculture and food security: a review. *Sustainable Agriculture.* pp.635-651.

Stahl, Y., Grabowski, S., Bleckmann, A., Kühnemuth, R., Weidtkamp-Peters, S., Pinto, K.G., Kirschner, G.K., Schmid, J.B., Wink, R.H. and Hülsewede, A. 2013. Moderation of *Arabidopsis* root stemness by CLAVATA1 and *ARABIDOPSIS* CRINKLY4 receptor kinase complexes. *Current Biology.* **23**(5), pp.362-371.

Stahl, Y. and Simon, R. 2013. Gated communities: apoplastic and symplastic signals converge at plasmodesmata to control cell fates. *Journal of experimental botany.* **64**(17), pp.5237-5241.

Stahl, Y., Wink, R.H., Ingram, G.C. and Simon, R. 2009. A signaling module controlling the stem cell niche in *Arabidopsis* root meristems. *Current Biology.* **19**(11), pp.909-914.

Stangoulis, J. 2019. Variation in root system architecture and morphology of two wheat genotypes is a predictor of their tolerance to phosphorus deficiency. *Acta Physiologiae Plantarum.* **41**(7), pp.1-13.

Strabala, T.J., O'donnell, P.J., Smit, A.-M., Ampomah-Dwamena, C., Martin, E.J., Netzler, N., Nieuwenhuizen, N.J., Quinn, B.D., Foote, H.C. and Hudson, K.R. 2006. Gain-of-function phenotypes of many CLAVATA3/ESR genes, including four new family members, correlate with tandem variations in the conserved CLAVATA3/ESR domain. *Plant Physiology.* **140**(4), pp.1331-1344.

Sun, J. and Zheng, N. 2015. Molecular mechanism underlying the plant NRT1. 1 dual-affinity nitrate transporter. *Frontiers in Physiology.* **6**, p386.

Sung, J., Lee, S., Lee, Y., Ha, S., Song, B., Kim, T., Waters, B.M. and Krishnan, H.B. 2015. Metabolomic profiling from leaves and roots of tomato (Solanum lycopersicum L.) plants grown under nitrogen, phosphorus or potassium-deficient condition. *Plant Science.* **241**, pp.55-64.

Svistoonoff, S., Creff, A., Reymond, M., Sigoillot-Claude, C., Ricaud, L., Blanchet, A., Nussaume, L. and Desnos, T. 2007. Root tip contact with low-phosphate media reprograms plant root architecture. *Nature Genetics.* **39**(6), pp.792-796.

Swarup, K., Benková, E., Swarup, R., Casimiro, I., Péret, B., Yang, Y., Parry, G., Nielsen, E., De Smet, I. and Vanneste, S. 2008. The auxin influx carrier LAX3 promotes lateral root emergence. *Nature Cell Biology.* **10**(8), pp.946-954.

Tabata, R., Sumida, K., Yoshii, T., Ohyama, K., Shinohara, H. and Matsubayashi, Y. 2014. Perception of root-derived peptides by shoot LRR-RKs mediates systemic N-demand signaling. *Science.* **346**(6207), pp.343-346.

Takahashi, F., Suzuki, T., Osakabe, Y., Betsuyaku, S., Kondo, Y., Dohmae, N., Fukuda, H., Yamaguchi-Shinozaki, K. and Shinozaki, K. 2018. A small peptide modulates stomatal control via abscisic acid in long-distance signalling. *Nature.* **556**(7700), pp.235-238.

Taleski, M., Imin, N. and Djordjevic, M.A. 2018. CEP peptide hormones: key players in orchestrating nitrogen-demand signalling, root nodulation, and lateral root development. *Journal of Experimental Botany.* **69**(8), pp.1829-1836.

Teng, S., Keurentjes, J., Bentsink, L., Koornneef, M. and Smeekens, S. 2005. Sucrose-Specific Induction of Anthocyanin Biosynthesis in *Arabidopsis* Requires the MYB75/PAP1 Gene. *Plant Physiology.* **139**(4), pp.1840-1852.

Terry, B.R., Matthews, E.K. and Haseloff, J. 1995. Molecular Characterization of Recombinant Green Fluorescent Protein by Fluorescence Correlation Microscopy. *Biochemical and Biophysical Research Communications.* **217**(1), pp.21-27.

Thieme, C.J., Rojas-Triana, M., Stecyk, E., Schudoma, C., Zhang, W., Yang, L., Minambres, M., Walther, D., Schulze, W.X., Paz-Ares, J., Scheible, W.R. and Kragler, F. 2015. Endogenous *Arabidopsis* messenger RNAs transported to distant tissues. *Nature Plants.* **1**(4), p15025.

Thole, J.M., Beisner, E.R., Liu, J., Venkova, S.V. and Strader, L.C. 2014. Abscisic acid regulates root elongation through the activities of auxin and ethylene in *Arabidopsis* thaliana. *G3: Genes, Genomes, Genetics.* **4**(7), pp.1259-1274.

Thomas, C.L., Bayer, E.M., Ritzenthaler, C., Fernandez-Calvino, L. and Maule, A.J. 2008. Specific targeting of a plasmodesmal protein affecting cell-to-cell communication. *PLOS Biology.* **6**(1), pe7.

Ticconi, C.A., Lucero, R.D., Sakhonwasee, S., Adamson, A.W., Creff, A., Nussaume, L., Desnos, T. and Abel, S. 2009. ER-resident proteins PDR2 and LPR1 mediate the developmental response of root meristems to phosphate availability. *Proceedings of the National Academy of Sciences.* **106**(33), pp.14174-14179.

Tilsner, J., Amari, K. and Torrance, L. 2011. Plasmodesmata viewed as specialised membrane adhesion sites. *Protoplasma.* **248**(1), pp.39-60.

Tilsner, J., Nicolas, W., Rosado, A. and Bayer, E.M. 2016. Staying Tight: Plasmodesmal Membrane Contact Sites and the Control of Cell-to-Cell Connectivity in Plants. *Annual Review of Plant Biology.* **67**, pp.337-364.

Tomoi, T., Kawade, K., Kitagawa, M., Sakata, Y., Tsukaya, H. and Fujita, T. 2020. Quantitative imaging reveals distinct contributions of SnRK2 and ABI3 in plasmodesmatal permeability in Physcomitrella patens. *Plant and Cell Physiology.* **61**(5), pp.942-956.

Truernit, E. and Sauer, N. 1995. The promoter of the *Arabidopsis* thaliana SUC2 sucrose-H+ symporter gene directs expression of β-glucuronidase to the phloem: evidence for phloem loading and unloading by SUC2. *Planta.* **196**(3), pp.564-570.

Turgeon, R. and Gowan, E. 1990. Phloem loading in Coleus blumei in the absence of carrier-mediated uptake of export sugar from the apoplast. *Plant Physiology.* **94**(3), pp.1244-1249.

Tylewicz, S., Petterle, A., Marttila, S., Miskolczi, P., Azeez, A., Singh, R., Immanen, J., Mähler, N., Hvidsten, T. and Eklund, D. 2018. Photoperiodic control of seasonal growth is mediated by ABA acting on cell-cell communication. *Science.* **360**(6385), pp.212-215.

Ubeda-Tomás, S., Federici, F., Casimiro, I., Beemster, G.T., Bhalerao, R., Swarup, R., Doerner, P., Haseloff, J. and Bennett, M.J. 2009. Gibberellin signaling in the endodermis controls *Arabidopsis* root meristem size. *Current Biology.* **19**(14), pp.1194-1199.

Ueki, S. and Citovsky, V. 2005. Identification of an interactor of cadmium ion-induced glycine-rich protein involved in regulation of callose levels in plant vasculature. *Proceedings of the National Academy of Sciences.* **102**(34), pp.12089-12094.

Uga, Y., Sugimoto, K., Ogawa, S., Rane, J., Ishitani, M., Hara, N., Kitomi, Y., Inukai, Y., Ono, K. and Kanno, N. 2013. Control of root system architecture by DEEPER ROOTING 1 increases rice yield under drought conditions. *Nature Genetics.* **45**(9), pp.1097-1102.

Vaattovaara, A., Brandt, B., Rajaraman, S., Safronov, O., Veidenberg, A., Luklová, M., Kangasjärvi, J., Löytynoja, A., Hothorn, M., Salojärvi, J. and Wrzaczek, M. 2019. Mechanistic insights into the evolution of DUF26-containing proteins in land plants. *Communications Biology.* **2**(1), pp.1-18.

Van den Berg, C., Willemsen, V., Hage, W., Weisbeek, P. and Scheres, B. 1995. Cell fate in the *Arabidopsis* root meristem determined by directional signalling. *Nature.* **378**(6552), pp.62-65.

van der Weele, C.M., Spollen, W.G., Sharp, R.E. and Baskin, T.I. 2000. Growth of *Arabidopsis* thaliana seedlings under water deficit studied by control of water potential in nutrient-agar media. *Journal of Experimental Botany.* **51**(350), pp.1555-1562.

Vatén, A., Dettmer, J., Wu, S., Stierhof, Y.-D., Miyashima, S., Yadav, S.R., Roberts, C.J., Campilho, A., Bulone, V. and Lichtenberger, R. 2011. Callose biosynthesis regulates symplastic trafficking during root development. *Developmental cell.* **21**(6), pp.1144-1155.

Verna, C., Ravichandran, S.J., Sawchuk, M.G., Linh, N.M. and Scarpella, E. 2019. Coordination of tissue cell polarity by auxin transport and signaling. *eLife.* **8**, pe51061.

Verstraeten, I., Schotte, S. and Geelen, D. 2014. Hypocotyl adventitious root organogenesis differs from lateral root development. *Frontiers in Plant Science.* **5**, p495.

Vidal, E.A., Araus, V., Lu, C., Parry, G., Green, P.J., Coruzzi, G.M. and Gutierrez, R.A. 2010. Nitrate-responsive miR393/AFB3 regulatory module controls root

system architecture in *Arabidopsis* thaliana. *Proceedings of the National Academy of Sciences.* **107**(9), pp.4477-4482.

Vidal, E.A., Moyano, T.C., Krouk, G., Katari, M.S., Tanurdzic, M., McCombie, W.R., Coruzzi, G.M. and Gutiérrez, R.A. 2013. Integrated RNA-seq and sRNA-seq analysis identifies novel nitrate-responsive genes in *Arabidopsis* thaliana roots. *BMC genomics.* **14**(1), p701.

Vu, M.H., Iswanto, A.B.B., Lee, J. and Kim, J.-Y. 2020. The Role of Plasmodesmata-Associated Receptor in Plant Development and Environmental Response. *Plants.* **9**(2), p216.

Wada, S., Miyake, C., Makino, A. and Suzuki, Y. 2020. Photorespiration Coupled With CO2 Assimilation Protects Photosystem I From Photoinhibition Under Moderate Poly(Ethylene Glycol)-Induced Osmotic Stress in Rice. *Frontiers in Plant Science.* **11**, p1121.

Wang, F.-L., Tan, Y.-L., Wallrad, L., Du, X.-Q., Eickelkamp, A., Wang, Z.-F., He, G.-F., Rehms, F., Li, Z. and Han, J.-P. 2021a. A potassium-sensing niche in *Arabidopsis* roots orchestrates signaling and adaptation responses to maintain nutrient homeostasis. *Developmental Cell.* **56**(6), pp.781-794. e786.

Wang, F., Muto, A., Van de Velde, J., Neyt, P., Himanen, K., Vandepoele, K. and Van Lijsebettens, M. 2015. Functional analysis of the *Arabidopsis* TETRASPANIN gene family in plant growth and development. *Plant physiology.* **169**(3), pp.2200-2214.

Wang, Y., Chen, Y.F. and Wu, W.H. 2021b. Potassium and phosphorus transport and signaling in plants. *Journal of Integrative Plant Biology.* **63**(1), pp.34-52.

Wang, Y., Ribot, C., Rezzonico, E. and Poirier, Y. 2004. Structure and expression profile of the *Arabidopsis* PHO1 gene family indicates a broad role in inorganic phosphate homeostasis. *Plant Physiology.* **135**(1), pp.400-411.

Wang, Y., Selinski, J., Mao, C., Zhu, Y., Berkowitz, O. and Whelan, J. 2020. Linking mitochondrial and chloroplast retrograde signalling in plants. *Philosophical Transactions of the Royal Society B.* **375**(1801), p20190410.

Wei, Z., Tan, S., Liu, T., Wu, Y., Lei, J.-G., Chen, Z., Friml, J., Xue, H.-W. and Liao, K. 2020. Plasmodesmata-like intercellular connections by plant remorin in animal cells. *bioRxiv.* p791137.

Williamson, L.C., Ribrioux, S.P., Fitter, A.H. and Leyser, H.O. 2001. Phosphate availability regulates root system architecture in *Arabidopsis*. *Plant Physiology.* **126**(2), pp.875-882.

Wilson, A.K., Pickett, F.B., Turner, J.C. and Estelle, M. 1990. A dominant mutation in*Arabidopsis* confers resistance to auxin, ethylene and abscisic acid. *Molecular and General Genetics MGG.* **222**(2-3), pp.377-383.

Wippel, K. and Sauer, N. 2011. *Arabidopsis* SUC1 loads the phloem in suc2 mutants when expressed from the SUC2 promoter. *Journal of Experimental Botany.* **63**(2), pp.669-679.

Wolf, S., Lucas, W.J., Deom, C.M. and Beachy, R.N. 1989. Movement Protein of Tobacco Mosaic Virus Modifies Plasmodesmatal Size Exclusion Limit. *Science.* **246**(4928), pp.377-379.

Wright, K.M., Wood, N.T., Roberts, A.G., Chapman, S., Boevink, P., MacKenzie, K.M. and Oparka, K.J. 2007. Targeting of TMV movement protein to plasmodesmata requires the actin/ER network; evidence from FRAP. *Traffic.* **8**(1), pp.21-31.

Wu, H.-C., Bulgakov, V.P. and Jinn, T.-L. 2018. Pectin methylesterases: Cell wall remodeling proteins are required for plant response to heat stress. *Frontiers in Plant Science.* **9**, p1612.

Wu, S., Lee, C.-M., Hayashi, T., Price, S., Divol, F., Henry, S., Pauluzzi, G., Perin, C. and Gallagher, K.L. 2014. A plausible mechanism, based upon Short-Root movement, for regulating the number of cortex cell layers in roots. *Proceedings of the National Academy of Sciences.* **111**(45), pp.16184-16189.

Xie, Y., Zheng, Y., Li, H., Luo, X., He, Z., Cao, S., Shi, Y., Zhao, Q., Xue, Y., Zuo, Z. and Ren, J. 2016. GPS-Lipid: a robust tool for the prediction of multiple lipid modification sites. *Scientific Reports.* **6**(1), p28249.

Xu, J., Li, H.-D., Chen, L.-Q., Wang, Y., Liu, L.-L., He, L. and Wu, W.-H. 2006. A protein kinase, interacting with two calcineurin B-like proteins, regulates K+ transporter AKT1 in *Arabidopsis*. *Cell.* **125**(7), pp.1347-1360.

Xu, Q. and Liesche, J. 2021. Sugar export from *Arabidopsis* leaves: Actors and regulatory strategies. *Journal of Experimental Botany.* **72**(15), pp.5275-5284.

Xu, W., Ding, G., Yokawa, K., Baluška, F., Li, Q.-F., Liu, Y., Shi, W., Liang, J. and Zhang, J. 2013. An improved agar-plate method for studying root growth and response of *Arabidopsis* thaliana. *Scientific Reports.* **3**(1).

Xu, X.M., Wang, J., Xuan, Z., Goldshmidt, A., Borrill, P.G., Hariharan, N., Kim, J.Y. and Jackson, D. 2011. Chaperonins facilitate KNOTTED1 cell-to-cell trafficking and stem cell function. *Science.* **333**(6046), pp.1141-1144.

Xu, Y., Buchholz, W.G., DeRose, R.T. and Hall, T.C. 1995. Characterization of a rice gene family encoding root-specific proteins. *Plant molecular biology.* **27**(2), pp.237-248.

Xu, Y., Yuan, Y., Du, N., Wang, Y., Shu, S., Sun, J. and Guo, S. 2018. Proteomic analysis of heat stress resistance of cucumber leaves when grafted onto Momordica rootstock. *Horticulture research.* **5**(1), pp.1-18.

Xue, Y., Liu, Z., Gao, X., Jin, C., Wen, L., Yao, X. and Ren, J. 2010. GPS-SNO: Computational Prediction of Protein S-Nitrosylation Sites with a Modified GPS Algorithm. *PLOS One.* **5**(6), pe11290.

Yadav, S.R., Yan, D., Sevilem, I. and Helariutta, Y. 2014. Plasmodesmata-mediated intercellular signaling during plant growth and development. *Frontiers in Plant Science.* **5**, p44.

Yan, D., Yadav, S.R., Paterlini, A., Nicolas, W.J., Petit, J.D., Brocard, L., Belevich, I., Grison, M.S., Vaten, A. and Karami, L. 2019. Sphingolipid biosynthesis modulates plasmodesmal ultrastructure and phloem unloading. *Nature Plants.* **5**(6), pp.604-615.

Yang, L., Perrera, V., Saplaoura, E., Apelt, F., Bahin, M., Kramdi, A., Olas, J., Mueller-Roeber, B., Sokolowska, E., Zhang, W., Li, R., Pitzalis, N., Heinlein, M., Zhang, S., Genovesio, A., Colot, V. and Kragler, F. 2019. m5C Methylation

Guides Systemic Transport of Messenger RNA over Graft Junctions in Plants. *Current Biology.* **29**(15), pp.2465-2476.e2465.

Yao, H., Wang, X., Chen, P., Hai, L., Jin, K., Yao, L., Mao, C. and Chen, X. 2018. Predicted *Arabidopsis* interactome resource and gene set linkage analysis: a transcriptomic analysis resource. *Plant Physiology.* **177**(1), pp.422-433.

Ye, H., Roorkiwal, M., Valliyodan, B., Zhou, L., Chen, P., Varshney, R.K. and Nguyen, H.T. 2018. Genetic diversity of root system architecture in response to drought stress in grain legumes. *Journal of Experimental Botany.* **69**(13), pp.3267-3277.

Ye, Z.-W., Chen, Q.-F. and Chye, M.-L. 2017. *Arabidopsis* thaliana Acyl-CoA-binding protein ACBP6 interacts with plasmodesmata-located protein PDLP8. *Plant Signaling & Behavior.* **12**(8), pe1359365.

Ye, Z.-W., Lung, S.-C., Hu, T.-H., Chen, Q.-F., Suen, Y.-L., Wang, M., Hoffmann-Benning, S., Yeung, E. and Chye, M.-L. 2016. *Arabidopsis* acyl-CoA-binding protein ACBP6 localizes in the phloem and affects jasmonate composition. *Plant Molecular Biology.* **92**(6), pp.717-730.

Yeats, T.H., Sorek, H., Wemmer, D.E. and Somerville, C.R. 2016. Cellulose Deficiency Is Enhanced on Hyper Accumulation of Sucrose by a H+-Coupled Sucrose Symporter. *Plant Physiology.* **171**(1), pp.110-124.

Zavaliev, R., Dong, X. and Epel, B.L. 2016. Glycosylphosphatidylinositol (GPI) Modification Serves as a Primary Plasmodesmal Sorting Signal. *Plant Physiology.* **172**(2), pp.1061-1073.

Zeng, S.M., Lo, E.K.W., Hazelton, B.J., Morales, M.F. and Torii, K.U. 2020. Effective range of non-cell autonomous activator and inhibitor peptides specifying plant stomatal patterning. *Development.* **147**(17), pdev192237.

Zhang, B., Van Aken, O., Thatcher, L., De Clercq, I., Duncan, O., Law, S.R., Murcha, M.W., Van der Merwe, M., Seifi, H.S. and Carrie, C. 2014a. The mitochondrial outer membrane AAA ATP ase At OM 66 affects cell death and pathogen resistance in A rabidopsis thaliana. *The Plant Journal.* **80**(4), pp.709-727.

Zhang, C., Han, L., Slewinski, T.L., Sun, J., Zhang, J., Wang, Z.-Y. and Turgeon, R. 2014b. Symplastic phloem loading in poplar. *Plant Physiology.* **166**(1), pp.306-313.

Zhang, G., Kong, G. and Li, Y. 2021a. Long-distance communication through systemic macromolecular signaling mediates stress defense responses in plants. *Physiologia Plantarum.* **173**(4), pp.1926-1934.

Zhang, H. and Forde, B.G. 1998. An *Arabidopsis* MADS box gene that controls nutrient-induced changes in root architecture. *Science.* **279**(5349), pp.407-409.

Zhang, H. and Forde, B.G. 2000. Regulation of *Arabidopsis* root development by nitrate availability. *Journal of Experimental Botany.* **51**(342), pp.51-59.

Zhang, H., Jennings, A., Barlow, P.W. and Forde, B.G. 1999. Dual pathways for regulation of root branching by nitrate. *Proceedings of the National Academy of Sciences.* **96**(11), pp.6529-6534.

Zhang, H., Yu, P., Zhao, J., Jiang, H., Wang, H., Zhu, Y., Botella, M.A., Šamaj, J., Li, C. and Lin, J. 2018. Expression of tomato prosystemin gene in *Arabidopsis* reveals systemic translocation of its mRNA and confers necrotrophic fungal resistance. *New Phytologist.* **217**(2), pp.799-812.

Zhang, L.-Y., Peng, Y.-B., Pelleschi-Travier, S., Fan, Y., Lu, Y.-F., Lu, Y.-M., Gao, X.-P., Shen, Y.-Y., Delrot, S. and Zhang, D.-P. 2004. Evidence for apoplasmic phloem unloading in developing apple fruit. *Plant Physiology.* **135**(1), pp.574-586.

Zhang, X.-Y., Wang, X.-L., Wang, X.-F., Xia, G.-H., Pan, Q.-H., Fan, R.-C., Wu, F.-Q., Yu, X.-C. and Zhang, D.-P. 2006. A shift of phloem unloading from symplasmic to apoplasmic pathway is involved in developmental onset of ripening in grape berry. *Plant Physiology.* **142**(1), pp.220-232.

Zhang, Y., Shen, C., Zhou, Y., Liu, C., Yin, W. and Xia, X. 2021b. Tuning drought resistance by using a root-specific expression transcription factor PdNF-YB21 in *Arabidopsis* thaliana. *Plant Cell, Tissue and Organ Culture (PCTOC).* **145**(2), pp.1-13.

Zhang, Y.J., Lynch, J.P. and Brown, K.M. 2003. Ethylene and phosphorus availability have interacting yet distinct effects on root hair development. *Journal of Experimental Botany.* **54**(391), pp.2351-2361.

Zhang, Z., Ruan, Y.-L., Zhou, N., Wang, F., Guan, X., Fang, L., Shang, X., Guo, W., Zhu, S. and Zhang, T. 2017. Suppressing a putative sterol carrier gene reduces plasmodesmal permeability and activates sucrose transporter genes during cotton fiber elongation. *The Plant Cell.* **29**(8), pp.2027-2046.

Zhang, Z., Zhu, J.-Y., Roh, J., Marchive, C., Kim, S.-K., Meyer, C., Sun, Y., Wang, W. and Wang, Z.-Y. 2016. TOR signaling promotes accumulation of BZR1 to balance growth with carbon availability in *Arabidopsis*. *Current Biology.* **26**(14), pp.1854-1860.

Zhao, B., Liu, Q., Wang, B. and Yuan, F. 2021. Roles of phytohormones and their signaling pathways in leaf development and stress responses. *Journal of Agricultural and Food Chemistry.* **69**(12), pp.3566-3584.

Zhao, S., Zhang, M.-L., Ma, T.-L. and Wang, Y. 2016. Phosphorylation of ARF2 relieves its repression of transcription of the K+ transporter gene HAK5 in response to low potassium stress. *The Plant Cell.* **28**(12), pp.3005-3019.

Zheng, H., Pan, X., Deng, Y., Wu, H., Liu, P. and Li, X. 2016. AtOPR3 specifically inhibits primary root growth in *Arabidopsis* under phosphate deficiency. *Scientific Reports.* **6**(1), p24778.

Zhu, J., Park, J.-H., Lee, S., Lee, J.H., Hwang, D., Kwak, J.M. and Kim, Y.J. 2020a. Regulation of stomatal development by stomatal lineage miRNAs. *Proceedings of the National Academy of Sciences.* **117**(11), pp.6237-6245.

Zhu, Y., Huang, P., Guo, P., Chong, L., Yu, G., Sun, X., Hu, T., Li, Y., Hsu, C.C. and Tang, K. 2020b. CDK8 is associated with RAP2. 6 and SnRK2. 6 and positively modulates abscisic acid signaling and drought response in *Arabidopsis*. *New Phytologist.* **228**(5), pp.1573-1590.

Zierer, W., Rüscher, D., Sonnewald, U. and Sonnewald, S. 2021. Tuber and Tuberous Root Development. *Annual Review of Plant Biology.* **72**.